Generating and Characterising Knockout and Transgenic Mouse Models of Frontotemporal Dementia Caused by CHMP2B Mutation

This thesis is submitted in fulfilment of the requirements for the degree of Doctor of Philosophy to University College London

By

Shabnam Ghazi-Noori

MRC Prion Unit and Department of Neurodegenerative Disease

Institute of Neurology

University College London

Declaration

I hereby declare that this thesis is my work and effort, and that it has not been submitted anywhere for any award. Wherever contributions of others are involved, every effort is made to indicate this clearly, with due reference to the literature, and acknowledgement of collaborative research and discussions.

Abstract

A mutation in the charged multivesicular body protein 2B (CHMP2B) gene, identified in a kindred from the Jutland region of Denmark, segregates with affected family members with clinical presentations of frontotemporal dementia (FTD) and is absent in control populations (Gydesen et al., 1987; Gydesen et al., 2002; Skibinski et al., 2005). The mutation is a G>C transition in the splice acceptor site of exon 6 resulting in two novel splice variants *CHMP2B*^{Int5} and *CHMP2B*$^{\Delta 10}$ leading to C-terminal truncation of the CHMP2B protein (Skibinski et al., 2005).

Chmp2b knockout (*Chmp2b*$^{-/-}$) mice and transgenic mice expressing either wild-type or C-terminally truncated mutant CHMP2B splice variants *CHMP2B*^{Int5} and *CHMP2B*$^{\Delta 10}$ were generated with the aims of examining the normal function of *Chmp2b* and the effect of mutant *CHMP2B* species *in vivo,* as well as providing insight into a potential common FTD mechanism of disease.

Quantification of Chmp2b protein in *Chmp2b*$^{-/-}$ mice demonstrates a significant (85%) depletion of endogenous Chmp2b in the mouse brain. No pathology is identified in the CNS or muscle tissue of these mice however, they do demonstrate significant motor and behavioural abnormalities.

CHMP2B^{Int5} transgenic mice demonstrate neurodegenerative changes including progressive gliosis, accumulation of CHMP2B, p62 and ubiquitin inclusions which are negative for TDP-43 and FUS proteins, consistent with the inclusion pathology observed in patients with *CHMP2B* mutation. Furthermore, these mice have reduced survival and develop progressive axonopathy characterized by axonal swellings and accumulation of mitochondria and vesicles likely from the endosome-lysosome and autophagy pathway, implicating altered axonal function in disease pathogenesis.

This thesis describes the first mouse models of FTD-3 caused by *CHMP2B* mutation and presents evidence consistent with a gain-of-function effect unique to the *CHMP2B*^{Int5} isoform and provides new insights into the mechanisms of CHMP2B-induced neurodegeneration.

Table of contents

List of tables

List of figures

List of video clips

Clips accompany section

Clip 1 21 month *Chmp2b wild type* (*Chmp2b*$^{+/+}$)

Clip showing wild type mouse gait and rearing

Clip 2 21 month *Chmp2b wild type* (*Chmp2b*$^{+/+}$)

Additional clip showing wild type mouse gait and rearing

Clip 3 14 month *Chmp2b knockout* (*Chmp2b*$^{-/-}$)

Clip showing typical *Chmp2b knockout* mouse 'splayed gait'

Clip 4 14 month *Chmp2b knockout* (*Chmp2b*$^{-/-}$)

Clip showing typical *Chmp2b knockout* mouse 'foot tapping'

Clip 5 12 month *Chmp2b*$^{-/-}$ and *Chmp2b*$^{+/+}$ mice, combined clips

- Time 0-15 seconds; kinked tail and difficulty initiating forward movement
- Time 16-26 seconds; curled paw and splayed gait
- Time 27-45 seconds; over-grooming, kyphosis and possible tremor
- Time 46-60 seconds- blank clip
- Time 1.01-1.06 minutes; splayed gait
- Time 1.07-1.25 minutes; wild type mouse gait and exploring behaviour
- Time 1.26-1.33 minutes; wild type mouse.

Abbreviations

ALS	Amyotrophic Lateral Sclerosis
CB	Citrate buffer
CHMP	Charged multivescular body protein
CHMP2B	Charged multivescular body protein 2B
Chmp2b$^{-/-}$	*chmp2b* (endogenous gene; knockout)
Chmp2b$^{+/+}$	*chmp2b* (endogenous gene; wild type)
CHMP2B$^{\Delta 10}$	Charged multivescular body protein 2B delta 10
CHMP2B^{int5}	Charged multivescular body protein 2B intron 5
CHMP2B^{WT}	Charged multivescular body protein 2B wild type
DAB	3'3' diaminobenzadine
DEPC	Diethylpyrocarbonate
DePeX	Distrene plasticizer xylene
DMSO	Dimethyl sulphoxide
EDTA	Ethylenediaminetetraacetic acid
EEA-1	early endosome antigen-1
EM	electron microscopy
EMG	electromyography
ENU	N-ethyl-N-nitrosourea
ESCRT	endosomal sorting complex required for transport
FTD	Frontotemporal dementia
FTLD	Frontotemporal lober degeneration
GAPDH	glyceraldehyde-3-phosphate dehydrogenase
GFAP	Glial fibrillary Acidic Protein
H&E	Haematoxylin and Eosin
Iba-1	ionized calcium binding adaptor molecule 1
Lamp-1	lysosome associated membrane protein 1
Lamp-2	lysosome associated membrane protein 2
LC-3 (I & II)	Light chain 3 (protein 1 and 2 respectively)

LM	light microscope
LMN	Lower Motor Neurons
M6PR	mannose-6-phosphate receptor
MIM	MIT-Interacting Motif
MIT	microtubule interacting and transport
MRI	Magnetic Resonance Imaging
MW	microwave
Non-Tg	non-transgenic
OCT	optimum cutting temperature
p62	Nucleoporin protein 62
PBS	phosphate buffered saline
PCR	polymerase chain reaction
PET	Positron Emission Tomography
PMA	Progressive Muscular Atrophy
PNFA	Progressive non-fluent aphasia
PPA	Primary progressive aphasia
RNA	ribonucleic acid
RPM	rotations per minute
RT	room temperature
RT-PCR	reverse transcriptase PCR
SD	Semantic dementia
SHIRPA	**S**mithKline Beecham Pharmaceuticals; **H**arwell, MRC Mouse Genome Centre and Mammalian Genetics Unit; **I**mperial College School of Medicine at St Mary's; **R**oyal London Hospital, St Bartholomew's and the Royal London School of Medicine; **P**henotype **A**ssessment
SPECT	Single Photon Emission Computed Tomography
TAE	tris base, acetic acid and EDTA
TBS	tris-buffered saline
Tg	transgenic

TDP-43	transactive response DNA-binding protein
WT	wild type

Antigen retrieval abbreviations

CB	citrate buffer
MCC1	mild cell conditioning
MW	microwave
PRT1	Protease 1 treatment
RT	room temperature

Researcher initials

AI	Dr. Adrian Isaacs
EA	Dr. Emmanuel Asante
MF	Mr. Mike Farmer
SB	Professor Sebastian Brandner
SBM	Miss Sarah Blakamore
SM	Mr Steven Morrel
SN	Shabnam Ghazi-Noori

Dedication

Let there be no doubt that this thesis is completely and whole heartedly dedicated to my mother and my father. If not for them and their strength, patience and unwavering support through this journey and life in general, *I* simply could not have reached this stage.

In loving memory of grandfathers and my grandmother who first noticed my little kidneys were not quite right. For my amazing, wonderful, beautiful, one and only auntie Farzi who has 'always always' been the person I can turn to for advice, to talk to and share a joke.

A particular debt of gratitude to my mother for being with me every step of the way and holding my hand and my soul for every blood test, being poked and prodded, the operations and of course my bad moods and my father for the ultimate act of courage, love and selflessness, donating one of his kidneys so that I could finish this PhD…….

A very huge thank-you to my brothers Reza and Arash who have always spurred me on, encouraged me and given me tummy aches from laughing so hard- the drinks are on you! To my wonderfully large and extended family, my grandmother, aunts, uncles, cousins, siblings and of course my little sister Lylah and the very talented Mr. Jermaine King Kabali.

This work is also dedicated to all the renal and transplant researchers, doctors, surgeons, nurses, phlebotomists, and NHS staff at Addenbrookes hospital and Guy's and St. Thomas' hospital. Mr. Geoff Koffman, Sir Roy Calne, Dr. John Scoble, Mr. Johnathan Olsburgh, Mr. Chris Callaghan, Dr. Sue Rigden, Dr. Evans, Prof. Sacks, Heather Johnson, Adi, Karlene Kerr, Anne-Marie, Marylene, Ceilia, Jane, Moira, Geraldine, Diane, Afori, Marylene, Georgina, the list is endless- Thank-you! ☺

To treatments and cures freely accessible to all for FTD, dementia and all neurological disease acquired and genetic.

'Dare Quam Accipere'
Thomas Guy 1644-1724

Acknowledgments
I am eternally grateful to my supervisors, Dr. Emmanuel Asante and Dr. Adrian Isaacs for giving me the opportunity to undertake this research project, sharing their knowledge and for their guidance and stout support. I am also grateful to Professor Lizzy Fisher for her time, patience, immense wisdom and for not letting me give up. I am grateful too to Frank Cooper MBE for having the time to listen to me and a strong shoulder to lean on and of course to Professor John Collinge for the opportunity to work in his amazing research unit. I would also like to thank Professors Angela Clow, Gillian Bates and Dominic Wells for seeding my career. I am in awe and admiration of all these amazing individuals and can only aspire to their achievements, for they are the giants on whose shoulders I may one day stand?!

I would like to say a huge and heartfelt thank-you to all my friends at the MRC Prion Unit. To the members of the Transgenic Group, Andrew G and Andy T who have always made me laugh, Funmi who welcomed me to the group and made me feel at home, Richard H for his expertise in generating transgenic mice, Kinga for her friendship and warmth, Tati and Shyma for the much needed coffee breaks and so much more and Asif for sharing his space and desk while I was writing. Also a big thank-you to Astrid A and Sarah M for their friendship, kindness and technical and scientific expertise.

This work has only been possible because so many people contributed their time and expertise. In loving memory of my dear friend and colleague Ben Woodman without whom the SHIRPA experiments (Chapter 4.1) would not have been possible. Unbelieveably, Ben passed away after a acute illness in hospital. He will always be remembered through his contributions to science, by his family, friends and colleagues. I would like to thank Mike Farmer who as well as making me laugh has been a constant source of advice on pretty much everything but in particular for his work on the mouse phenotyping experiments (Chapter 4) I will always be grateful, And of course none of this work would be possible without the Wakefield Street crew! A huge thank-you to Steven Morrel who first spotted the *Chmp2b* knockout mice gait, I would also like to thank Gavin, Claire, Lee, Sarah Blackamore and everyone at Wakefield Street for their hard work and rapid response to requests, you are all amazing.

A special thank-you to Camila Batmanghelidjh for her all encompassing compassion, generosity, her wings that spread so far and help to protect the most vulnerable children, young people and families in society and for being such an inspiration.

I would like to thank my friend Bee Lian Sim for her compassion, kindness and friendship throughout the years. I would also like to thank my bestest friend ever Natasha and her husband Thomas, my two beautiful God sons Aidan and Joshua for their love, support and friendship. To my amazing friends who have encouraged and supported me and put up with me; shahlaa, Samara, Sunny, Sara Montiero, Alex Santacreu and of course my love Emmanuel Mintias ☺

1 Introduction

1.1 Project Overview

Frontotemporal Dementia (FTD) is the second most common form of presenile dementia after Alzheimer's disease (AD) (Neary et al., 1998). FTD encompasses a heterogeneous class of neurodegenerative diseases that clinically present with personality change, language disorder and cognitive decline and at post-mortem with extensive atrophy of the frontal and temporal lobes (Neary et al., 2005; Weder et al., 2007). There is a strong genetic component in FTD so that in 25-50% of FTD cases there is a first degree relative diagnosed with dementia (Stevens et al., 1998; Chow et al., 1999; Rosso et al., 2003).

In 2005 Skibinski *et al.* identified the potential disease gene previously linked to chromosome 3 that was associated with a form of FTD in a large Danish Family (FTD-3). The mutation identified in the Charged Multivesicular Body Protein 2B (*CHMP2B*) gene results in two aberrant transcripts, *CHMP2B*^{Int5} and *CHMP2B*^{Delta10} (Skibinski et al., 2005), neither of which were found in any bioinformatic database. The aim of this study was to generate and characterise transgenic and knock-out murine models that may recapitulate hallmark characteristics of human FTD-3 disease. This will aid the study of both the pathology of FTD-3 and the development of potential drug therapies.

1.1.1 A brief history of clinical understanding of FTD

The concept of frontal and temporal lobar degeneration (FTLD) was originally introduced when a form of presenile dementia with circumscribed frontotemporal lobar atrophy was first reported by Arnold Pick in 1892 and later termed Pick's Disease (PiD) (Pick A, 1892; Kertesz, 2004; Weder et al., 2007). However, characteristic histological lesions of PiD, typically well defined, spherical, argyrophilic (bind silver salt stains), tau-immunoreactive, neuronal intracytoplasmic inclusions

(NII) and ballooned neurons referred to as Pick cells were first described by Alois Alzheimer in 1911 (Alzheimer A, 1911; Alzheimer et al., 1995). The term Pick's disease was consequently used to differentiate the clinically and pathologically distinct disorder FTLD from Alzheimer's disease (AD) (Pick A, 1892; Graff-Radford and Woodruff, 2007). Since this distinction several classification systems for FTLD have been presented with each successive classification including more disorders under the umbrella of FTLD (Sjogren and Andersen, 2006; Mackenzie et al., 2009; Josephs et al., 2011).

The term frontotemporal dementia (FTD) was introduced by the Lund and Manchester group in 1994 to describe a specific progressive behavioural syndrome (Brun and et al, 1994) and superseded terms such as frontal lobe dementia, dementia of the frontal lobe and non-Alzheimer's dementia (Brun and et al, 1994; Graff-Radford and Woodruff, 2007; Seelaar et al., 2011). The clinical and pathological criteria the group developed facilitated accurate diagnosis and better appreciation of the prevalence of FTD, thereby aiding discrimination between the diagnosis of Alzheimer's disease (AD) and FTD (Brun and et al, 1994).

The criteria prepared the way for significant progress to be made in the field of FTD but in practice clinicians in the wider neurology community found the criteria set out by the Lund and Manchester consortium limiting (Neary et al., 1998). The consensus was that the criteria lacked guidance as to the number of clinical features required for diagnosis and the relative importance of each feature (Neary et al., 1998). In addition other clinical syndromes determined by the hallmark distribution of pathology within the frontal and temporal lobes of the brain such as progressive aphasia and semantic dementia were not included as part of this diagnostic criteria (Brun and et al, 1994; Neary et al., 1998).

Clinical criteria published by Neary and colleagues in 1998 proposed Frontotemporal Lobar Degeneration (FTLD) as a blanket term encompassing the three clinical syndromes irrespective of underlying histology (Neary et al., 1998). They divided patients into three categories; frontotemporal dementia (FTD) in which behavioural change is by definition the dominant feature of the disease, progressive non fluent aphasia (PNFA), predominantly a disorder of expressive language in which patients have severe trouble in word retrieval in the context of preserved word comprehension, and semantic dementia (SD) in which the most common initial presentation is language abnormality including loss of memory for words or loss of word meanings (Neary et al., 1998).

In order to further define and accommodate the need for clinicians to easily make prompt diagnosis of FTD, McKhann and colleagues simplified the criteria of Neary *et al.* 1998 (McKhann et al., 2001). The McKhann criteria combines PNFA and SD together with FTD and proposes the following six features: (1) development of behavioural and cognitive deficits (2) early and progressive change in personality or language (3) significant impairment in social or occupational ability (4) deficits show a progressive course (5) presence of symptoms in the absence of delirium and (6) exclusion of other psychiatric disease (McKhann et al., 2001). This demonstrates the vast progress that has been made since FTD was originally identified by Pick and Alzheimer when the only conclusive diagnosis was the presence of gross frontotemporal atrophy with the presence of characteristic cell pathology.

Classification criteria by Neary *et al* (1998) and McKann *et al* (2001) identified a proportion of patients with FTD that developed parkinsonism symptoms at later stages of disease (Neary et al., 1998; McKhann et al., 2001) these patients were classified as FTD with parkinsonism linked to chromosome 17 (FTDP-17) based on their clinical symptoms and because the disease locus had previously been linked to chromosome 17 (Wilhelmsen et al., 1994; Lynch et al., 1994; Foster et al., 1997).

Frontotemporal dementia with motor neuron disease (FTD-MND) is an additional form of FTD (Neary et al., 1990; Valdmanis et al., 2007). There is now a general consensus that FTD, FTD-MND and MND are diseases with clinical, pathological and biochemical presentation within the same clinical spectrum (Seelaar et al., 2011; Seilhean et al., 2011; Rohrer et al., 2011b).

In recent years (2006-2011) advances in molecular pathology and genetics as well as improved imaging techniques coupled with refined clinical descriptions have contributed to enormous progress in the fields of FTD and ALS. As a result of this rapid progress the general consensus prevailed that the most commonly applied Neary diagnostic criteria (Neary, 1990) needed to be updated and in response to this, experts in the field have published updated and revised nomenclature and nosology studies (Mackenzie et al., 2009; Mackenzie et al., 2010; Josephs et al., 2011; Seilhean et al., 2011).

In accordance with current accepted terminology, in this study the term FTD is used to refer to the clinical presentation of FTD syndromes and the term FTLD reserved to describe the pathological basis of the disease including gross pathology and histology (Brun and et al, 1994; Neary et al., 1998; Sampathu et al., 2006; Mackenzie et al., 2009; Mackenzie et al., 2010; Josephs et al., 2011; Seilhean et al., 2011).

1.1.2 Frontotemporal dementia linked to chromosome 3 in a Danish family- Historical perspectives

The first report of a Danish family with pre-senile dementia was published in 1987 (Gydesen et al., 1987). The study described a family in which 14 out of 73 family members were clinically symptomatic for an unspecified form of early onset dementia distinct from Alzheimer's and Pick's disease. In this initial report of the family only two post-mortem brains were available; they showed cerebral atrophy

but no other characteristics of any known dementia syndrome of the time. The only other observation noted was increased cerebral blood flow in one affected member of the family with early stage disease (Gydesen et al., 1987).

Figure 1.1 Picture of the FTD-3 family.

Danish Family, farmer's wife (seated second from left) and her husband (seated third from left) surrounded by their 12 children (taken ~1930).

This family first came to the attention of clinicians and scientists when an affected family member (patient III-15) approached Dr. Susan Gydesen at the Department of Psychiatry, University of Copenhagen, Denmark (Gydesen et al., 1987). This original contact by patient III-15 initiated collaborations between Denmark and the UK to investigate '*the family disease*' including clinical diagnosis, neuropsychological testing, neuroimaging, neuropathological analysis and molecular genetics (personal communications).

Based on the study of the family pedigree the founding affected matriarch had twelve children (figure 1.1) and went on to develop dementia by the age of 56 years (born 1876) and died twelve years later (1944). Eight of her children also developed dementia later in life (Brown et al., 1991; Brown et al., 1993; Gydesen et al., 2002). These eight individuals also went on to have large families, from which there were 50 at risk individuals in the third generation of this kindred and 13 of them developed dementia (Brown, 1998). The family now spans 6 generations with over 450 members and 38 known affected individuals (figure 1.2). In 2005 a mutation in the *CHMP2B* gene was identified as the cause of the Danish family dementia (Skibinski et al., 2005).

A new branch of the FTD-3 family was identified from an affected individual who had been adopted at birth (Lindquist et al., 2008). Information about the course of disease was obtained from an unaffected half sibling who was brought up by the affected biological parent. Genetic screening identified *CHMP2B* mutation identical to that of FTD-3 family in this adopted individual and another half sibling (Lindquist et al., 2008). In a Belgian series of patients a novel missense mutation was identified in a familial FTD patient (van der Zee J. et al., 2008). Five additional *CHMP2B* missense mutations of unknown pathogenicity have been identified in eight individuals with a range of FTD-MND spectrum disorders (Skibinski et al., 2005; Parkinson et al., 2006; Rizzu et al., 2006; Lindquist et al., 2008; Cox et al., 2010; Isaacs et al., 2011).

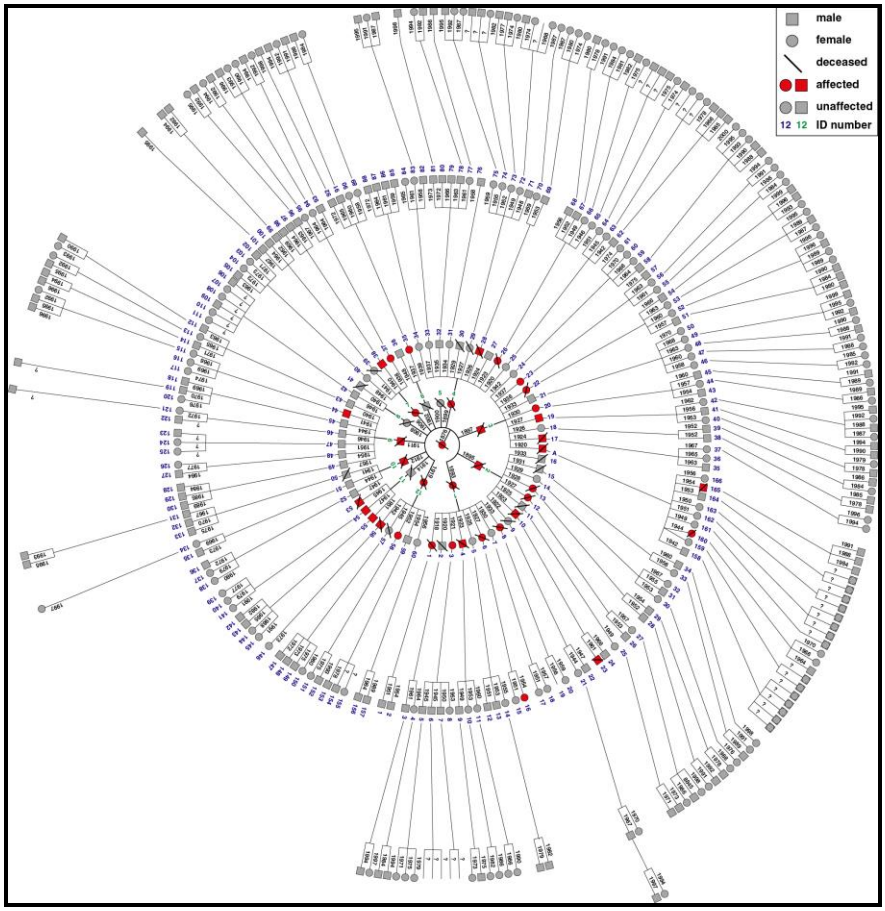

Figure 1.2 Danish FTD-3 pedigree

Generations 1 to 6 of affected and unaffected male and female family members.

1.2 Clinical Presentation and Classification

FTD can be classified into three clinical syndromes depending on the early and predominant symptoms- behavioural variant frontotemporal dementia (bvFTD), progressive non-fluent aphasia (PNFA) and semantic dementia (SD)- all share an insidious onset with inexorably progressive characteristics but with variable rates of decline. Typical clinical presentations including, lack of insight into their disease, emotional blunting, apathy, neglect of personal hygiene and selfishness are commonly associated with bvFTD but may be seen in all subtypes (Bathgate et al., 2001; Seelaar et al., 2011). The language variants of FTD (PNFA and SD) are collectively termed primary progressive aphasia (PPA) with patients exhibiting

progressive impairment in speech and semantic memory respectively (Bathgate et al., 2001; Gorno-Tempini et al., 2004; Rascovsky et al., 2007; Seelaar et al., 2011). Not all clinical presentations of PPA can categorically be classified as PNFA or SD. Such cases typically present with hesitant speech with prominent word finding difficulty and may be classified under the recently described term Logopenic Progressive Aphasia (LPA) mostly associated with atypical Alzheimer's disease (Leyton et al., 2011).

The symptoms demonstrated by patients are closely correlated with the distribution of pathology in the brain. A combination of imaging and post-mortem studies has shown that in FTD patients with disinhibition symptoms the orbitofrontal cortex is affected with involvement of the temporal cortex (Neary et al., 2005). Functional imaging including studies of single photon emission computed tomography (SPECT), positron emission tomography (PET), and perfusion magnetic resonance imaging (MRI) show reduced perfusion of the frontal and temporal lobes which can be strikingly asymmetrical and may be considered as an additional diagnostic tool (Seelaar et al., 2011; Zhang et al., 2011).

In addition to the main FTD syndromes (bvFTD, PNFA, SD) presented above, a number of other neurodegenerative diseases present with clinical symptoms, cellular biochemistry and genetics highly consistent with FTD and have over time been added to the umbrella of FTD syndromes. The most striking of these is autosomal dominant familial frontotemporal dementia with parkinsonism linked to chromosome 17 (FTDP-17) (Foster et al., 1997). Other neurological disorders that share overlapping clinical presentation, cellular biochemistry and genetics with FTD include progressive supranuclear palsy, (PSP), corticobasal degeneration (CBD) and inclusion body myopathy with Paget's disease of the bone and FTD (IBMPFD) (Mackenzie et al., 2011; Rohrer et al., 2011b).

Frontotemporal Dementia with motor neuron disease (FTD-MND) is an additional neurodegenerative disease that shares significant clinicopathological similarity with FTD syndromes. MND can present with significant overlap with FTD but also with PSP, CBD and other FTD syndromes (Mackenzie et al., 2009). Affected individuals may present with characteristic FTD symptoms, preceded, followed or with simultaneous symptoms of motor neuron disease including muscle atrophy, weakness and fasiculations in the upper extremities (Lomen-Hoerth et al., 2002; Seelaar et al., 2007; Seelaar et al., 2010; Espay and Litvan, 2011).

There is a strong genetic component to FTD-MND (Graff-Radford and Woodruff, 2007) and families were linked to chromosome 9 (Hosler et al., 2000; Morita et al., 2006; Vance et al., 2006; Valdmanis et al., 2007; Pearson et al., 2011). The same region of chromosome 9 defined by 3.7Mb region containing only five known genes (Gijselinck et al., 2010; Pearson et al., 2011) was associated in several genome wide association studies to sporadic FTD, ALS and FTD-MND (van Es et al., 2009; Laaksovirta et al., 2010; Shatunov et al., 2010; Mok et al., 2012). The genetic basis of chromosome 9-linked FTD/ALS has been identified as a hexanucleotide (GGGGCC) repeat expansion in chromosome 9 open reading frame 72 (*C9orf72*). The expanded GGGGCC repeat is found in the non-coding region of *C9orf72* encoding an uncharacterised protein of unknown function (Renton et al., 2011; Dejesus-Hernandez et al., 2011).

1.2.1 Behavioural variant frontotemporal dementia

The prevailing feature of bvFTD is an insidious onset of progressive behavioural and personality change. In some patients the frontal cortex may be predominately affected with pathology bias for the right hemisphere (Seelaar et al., 2008b; Seelaar et al., 2010) and other patients may show bilateral frontal and temporal atrophy (Kipps et al., 2008; Burrell and Hodges, 2010). Patients with FTD may exhibit lack of insight, apathy, loss of appropriate emotional expression and stereotyped behaviour

or conversely they may demonstrate loss of social inhibitions such as impulsive or inappropriate behaviour including hyperorality, become overactive or fatuous. Patients may change their dietary habits or even religious or political beliefs from their pre-morbid state (Neary et al., 1998; Weder et al., 2007)

In patients with symptoms of apathy there is widespread frontal involvement extending to the dorsolateral frontal cortex, whilst patients with stereotyped behaviour show greater anterior temporal lobe atrophy with striatum involvement (Neary et al., 2005). Overall, patients with more behaviour change have greater right hemisphere atrophy (Neary et al., 2000a; Snowden et al., 2001; Neary et al., 2005; Weder et al., 2007)

1.2.2 Semantic dementia

Semantic Dementia (SD) is primarily a disorder of language dysfunction (Neary et al., 1998; Neary et al., 2005; Weder et al., 2007) but patients may also show behavioural changes in the course of disease similar to bvFTD. In particular SD sufferers have a tendency to become egocentric and develop habitual routines. Patients can speak fluently with appropriate grammar and pronunciation but seem to lose the ability to connect meaning of words to images, for example naming pictures.

They become unable to recognise the significance of faces, and matching pictures to words, in addition patients are often unaware of their language deterioration (Neary et al., 1998; Weder et al., 2007). Deficits in non-verbal tasks including auditory and visual tasks are also observed (Neary et al., 1998; Weder et al., 2007). Patients with SD have circumscribed atrophy of the temporal lobe with left hemisphere bias (Hodges et al., 1992; Sjogren and Andersen, 2006).

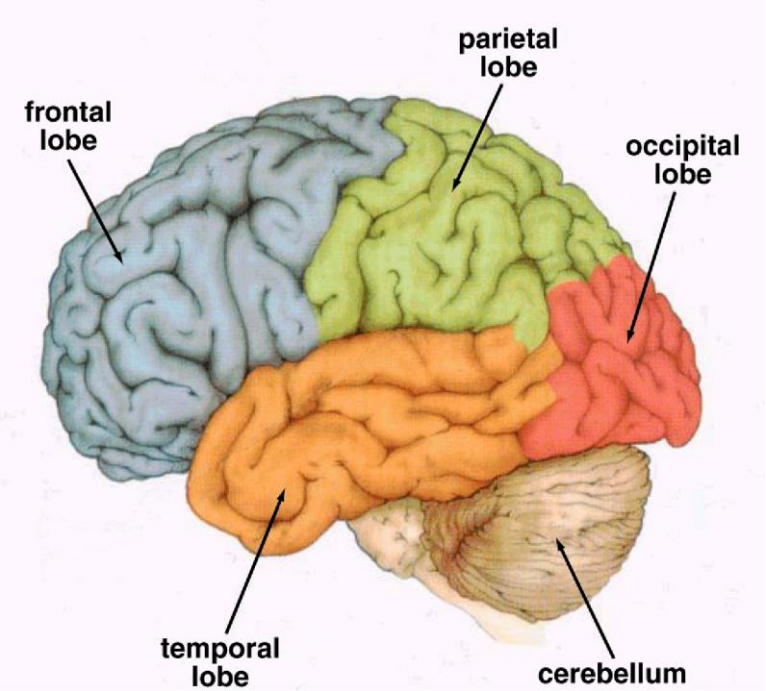

Figure 1.3 The four lobes of the brain.

Frontal lobe (blue), parietal lobe (green), occipital lobe (red) and temporal lobe (orange), the cerebellum is also indicated. Adapted from www.city.ac.uk/optometry/Biolabs/Brainlab/Brainlab.htm

1.2.3 Primary non-fluent aphasia

Progressive non fluent aphasia (PNFA) is a disorder of expressive language typified by characteristic economy of speech, dysnomia and loss of generative capacity (Neary et al., 2005). Patients with PNFA present with apraxia of speech with changes in fluency, pronunciation or have word finding difficulty and gradually become mute (Neary et al., 1993; Snowden and Neary, 1993; Neary et al., 1998; Neary et al., 2005; Weder et al., 2007). Object knowledge and single word comprehension are noted to be relatively preserved. Behavioural changes such as those identified with bvFTD are less common, however at the end stage of disease they may also show some behavioural changes. This form of FTLD is associated with asymmetric left hemisphere atrophy (Neary et al., 1993; Snowden and Neary, 1993; Neary et al., 1998; Neary et al., 2005; Weder et al., 2007).

1.3 FTD Clinical Variation

1.3.1 FTDP-17

FTDP-17 presents with classic clinical symptoms of FTD including behavioural and personality change with presenile dementia (Espay and Litvan, 2011). In addition FTDP-17 patients also co-exhibit symptoms of parkinsonism characterised by rigidity, bradykinesia and resting tremor. Parkinsonism symptoms have also been reported to be the presenting clinical feature in some cases (Fujioka and Wszolek, 2011). A number of mutations in tau and progranulin genes both on chromosome 17 have been identified in FTDP-17 families (Hutton et al., 1998; Cruts et al., 2005; Baba et al., 2007; van Swieten, 2007; Fujioka and Wszolek, 2011).

1.3.2 FTD-3

Clinical assessment has confirmed that all affected family members fulfil the clinical and pathological criteria for FTLD diagnosis (Neary et al., 1998; McKhann et al., 2001; Gydesen et al., 2002). FTD-3 is an insidious and progressive disease. The age of onset in this family ranges between 48 and 67 years (mean 57 years) with a duration of 3-21 years. Cognitive decline and personality change, associated with frontal lobe pathology, is often the first sign of disease onset and may present in a non-uniform manner. Individuals will either lose interest in their friends and family, becoming generally apathetic, or they may become aggressive compared to their pre-morbid state and lose their social inhibitions (Gydesen et al., 1987; Gydesen et al., 2002).

Stereotyped behaviour is often observed in FTD-3 and can present as part of personality change, typical presentations include disinhibition, inappropriate emotional response, lack of concern for others, lack of concern for self including unkempt appearance, and restlessness progressing to aggressive behaviour (Gydesen et al., 1987; Gydesen et al., 2002). For example, six months before

developing symptoms of cognitive decline case III-22 (figure 1.8) became irritable and was unable to manage daily grooming practices and domestic abilities. She also developed repetitive questioning and repeatedly bought certain food items that she did not use. Other patients have been noted to develop hyperorality (placing non-food objects in their mouth and excessive eating), which is associated with temporal lobe dysfunction. In addition all patients lack insight into their illness (Brown, 1998). Patients may also struggle with word finding that progresses to aphasia but not with classic features of PFNA or SD, eventually becoming mute (Gydesen et al., 2002). Early dyscalculia was identified in 8 and stereotyped behaviour in 11 of 22 affected FTD-3 family members (Isaacs et al., 2011).

Motor symptoms develop approximately 5 years after initial symptom onset (Gydesen et al., 1987). Patients demonstrate apraxia due to frontal cortex dysfunction and pyramidal symptoms with parkinsonian features and dystonia (Gydesen et al., 1987). In FTD-3 patients, abnormal posture of head and neck due to muscle spasm are also common, patients become incontinent and sudden spasms leading to jerking of arms (myoclonus) can occur (Gydesen et al., 1987). Interestingly, there are reports of some patients that develop arm dystonia in which they have one arm permanently extended (Gydesen et al., 1987; Gydesen et al., 2002). None of the affected family members show clinical signs of upper motor neuron (UMN) or lower motor neuron (LMN) impairment and to date there are no neurophysiological studies or EMG data available (Isaacs et al., 2011).

At end stage patients are unable to feed themselves and require round the clock care and may also develop problems in swallowing (Brown, 1998; Gydesen et al., 2002; Brown et al., 2004). Although patients demonstrate post morbid cognitive deficits as determined by the Queen Square Screening Test for Cognitive Deficits, day to day memory is maintained, thus categorically distinguishing FTD-3 from Alzheimer's disease (Brown, 1998).

The two half siblings from the additional branch of the family also demonstrated clinical symptoms consistent with the affected member of the FTD-3 family. Both show personality and behaviour change in their 50s including apathy, aggression and decline in speech with disease progression (Lindquist et al., 2008). The Belgian patient first showed signs of disease at 58 years of age including early onset progressive dysgraphia, mild disinhibition and aphasia, but delayed recall was preserved (van der Zee J. et al., 2008).

A screening study found *CHMP2B* missense mutations in approximately 10% of patients with progressive muscular atrophy (PMA) a form of MND affecting LMN (Cox et al., 2010), one missense mutation (N143S) is associated with CBD (van der Zee J. et al., 2008) and another missense mutation (D148Y) with semantic dementia (Skibinski et al., 2005). The pathogenicity of these missense mutations is currently unclear (Isaacs et al., 2011).

1.3.3 FTD-MND

The term motor neuron disease (MND) encompasses a group of neurodegenerative diseases with progressive motor neuron loss that are ultimately terminal. The most frequent clinical presentation of MND is Amyotropohic lateral sclerosis (ALS) with >75% of MND patients diagnosed with ALS (Ince et al., 1998; Lillo and Hodges, 2009). ALS is characterised by loss of both Lower Motor Neurons (LMN) in the anterior horn of the spinal cord and brain stem as well as the progressive loss of upper motor neurons (UMN) in layer V of the motor cortex. A second variant of MND is progressive muscular atrophy (PMA) in which only LMN degeneration occurs and has a clinically slower decline. Between 10-20% of MND cases are diagnosed with PMA (Lillo and Hodges, 2009).

In patients diagnosed with FTD, 5-25% of cases are preceded, accompanied, or followed by signs of MND (Peavy et al., 1992; Massman et al., 1996; Lomen-Hoerth et al., 2002; Rosso et al., 2003; Johnson et al., 2005; Seelaar et al., 2007; Lillo and Hodges, 2009; Lillo et al., 2010; Burrell et al., 2011).

The term frontotemporal dementia with motor neuron disease (FTD-MND) was used by the Lund and Manchester group to describe patients originally diagnosed with FTD exhibiting motor neuron symptoms (Lund and Manchester group 1994). In parallel ALS patients with cognitive impairment have also been classified as FTD-MND (Massman et al., 1996; Portet et al., 2001). In the face of mounting evidence it is now accepted that FTD and MND form a clinicopathological spectrum (Neary et al., 2000b; Lillo and Hodges, 2009; Lillo et al., 2010; Boeve, 2011; Simon-Sanchez et al., 2012).

1.4 Epidemiology

Population based studies have shown a wide range of estimates in the prevalence of FTD (Seelaar et al., 2011). In the first published FTD population study, the prevalence of FTD in Cambridgeshire UK was estimated to be 15 per 100,000 in 45-64 year old population (Ratnavalli et al., 2002). In a population of approximately 3000, 17 patients were identified with FTD of whom 11 were under the age of 65 years with a mean age of 52.8 years (Ratnavalli et al., 2002).

Another study investigating the prevalence of all causes of young onset dementia (before the age of 65 years) in the West London catchment area in the UK reported a comparable prevalence of 15.4 per 100,000 for FTD as a subgroup of all causes of dementia (Harvey et al., 2003). In this study 12% of all dementia cases fulfilled the Lund-Manchester diagnostic criteria for FTD (Harvey et al., 2003).

The prevalence of FTD in the Zuid-Holland province of the Netherlands was estimated to be much lower than the UK studies at 3.6 per 100,000 in 50-59 years age group, increasing to 9.4 per 100,000 in 60-69 years, and 3.8 per 100,000 in the 70-79 years age group (Rosso et al., 2003). For comparison with the Cambridge and West London studies the prevalence in 45-64 year age group was estimated to be 4 per 100,000 (Rosso et al., 2003; van Swieten, 2007). The lower prevalence reported in this study is likely to be due to study design. Whereas the Cambridge study included all cases of dementia in their defined population, the Dutch study only recruited referred cases (Seelaar et al., 2011).

In Rochester, Minnesota USA between 1990 and 1994 the incidence rate of FTD was estimated to be 2.2 per 100,000 per year in the 40-49 year age range, 3.3 per 100,000 in the 50-59 year age range, increasing to 8.9 new cases per year per 100,000 persons in the 60-69 age range (Knopman et al., 2004). The overall incidence rate was estimated to be 4.1 per 100,000 FTD cases per year in the 49-69 year age range (Knopman et al., 2004). The authors suggested that based on incidence and median survival calculations, the prevalence of FTD in this small group would be estimated to be 53.4 cases per 100,000 persons, significantly higher than other published reports (Knopman et al., 2004). This significantly higher calculated prevalence is likely to be because this study included dementia types other than FTD (Knopman et al., 2004).

A second study estimating the incidence of early onset dementias in the Cambridgeshire area served by Addenbrookes Hospital between 2000 and 2006 found a remarkably comparable incidence rate of 3.5 new cases per year per 100,000 persons in the 45-64 year age range (Mercy et al., 2008). Incident rates extrapolated from this analysis would suggest that 460 new FTD cases per year would be expected in the UK population aged 45-64 years of age (Mercy et al., 2008).

Mean age of onset of FTLD is variable but ranges between 45-65 years of age with mean age varying somewhere in the 5th decade in most studies. Age of onset in familial and sporadic cases is found to be comparable with slightly earlier age of onset associated with sporadic FTD (Ratnavalli et al., 2002; Rosso et al., 2003).

Although FTD is generally considered a presenile dementia 20-25% of FTD cases are over the age of 65 years (Ratnavalli et al., 2002; Johnson et al., 2005; Rabinovici and Miller, 2010). When screening individuals over the age of 85 years from Gothenburg Sweden, investigators estimated a prevalence of 3.1 in 100 in their cohort, a surprisingly high occurrence (Gislason et al., 2003; Seelaar et al., 2011).

Survival, age of onset and diagnoses vary greatly at different centres. Centres report median survival of approximately 4 years from diagnosis and around 6-11 years from symptom onset (Hodges et al., 2003; Kertesz, 2004; Rascovsky et al., 2005; Roberson et al., 2005). FTD-MND is associated with early mortality of less than 5 years, while in uncomplicated FTD, bvFTD has been associated with the shortest survival <9 years (Rabinovici and Miller, 2010).

Most studies report that FTD affects men and women equally (Knopman et al., 2004; Seelaar et al., 2011). However, the Cambridge study reported a striking 14:3 male to female ratio in their population (Ratnavalli et al., 2002). Further studies based on a breakdown of clinical syndrome data report a male preponderance in bvFTD and SD and a female preponderance in PFNA (Ratnavalli et al., 2002; Hodges et al., 2003; Johnson et al., 2005; Rascovsky et al., 2005; Rabinovici and Miller, 2010).

Variation amongst studies is likely to be due to differences in definitions used to diagnose patients, cohort size and post-mortem tissue available for confirmation of FTD, as well as genetic distribution of FTD across continents and countries.

1.5 Genetics

A positive family history is identified in 30-50% of FTD cases with at least one other family member being affected (Chow et al., 1999; Seelaar et al., 2008b). FTD-MND demonstrates the highest heritability, up to 60% in some studies (Stevens et al., 1998; Goldman et al., 2005; Seelaar et al., 2008a; Rohrer et al., 2009b; Seelaar et al., 2011).

In 10-27% of familial cases there is an autosomal dominant mode of inheritance (Stevens et al., 1998; Chow et al., 1999; Goldman et al., 2005; Seelaar et al., 2008a; Seelaar et al., 2008b). Mutations in the microtubule associated protein tau (*MAPT*) account for 5-20% of familial cases and progranulin (*GRN*) mutations account for 5-20% of familial cases and 1-5% of sporadic cases, while the recently identified C9orf72 expansion accounts for 21% of famililal FTD and 6% of sporadic cases in North American and European populations, (www.molgen.ua.ac.be/FTDMutations/, 2012; Gijselinck et al., 2008; Seelaar et al., 2011; Josephs et al., 2011; Ferrari et al., 2011; Rohrer et al., 2011b; Majounie et al., 2012; Rademakers et al., 2012).

Other genes with rare causative mutations in FTD include TAR-DNA binding protein 43 (*TDP-43*), fused in sarcoma (*FUS*), charged multivesicular protein 2B (*CHMP2B*), and valosin-containing protein (*VCP*) whose combined effect contribute to less than 5% of familial FTD cases (Seelaar et al., 2011; Ferrari et al., 2011)

1.5.1 CHMP2B

The presenile dementia in the Danish family is autosomal dominant with high penetrance. Linkage studies mapped the disease gene in affected family members to the pericentromeric region of chromosome 3 and subsequent haplotype analysis further reduced the critical area to a 15.5Mb region with 13 known genes on the long arm of chromosome 3 (figure 1.4) (Brown et al., 1995; Skibinski et al., 2005).

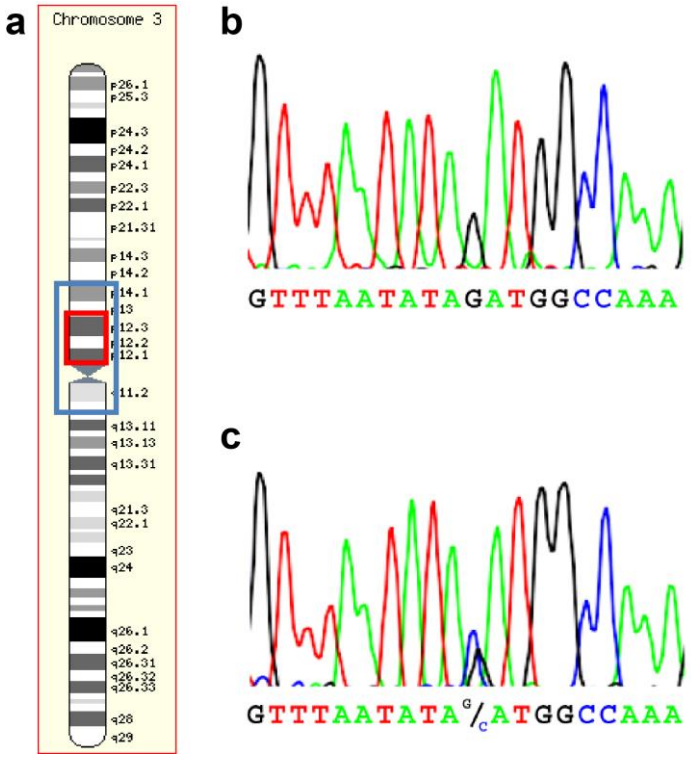

Figure 1.4 Pericentromeric region of chromosome 3 and electropherograms of mutation found in affected FTD3 family members.

a) pericentromeric region of chromosome 3 harbouring CHMP2B mutation. b) Unaffected pedigree members show a homozygous G at mutation site and c) heterozygote G/C splice site mutation in affected pedigree members.

Sequencing of candidate genes in the critical region uncovered only one mutation, a G>C transition in the splice acceptor site of exon 6 in the Charged Multivesicular Body Protein 2B (*CHMP2B*) (figure 1.4) (Skibinski et al., 2005). This mutation segregated in all affected members of the family and was absent in unaffected family members and 120 Centre d'Etude du Polymorphisme Humain (CEPH) control samples and 100 control samples from the Danish population (Skibinski et al., 2005).

RT-PCR amplification of *CHMP2B* from total RNA extracted from patient brain and lymphoblast cell lines revealed two novel splice variants absent in control samples. Sub-cloning and sequence analysis of the aberrant amplification products revealed that one transcript contains a 201bp intronic sequence between exon 5 and 6 ($CHMP2B^{Int5}$) (figure 1.5) resulting in a premature stop codon and a 36 amino acid

carboxy terminal truncation (figure 1.6) (Skibinski et al., 2005). The second transcript contains a 10bp deletion at the beginning of exon 6 due to the use of a cryptic splice site located 10bp from the 5' end of exon 6 ($CHMP2B^{\Delta 10}$) (figure 1.5). This frame shift mutation leads to the final 36 amino acids of CHMP2B being replaced with 29 nonsense-coding amino acids at the carboxy terminus (figure 1.6) (Skibinski et al., 2005). Both transcripts are present in brain tissue from affected family members $CHMP2B^{Int5}$ at ~35% and $CHMP2B^{\Delta 10}$ ~10% relative to the wild type transcript (Urwin et al., 2010b).

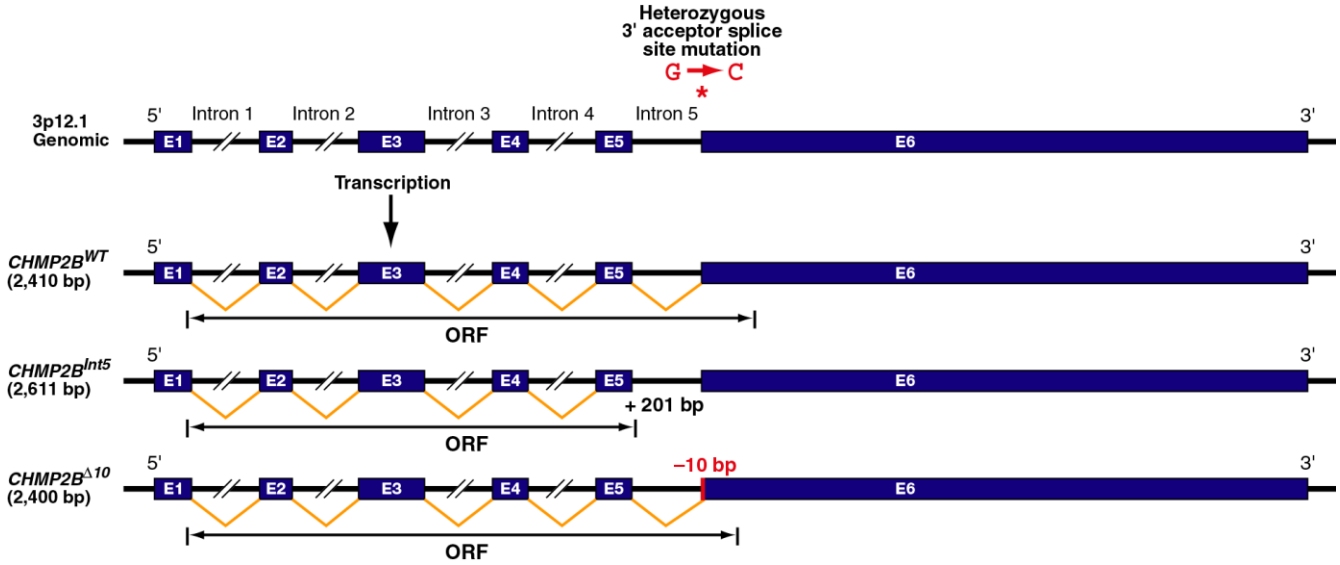

Figure 1.5 Pictorial representation of CHMP2B aberrant transcripts

G>C splice variant in genomic sequence (* in diagram) results in aberrant transcripts CHMP2B^{Int5} and CHMP2B$^{\Delta 10}$. CHMP2B^{Int5} includes the 201bp intron 5, which contains a premature stop codon leading to C-terminal truncation. CHMP2B$^{\Delta 10}$ results from a 10bp deletion at the beginning of exon 6 due to the use of a cryptic splice site causing a frameshift mutation leading to the final 36 amino acids of CHMP2B being replaced with 29 nonsense coding amino acids at the carboxy terminus.

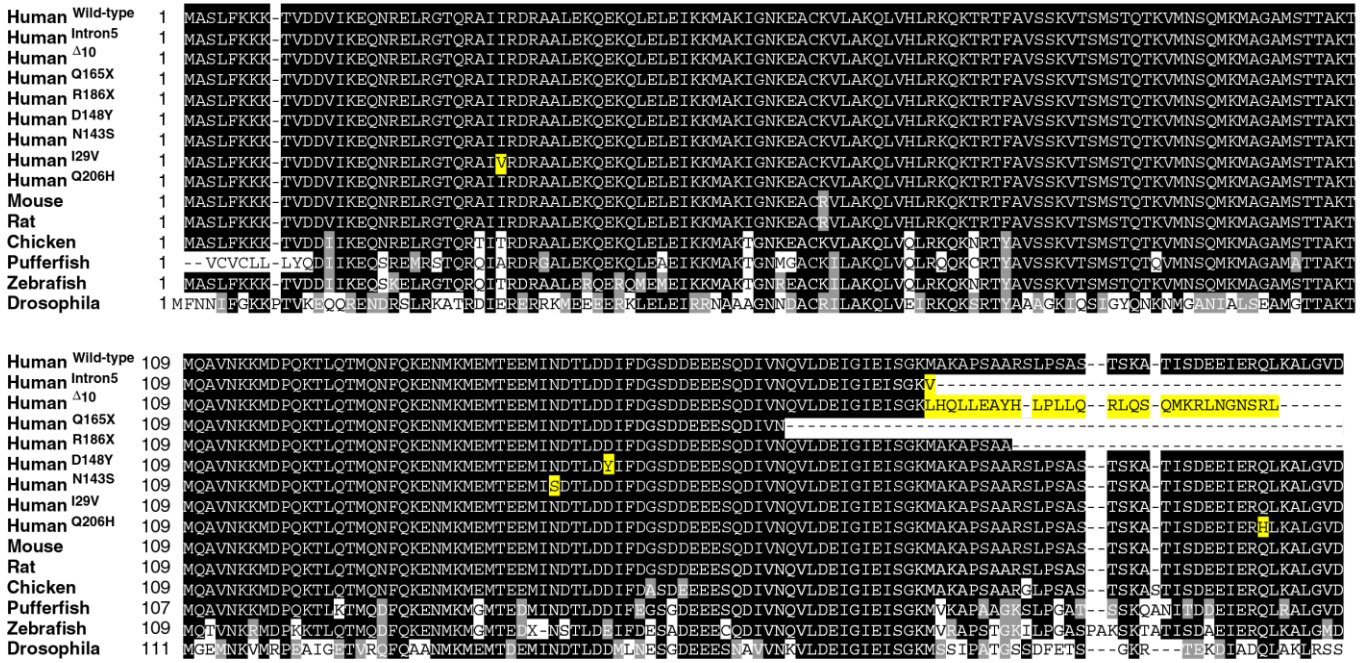

Figure 1.6 Multiple alignment of CHMP2B protein sequences

CHMP2B protein sequences from selected species and CHMP2B mutant protein sequences. Yellow highlight indicates identified coding mutations.

Since the identification of the gene responsible for FTD-3, several groups have screened other cases of FTD for CHMP2B mutation, (www.molgen.ua.ac.be/FTDMutations/, 2012). A C>T transition in exon 5 of CHMP2B was identified in a single familial Belgian FTD case from a group of Belgian patients tested (*N*=146) that was absent in control samples (van der Zee J. et al., 2006). This missense mutation (Q165X) is predicted to induce a premature stop codon resulting in a C-terminal truncation (van der Zee J. et al., 2006). In order to eliminate the possibility that the CHMP2B mutation may not be the true disease mutation, but hitchhiking on the real disease gene, sequencing of all open reading frames within the disease haplotype was carried out. No other unique variants were identified; this increases the likelihood that the splice site mutation reported underlies FTD-3 (Momeni et al., 2006a).

Other than the FTD-3 and Belgian mutations, several CHMP2B missense mutations of uncertain pathogenicity have been described. A G442T missense mutation resulting in a D148Y substitution in exon 5 was also reported in an unrelated individual with FTD that was absent in 100 control samples from CEPH in the original paper by Skibinski *et al* (2005 (Skibinski et al., 2005).

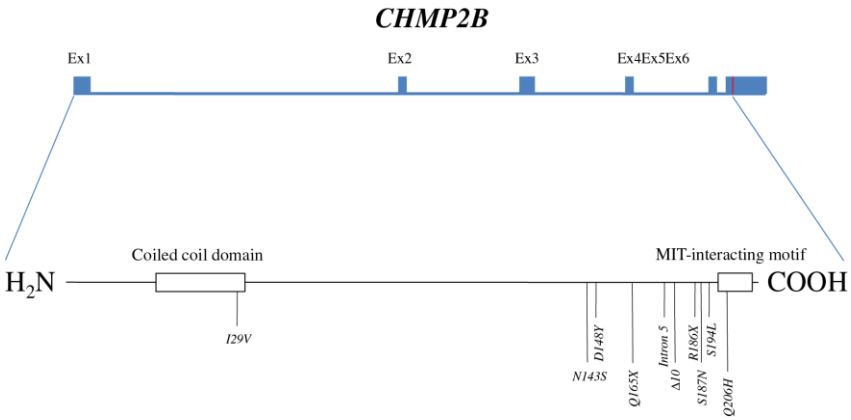

Figure 1.7 Clustering of CHMP2B mutations identified to date.

CHMP2B mutations clustering at C-terminal region of CHMP2B gene. Adapted from Ferarri *et al* (2011); (Ferrari et al., 2011)

CHMP2B missense mutations have been identified in a range of FTD-MND spectrum syndromes. These include the I29V mutation in the N-terminal coiled coil domain identified in a case of FTD-MND (Parkinson et al., 2006), a case of

FTD (Rizzu et al., 2006) and also in a single case with no clinical symptoms (Cannon et al., 2006). Other missense mutations are T104N and Q206H in two PMA cases (the I29V mutation was also identified in two PMA cases in the same study) (Cox et al., 2010) and N143S in a CBD case (van der Zee J. et al., 2008). Other missense mutations include S187N identified in a single case of FTD but also in an individual without neurological symptoms (Ghanim et al., 2010; Ferrari et al., 2011), S194L identified in a single case of FTD and not found in controls, T72M found in a familial FTD case, but not segregating with disease, indicating it is non-pathogenic, and R69Q identified in one control and no cases (Ghanim et al., 2010). It is interesting that mutations concomitant with clinical presentations of FTD-MND spectrum syndromes are predominantly (except I29V) clustered in the *CHMP2B* C-terminal region (figure 1.7) which houses the (microtubule interacting and transport (MIT))-interacting motif (MIM) (figure 1.7) (Williams and Urbe, 2007; Urwin et al., 2009; Ferrari et al., 2011). However, the pathogenicity of these missense mutations is currently unresolved. Of note is the chance finding of a C556T mutation in two middle-aged children of an affected man from a large six-generation Afrikaner family (Momeni et al., 2006b). This mutation changes codon 186 (CGA>TGA) of the *CHMP2B* sequence and is predicted to result in a C-terminal truncation (Momeni et al., 2006b). Although the authors report that the two middle aged children with this mutation are unaffected, expression of this mutation *in vitro* is reported to result in phenotype comparable to the FTD-3 *CHMP2B* mutation (van der Zee J. et al., 2008). It would be useful to obtain post-mortem analysis of these two Afrikaner individuals in due course as FTD-3 *CHMP2B* mutation has a wide age of symptomatic onset and the possibility remains that the Afrikaner individuals are yet to develop clinical presentation.

1.6 Neuropathology

The heterogeneous neurological disorders grouped under the umbrella of FTD share common gross and cellular pathology, with each subtype demonstrating particular distinguishing hallmarks (Neumann et al., 2009b).

Gross neuropathological changes observed in FTLD are predominantly atrophy of the frontal and temporal lobes (Snowden et al., 2002) with sparing of the posterior lobes; although other major anatomical brain regions are also affected. The hippocampus, basal ganglia (particularly the head of the caudate nucleus), and striatum show atrophy and enlargement of the ventricles is also observed (Graff-Radford and Woodruff, 2007). There is marked sparing of the posterior regions of the brain in early stages of the disease, but these regions ultimately become involved as disease progresses to late terminal stages (Broe et al., 2003).

There is considerable variation in cellular pathology across FTD syndromes (Broe et al., 2003). At the cellular level FTD syndromes share some common non-specific neurodegenerative pathology including neuronal loss, gliosis and inclusion bodies. In recent years identification of novel molecular inclusions unique to FTD subtypes has spurred the classification of FTLD pathology based on presumed molecular defects (Neumann et al., 2009b).

FTLD can be classified into four main groups based on the major proteins deposited in the brain: 1) FTLD-tau 2) FTLD-TDP and 3) FTLD-FUS and 4) FTLD-other which incorporates FTLD with no inclusions (ni) FTLD-ni and FTLD with inclusions from ubiquitin proteasome system (UPS)- FLTD-UPS (Mackenzie et al., 2009; Mackenzie et al., 2010; Seelaar et al., 2011; Josephs et al., 2011; Rohrer et al., 2011b). Pathological identity can be further sub-classified within each of these three groups based on inclusion morphology and distribution and tau isoform dominance. Greater than 99% of FTLD cases can be classified on the basis of specific protein deposition with only rare cases classified as FTLD-other <1% (Graff-Radford and Woodruff, 2007).

At post mortem FTD *tau pathology* accounts for ~40% of FTLD cases (Goedert et al., 1989; Knopman et al., 2004); FTLD with TDP pathology generally accounts for ~50% of cases (Josephs et al., 2004; Rohrer et al., 2011b) and FTLD-FUS accounts

for approximately 5-10% of FTD cases (Knopman et al., 2004; Lashley et al., 2011; Rohrer et al., 2011a).

1.6.1 FTLD-tau

The microtubule associated protein tau (MAPT) is a soluble phosphoprotein abundantly expressed both in the central and peripheral nervous system. Tau plays a fundamental role in maintaining neuronal integrity and axoplasmic transport by promoting microtubule (MT) assembly and stability (Goedert et al., 1989; Neumann et al., 2009b).

The accumulation of intraneuronal insoluble hyperphosphorylated tau deposits is one of the most common observations in FTLD accounting for ~40% of cases (Josephs et al., 2004; Taniguchi et al., 2004; Rohrer and Warren, 2011). This abnormal accumulation of tau is also a pathological characteristic in a number of other FTD clinical syndromes including progressive supranuclear palsy (PSP), corticobasal degeneration (CBD) and some cases of frontotemporal dementia and Parkinsonism linked to chromosome 17, collectively termed 'tauopathies' (Neumann et al., 2009b). Tauopathies may be further sub classified based on both phosphorylation and isoform composition; *i.e.* tauopathies can be allocated as disorders with inclusions composed predominantly of tau containing either 3 or 4 microtubule binding domain repeats (3R or 4R isoforms) (Mackenzie et al., 2009).

Tauopathies typically exhibit atrophy of both the frontal and temporal lobes (Pickering-Brown et al., 2004). This is associated microscopically with neuronal loss, astrocytosis, microvacuolation and swollen neurons together with a spectrum of tau protein specific pathology including intraneuronal neurofibrillary tangle-like inclusions and pretangles, intraneuronal Pick body inclusions, astrocyte tangle-like inclusions and dystrophic neurites (Taniguchi et al., 2004) as well as glial tangles and coiled bodies found in white matter (Seelaar *et al.,* 2010). Although there is considerable clinical and neuropathological overlap

between the FTLD-tau pathologies, each distinct type of tauopathy can be distinguished by the distribution, degree and morphology of tau inclusions (Spillantini et al., 1998; Goedert et al., 1998).

1.6.2 FTLD-TDP

In patients diagnosed with FTD, tau inclusions are not found in 50% of cases at post-mortem (Kertesz et al., 2000; Mackenzie and Rademakers, 2007). Instead, varying degrees of ubiquitin positive rounded intraneuronal inclusions are present originally termed FTLD with ubiquitin inclusions (FTLD-U) (Kertesz et al., 2000; Mackenzie and Rademakers, 2007). In 2006 Neumann and colleagues identified *Transactivation response* (TAR) *DNA binding protein with molecular weight 43kDa* (TDP-43/TARDTBP) as the ubiquitinated protein in the vast majority of FTLD-U cases (Neumann et al., 2006). Consequently cases of FTLD-U with TDP-43 positive staining were reassigned as FTLD-TDP (Mackenzie et al., 2009; Mackenzie et al., 2010; Mackenzie et al., 2011). Furthermore the previously recognised characteristic pattern of staining seen with ubiquitin antibodies could be recapitulated using TDP-43 immunohistochemistry (Sampathu et al., 2006; Mackenzie et al., 2006a). A harmonised classification system for FTLD with TDP-43 pathology has recently been established to supersede the original classification system described by Mackenzie and Sampathu for ubiquitin pathology (Mackenzie et al., 2011).

The harmonised classification system identifies four distinct patterns of pathology identified by TDP-43 antibodies (figure 1.8) (Mackenzie et al., 2011). Type A pathology is characterised by numerous short dystrophic neurites (DNs) and oval cytoplasmic inclusions concentrated in neocortical layer 2. A moderate number of lentiform neuronal intranuclear inclusions (NII) are also a common but inconsistent feature. Type B pathology is characterised by a moderate number of neuronal cytoplasmic inclusions (NCI) throughout all cortical layers, but with very few DNs. Type C pathology is characterised by a predominance of elongated DNs in upper cortical layers with very few NCI. Type D pathology

refers to inclusion body myopathy with Paget's disease of the bone and FTD (IBMPFD) characterised by numerous short DN and frequent lentiform NII. This pathological group is now referred to as FTLD-TDP (Mackenzie et al., 2011).

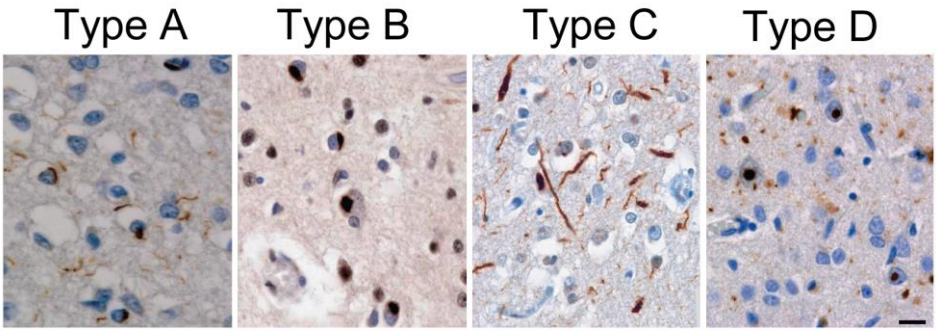

Figure 1.8 FTLP-TDP harmonised subtype classification.

FTLD-TDP pathology is heterogeneous with respect to the morphology and laminar distribution of pathological inclusions leading to the description of four distinct pathological subtypes classified as subytpes A-D in the harmonised classification system. Type A pathology; numerous short dystrophic neurites (DNs) and oval cytoplasmic inclusions concentrated in neocortical layer 2. A moderate number of lentiform neuronal intranuclear inclusions (NII) are also a common but inconsistent feature, clinical phenotype commonly bvFTD and PNFA. Type B pathology; a moderate number of neuronal cytoplasmic inclusions (NCI) throughout all cortical layers, but with very few DNs clinical phenotype commonly bvFTD and MND with FTD. Type C pathology; a predominance of elongated DNs in upper cortical layers with very few NCI, clinical phenotype commonly bvFTD and SD. Type D pathology refers to inclusion body myopathy with Paget's disease of the bone and FTD (IBMPFD) characterised by numerous short DN and frequent lentiform NII. Adopted from Neuman *et al.* 2009 (Neumann et al., 2009b)

1.6.2.1 FTLD-TDP Clinical and Genetic Associations

FTLD-TDP pathology has been identified in both sporadic and familial FTD cases with mutations in *GRN, VCP, TARDBP* and most recently *C9orf72* repeat expansion (Renton et al., 2011; Dejesus-Hernandez et al., 2011; Rademakers et al., 2012).

Several studies have looked at the relationship between FTD-TDP subtypes, FTD clinical syndromes- and the mutations in FTD-TDP associated genes *GRN, VCP, TARDBP* and *C9orf72*. The majority of FTD-TDP cases are linked to *GRN* and *C9orf72* repeat expansion. In one study of autosomal dominant families with clinical FTD and FTD-TDP pathology 53% were explained by *C9orf72* repeat

expansion and 47% with *GRN* mutations- this study did not identify sporadic cases (Hsiung et al., 2012a).

Although there is heterogeneous clinical presentation across FTD-TDP subtypes, an increasing body of evidence has shown that FTD-TDP B pathology is the result of *C9orf72* repeat expansion (Sampathu et al., 2006; Josephs et al., 2011; Mackenzie et al., 2011; Rohrer et al., 2011b; Simon-Sanchez et al., 2012; Hsiung et al., 2012b) accounting for the majority (80%) of FTD-MND clinical syndrome, approximately 30% of bvFTD and 10% each of SD and PNFA based on pooled data from a large clinicopathological study by Josephs and colleagues (Sampathu et al., 2006; Josephs et al., 2011; Mackenzie et al., 2011; Rohrer et al., 2011b; Simon-Sanchez et al., 2012; Hsiung et al., 2012b).

FTD-TDP A pathology is associated with *GRN* mutation, with bvFTD and PFNA as the main presenting clinical syndromes (van Swieten and Heutink, 2008; Rohrer and Warren, 2011; Mackenzie et al., 2011; Rohrer et al., 2011a). FTD-TDP C pathology is found in patients with clinical pretentions of SD and bvFTD (Rohrer 2011). FTD-TDP D is the least frequent of the FTD-TDP subtypes associated primarily with IBMPFD with *VCP* mutation (Forman et al., 2006; Rohrer and Warren, 2011; Mackenzie et al., 2011; Rohrer et al., 2011a).

1.6.3 FTLD-FUS

A number of FTLD cases with ubiquitin-positive inclusions (~10%) do not stain for either tau or TDP pathology (Roeber et al., 2008; Hatanpaa et al., 2008). *FUS* mutations were first reported in familial ALS cases characterised by tau and TDP-43 negative inclusions, but were found to be positive for FUS staining (Vance et al., 2009; Kwiatkowski et al., 2009). Consequently, FUS was found to be the characteristic protein marker in FTD cases negative for tau and TDP-43 (Roeber et al., 2008)

1.6.4 FTLD-Other

Less than 1% of cases remain that do not show immunoreactivity for any of the major FTD protein markers; tau, TDP-43 or FUS. The term FTLD with inclusions of the ubiquitin proteasome system (FTLD-UPS) is reserved for cases of FTD with ubiquitin and p62 positive inclusions which are negative for tau, TDP-43 and FUS. FTD caused by CHMP2B mutation, first identified in the FTD-3 family, is the major FTLD-UPS subtype (Skibinski et al., 2005; Cairns et al., 2007b; Holm et al., 2009; Urwin et al., 2010b).

Furthermore, a collaborative study identified two FTD cases that do not show immunoreactivity to tau, TDP-43, FUS or any ubiquitinated inclusions; that is there is no evidence of any known inclusions in these cases. These cases are classified as FTLD with no inclusions (FTLD-ni), previously termed Dementia Lacking Distinctive Histology (DLDH) (Mackenzie et al., 2006b; Mackenzie et al., 2010; Urwin et al., 2010b).

1.6.5 FTD-3 Neuropathology

Post-mortem and imaging studies of affected FTD-3 family members show gross global and central cortical atrophy consistently involving the frontal and temporal cortices (figure 1.9), the parietal lobe may also be affected but the cerebellum is spared (Brown, 1998; Gydesen et al., 2002; Holm et al., 2007). MRI and CT scans of *CHMP2B* mutation carriers reveal global as well as focal atrophy in pre-symptomatic individuals progressing to increasing generalised atrophy with advancing of disease (Gydesen et al., 2002; Eskildsen et al., 2009; Rohrer et al., 2009a)

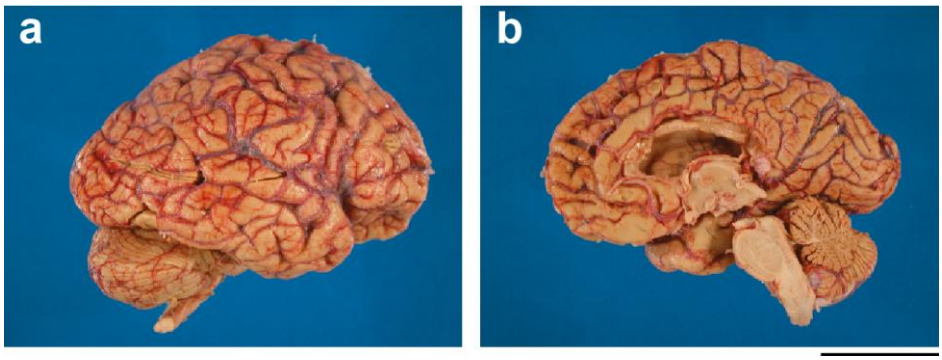

Figure 1.9 Case III-22 gross brain appearance.

Demonstrating cerebral atrophy of a) frontal and temporal cortex and b) dilatation of ventricle.Scale bar = 5 cm. Adopted from Holm *et al*. 2007;(Holm et al., 2007)

A study of recently deceased and archived post-mortem tissue from family members has provided new insights into the neuropathology of FTD-3 (Holm et al., 2007). Chronic neurodegenerative changes were confirmed including spongiosis, gliosis and astrocyte infiltration seen predominantly in layer II of the frontal cortex with involvement of the entire thickness of the cortex to some degree (figure 1.10) (Holm et al., 2007). Mild degeneration is present in the temporal cortex with the amygdala and hippocampus being spared with no hippocampal sclerosis (Holm et al., 2007). Loss of myelin was seen coupled with white matter changes complementing cortical degeneration in the presence of astrocytosis but in the absence of macrophages (Holm et al., 2007).

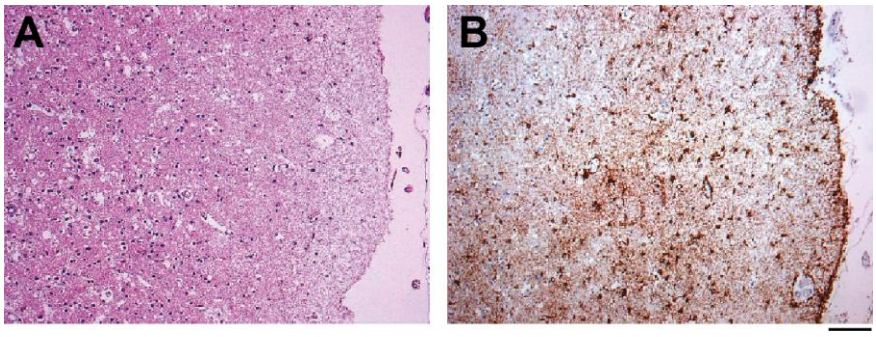

Figure 1.10 Gross neuropathology of FTD-3.

Haematoxylin and eosin (A) and glial fibrillary acidic protein (B) immunohistochemical staining of sections from frontal cortex of an FTD-3 patient. Pronounced microvacuolisation and gliosis are the most characteristic features. Scale bar = 50 µm. Adapted from Holm *et al*. 2007 (Holm et al., 2007).

Ubiquitin staining shows consistent pathology with characteristic ubiquitin immunoreactive (UB-IR) and p62 neuronal cytoplasmic inclusions (NCI) in the dentate granule cell layer of the hippocampus and to a lesser extent in the frontal cortex (Holm et al., 2007). The UB-IR NCI's are round, well defined and solid with only a few granular NCI seen occasionally. In layer II of the frontal and temporal cortex only sparse granular UB-IR NCI were seen. These UB-IR NCI's were absent from the striatum and lower motor neurons, none of the control tissue showed UB-IR NCI or NII (Holm et al., 2007).

Immunostaining for TDP-43 and FUS revealed that neither TDP-43 or FUS co-localise to UB-IR NCI's in FTD-3 patients (Holm et al., 2007; Holm et al., 2009). In contrast p62 inclusions of the same number, morphology and distribution are seen to co-localise to UB-IR NCI (figure 1.11) (Holm et al., 2007). In summary the distribution of UB-IR are cytoplasmic rather than nuclear or neuritic, they are found to be more abundant in the hippocampus and sparse in the cortical regions. Based on these histological findings FTD-3 previously classified as FTLD-U (Holm et al., 2007) has been reclassified under FTLD-other as an FTLD-UPS (Holm et al., 2007; Mackenzie et al., 2011).

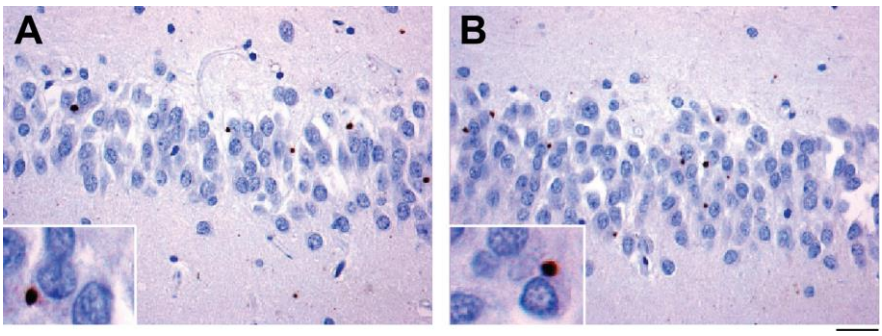

Figure 1.11 Ubiquitin and p62 positive inclusions in the dentate granule cell layer of FTD-3 patient brain.

Immunohistochemical staining for ubiquitin (A) and p62 (B) in the hippocampal dentate granule cells showing neuronal cytoplasmic inclusions (NCI). Scale bar = 25 μm. Adapted from Holm *et al*. (2007) (Holm et al., 2007).

More detailed analysis of FTD-3 pathology revealed the presence of enlarged vacuoles in neurons of the frontal, temporal and occipital cortex, but not in cerebellar neurons (Urwin et al., 2010a) consistent with the areas affected on imaging and neuropathology. These vacuoles are positive for mannose-6-phosphate receptor (M6PR) a marker of late endosomes, indicating enlarged aberrant late endosomes (Urwin et al., 2010a). Furthermore, fibroblast cell lines derived from patients' skin cells also demonstrate these distinctive aberrant endosomal vacuoles (Urwin et al., 2010a).

FTD-3 brains do not demonstrate abnormal aβ, α-synuclein, neurofilament or prion protein staining (Holm et al., 2007). Although some tau pathology has been observed in the frontal cortex of three FTD-3 brains, it is at insufficient levels for FTLD-tau diagnosis and is consistent with typical aging (Yancopoulou et al., 2003).

1.7 Endosomal Sorting Complex Required for Transport Proteins and Multivesicular Bodies

CHMP2B is a subunit of the Endosomal Sorting Complex Required for Transport (ESCRT) III. Four groups of ESCRT proteins have been identified: ESCRT 0, ESCRT I, ESCRT II and ESCRT III (Williams and Urbe, 2007). They are a group of multiprotein subunits that act sequentially to enable the recruitment, sorting and delivery of endocytosed transmembrane proteins into intraluminal vesicles of morphologically distinctive endosomes known as multivesicular bodies (MVBs) (figure 1.12). Early endosomes have tubulovesicular structures that constitute a major sorting platform and late endosomes have typical spherical characteristics and are able to fuse with lysosomes (Gruenberg and Stenmark, 2004). Transition from early to late endosomes is thought to occur via the inward budding and scission (pinching off) of the endosome limiting membrane to form intraluminal vesicles (ILV) and the degradation of internalised material via fusion and expulsion of material into lysosomes. ESCRT-III has been implicated in mediating the ILV scission event (Wollert et al., 2009). The lipid and protein composition

changes from early to late endosomes to fusion with lysosomes. The fusion of MVBs with lysosomes results in degradation of protein by lysosomal acidic hydrolases (Kobayashi et al., 2002; Gruenberg and Stenmark, 2004).

ESCRT proteins have been implicated in an array of other cellular functions that require membrane scission including cytokinesis, viral budding and autophagy (Hurley, 2010). It is beyond the scope of this study to discuss and do justice to each ESCRT function. This section will therefore focus on the role of CHMP2B and ESCRT-III in endosome-lysosome trafficking and autophagy and their relevance to neurodegeneration.

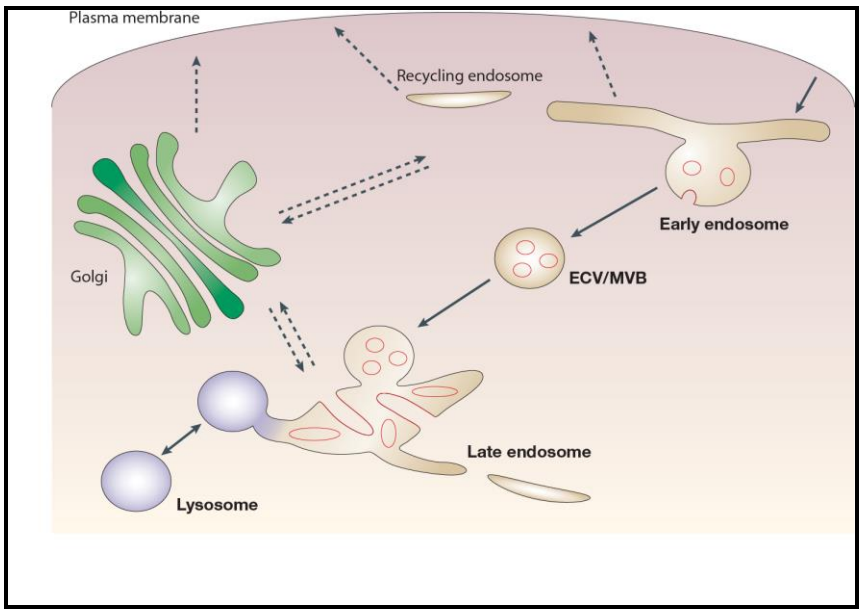

Figure 1.12 Biogenesis and recycling of endosomes from plasma membrane to lysosome.

ECV; endosomal carrier vesicles/MVB, multivesicular bodies Receptors and protein membranes are engulfed by early endosomes and consequently delivered to lysosomes for degradation via ECV/MVB. Adapted from Gruenberg *et al* (2004) (Gruenberg and Stenmark, 2004)

1.7.1 Human homologues of yeast ESCRT III proteins

ESCRT proteins were first identified in yeast reviewed by Hurley and Emr (2006 (Hurley and Emr, 2006). The human homologues of yeast ESCRT III proteins are the Charged Multivesicular body Proteins, also known as chromatin modifying proteins, (CHMP). To date 12 ESCRT III CHMP proteins have been identified in

humans and are subdivided into six groups based on the six yeast orthologous subunits and CHMP7 which has no yeast orthologue (Horii et al., 2006). CHMP1, CHMP2, CHMP3, CHMP4, CHMP6 and CHMP7 make up the core ESCRT III components, which are sufficient for membrane scission (Wollert and Hurley, 2010), and CHMP1 and CHMP5 are thought to play regulatory and peripheral roles (Babst et al., 2002; Horii et al., 2006; Hurley, 2010). The other ESCRT III subunits (which are not CHMP proteins) Did2, Ist1 and VPS60 assemble with the rest of the ESCRT III complex at a late stage (Nickerson et al., 2007; Hurley, 2010). CHMP1 and CHMP2 each have two isoforms, CHMP1A, CHMP1B and CHMP2A and CHMP2B respectively and CHMP4 has three isoforms, CHMP4A, CHMP4B and CHMP4C (Hurley, 2008; Hurley, 2010). The bulk of ESCRT III proteins are localised as monomeric subunits in the cytosol; they form a heteromeric ESCRT III complex when they are recruited to the endosomal membrane (Babst et al., 2002)

CHMP proteins are predicted to have similar protein structures composed of a highly polarised 5-helix core (Muziol et al., 2006). The first two N-terminal helices have a basic charge binding strongly to acidic membranes (Hurley, 2010). Helices 3-5 at the C-terminal region are acidic and have consistently been shown to autoinhibit assembly of the ESCRT III complex, by binding to the basic N-terminus, thus maintaining the complexes in a soluble monomeric state in the cytosol (Zamborlini et al., 2006; Shim et al., 2007; Lata et al., 2008). C-terminal truncation of subunits promotes complex assembly (Zamborlini et al., 2006; Shim et al., 2007).

Structural data has shown that ESCRT-III subunits contain a C-terminal MIT-interacting motif (MIM) which recruits MIT domain containing proteins such as the VPS4 AAA ATPase (Obita et al., 2007; Stuchell-Brereton et al., 2007). Release of ESCRT complexes from the membrane requires the ATPase activity of the VPS4 proteins and is the main thermodynamic driving force of the ESCRT cycle. VPS4 ATPase activity allows the ESCRT machinery to recycle through multiple rounds of vesicle formation and may also provide the energy necessary for protein

sorting and/or vesicle formation (Williams and Urbe, 2007). The disassembly of the membrane-bound ESCRT III complex is required to complete the ESCRT cycle and replenish the cytosolic pool of ESCRT III subunits (Hurley, 2010). ESCRT dysfunction is implicated in a number of human diseases including cancer, viral infection, in particular HIV infection, and neurodegeneration (Saksena et al., 2009). The focus of this study is the role of CHMPB in FTLD.

1.7.2 Mutant CHMP2B Causes dendritic spine and late endosome pathology

CHMP2B is a 213 amino acid protein containing a MIM domain at its C-terminal region (Skibinski et al., 2005; Hurley, 2010).

Studies of CHMP2B by *in situ* hybridisation in mouse brain show that it is expressed in all layers of the adult cerebral cortex, hippocampus and cerebellum (Skibinski et al., 2005). Belly and colleagues (2010) report that depletion of endogenous CHMP2B with shRNA led to a highly significant reduction in spine diameter per neuron (Belly et al., 2010). Spine classification reveals a 50% drop in the average proportion of spines with mushroom morphology. These observations were not associated with neuronal death but demonstrate that endogenous CHMP2B is necessary for healthy neuronal morphology (Belly et al., 2010).

Expressing mutant $CHMP2B^{Int5}$ in mature cortical neurons results in dramatic retraction of dendritic trees and 50% cell loss (Lee et al., 2007; Belly et al., 2010).

Confirmed familial pathogenic CHMP2B mutations identified to date (the Danish FTD-3 mutation and the Belgian Q165X mutation) result in C-terminal truncation of the wild type protein (figure 1.6). Over-expression of Danish mutant CHMP2B proteins, $CHMP2B^{Int5}$ and $CHMP2B^{\Delta 10}$ in various cell lines (PC12, COS-7, HEK-7, SK-N-SH, cortical neurons) produces enlarged endosomal structures (e.g. figure 1.13) that are positive for late endosome markers, while over-expression of $CHMP2B^{wt}$ in transfected cells show diffusely stained endosomes (Skibinski et al.,

2005; Filimonenko et al., 2007; Lee et al., 2007; Cox et al., 2010; Belly et al., 2010; Urwin et al., 2010a; Lee et al., 2011). Expression of the CHMP2B Belgian mutation $CHMP2B^{Q165X}$ (C-terminal truncation mutation) in a neuroblastoma cell line also results in large vesicular structures positive for late endosome markers CD63 (van der Zee J. et al., 2008).

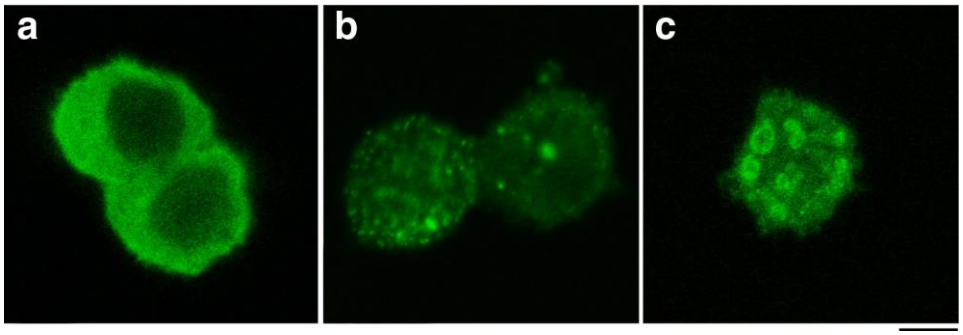

Figure 1.13 CHMP2B C-terminal truncations lead to enlarged endosomes.

PC12 cells transfected with a) $CHMP2B^{wt}$, b) $CHMP2B^{Int5}$, c) $CHMP2B^{\Delta 10}$ demonstrating aberrant endosomes adapted from Skibinksi *et al* (2005) (Skibinski et al., 2005)

Fibroblast cell lines derived from skin biopsies of Danish FTD-3 and Belgian mutation patients reveal enlarged late endosomal vesicles (Urwin et al., 2010a). With electron microscopy these structures were seen to be enlarged vacuoles with aberrant membrane deformation at the periphery or intraluminal vesicles (ILVs) which did not fill the lumen suggesting these enlarged structures may be dysmorphic MVBs (figure 1.14) (Urwin et al., 2010a).

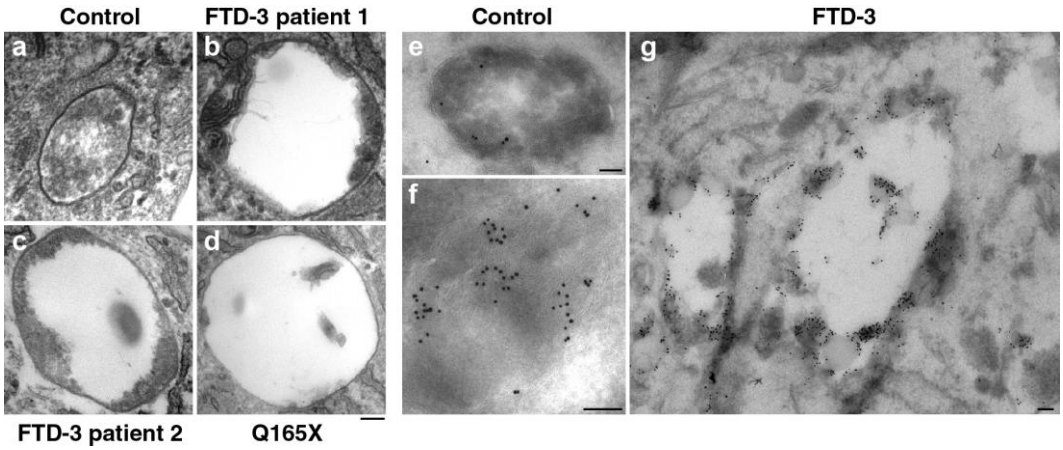

Figure 1.14 Enlarged aberrant endosomes in FTD-3 patient fibroblasts.

Mutant CHMP2B causes aberrant enlarged endosomes. FTD-3 and Control fibroblast EM; (a) Ultrastructural of unaffected patient fibroblasts (b and c) aberrantly formed multivesicular bodies (MVBs) identified in fibroblast cell lines from two FTD-3 patients and (d) in Q165X patient. FTD-3 patient MVBs are typically enlarged and showed unusual peripheral membrane deformation or sparsity of ILVs.. Aberrant structures are positive for CD63, which also surround normal MVBs and heavily surround lysosomes in (e) patient and control cell lines. (f) Normal MVB from a control cell line; normal lysosome from a control cell line; (g) abnormal compartments from an FTD-3 cell line. Anti-CD63, 10 nm gold. Scale bars =25 nm. Adopted from Urwin *et al* 2010; (Urwin et al., 2010a)

1.7.3 Mutant CHMP2B impairs the endosome-lysosome pathway

There is considerable evidence that mutant CHMP2B impairs delivery of cargoes from endosomes to lysosomes. CHMP2B^{Int5} alters intracellular sorting and degradation of endosomal cargo proteins such as glutamate receptor subunit NR1 and epidermal growth factor receptor (EGFR) (Lee et al., 2007). To address the question of whether CHMP2B mutations impair endosome-lysosome fusion or the earlier step of delivery of cargoes to ILVs, cells were treated with fluorescently labelled epidermal growth factor (EGF-488), as EGF has been shown to be delivered from endosomes to lysosomes in an ESCRT-dependent manner (Katzmann et al., 2002). Successful endosome-lysosome fusion was identified by co-localisation of the lysosomal marker LAMP-1 with EGF-488. This assay showed CHMP2B^{Int5} impaired endosome-lysosome fusion when expressed in human neuroblastoma cells, and the defect was confirmed in patient fibroblasts (Urwin et al., 2010a).

Impaired endosome-lysosome fusion may be the result of CHMP2B^{Int5} leading to impaired recruitment of other endosomal proteins. The recruitment of Rab7 is required for the successful fusion of endosomes to lysosomes. Both CHMP2B mutants CHMP2B^{Int5} and CHMP2B$^{\Delta 10}$, show at least a third reduction in recruitment of Rab7 onto endosomes compared with CHMP2B^{wt} suggesting this could be a potential mechanism explaining impairment of endosome-lysosome fusion (Urwin et al., 2010a).

1.7.4 Mutant CHMP2B impairs autophagy

Autophagy, literally meaning self-digestion, is an evolutionarily conserved highly regulated process responsible for the degradation of long lived proteins, organelles, misfolded proteins and aggregates that converges onto the MVB-lysosome pathway (Mizushima et al., 2008; Lee et al., 2009; Metcalf and Isaacs, 2010; Lee et al., 2011). LC3 is a widely used marker of autophagy, LC3-I is a 18kD cytosolic protein which, on autophagy induction, can be converted to LC3-II a 16kD lipidated protein that binds to autophagosomes. Therefore an increase in LC3-II staining indicates an increase in autophagosome formation and an increased LC3-I/LC3-II ratio is a good method of measuring cellular autophagy. The p62 protein is also a marker of autophagy and binds both LC3 and ubiquitinated aggregates enabling them to be degraded by autophagy (figure 1.15) (Filimonenko et al., 2007). Ubiquitin positive inclusions also positive for the autophagy marker p62 have been identified in FTD-3 patient tissue, suggesting that autophagy may be a likely neurodegenerative mechanism (Filimonenko et al., 2007; Lee et al., 2007; van der Zee J. et al., 2008; Lee et al., 2009; Metcalf and Isaacs, 2010; Urwin et al., 2010a).

An accumulation of GFP-LC3 positive autophagosomes are seen in cortical neurons expressing CHMP2B^{Int5} (Lee et al., 2007). Furthermore, HEK293 cells transfected with CHMP2B^{Int5} show accumulation of autophagosomes under EM and increased levels of LC3-II that could be prevented by application of an

autophagy inhibitor (Lee et al., 2007). Furthermore, expressing a dominant negative form of the VPS4 AAA ATPase involved in ESCRT III disassembly produces similar results with the accumulation of autophagosomes and LC3-II increase (Lee et al., 2007). These data suggest that mutant CHMP2B^{Int5} causes failure of ESCRT III to dissociate from endosomal membranes and the accumulation of enlarged aberrant autophagosomes likely due to their failure to fuse with lysosomes (Lee et al., 2007).

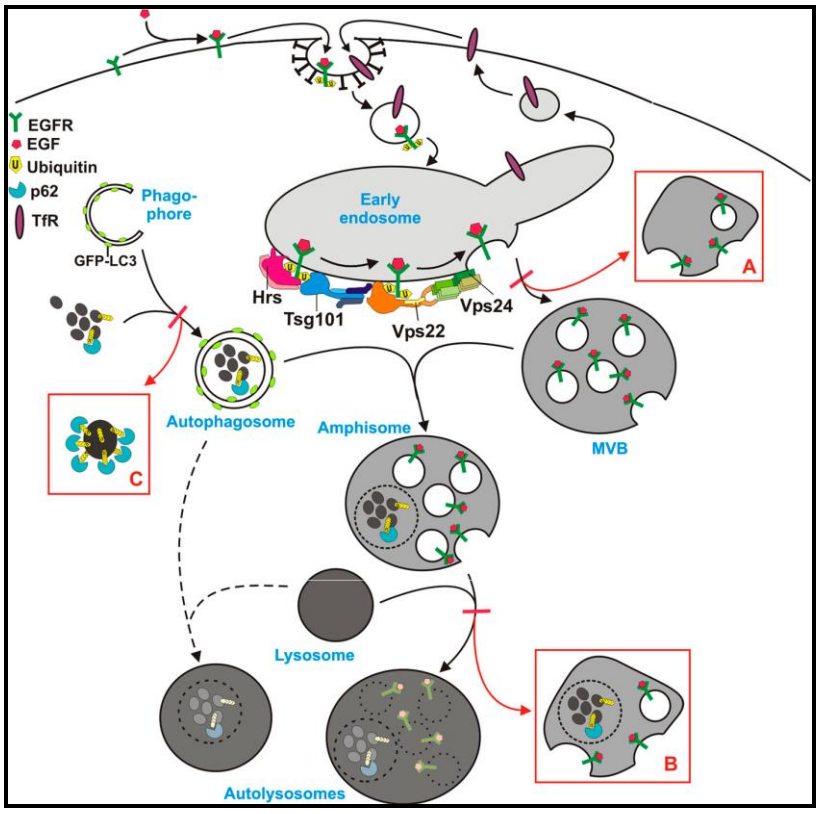

Figure 1.15 Diagrammatic representation of the autophagy pathway.

Autophagy degradation pathway in control and ESCRT-depleted cells. In control cells, internalised cytoplasmic cargo are sequestered by an isolation membrane (phagophore), forming double-membrane autophagosomes that can fuse with MVBs, forming amphisomes. Amphisomes, containing both endocytic and autophagic cargo, then fuse with lysosomes, forming autolysosomes, where the content is degraded. Autophagosomes may also fuse directly with lysosomes. The ESCRT complexes are required for correct sorting and degradation of ubiquitinated integral membrane proteins (e.g., EGFR) and for proper MVB morphology, and depletion of ESCRT subunits results in the formation of aberrant MVBs (red box A). Degradation of autophagic cargo is also inhibited in ESCRT- depleted cells, thought to be due to inhibited formation of autolysosomes (red box B), although autophagosomes and amphisomes are still formed. In addition, large p62 and ubiquitin-positive membrane-free aggregates accumulate in ESCRTdepleted cells (red box C), indicating that continuous autophagic clearance of cytoplasmic proteins is important to avoid accumulation of ubiquitin-positive aggregates that may cause neurodegeneration. Figure adapted from Filimonenko *et al* (2007) (Filimonenko et al., 2007)

Consistent with these findings depletion of ESCRT I (Tsg101) and ESCRT III (vps24) subunits or expression of CHMP2B^{Int5} in HeLa cells results in the accumulation of large ubiquitin, p62 and LC3 positive structures, indicating impaired autophagy (Filimonenko et al., 2007). Taken together, these data provide evidence that CHMP2B^{Int5} inhibits autophagic fusion and degradation leading to a build-up of autophagosomes as identified by increase of LC3 and accumulation of ubiquitin and p62 (Filimonenko et al., 2007; Lee et al., 2009)

1.8 Mouse Models of FTD

Since the identification of mutations in *MAPT*, *GRN* and TDP-43 responsible for a proportion of FTD-ALS spectrum of disease, numerous mouse models have been generated expressing disease mutations in the hope of shedding light on the pathogenesis and mechanism of disease as well as creating potential models for the development of therapeutic drugs (Lewis et al., 2000; Ramsden et al., 2005; SantaCruz et al., 2005; Deters et al., 2008; Gotz and Ittner, 2008; Wegorzewska et al., 2009; Yin et al., 2010a). With the identification of additional new mutations in novel genes such as the *C9orf72* expansion, more mouse models will undoubtedly continue to be generated. It is important to appreciate that no single mouse model recapitulates exactly the pathology and phenotype identified in human disease associated with a particular mutation; reviewed by Gotz and Ittner (2008) (Gotz and Ittner, 2008)

The CHMP2B protein in which mutations were originally identified in the Danish FTD-3 family appears to have different functions to other FTD disease proteins discussed in this chapter. CHMP2B belongs to the ESCRT group of proteins that are highly conserved across evolution in both function and structure (Hurley, 2010). With this in mind the literature review in this chapter will focus on mouse models of ESCRT subunits.

1.8.1 ESCRT subunit mouse models

In vitro cell culture models have been useful in helping to unravel the potential functions and dysfunction of CHMP proteins in the endosome-lysosome and autophagy pathways. Knockout mouse models of ESCRT subunits and autophagy genes largely support *in vitro* data (Hara et al., 2006; Komatsu et al., 2006; Shim et al., 2006; Lee et al., 2007). However, knocking out ESCRT III subunits does not produce viable mice (Shim et al., 2006; Lee et al., 2007).

To date few research articles have been published showing the effect of ESCRT III proteins *in vivo*. In 2006 Shim *et al*. published the first knockout mouse model of an ESCRT protein. They generated a null mutation in *CHMP5* (composed of eight small exons) by replacing exons 3-7 with a loxP-flanked neomycin resistant cassette using homologous recombination. They found that the resulting homozygous mice were embryonic lethal (E10). Compared to the wild type embryos and after E7.5 the CHMP5 null embryos demonstrated severe developmental abnormalities including abnormal neural tube formation (Shim et al., 2006). There were also severe abnormalities seen in the head fold and heart amongst other defects. Cultured primary embryonic cells showed the accumulation of late endosomal MVB compartments, thought to be due to failure in delivering internalised contents to lysosomes (Shim et al., 2006). A knockout mouse model of CHMP4B created by the random insertion of a β-geo cassette into the last intron of CHMP4B is embryonic lethal at E7.5-E8.5 although no further investigations were pursued on the embryonic tissues, cortical cell cultures did show failure of dendritic branching (Lee et al., 2007).

Hepatocyte growth factor-regulated tyrosine kinase substrate (Hrs) is part of the ESCRT 0 complex that recruits ubiquitinated receptors and proteins to endosomes and is essential for recruiting ESCRT I complex. Hrs is ubiquitously expressed in mouse brain with higher expression found in the hippocampus, cerebral cortex and hypothalamus. A greater degree of Hrs expression is observed in the hippocampal CA3 pyramidal neurons compared to the CA1 neurons (Tamai et al., 2008).

Tamai and colleagues (2008) used Cre-lox recombination to specifically delete Hrs in mouse neurons, leading to a 60% reduction of neuronal Hrs expression (Tamai et al., 2008). In contrast to the ESCRT III knock-out mice; these mice are viable at birth and no differences are noted from their wild type litter mates. At 5 weeks progressive accumulation of ubiquitinated proteins including aggregated AMPAR and NMDAR receptors as well as the autophagy associated protein p62 is seen, this is followed by progressive neuronal cell loss specifically in the pyramidal CA3 neurons of the hippocampus. Even though ubiquitinated aggregated proteins are seen in all brain regions viewed (substantia nigra, striatum, cerebellum and hypothalamus) cell loss is localised to CA3 pyramidal neurons while the CA1 hippocampal region is not affected (Tamai et al., 2008). The CA3 pryamidal cells are found to be positive for GFAP suggesting neuronal damage and several TUNEL positive cells are seen in the same region demonstrating apoptotic cell death (Tamai et al., 2008)

Hrs depleted mice also show growth retardation from 3 weeks, and distinct learning and locomotor impairments characteristic of a neurodegenerative phenotype (Tamai et al., 2008). In the open field test, they have significantly less vertical rearing activity compared to their wild type littermates, although this is not due to muscle weakness as no difference is found in the wire hanging test or footprint analysis of gait. In the forced swimming test, Hrs depleted mice also demonstrate significantly longer immobility duration (Tamai et al., 2008).

Tamai and colleagues (2008) suggest that depletion of Hrs impairs the endosome dependent degradative (autophagy) pathway as the mice develop progressive ubiquitinated protein aggregates with age, these include the p62 protein, and that the lack of LC3 staining may suggest that Hrs plays a crucial role in autophagosome maturation (Tamai et al., 2008). Certainly in these mice Hrs depletion has a significant and specific detrimental effect on CA3 pyramidal neurons. This may be because this particular neuronal population which normally has higher Hrs expression is particularly sensitive to Hrs depletion

perhaps because cargos critical for their survival are dependent on Hrs sorting and degradation (Tamai et al., 2007; Tamai et al., 2008).

It is also possible that when Hrs, which is the first step in the recruitment of ubiquitinated receptors and proteins to the ESCRT machinery is not available, a 'back log' of ubiquitin and ubiquitinated proteins builds up leading to a more global neurodegenerative mechanism. This notion is supported by data showing that in mice loss of autophagy genes *atg7* and *atg5* specifically in the CNS results in massive neuronal loss and accumulation of ubiquitinated protein aggregates in the cerebellar cortex and cerebellum (Hara et al., 2006; Komatsu et al., 2006). Furthermore, these mice too have significant locomotor deficiency and significantly reduced life span (Hara et al., 2006; Komatsu et al., 2006).

1.8.2 CHMP2B mouse models

Advances in genomic technologies have enabled a vast number of mouse models of many human diseases to be generated. This of course includes murine models that aim to replicate human neurodegenerative diseases of genetic aetiology. All the FTD-3 transgenic and knockout mouse lines described in this thesis were generated at the MRC Prion Unit facilities by the transgenic team as detailed in chapter 3 (*Chmp2b* knockout mice) and chapter 5 (CHMP2B transgenic mice).

1.9 Project Aims

The aims of this study have been to generate mouse models of FTD-3 which (1) have been depleted of endogenous mouse *Chmp2b* and (2) express mutant human *CHMP2B*^{Int5}, *CHMP2B*$^{\Delta 10}$ and wild type human CHMP2B isoforms. A further aim of this study has been to characterise these mouse models to gain a better understanding of the normal function of Chmp2b and to assess whether FTD-3 mutations are likely to cause disease by a loss of function or toxic gain of function mechanism.

2 MATERIALS AND METHODS

2.1 Equipment and Reagents

2.1.1 Equipment

7500 Real-Time PCR system (Applied Biosciences)

AnalySIS imaging software (Olympus).

Bench top centrifuge 5415R (Eppendorf)

Click boxes (Sanger Institute)

ColorView II digital camera (Soft Imaging System)

Compact X4 Xograph (Kodak)

Cryostat (Bright OTF 5000)

Electrophoresis tank (Invitrogen)

Eppendorf benchtop centrifuge

Gel Doc EQ UV-transilluminator (Bio-Rad)

Gilson Pipetman P1000, P200, P100, P50, P20, P5 (VWR)

Grip Strength Meter (Harvard Apparatus, 76007-BSRSIC)

Heating block (Eppendorf, thermomixer)

Hot plate (Fisher Scientific; Bibby HB502)

Kodak Biomax MMR film (VWR 103741)

Modified-SHIRPA equipment (made to order)

NanoDrop ND1000 Spectrophotometer & software (Labtech)

Nestlets 5x5 cm (Lillico Biotechnology)

Nexus staining apparatus (Ventana Medical Systems)

Plastic water downpipe (L 320mm x D 100mm; B&Q)

Power pack (Invitrogen)

Rotarod (Panlab, 760237)

Sony DCR-DVD 106 E digital camera

Tetrad 2 Peltier thermal cycler (BioRad)

Water bath (Grant)

Zeiss Axioplan microscope

2.1.2 Plastic and glassware

96 Well PCR Optical plates for PCR (Abgene; AB-0600)

Conical tubes 15ml (VWR 734-0451)

Conical tubes 50ml (VWR 734-0453)

Duran bottles (VWR, various sizes)

Eppendorf microtubes 0.5ml (VWR; 211-2140)

Eppendorf microtubes 1.5ml (VWR; 211-2130)

PCR microtubes for PCR (BioRad; TBC-0802)

RNAse free conical tubes 15ml (Ambion; AM2500)

RNAse free conical tubes 15ml (Ambion; AM2502)

RNAse free microfuge tubes 50ml (Promega; AM12300)

RNAse free microfuge tubes 50ml (Promega; AM12300)

TaqMan Real-Time PCR Plates (ABI; 4346906)

2.1.3 Commercial kits

Commercial kit	Company	Catalogue number
Human CHMP2B probe (5'FAM-3'TAM) (20 µM)	ABI	Made to order
Omniscript cDNA synthesis kit	Qiagen	205111
Quantitect RT PCR kit Including QuantiTect Probe PCR Master Mix, 100 ul UNG solution and RNase-Free Water	Qiagen	204343
RNeasy mini kit	Qiagen	74104
Rodent GAPDH RT-Kit including forward and reverse primers (20µM) and probe (VIC) (20µM)	ABI	4308313

Table 2.1 List of commercial kits

2.1.4 Antibodies

Primary Antibody	Species raised in	Dilution	Antigen retrieval method	Antibody incubation	Company	Catalogue number
Calbindin	Anti-rabbit	1:100	MCC1	42 °C 48 min	Millipore	AB1778
CHMP2B- 3371	Anti-rabbit	1:400	MCC1	RT 1h	Biogenes	Custom antibody
$CHMP2B^{WT}$ C-Terminal	Anti-rabbit	1:1000	MW+CB	37°C 1h	Abcam	Ab33174
EEA-1	Anti-rabbit	1:2000	MW+CB	37 °C 1h	Abcam	Ab2900
GFAP	Anti-rabbit	1:1000	PRT1	37°C 1h	DAKO	Z0334
IBA-1	Anti-rabbit	1:500	MCC1	RT 4h	Wako	016-20001
LAMP-1	Anti-rabbit	1:100	MW+CB	37 °C 1h	Abcam	Ab24170
LC-3	Anti-rabbit	1:100	MCC1	RT 4h	Novus Biological	NB100-2220
M6PR	Anti-rabbit	1:100	MW+EDTA	37 °C 1h	Cambridge Bioscience	MA-066
p62	Anti-guinea pig	1:400	MW+CB	RT 6h	Progen	GP62-C
Synaptophysin	Anti-rabbit	1:200	MW+EDTA	37 °C 44min	Invitrogen	080130
TDP-43	Anti-rabbit	1:2000	MW+CB	12h	Novus Biological	10782-2-AP
Ubiquitin	Anti-mouse	1:5000	MCC2	RT 4h	Santa Cruz	SC8017
Ubiquitin	Anti-rabbit	1:1000	MW+CB	37°C 1h	Dako	Z0458

Table 2.2 Primary antibodies used in immunohistochemistry protocols

Primary Antibody	Dilution	Company	Catalogue number
N-Terminal CHMP2B^{WT} 0762-B1	1:8000	21 Century Biochemicals	Custom antibody
N-terminal CHMP2B^{-}3335	1:2000	Biogenes	Custom antibody
LC-3	1:1000	Novus Biological	NB100-2220
Actin	1:10000	Sigma-Aldrich	A3853-200UL

Table 2.3 primary antibodies used in western blot protocols

Secondary Antibody	IHC Dilution	Western blot Dilution	Company	Catalogue number
Biotinylated anti-guinea pig	1:250	NA	Dako	P014102-2
Biotinylated anti-mouse	1:1000	NA	Dako	E043301-2
Biotinylated anti-rabbit	1:500	NA	Dako	E035301-2
Universal secondary antibody	Automated dosing	Not applicable	Ventana	760-4205
Anti-rabbit HRP	NA	1:2500	Jackson Immunoresearch	111035144
Anti-mouse HRP	NA	1:1000	Dako	P0260

Table 2.4 Secondary antibodies used in immunohistochemistry and western blot protocols

Ancillary products	Dilution	Company	Catalogue number
Antibody diluent	N/A	Ventana	251-018
Endogenous biotin blocking kit	Neat	Ventana	760-050
MCC1 (proprietary cell conditioning reagent)	Automated dosing	Ventana	950-124
Protease 3 (proprietary reagent)	Automated dosing	Ventana	760-2020
Universal DAB detection kit	Automated dosing	Ventana	760-500

Table 2.5 Ancillary reagents used in western blotting and immunohistochemistry

2.1.5 Reagents

Reagent	Company	Catalogue number
10mM ATP, 10mM GTP, 10mM TTP, 10mM CTP	Sigma	D7295
10x PCR buffer	Sigma	P2192
1kb Plus DNA ladder	Invitrogen	10787-018
1mol Acetic Acid	Sigma	34256-1L-R
25% EM grade gluteraldehyde	Agar Scientific	R1010
Agarose DNA pure grade	Sigma	443666A
Araldite CY212 resin	Agar Scientific	R1040
Cresyl Violet Acetate	Sigma	C5042-10G
DEPC treated water 1L	Ambion	102884
DePex	Sigma	361254D
Dimethyl Sulphoxide (DMSO)	Sigma	D9170
DirectPCR Ear	Viagen	402-E
Distilled water	Sigma	W1754
Ethanol	VWR	20821.321
Ethidium bromide 1% in dH_2O	Sigma	46067
Ficoll	Sgima	F4375-25G
Isopropanol	VWR	437423R
Laemmli sample buffer	Sigma	S3401
MegaMix Gold	Microzone	2MMG-5
Nupage 20x Transfer buffer	Invitrogen	NP00061
Nupage 4x LDS Sample buffer	Invitrogen	NP0007
Osmium tetraoxide	Agar Scientific	R1090
Phosphate buffer	VWR	E504-500ML
Proteinase K 500μg/ml	Sigma	P2308
Protein Precipitation solution	Promega	A7953
QIAzol	Qiagen	79306

Table 2.6 Commercially purchased reagents

Reagent	Company	Catalogue number
Random Hexamers	Promega	C118
RNA later solution	Qiagen	76106
RNAse zap	Ambion	AM9780
RNAse zap wipes	Ambion	AM9786
RNAsin Plus (2500U)	Promega	N2611
B-mercaptoethanol concentration (14.3M)	Sigma	M7522-100ML
SeaBlue Plus2 Pre-stained protein standard	Invitrogen	LC5929_46528852
Shandon Cryomatrix	Thermo-Shandon Ltd	SKU6769006
SuperSignal West Pico Chemiluminescent	Fisher Scientific	34080
Tris-Glycine Protein gradient gels 4-20%	Invitrogen	EC60252BOX-46528852

Table 2.6 continued commercially purchased reagents

2.1.6 Prepared solutions

1% Acidified Cresyl violet solution

Cresyl violet	1 g
Distilled water	100 ml

Add 10 drops (or 0.3 ml) of acetic acid and filter

10mM Tris-EDTA pH 8.0

1M Tris-HCl (VWR)	500µl
0.1M EDTA (Sigma)	2.5µl
dH_2O	make to 500ml

Concentrated HCl to buffer to pH8.0

Digestion Buffer

1M Tris-HCl (VWR)	50ml
0.5M EDTA (Sigma)	200ml
5M NaCl	20ml
dH_2O	make to 1L

Concentrated HCl to buffer to pH8.0

Autoclave

0.5M TAE buffer (50x concentrate)

Tris-HCl	242g
Glacial Acetic Acid	57.1ml
0.5M EDTA	100ml
Deionised H_2O	make to 1L

0.1M Citrate Buffer pH6

0.1M Solution A: 21.14g citric acid monohydrate

0.1M Solution B: 29.41g trisodium citrate dehydrate

For 1L of pH6 citrate buffer add 11.5ml of 0.1M solution A to 88.5ml of solution B. Make up to 1L using deionised water

10x Tris-EDTA pH7.8

EDTA	5g
Tris-Base	2.5g
Tri-sodium citrate	3.2g
Deionised H_2O	make to 1L

1.5% Agarose Gel

Agarose DNA pure grade	7.5g
TAE	500ml
Ethidium bromide [1% in dH_2O]	10µl

Orange G (azo dye)

1M Tris HCl pH 7.8	500µl
0.5M EDTA	100µl
Ficoll	10g
Sterile distilled H_2O	25ml
Mix then add:	
Orange G (added last)	50mg
Sterile distilled H_2O	made up to 100ml

Solution is heated and gently stirred on a heating block until dissolved and topped up to 50ml with sterile H_2O.

2.2 Mouse Strains

2.2.1 *CHMP2B* transgenic mouse colony

The generation of *CHMP2B* transgenic mice up to and including the surgical implantation of two-cell eggs into the oviducts of pseudopregnant mice was performed by the MRC Prion unit transgenic team under the direction of EA. *CHMP2B* transgenic mouse colonies were generated on a CBAxC57BL/6J mixed genetic background as described in section 5.1.

2.2.2 *Chmp2b* knockout mouse colony

Chmp2b knockout mice were generated from commercially purchased frozen embryos harbouring the pGT0lxf gene trap within intron 2 of mouse *Chmp2b* gene Frozen embryos. Resusitation and surgical implantation of embryos was performed by the MRC Prion unit transgenic team under the direction of EA *Chmp2b* knockout colony was generated on a 129P2/OlaHsd xC57BL/6J mixed genetic background as described in section 3.2. The official nomenclature for these gene trap mice is $Chmp2b^{Gt(XL952)Byg}$. However, for simplicity and ease of reference, the terminology knockout ($Chmp2b^{-/-}$) is used throughout this thesis, while recognising that complete knockout of the *Chmp2b* gene was not achieved by this approach, as described in Chapter 3.

2.3 Animal Husbandry and Ethical Approval

Ethical approval was granted by Local Ethical Committee and all personnel involved in animal experimentation obtained appropriate training and Home Office licences. Mice were housed in Sealsafe®1284 IVC cages [overall Dimensions L 365x W 207x H 140 mm; floor area: 530 cm^2] (Tecniplast; 1284L) containing high quality, dust free Aspen wood wool bedding (Lillico; Aspen) and 1 inner cardboard from toilet roll for environmental enrichment at the MRC Prion Unit's Biological Services Facility with a 12 hour light-dark cycle. Mice were fed a diet of RM1 [wheat, barley, wheat feed, de-hulled extracted toasted soya, soya protein concentrate, macro minerals, soya oil, whey powder, amino acids,

vitamins, micro minerals] 9.5mm pellets for stock mice and RM3 [wheat, wheatfeed, de-hulled extracted toasted soya, barley, macro minerals, yeast, dextrose monohydrate, potato protein, hydrolised wheat gluten, full fat soya, soya oil, maize gluten meal, amino acids, vitamins, micro minerals] 9.5 mm pellets for breeding animals (Special Diet Services; RM1-P catalogue number 801010 and RM3-P catalogue number 801030 respectively).

2.4 Molecular Methods

2.4.1 Primer design

Sequences for designing primers for screening *Chmp2b* knockout, CHMP2B transgenic and wild type mice were obtained from NCBI (http://www.ncbi.nlm.nih.gov/) and BayGenomics (BayGenomics, 2012) websites. Primers for quantitative PCR and genotyping were designed using the program Primer 3 (http://frodo.wi.mit.edu/cgi-bin/primer3/primer3). Primer sequences are listed in table 2.1.

2.4.1.1 Primer sequences

Primer	Application	Sequence
SalF	*CHMP2B* transgenic PCR	5'ATTGTCGACACCATGGCGTCCCTCTTCAAG AAG-3
F19105	*CHMP2B* transgenic PCR & RT-PCR	5'-CACCTCTAAAAGAGCTACGGTGG-3'
XhoR1	*CHMP2B* transgenic RT-PCR	5'ATCTCGAGCTAATCTACTCCTAAAGCCTTGA G-3'
Int2_F	*Chmp2b* knockout PCR	5'CCATTGCCACTTGGATGTAA-3'
Int2_485R	*Chmp2b* knockout PCR	5'GACGCACTTTAAGGTCACAGC-3'
KO_386R	*Chmp2b* knockout PCR	5'CCATTGCCACTTGGATGTAA-3'
HCHMP2B_F	TaqMan PCR	5'-AAAGCTCCATCAGCTGCTC-3'
HCHMP2B_R	TaqMan PCR	5'-TCCTAAAGCCTTGAGTTGC-3'
GAPDH	TaqMan PCR	Commercially purchased (ABI; 4308313)

Table 2.7 Table of primer sequences.

List of primer sequences used in PCR and TaqMan RT-PCR amplification

2.4.2 Tissue digestion and DNA extraction

Tailor biopsies ear punches were taken from mice at weaning and were retained for DNA extraction. Tail biopsies (0.5 cm) were taken from weaned pups by applying local anaesthetic (EMLA®) to the tip of the tail before being biopsied using mouse tail guillotine. Both ear and tail samples were stored at -20°C until required.

Samples were digested using 20µl proteinase K enzyme (500µg/ml) and 480ml digestion buffer and incubated in a water bath at 55°C overnight (~16h). The next day the samples were removed from the water bath and briefly vortexed; 160µl of protein precipitation buffer was added to the digested samples. The samples were vortexed again for 10 minutes and incubated on ice for 6 minutes, followed by centrifugation at 13000 rpm for 5 min at room temperature. DNA extraction using isopropanol was applied to both tail and ear tissue digests as follows:

The supernatant from the digested samples was transferred to new labelled tubes and 500µl of isopropanol was added. The protein pellets were discarded. The samples were shaken for 20 seconds and spun again for 5 minutes at 13000 rpm at room temperature. The supernatant was discarded and the tubes with DNA pellets placed upside down on absorbent blue sheet to drain excess ethanol (~2 minutes).

The DNA pellets were washed with 200µl of 70% ethanol and spun for 5 min at 13000 rpm at room temperature. A 200µl Gilson pipette tip was used to aspirate the residual 70% ethanol, with a fresh yellow tip being used per sample to avoid cross-contamination. DNA pellets were allowed to air dry for ~20 minutes. The DNA pellets were re-suspended in 10mM Tris-EDTA pH8.0. DNA samples were used for genotyping and real-time PCR analysis. Samples were stored at 4°C in the short term or archived at minus 80°C for long term storage. In some cases the crude ear digest was used directly in PCR.

2.4.3 RNA extraction and reverse transcription-PCR

RNA Extraction:

Commercially available RNeasy mini kits (Qiagen) were used to extract total RNA from RNA Later® (Qiagen) stabilised or snap frozen tissue. The only deviation from the kit instructions was to use Qiazol (Qiagen) extraction buffer according to manufacturer's instructions in place of RNeasy mini kit RDD extraction buffer. The RNA concentration was measured using NanoDrop ND1000 Spectrophotometer (Labtech).

Reverse transcription-PCR:

The master mix for cDNA synthesis was prepared as follows: 2μl each of 5mM dNTP mix, 10x buffer from Omniscript cDNA synthesis kit (Qiagen) and random hexamers (Promega) plus 0.25μl RNasin (Promega) RNAse inhibitor, 1μl Omniscript enzyme and 2.75μl RNAse-free water both from Omniscript cDNA synthesis kit (Qiagen). For first strand cDNA synthesis RNA extracted using RNeasy mini kit was diluted to 0.1μg/μl using RNAse-free water. For each reaction 10μl of cDNA synthesis master mix and 10ul of RNA (0.1μg/μl) were incubated for 10 minutes at room temperature (21°C), followed by 1 hour incubation at 37°C for cDNA synthesis to occur and finally 10 minutes at 70°C to inactivate enzymes.

The single stranded cDNA (5ul) was used as template for PCR using 0.5 μl of 10μM each of CHMP2B specific primers, F19105 forward primer and XhoR1 reverse primer (table 2.7), 15μl of PCR master mix and 4μl of PCR water in a total reaction volume of 25ul. The same thermal cycling programme and DNA gel electrophoresis methods were applied as described for CHMP2B transgenic PCR (table 2.9).

2.4.4 DNA amplification by PCR

DNA sequences of interest were amplified using crude ear digest or genomic DNA extracted from tail biopsies or ear punches in PCR to genotype either the

Chmp2b knockout line or CHMP2B transgenic lines. All PCRs were carried out in either 96 well plates or PCR microtubes.

2.4.4.1 *Chmp2b* knockout multiplex-PCR

The *Chmp2b* knockout multiplex PCR master mix was prepared as follows: 6.25µl of MegaMix gold (Microzone), 1µl of forward primer (5µM Int2_F), 0.5µl of reverse primer designed against *Chmp2b* knockout genetrap sequence (5µM KO_386R), 0.5µl of reverse primer targeting *Chmp2b* intron 2 sequence (5µM Int2_485R) and 4.25µl sterile water (Sigma) were mixed in an Eppendorf tube on ice for each sample. 0.5µl of genomic DNA (0.5-100ng/µl) extracted with isopropanol or crude ear lysis was added.

Thermal cycling conditions on Tetrad 2 Peltier thermal cyclers (BioRad) used for the amplification of *Chmp2b* knockout and wild type sequences were as detailed in table below (table 2.8). PCR products were analysed using agarose gel electrophoresis as described below.

Temperature (°C)	Time	PCR function (35 cycles)
94	5 minutes	Initialisation
94	30 seconds	Denaturation
55	45 second	Annealing
72	45 seconds	Elongation
72	7 minutes	Final elongation

Table 2.8 *Chmp2b* knockout PCR conditions

2.4.4.2 CHMP2B transgenic PCR

One common PCR recipe was used to amplify transgenic sequences for *CHMP2B*^{WT} and both the mutant *CHMP2B*^{Int5} and *CHMP2B*$^{\Delta 10}$ sequences.

The transgenic PCR master reaction mixture was prepared as follows: 2.5μl of 10x PCR Buffer (Sigma), 2μl of 1.25Mm dNTPs, 1.25μl DMSO, 0.25μl of 20μM SalF forward primer, 0.25μl of 20μM F1905 reverse primer and 18.25μl sterile water (Sigma) with 0.5μl of Taq polymerase enzyme (Sigma) were mixed in an Eppendorf tube on ice for each sample.

For PCR using genomic DNA extracted from tail or ear biopsies 24.5μl of transgenic PCR master mix was used with 0.5μl DNA (0.5-300ng/μl). For PCR using crude ear lysate 23μl of transgenic PCR master mix was used with 2μl of ear lysate (DNA estimated at 80-200ng/μl).

Thermal cycling conditions on Tetrad 2 Peltier thermal cyclers (BioRad) used for the amplification of human *CHMP2B*^{WT}, *CHMP2B*^{int5} and *CHMP2B*$^{\Delta 10}$ sequences detailed in table 2.9. PCR products were analysed using agarose gel electrophoresis as described below.

Temperature (°C)	Time	PCR function (30 cycles)
94	5 minutes	Initialisation
94	30 seconds	Denaturation
55	30 second	Annealing
72	50 seconds	Elongation
72	7 minutes	Final elongation

Table 2.9 *CHMP2B* transgenic PCR conditions

2.4.4.3 Gel Electrophoresis

Agarose gel (1.5%) for DNA gel electrophoresis was made by dissolving 7.5mg of Ultra-Pure Agarose (Invitrogen) in 500 of 1x TAE (Invitrogen) on stirring hotplate (VWR). Once dissolved, 10 µl of 1% ethidium bromide (0.1µg/ml) (Sigma) was added to the cooled solution. The dissolved liquid gel was set in an agarose gel tray assembled with a loading well gel comb. PCR products (10-15µl) and 1kb HotStarTaq DNA ladder (15µl) (Invitrogen) were loaded into wells and a current of 120V was passed through the agarose gel for 30-45 minutes. The resolved DNA bands were visualised on a Gel Doc EQ UV-transilluminator (Bio-Rad) and a record was printed out using a video printer (Bio-Rad). PCR product size was estimated against standard commercially available 1Kb DNA marker.

2.4.5 Real-time PCR (TaqMan®) assay

DNA samples extracted from tail biopsies were diluted 1/30 and DNA from ear samples similarly extracted were diluted 1/10 using distilled water (Sigma).

PCR master mix for the Real-Time TaqMan assay was prepared as follows: To 12.5µl of QuantiTect Mix (Qiagen), which contains reaction buffer, dNTPs, HotStarTaq DNA polymerase and ROX dye (normalises fluorescent signals on ABI

systems), 0.5µl of 10µM human specific CHMP2B sequence forward primer (hCHMP2B_F), 0.5µl 10µM human sequence specific CHMP2B reverse primer (hCHMP2B_R), 0.5µl 10µM of CHMP2B human specific primer fluorescent reporter (FAM) probe, 0.25µl of each of commercially available 20µM rodent GAPDH forward and reverse primers (ABI), 0.25µl of rodent 20µM GAPDH fluorescent reporter (VIC) probe and1.25µl of distilled water (Sigma) was added per sample.

For each test sample 16ul of master mix was added to Real-Time PCR optical 96-well plates together with 9µl of DNA (25µl total volume per well). DNA samples were exponentially amplified using the programme detailed in table 2.10 on 7500 Fast Real-Time PCR system (Applied Biosciences). Potential homozygous mice were identified using the comparative Ct method described in section 2.4.5.1.

Temperature (°C)	Time
94	15 minutes
94	15 second (40 repeats)
60	60 seconds (40 repeats)
72	7 minutes

Table 2.10 TaqMan PCR conditions

2.4.5.1 delta Ct method

Cyle threshold (Ct) is a measure of the cycle number at which the fluorescence of a particular sample crosses a threshold set for all samples in the batch. The comparative Ct method involves comparing the Ct values of the samples of interest with a control or calibrator such as a non-treated sample that is used as an internal standard. The Ct values of both the control and the samples of interest are normalized to an appropriate endogenous housekeeping gene. The housekeeping gene is selected on the basis that it is not expected to be affected by the experimental treatment. In this study, the known hemizygote is the control sample and GAPDH is used as the endogenous housekeeping or reference gene.

Standard curves were set up for each of the transgenic lines using Real-Time PCR method described above with the exception that the DNA used was from a known hemizygous offspring from a first generation mating. The DNA concentration was determined using a NanoDrop ND1000 Spectrophotometer (Labtech) and diluted to a concentration of 250ng DNA per 9µl volume (27.7ng/ul). 250ng is the highest concentration point in the standard curve. Further concentrations were achieved by diluting the 250ng sample 1:2

sequentially so that the range of the standard curve per 9µl volume was as follows 250.0ng, 125.0ng, 62.5ng, 31.3ng, 15.6ng, 7.8ng and 3.9ng.

Amplification plot and Ct values were taken from 7500 Fast-System software, an example of the concentration curves obtained for Tg158 is given (figure 2.1). Cycle threshold (Ct) values from this graph were used to determine a log-linear graph for CHMP2B (figure 2.2a) and GAPDH (figure 2.2b) by plotting the log of standard concentrations against the mean cycle threshold (mean Ct). The R^2 values of CHMP2B (0.9964) and GAPDH (0.9991) demonstrate a highly significant correlation between Log concentration and mean Ct. and the slope values indicate GAPDH and CHMP2B are amplified with very similar efficiency (figures 2.2a and 2.2b).

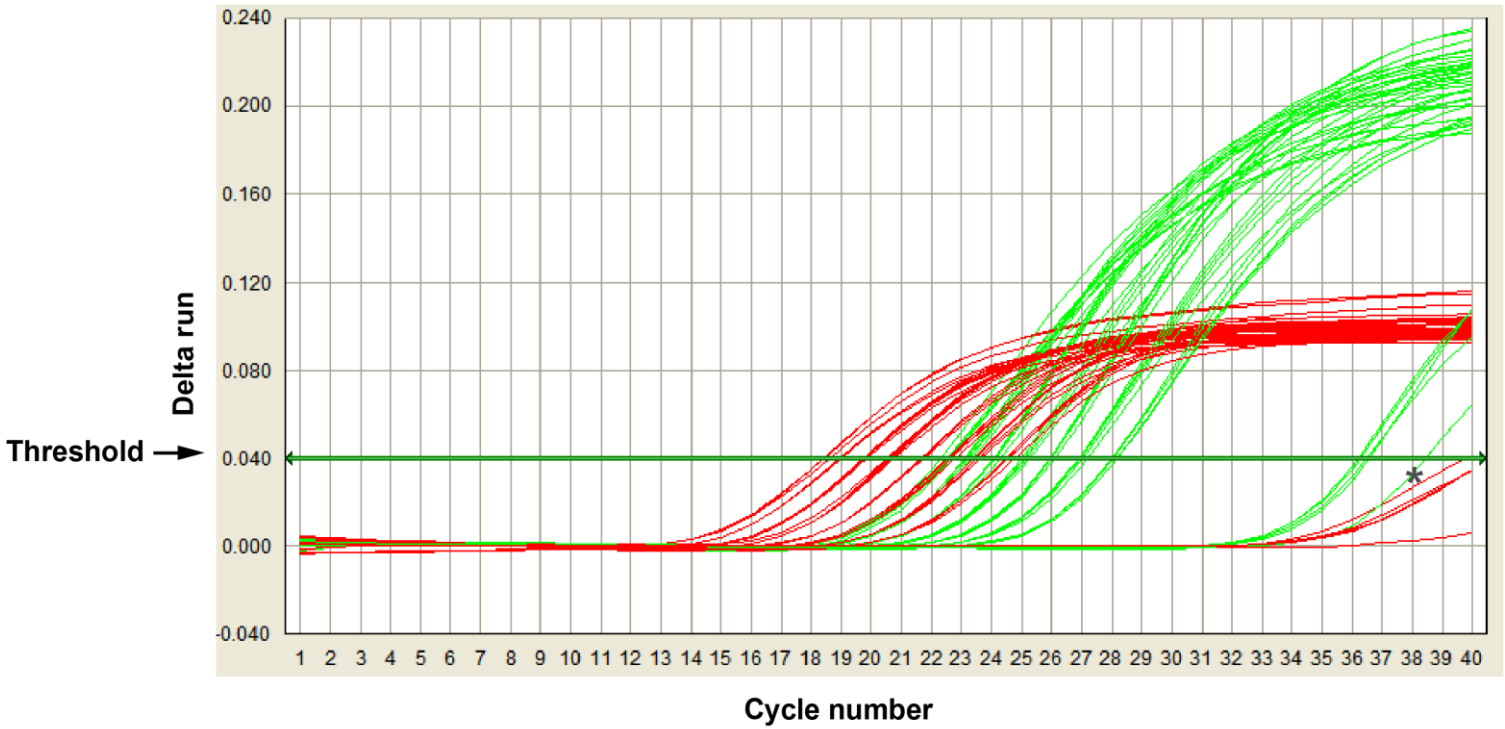

Figure 2.1 TaqMan Real-Time PCR assay. Typical standard curve amplification plot Green= CHMP2B amplification curves, Red= GAPDH amplification curves values; *water DNA negative. Five replicates were run for each sample.

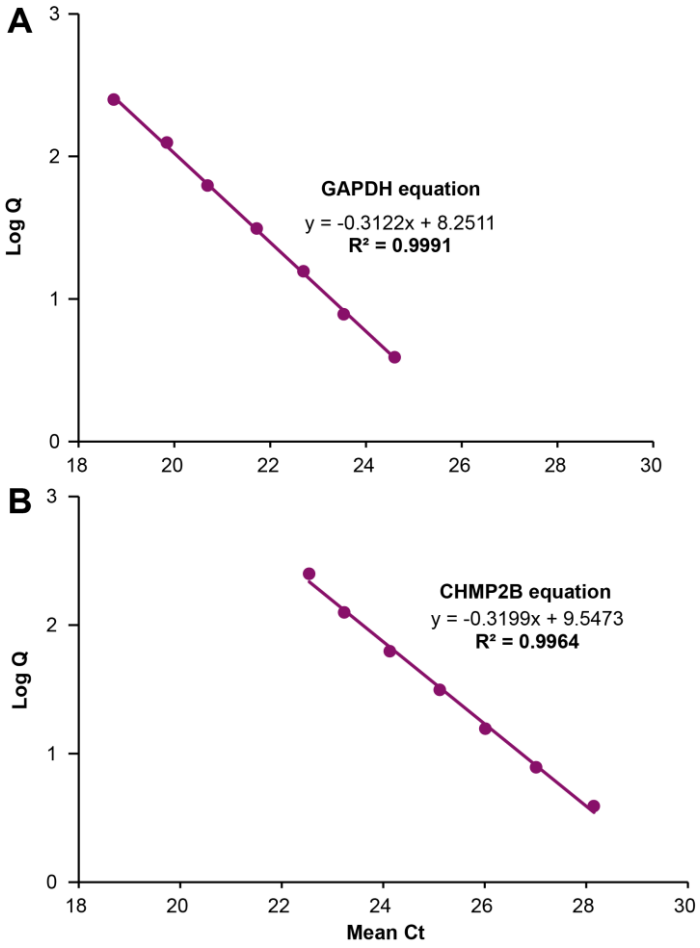

Figure 2.2 TaqMan mean Ct standard curves exemplified by Tg158 samples.
The equation of the graph A) GAPDH and B) CHMP2B allows determination o log concentration (log Q) from a measured Ct; R^2 values demonstrate a very high correlation between mean Ct and LOG Q.

The difference in Ct values between GAPDH and CHMP2B for test samples and a known hemizygous samples were calculated:

[delta]Ct = [delta]Ct sample - [delta]Ct reference

Where, [delta] Ct sample is the Ct value for any sample normalized to the endogenous housekeeping gene and [delta] Ct reference is the Ct value for the known hemizygous sample also normalized to the endogenous housekeeping gene.

As an additional precaution and to confirm homozygosity, mice indicated to be homozygous by the Real-time TaqMan PCR were subjected to progeny test matings by breeding them to wild type mice. Homozygous mice produced hemizygous litters which all tested positive for *CHMP2B* transgene by PCR genotyping. At least three litters were tested for each mouse.

2.5 Histology

2.5.1 Snap freezing for protein analysis

Brain tissues for protein analysis by western blotting were dissected from appropriate mice and cut in half mid-sagittally. The right half of the brain was snap frozen by placing it in a beaker containing isopentane (BDH) cooled by dropping 2-3 pellets of dry ice. The beaker was placed on dry ice and the brain left in the cooled isopentane for at least 2 minutes to ensure thorough freezing. Samples were transferred to labelled plastic bijou tubes and stored at -80°C until required.

2.5.2 Tissue for histology

The left half of the brain was fixed in 10% buffered formal saline and embedded in paraffin for histology.

Where required the left half of the brain was covered in a thin layer of OCT cryomatrix and snap frozen by placing it in a beaker of isopentane cooled with dry ice for 2 minutes. Brains were mounted onto a cork disc using cryomatrix (Shandon Scientific) and stored in a labelled 5ml bijou container at -80°C until required. When required 15μm sections were cut on a cryostat (Bright OTF 5000).

2.5.3 Histology and immunohistochemistry

2.5.3.1 Haematoxylin and eosin staining

Paraffin sections (3-4μm) were dewaxed in a series of xylene changes (3 xylene changes at 5-minute intervals) and re-dehydrated through an ethanol:dH_2O series: 100% ethanol 2 changes , 75% ethanol, 50% ethanol and 100% distilled water) and placed in haematoxylin for 1 minute, thoroughly rinsed in distilled water, then placed in eosin for 3-5 minutes and rinsed in distilled water. The samples were then dehydrated for 5 minutes in each of increasing ethanol:dH_2O series: 50% ethanol, 75% ethanol and 100% ethanol, and then xylene and finally cover slipped using DePex mountant.

2.5.3.2 Cresyl violet staining

Paraffin sections (3-4μm) were dewaxed in a series of xylene changes (3 xylene changes at 5-minute intervals) and re-dehydrated through an ethanol:dH_2O series: 100% ethanol 2 changes , 75% ethanol, 50% ethanol and 100% distilled water) and placed in 1% acidified Cresyl violet solution for 5 minutes. Sections were rinsed in distilled water to obtain contrast between grey and white matter of the CNS ~1-3 minutes. The samples were then dehydrated for 5 minutes in each of increasing ethanol:dH_2O series: 50% ethanol, 75% ethanol and 100% ethanol, and then xylene and finally cover slipped using DePex mountant.

2.5.3.3 Immunohistochemistry

Antigen retrieval methods

Antigen retrieval specific to each primary antibody was applied. Antigen retrieval methods used were:

- Citrate butter **(CB)** antigen retrieval: 0.01M citrate buffer in microwave **(MW)** at full power for 30 minutes.
- Tris-EDTA buffer **(EDTA)** antigen retrieval: 0.05M Tris-EDTA in microwave at full power for 30 minutes
- Protease **(PRT3)** antigen retrieval: Ventana commercially purchased protease 3 automated dosing for 15 minutes
- Ventana proprietary mild cell conditioning treatment **(MCC1)** antigen retrieval: slides were incubated on cell conditioning solution for 15 minutes.

Immunohistochemistry was carried out using the automated Nexus staining apparatus (Ventana Medical Systems) according to the manufacturer's guidelines, using IView-DAB detection system kit (Ventana Medical Systems). In brief, sections were dewaxed and re-hydrated as described in section 2.5.3.1. Non-specific proteins were blocked using commercial blocking reagent for 15 minutes (Ventana Medical System) followed by application of primary antibody at defined temperature and duration (table 2.2.) followed by the application of commercial biotinylated HRP secondary antibody (table 2.4) and the signal visualised using purchased 3’3 diaminobenzidine (DAB) and hydrogen peroxide commercial kit (Ventana Medical System).

Samples were dehydrated in series of ethanol as described above and cleared in three changes of xylene (section 2.5.3.1) and cover slipped using DePex mountant.

Photographs were obtained on a ColorView II digital camera (Soft Imaging System) mounted on a Zeiss Axioplan microscope and prepared for presentation in Adobe Photoshop.

2.5.3.4 Electron microscopy

Mice were perfused through the heart with 3% glutaraldehyde in phosphate buffer; their brains were removed and post-fixed in 3% glutaraldehyde overnight. Brains were treated with 1% osmium tetroxide for three hours at 4° C and embedded in Araldite CY212 resin. Ultrathin sections (70 mM) were stained with lead citrate and uranyl acetate and digital images taken on a Phillips CM10 electron microscope with a Megaview III digital camera (Olympus). EM processing and ultrathin section cutting was performed by the Institute of Neurology core facility.

2.5.3.5 Quantification of pathological findings

Quantification was performed blinded on 4 mice per genotype ($CHMP2B^{WT}$, $CHMP2B^{Int5}$and non-transgenics) at 6, 12 and 18 months of age using brightfield images. For p62 inclusion quantification three 40X images (21069 μm^2per image) were taken in the thalamus and cortex and six in the corpus callosum and inclusions counted using the touch count tool in analySIS imaging software (Olympus).

For quantification of GFAP and Iba1 staining, six 10X images (335628 μm^2per image) were taken in the cortex and the thalamus. The same threshold for GFAP staining was applied to all images using Volocity image analysis software (Perkin Elmer) and the area covered by GFAP immunoreactivity quantified. Activation of Iba1-positive microglia was performed by scoring each image from 1-4 (1 = ramified, 2 = reactive, 3 = ameboid and 4 = phagocytic) as previously described (Ahmed et al., 2010), and taking the average of all images per region.

Statistical testing was performed with Graphpad Prism 5 software using a two-way ANOVA and post-hoc Bonferroni test.

2.6 Western Blot

2.6.1 Brain homogenates

Snap frozen brain samples (section 2.5.1) were used to make 10% brain homogenates using 10mM phosphate buffered saline (PBS) (VWR) with protease inhibitors (x1 protease inhibitor tablet) (Roche) per 10ml of PBS. Samples were weighed (milligrams) to 2 decimal places and the volume of homogenisation buffer required was calculated using the following standard formula;

$$V=BW \times 2(4.5)$$

Where V is the required volume of PBS (ml) and BW is the weight of the brain (mg). 2(4.5) = An initial volume of BW x 4.5ml PBS was added to the brain and the brain homogenised using ribolyser beads and a Hybaid Ribolyser for 2 x 45 seconds at speed 5.5 rpm; a second volume of BW x 4.5ml PBS was added to the resulting 5% brain homogenate transferred to a Bijou tube, and thoroughly mixed to obtain a final concentration of 10% brain homogenate.

2.6.2 Sample preparation and western blotting

Sample preparation:

Homogenised brain samples (section 2.6.1) were equally divided into 2 aliquots, and to one aliquot, an equal volume of 2x Laemmli sample buffer (BioRad) containing β-mercaptoethanol (50µl β-mecaptoethanol to 450µl 2x Laemmli sample buffer) was added. This sample was boiled for 3 minutes at 100°C on a thermomixer hotplate (Eppendorf) and subsequently further divided into

aliquots as required. All samples and aliquots were labelled and stored at -80°C until required.

Western blotting:

For protein electrophoresis aliquots of brain homogenate prepared in Laemmli sample buffer were boiled for 1 minute at 100°C on a thermomixer hotplate. Pre-cast Tris-glycine 4-20% gradient protein gels (Invitrogen) were loaded with 5µl of denatured brain homogenate and subjected to electrophoresis at 125V for 1.5h in Tris-glycine-SDS buffer (National Diagnostics).

Proteins were transferred from the gel onto Polyvinylidene difluoride (PVDF) membrane using the XCell II Blot wet transfer module (Invitrogen). Electroblotting was carried out at 35V for 2 hours.

To visualise the proteins of interest the PVDF membrane was removed and washed in 10mM PBS containing 0.01% Tween 20 (PBS/T) with three wash buffer changes at 3-minute intervals. Dried milk (5% Marvel) was used to block non-specific proteins at room temperature for 1 hour. The membrane was washed again as described above and incubated with appropriate primary antibody at 4°C overnight or 1 hour at room temperature. The membrane was washed 3 times again and incubated for 1 hour at room temperature with HRP conjugated secondary antibody. After a final three washes in PBS, the membrane was incubated with SuperSignal West Pico chemiluminesence substrate (Thermo Scientific) and exposed to Kodak photographic film (Sigma) for varying durations and developed on an automated machine (Compact X4 Xograph Imaging system).

2.7 Behavioural Phenotyping

2.7.1 Kaplan-Meier survival analysis

Kaplan-Meier survival analysis was performed on IBM SPSS Version 19 statistical programme.

2.7.2 Assessors

All assessors (SN, MF, SM, SBM) were in possession of appropriate Home Office licences to work with animals and were trained in performing the phenotyping protocols detailed in this section prior to assessing mouse test cohorts. Assessors were blinded to test cohort genotypes, gender and age when performing phenotyping assessments.

2.7.3 Modified SHIRPA

The modified SHIRPA protocol was adopted from the procedure described on the MRC Harwell Mammalian Genetics website (http://empress.har.mrc.ac.uk/). The modified-SHIRPA protocol detailed below was used as a primary phenotyping screen of *Chmp2b* knockout mice (EMPReSS, 2008).

Modified-SHIRPA was performed on a cohort of 12 month-old *Chmp2b* knockout mice; N=16 Chmp2b-/- mice; N=15 Chmp2b+/+ mice.

Equipment

One set of the modified-SHRIPA equipment listed below was kindly lent to us by Mr Ben Woodman from Professor G. Bates' laboratory from the MRC Neurogenetics group at King's College London and a second set was made to order by the works department at King's College London Guy's hospital site, generously organised by Mr Ben Woodman. The click box which emits a 20-KHz sound at 90dB and was used to test the auditory startle responses (pinna reflex test) of the mice was purchased from the Sanger Institute.

- Clear Perspex cylindrical viewing jar (14 cm diameter, 18 cm height)
- Tripod (7.5 cm height).
- Plastic sheet [sandpapered down to create a surface that is not smooth] (20 cm x 20 cm)
- Clear Perspex arena (60 cm length, 37 cm width and 18 cm height). In the floor of the arena is a Perspex sheet marked with 15 squares (11 cm). A grid (40 cm x 20 cm) with 12 mm mesh (approximate) is secured across the top of the width of the box
- Click-box (generates a brief 20 KHz tone at 90 dB)
- Clear Perspex tube (3 cm diameter, 20 cm length)
- Stopwatch
- Commercially available cotton ear buds used as probe (Boots own brand)
- Modified-SHIRPA score sheet

<u>Supplies</u>

- Tissues
- Alcohol wipes for wiping down equipment between each mouse

<u>Procedure</u>

Modified-SHIRPA protocol assessment was carried out by three assessors (SN, SM, SBM). Mice were weighed using electronic laboratroy scales and their weights recorded to two decimal places prior to being placed in a viewing jar.

Procedure for behaviour assessed in the viewing jar:

Refer to the score sheet (section 2.7.3) for guidance on scoring, a short description of each test is provided below.

Wipe the viewing jar area clean with alcohol wipes and allow it to dry before use. Place the viewing jar upright on top of the plastic sheet. Remove a mouse from its home cage, gripping the tail between the thumb and the forefinger and place into the viewing jar.

The following highlighted behaviours were recorded without disturbing the mouse. Any incidents of bizarre behaviour, stereotypy and convulsions were recorded separately.

Body Position: observe the mouse and identify whether it appears to be inactive, active or excessively active.

Tremor: Make a note of whether or not the mouse appears to tremble.

Palpebral Closure: Study the mouse for palpebral closure.

Coat Appearance: Look carefully at the mouse's coat and determine how tidy and well groomed it is, making a note of any abnormalities such as piloerection.

Whiskers: Make a note of whether the mouse has intact or trimmed whiskers.

Lacrimation: Make a note of the presence or absence of lacrimation.

Defecation: Make a note of whether or not the mouse defecates.

Procedure for behaviour assessment in the observation arena

Wipe the arena clean with alcohol wipes and allow it to dry before use.

Transfer a mouse to the centre of the arena inside the viewing jar, using the plastic sheet underneath the jar. Carefully remove the plastic sheet from underneath the viewing jar at approximately 25 cm above the arena floor allowing the mouse to fall into the observation arena.

Transfer Arousal:

Observe the immediate reaction of the mouse to the new environment and make a note of whether it appears to freeze for a period longer than 5 seconds, freezes briefly before it begins to move, or moves immediately.

Locomotor Activity:

Start the stopwatch and make a note of the total number of squares the mouse enters with all four feet in 30 seconds.

Gait:

Study the gait of the mouse and determine how fluid its movement is as well as the extent to which the pelvis is elevated during forward motion.

Tail Elevation:

During forward motion, observe the position of the tail making a note of whether it is dragging, horizontally extended or is elevated.

Startle Response:

Hold the IHR click-box approximately 30 cm above the arena and emit 90 dB tone. Observe the response of the mouse

Touch Escape:

Approach the mouse from the front with a bent index finger before stroking on the back of the neck. Observe the response of the mouse.

<u>Procedure for behaviour assessed above the arena</u>

Remove the mouse from the arena and observe the following

Positional passivity:

Measure the immediate response to sequential handling of the mouse. Identify whether the mouse struggles when held by its tail (terminate further handling if apparent). Identify whether the mouse struggles when held by the neck, a loose scruff between the forefinger and thumb (terminate further handling if apparent). Identify whether the mouse struggles when lying supine (terminate further handling if apparent).

Skin Colour:

Make a note of the colour gradations of plantar surface and digits of forelimbs.

Trunk Curl:

Make a note of forward curling (i.e. head to abdomen) of the mouse when held by the tail.

Limb Grasping:

Make a note of the mouse grasping its limbs when held by the tail.

Pinna Reflex:

Place the mouse gently on to a grid and touch the proximal part of the inner canthus lightly with the tip of a fine cotton probe, observing ear retraction.

Corneal Reflex:

Whilst the mouse is on the grid, touch the cornea lightly with the tip of a fine cotton probe, observing the eye-blink response.

Contact Righting Reflex:

Place the animal into the clear Perspex plastic tube and roll the tube slowly until the mouse inside it is upside down. Observe the righting reflex.

Evidence of Biting:

Make a note of whether or not the mouse bites during the screen.

Vocalisation:

Make a note of whether or not the mouse is vocal during the screen.

Modified-SHIRPA score sheet

Behaviour recorded in viewing jar

Body Position

0 = Inactive
1 = Active
2 = Excessive activity

Tremor

0 = Absent
1 = Closed

Palpebral Closure

1 = Eyes Open
2 = Eyes Closed

Coat Appearance

0 = Tidy and well groomed
1 = Irregularities such as piloerection

Whiskers

0 = Present
1 = Absent (include any further comments)

Lacrimation

0 = Absent
1 = Present

Defecation

0 = Present
1 = Absent

Behaviour recorded in observation arena

Transfer Arousal

0 = Extended freeze (over 5 seconds)
1 = Brief freeze followed by movement
2 = Immediate movement

Locomotor Activity

The total number of squares the mouse enters with all four feet in 30 seconds

Gait

0 = Fluid movement and approximately 3mm pelvic elevation
1 = Lack of fluidity in movement (include comments *e.g.* retropulsion, more than 3mm pelvic elevation)

Tail Elevation

0 = Dragging
1 = Horizontal Extension
2 = Elevated/Straub Tail

Startle Response
0 = None
1 = Preyer Reflex (backwards flick of the pinnae)
2 = Reaction in addition to the Preyer reflex (*e.g.* startled response)

Touch Escape
0 = No response
1 = Response to touch
2 = Flees prior to touch

<u>Behaviour recorded above the arena</u>
Positional Passivity
0 = Struggles when held by the tail
1 = Struggles when held by the neck (loose scruff between the forefinger and thumb)
2 = Struggles when laid supine
3 = No struggle

Skin Colour
0 = Blanched
1 = Pink
2 = Bright, deep red flush

Trunk Curl
0 = Absent
1 = Present

Pinna Reflex (Ears flick)
0 = Present
1 = Absent

Corneal Reflex
0 = Present (blink)
1 = Absent
Contact Righting Reflex
0 = Present
1 = Absent

Evidence of biting
0 = None
1 = biting in response to handling

Vocalisation
0 = None
1 = Vocal

Additional Observations

Foot tapping, splayed gait, twitching, leaning, rapid breathing, kinked tail, hunched back:

0 = Absent
1 = Present

Modified-SHIRPA record sheet

Mouse identifier number				
Date				
Operator				
Weight(g)				
Gender				
VIEWING JAR				
Body Position (0-2)				
Tremor (0-1)				
Defecation				
Urination				
Palpebral Closure (0-1)				
Coat Appearance (0-1)				
Whiskers (0-1)				
Lacrimation (0-1)				
Evidence of Biting (0-1)				
Vocalization (0-1)				
ARENA				
Transfer Arousal (0-2)				
LMA (No.)				
Gait (0-1)				
Tail elevation (0-2)				
Startle Response (0-2)				
Touch Escape (0-2)				
Positional Passivity (0-3)				
ABOVE ARENA				
Trunk Curl (0-1)				
Limb Grasping (0-1)				
Pinna Reflex (0-1)				
Corneal Reflex (0-1)				
RESTRAINT & OTHER				
Skin Colour (0-2)				
Contact Righting Reflex (0-1)				
Extra notes				

Table 2.11 Modified-SHIRPA protocol used to score mouse behaviour.

Score of 0= phenotype absent, 1= phenotype present, 2= increase in phenotype intensity relative to scoring 1, 3= increase in phenotype intensity relative to scoring 2.

2.7.4 Rotarod

The rotarod protocol was adopted from that published on the MRC Harwell Mammalian Genetics website (http://empress.har.mrc.ac.uk/) (EMPReSS, 2008).

On the day of testing whilst in their home cages; mice were placed in the testing room for at least 15 minutes prior to rotarod assessment to help them to acclimate to the testing room (acclimation phase).

The test phase is composed of three trials separated by 15-minute inter-trial intervals (ITI). No training period was used prior to the test phase apart from an initial run on the apparatus 15 minutes before the first test for the mice to experience the equipment. The rotarod (Panlab, 760237) was set to accelerating mode (4 to 40rpm in 300s).

Test trial 1 (T1): Test mice were placed on the rotarod lanes while the rod initially rotated at 4rpm constant speed. Once all the mice were able to walk forward for a few seconds at 4 rpm the accelerating mode was started and the rod started to accelerate from 4 rpm to 40 rpm in 300 seconds. The latency at which each mouse fell off the rod (latency) was recorded. The apparatus was cleaned with water and 50% ethanol and wiped dry. A 15 min inter trial interval (**ITI**) was allowed between consecutive trials of the same mice. Test trials 2 and 3 (**T2** and **T3**) were performed in exactly the same way as T1 and rotarod latency was recorded for each mouse in the test cohort in order of T1-ITI-T2-ITI-T3.

2.7.5 Grip Strength

The grip strength protocol was adopted from that published on the MRC Harwell Mammalian Genetics website (http://empress.har.mrc.ac.uk/) (EMPReSS, 2008).

Commercially available Grip Strength Meter (Harvard Apparatus, 76007-BSRSIC)) was used. The system is supplied with a single grid which connects to the sensor.

The Assessor removed a single test mouse at a time from its home cage by gripping the base of its tail between their thumb and forefinger.

Mouse forelimb and hindlimb measurement was taken by gently lowering the mouse over the top of the grid so that both its front and hind paws could grip the grid. The mouse's torso was kept horizontal and the mouse was pulled back steadily (not jerking) until its grip was released down the complete length of the grid. When the mouse released the grid, the maximal grip strength value of the animal was displayed on the apparatus screen and the value (grams) recorded. This procedure was repeated two further times to obtain 3 forelimb and hindlimb grip strength measurements G1, G2 and G3.
The grid was cleaned with 50% ethanol and dried with tissue, before measuring grip strength for each test mouse.

2.7.6 Burrowing

The burrowing protocol described here was adapted from Deacon, R Nature Protocols (Deacon, 2006b).

A sawn section from commercially purchased plastic water downpipe measuring 320mm long and 100mm in diameter (B&Q) was adapted as the burrowing tube and filled with 200g of RM1 food pellets (Special Diet Services) as burrowing material. One end of the tube was left open and raised 60mm above the cage floor by two 80mm bolts, placed 25 mm in from the end of the tube, spaced 70 mm apart. The other end was covered by a plastic plug.

The burrowing tube was placed in a mouse cage overnight together with a singly-housed mouse 1 hour before the dark cycle. The amount of burrowing material left in the burrowing tube was measured (in grams) the next day during the light

cycle. The amount of food pellets burrowed was determined by subtracting the amount of pellets remaining the next day from the starting amount of food pellets (200g). Each mouse was allowed a single practice run for 2 hours prior to being tested overnight.

2.7.7 Nesting

The nesting protocol described here was adapted from Deacon, R Nature Protocols (Deacon, 2006a).

Test mice were singly-housed and commercially purchased 5x5 cm Nestlet squares (Lillico Biotechnology) were placed into the mouse cages 1 hour before the dark cycle. Standard cage bedding (section 2.3) was available in the mouse cage but all forms of environmental enrichment such as inner toilet roll tubes were removed.

The nests were scored the next day according to the scoring system demonstrated in figure 2.4 and table 2.12

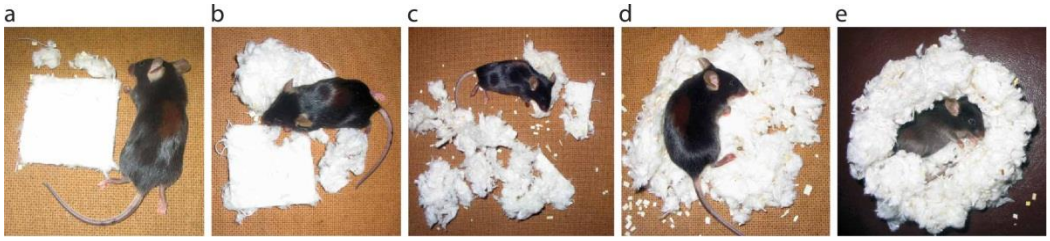

Figure 2.3 Pictorial representation of typical Nestlet scores.

Nests are scored 1-5 (a-e respectively) based on degree of Nestlet tearing and nest formation. Adapted from Deacon (2006) (Deacon, 2006a).

Nest Score	Corresponding to figure 2.5	Description
1	**a**	Nestlet not noticeably touched; >90% intact Nest structure absent
2	**b**	Nestlet partially torn; 50-90% remaining intact Nest structure absent
3	**c**	Nestlet is mostly torn 50-90% torn/shredded Nest structure absent
4	**d**	Most of Nestlet is torn >90% torn/shredded Identifiable gathered *flat* nest structure
5	**e**	Most of Nestlet is torn >90% torn/shredded Near perfect gathered *concave* nest structure with walls higher than the height of the mouse lying in the nest on its side.

Table 2.12 Description of nest scores accompanying Figure 2.5.

Adapted from Deacon 2006 (Deacon, 2006a).

2.7.8 Videoing mice

Mice were videoed in the SHIRPA observational arena with white flooring (60 cm length, 37 cm width and 18 cm height) to demonstrate phenotypes including splayed gait and foot tapping (chapter 3) using Sony DCR-DVD 106 E digital camera. Video clips were edited using Adobe Premiere video editing software.

3 Characterising Chmp2b Knockout Mice

3.1 *Chmp2b* Knockout Mice

The autosomal dominant CHMP2B splice site mutation originally identified in the Danish kindred results in the formation of two aberrant transcripts termed CHMP2B Intron5 and CHMP2B Delta10, and therefore the loss of one normal CHMP2B allele (Skibinski et al., 2005). This Chapter describes the generation and characterisation of *Chmp2b* knockout (*Chmp2b*$^{-/-}$) mice to investigate whether loss of function of *Chmp2b* contributes to disease and to elucidate the normal function of Chmp2b protein.

Chmp2b knockout mice were resuscitated from commercially available *Chmp2b* knockout mouse frozen embryos. The amount of protein depletion in the *Chmp2b* knockout mice was determined using quantitative western blot analysis. A systematic histopathological study was undertaken to examine the brain, spinal cord, sciatic nerve and quadriceps muscle for the presence of pathology in homozygous *Chmp2b* knockout mice across increasing age compared to wild type age-matched mice.

3.2 Generation of Chmp2b Knockout Mice

Commercially available embryonic stem cells in which the pGT0Lxf gene trap vector was found to randomly insert within intron 2 of *Chmp2b* sequence (figure 3.1) were purchased from BayGenomics California (Stryke et al., 2003; BayGenomics, 2012).

Briefly, the targetted ES cells (genetic background 129P2/OlaHsd) were produced as follows: the pGT0Lxf gene trap vector which harbours a splice acceptor (SA) site and intron 1 of the *Engrailed-2* gene followed by β-geo cassette and a polyA (pA) sequence (figure 3.1) was electroporated into XL952 embryonic stem (ES) cells derived from the Sv129 mouse strain. The pGT0Lxf gene trap vector

randomly inserts into intronic sequence of a gene. In this case the pGT0Lxf gene trap vector inserted into intron 2 of *Chmp2b* (figure 3.1), which was confirmed by RT-PCR and sequence analyses of DNA extracted from aliquots of the ES cells prior to generation of the *Chmp2b* knockout mice (Stryke et al., 2003; BayGenomics, 2012). ES cells confirmed to be harbouring the gene trap vector in intron 2 of the *Chmp2b* gene were injected into blastocysts of C57BL6/J mice by Bay Genomics (Stryke et al., 2003).

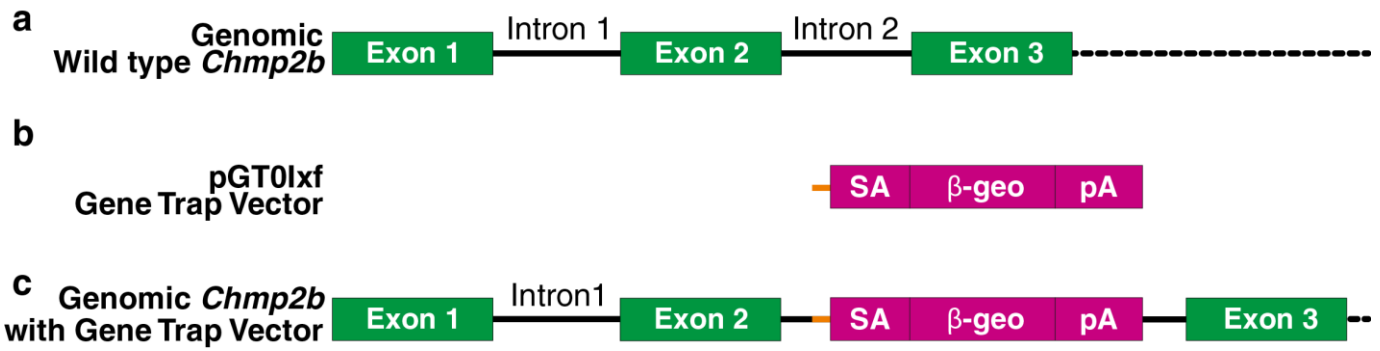

Figure 3.1 *Chmp2b* genomic wild type and *Chmp2b* knockout sequence schematics.

Schematic representation of (a) *Chmp2b* wild type sequence (b) pGT0lxf gene trap vector including intron 1of the *Engrailed-2* gene in orange, SA is splice acceptor site, β-geo is beta galactosidase-neomycin fusion cassette, pA is polyadenylation site and (c) *Chmp2b* sequence with pGT0lxf gene trap vector inserted within *Chmp2b* intron 2.

Two male chimaeric mice were born, with each predicted to be over 90% chimaeric based on coat colour. Both males were bred to C57BL6/J females and pups recovered and genotyped. Several XL952/BL6/J F1 mice were produced over several litters. Sperm from male F1s was recovered and used to produce approximately 300 2-cell embryos by *in vitro* fertilisation of BL6/J eggs (BayGenomics, 2012). These embryos were frozen and imported into the MRC Prion Unit where they were resuscitated and implanted into pseudopregnant mice by the MRC Prion Unit Transgenic Team. The official nomenclature for these gene trap mice is *Chmp2b*$^{Gt(XL952)Byg}$. However, for simplicity and ease of reference, the terminology knockout (*Chmp2b*$^{-/-}$) is used throughout this thesis, while recognising that complete knockout of the *Chmp2b* gene was not achieved by this approach.

3.2.1 Establishing Chmp2b knockout colony

Tail biopsies were taken from the resulting pups and screened by PCR for the presence of the *Chmp2b* knockout cassette in intron 2, using PCR primers designed to allow discrimination of *Chmp2b* knockout mice from wild type mice. Details of the genotype-specific primers and PCR protocol are provided in chapter 2. Confirmed knockout mice were mated at 6 weeks of age to C57BL/6J wild type mice and therefore the *Chmp2b* knockout colony established for use in this study is on a mixed 129 x C57BL/6J genetic background.

3.2.2 Breeding scheme

The initial mating of *Chmp2b* heterozygous (*Chmp2b*$^{+/-}$) mice to wild type C57BL/6J mice (*Chmp2b*$^{+/+}$) produced 50% *Chmp2b* heterozygous (*Chmp2b*$^{+/-}$) mice and 50% *Chmp2b*$^{+/+}$ wild type mice (figure 3.2). To obtain *Chmp2b* homozygous (*Chmp2b*$^{-/-}$) knockout mice, heterozygous *Chmp2b* (*Chmp2b*$^{+/-}$) knockout mice harbouring one copy of the β-geo knockout cassette were mated to each other (figure 3.2) so that the resulting litter would be expected to produce 25% *Chmp2b*$^{-/-}$, 50% *Chmp2b*$^{+/-}$ and 25% *Chmp2b*$^{+/+}$ offspring. Finally, to establish and maintain the *Chmp2b* homozygous colony, *Chmp2b*$^{-/-}$ mice were mated to each other.

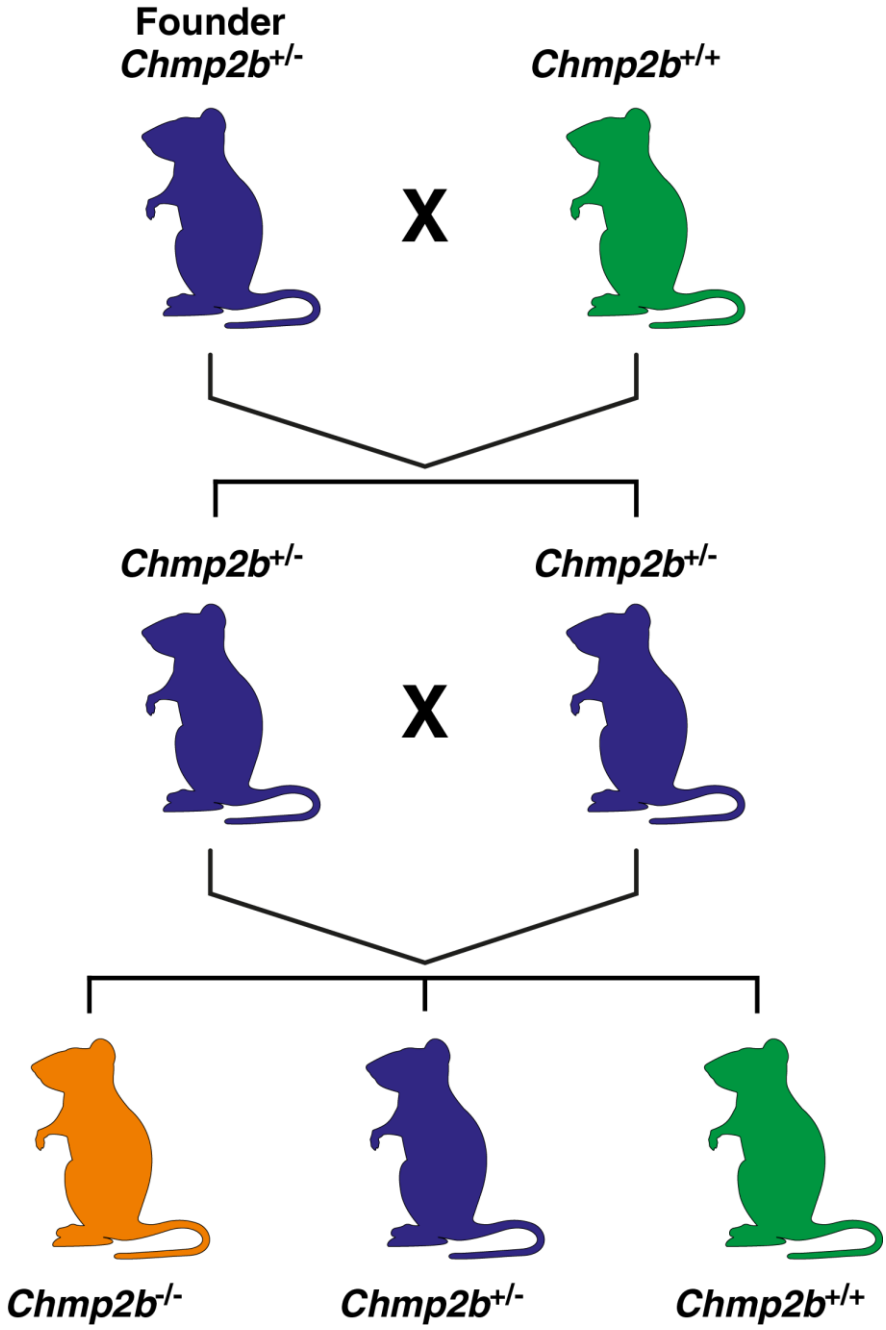

Figure 3.2 *Chmp2b* knockout colony breeding scheme.

Mating of *Chmp2b* hemizygous (*Chmp2b*$^{+/-}$) founder to C57BL/6J wild type (*Chmp2b*$^{+/+}$) mice and subsequent *Chmp2b* heterozygous (*Chmp2b*$^{+/-}$) X heterozygous (*Chmp2b*$^{+/-}$) breeding to produce the initial *Chmp2b* homozygous knockout (*Chmp2b*$^{-/-}$) offspring (orange).

3.3 Molecular Characterisation of *Chmp2b* Knockout Mice

3.3.1 PCR primers and multiplex PCR

To genotype the *Chmp2b* knockout mice a multiplex PCR was designed where two gene regions of interest could be simultaneously amplified. As the β-geo cassette is known to be inserted into intron 2 of the *Chmp2b* gene, intronic primers were designed at the start of intron 2 (Int2_F forward primer) and reverse primers either to intron 2 (Int2_485R) or to the β-geo cassette in the *Engrailed-2* gene intronic sequence (KO_386R) (figure 3.3). Because the intronic reverse primer (Int2_485R) is downstream of the β-geo cassette it does not amplify with the forward primer when the cassette is present making this amplification product specific for the wild-type allele (figure 3.3).

Therefore, in *Chmp2b* wild type mice, in which the β-geo cassette is *not* inserted into intron 2, only a single wild type band of ~485bp is amplified. In *Chmp2b* homozygous knockout mice, where both *Chmp2b* alleles have the β-geo cassette inserted in intron 2, a single band of ~386bp is amplified. In heterozygous mice, where one wild type and one knockout allele is present, both PCR products of ~485bp and ~386pb are amplified (figure 3.4).

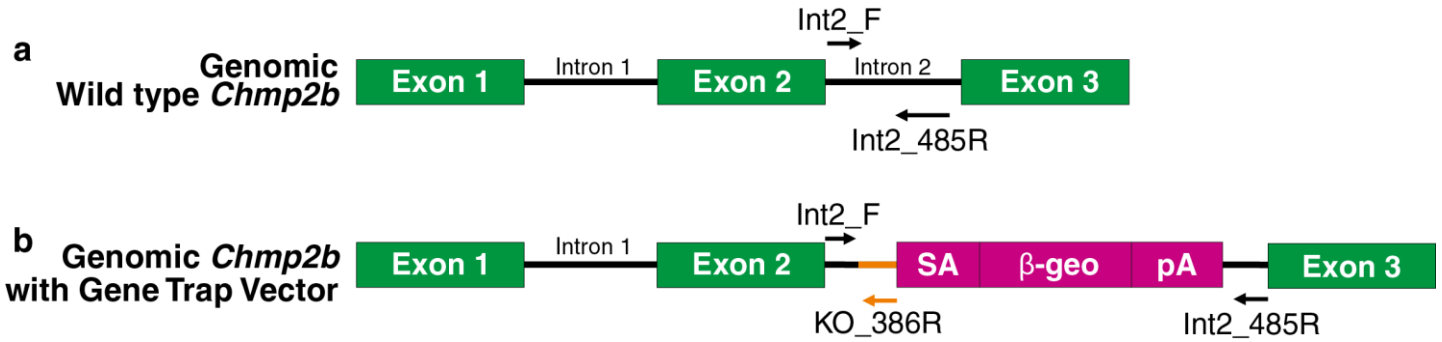

Figure 3.3 Schematic representation of primers targeting *Chmp2b* wild type and knockout sequence used in PCR genotyping.

Intron 2 forward primer (Int2_F) is the common forward primer to both sequences. (a) The reverse primer (Int2_485R) enables amplification of the endogenous *Chmp2b* wild type sequence. (b)The reverse primer (KO_386R) enables amplification of the *Chmp2b* knockout sequence by targeting intron 1 of the *Engrailed-2* gene (orange) within the pGT0lxf gene trap vector.

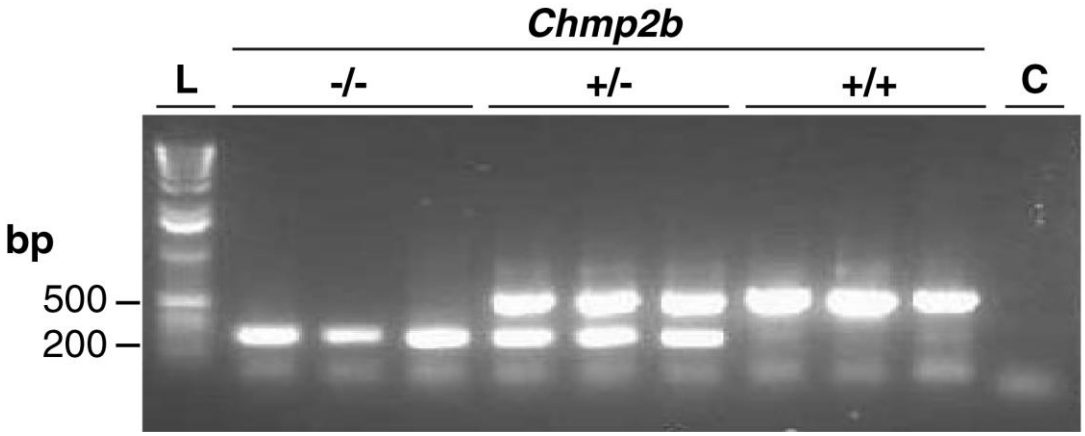

Figure 3.4 Typical DNA genotyping bands for *Chmp2b* knockout mice.

Chmp2b homozygous knockout (-/-), heterozygous (+/-) and wild type (+/+) bands amplified with the multiplex PCR used to genotype *Chmp2b* knockout mice. L is 1kb DNA ladder and C is no DNA sterile distilled water control. Genotyping using Int2_F, Int2_485R and KO_386R primers amplifies *Chmp2b* wild type bands 485bp; *Chmp2b* knockout bands 386bp and in the case of heterozygous mice carrying both alleles both wild type 485bp and knockout 386bp bands are amplified.

3.3.2 Chmp2b protein expression

To determine the extent of Chmp2b protein depletion in *Chmp2b* knockout mice 10% brain homogenates (N=3 $Chmp2b^{-/-}$ *and* $Chmp2b^{+/+}$) were run on an SDS-PAGE gel, western blotted and then probed with commercially purchased C-terminal CHMP2B polyclonal antibody (Abcam) (figure 3.5). The relative level of Chmp2b depletion was determined using a quantitative imaging analysis (figure 3.6).

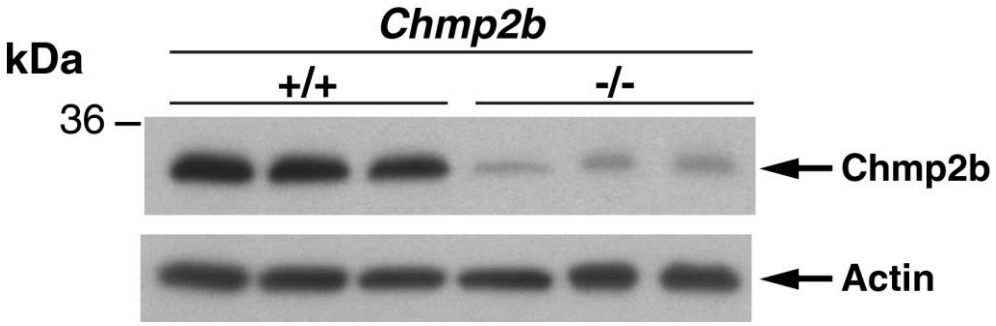

Figure 3.5 Chmp2b protein blot with C-terminal CHMP2B antibody.

10% Brain homogenates were probed with C-terminal CHMP2B antibody (Abcam). The top blot shows Chmp2b protein expression in *Chmp2b* wild type (+/+) and knockout (-/-) brain homogenates. The bottom blot is the same blot re-probed with anti-Actin antibody demonstrating equal loading.

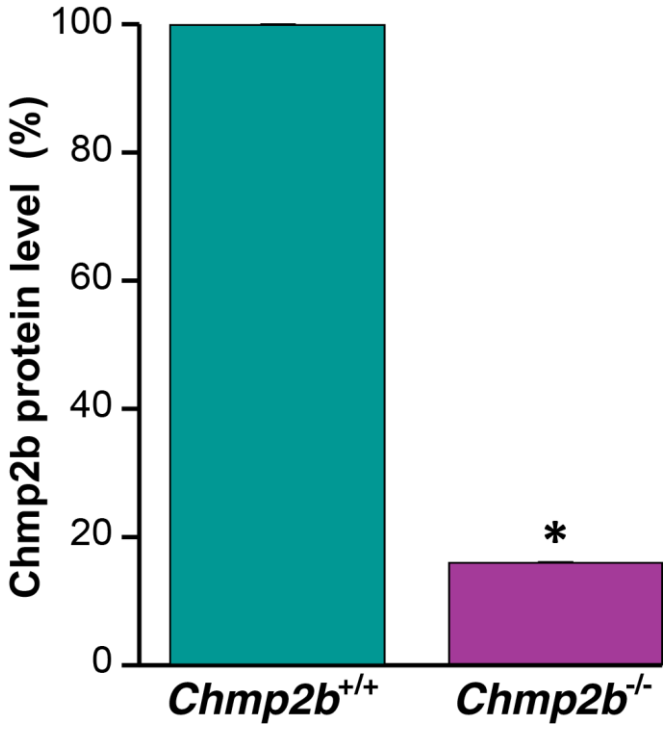

Figure 3.6 Quantification of Chmp2b protein depletion in 12- month-old mouse brain.

The level of Chmp2b depletion in *Chmp2b*$^{-/-}$ mice was determined from the western blot (figure 3.5) using the Volocity program (error bars= SEM). Quantitative analysis reveals that the *Chmp2b*$^{-/-}$ mouse brains have 85% depletion of Chmp2b protein expression relative to *Chmp2b*$^{+/+}$ mice. N=3 for each genotype. *Chmp2b* depletion is highly significant; p>*0.0005 determined using T-test.

Quantitative analysis of the western blot reveals that the *Chmp2b*$^{-/-}$ mice (N=3) have ~85% (*p*>0.0005*)* of their endogenous Chmp2b protein depleted compared to *Chmp2b*$^{+/+}$ (N=3) (figure 3.6); *Chmp2b* heterozygous (*Chmp2b*$^{+/-}$) mice (N=2) have ~25 % Chmp2b protein depletion (data not shown).

3.4 *Chmp2b*$^{-/-}$ Pathology

Histological studies of affected members of the Danish FTD-3 family show global frontotemporal atrophy with the amygdala and hippocampus being spared (Gydesen et al., 2002; Holm et al., 2007). Gliosis in the absence of macrophages is seen in layer II of the frontal cortex (Holm et al., 2007). A hallmark feature of FTD-3 is the presence of ubiquitin and p62 cellular inclusions seen in the frontal cortex and hippocampus but distinctively with the absence of TDP-43 and FUS staining (Holm et al., 2007; Holm et al., 2009). The presence of enlarged vacuoles positive for M6PR a marker of late endosomes, demonstrate enlarged aberrant late endosomes in neurons of the frontal, temporal and occipital cortex, but not in cerebellar neurons (Urwin et al., 2010a).

To determine whether the *Chmp2b* knockout mice generated recapitulate key neuropathological features observed in human post-mortem brain tissue, a systematic histological study was undertaken to identify gross pathological changes in the brain, spinal cord, quadriceps muscle and the sciatic nerve. Furthermore, brain and spinal cord tissues were examined for gliosis, cellular or synaptic density loss as well as immunostaining for ubiquitin, a key marker of neurodegeneration and p62 a marker of autophagy and a hallmark feature of FTD-3. In addition late endosome markers mannose-6-phosphate receptor (M6PR) and lysosomal associated membrane protein-1 (LAMP-1) and the early endosome marker; early endosome antigen-1 (EEA1) markers were used to examine whether the *Chmp2b* knockout mouse brains demonstrate any change in expression of endosome markers characteristic of FTD-3 pathology. The

immunohistological expression of TDP-43, a key protein shown to be the ubiquitinated protein in a subset of FTLD cases reclassified as FTLD-TDP (Neumann et al., 2006; Mackenzie et al., 2011) but not specifically associated with FTD-3 pathology, was also assessed in *Chmp2b* knockout mouse brain.

Chmp2b knockout and age-matched wild type control formalin fixed paraffin embedded brain and lumbar spinal cord sections were stained with the panel of antibodies and histological stains (N=3 for each genotype at 12, 18 and 24 months of age). Detailed description of protocols can be found in chapter 2. Brain and spinal cord sections were viewed using light microscopy with consultant neuropathologist SB. The frontal cortex, CA3 region of the hippocampus, cerebellum and lumbar regions of the spinal cord were photographed.

3.4.1 Brain pathology

The frontal cortex and hippocampus were selected as these are the regions of inclusion pathology in FTD-3 human disease (Holm et al., 2007; Holm et al., 2009). The cerebellum was chosen as an additional region of interest as the *Chmp2b* knockout mice demonstrate a lower limb gait phenotype (chapter 4) and that published data from Hara (2006) and Komatsu (2006) report knocking out autophagy genes (*Atg5* and *Atg 7)* specifically in the central nervous system results in loss of Purkinje cells, shown by loss of calbindin expression in the cerebellum and gait phenotype (Hara et al., 2006; Komatsu et al., 2006). Therefore to investigate if the *chmp2b* knockout gait phenotype is caused by the loss of cerebellar neurons, calbindin expression was examined in the cerebellum. Optimisation of autophagosome staining with an LC-3 antibody was also attempted but without success, and was therefore excluded from the panel of antibodies used in this study.

3.4.1.1 Gross morphology, astrogliosis and microglial activation

Hematoxylin and Eosin (H&E) staining is the most widely used of all histological staining protocols for the vast majority of tissues in both research and clinical laboratories due to the striking clarity with which the two dyes distinguish cellular matrix (cytoplasm), connective tissue and nuclei (Bancroft and Gamble, 2002). Hematoxylin is a cationic dye that stains basophilic components of the cell (Spitalnik and Witkin, 2012). Positively charged metal-hematein, complexes in hematoxylin, bind to the negatively charged phosphate backbone of DNA, and consequently stain cellular nuclei blue (Bancroft and Gamble, 2002; Merck, 2012).

Eosin is an acidic anionic red-pink dye that mainly binds negatively charged proteins (Spitalnik and Witkin, 2012). It is an especially useful stain as it can distinguish between the cytoplasm and different types of connective tissue fibres and matrices by staining them different shades of red and pink with appropriate differentiation (Bancroft and Gamble, 2002; Merck, 2012). It is also the most useful stain to combine with hematoxylin due to the contrast in colour of the two dyes, pink and blue respectively, demonstrating the tissues' general histological architecture and gross morphology (Bancroft and Gamble, 2002; Merck, 2012). Accordingly, in this study H&E staining has been used to look at the general histological architecture and gross morphology of the mouse brain and spinal cord regions of interest.

Glial Fibrillary Acidic Protein (GFAP) is 50kDa intracytoplasmic type III intermediate filament (IF) protein and a classic marker of mature astrocytes (Middeldorp and Hol, 2011). The enlargement of astrocytes and extension of their processes as well as increased expression of GFAP is a marker of reactive gliosis, a cellular response associated with brain damage and aging (Middeldorp and Hol, 2011). GFAP antibodies used to visualise astrocytes demonstrate cells with a stellate morphology, characteristic for differentiated astrocytes (Middeldorp and Hol, 2011).

GFAP mRNA and protein expression increases progressively during aging in humans and laboratory rodents (Goss et al., 1991; Morgan et al., 1997; Morgan et al., 1999). With increasing age an increase in GFAP is observed in the hippocampus, frontal cortex and temporal cortex of human brains (Nichols et al., 1993). Astrogliosis and increase of GFAP expression is associated with neurodegeneration and neuronal death in a number of neurodegenerative diseases including ALS, Huntington's Disease (HD), PiD, Parkinson's disease (PD), and Alzheimer's disease (AD) (Eng and Ghirnikar, 1994; Eng et al., 2000; Middeldorp and Hol, 2011). The anatomical region, severity of gliosis, and age of onset vary between the different neurodegenerative diseases (Middeldorp and Hol, 2011). In the Danish FTD-3 family astrogliosis is observed in all layers of the frontal cortex but the hippocampus and cerebellum are spared (Holm et al., 2007). The hippocampus, although spared of atrophy in Danish FTD-3 pathology, does contain p62-positive inclusions and is the site of extensive neuropathology in a number of neurodegenerative diseases including HD (Hassel et al., 2008) and AD (Muramori et al., 1998). The cerebellum is involved in motor control, gait and balance and is also affected in a number of neurodegenerative diseases including the spinocerebellar ataxias (Orr, 2012). Furthermore the CHMP2B knockout mice demonstrate limb and gait abnormalities (chapter 4). In this study immunohistochemical (IHC) staining for GFAP has been used as a marker of astrogliosis.

Ionized calcium binding adaptor molecule 1 (Iba1) is uniquely expressed in microglia (Ito et al., 1998). In the CNS, microglia have a similar role to macrophages in peripheral tissue; they are highly specialised cells that are greatly influenced by their cellular environment and have a number of distinctive features including their ramified morphology and low level basal occurrence in the absence of pathology (Hanisch and Kettenmann, 2007; Perry et al., 2010). In response to acute brain injury or chronic neurodegenerative disease, microglia are up-regulated resulting in 'activated microglia'. Activated microglia undergo a change in their cellular morphology which is characterised by shortened and

extensively branched processes and hypertrophy of the cell body (Perry et al., 2010).

The presence of activated microglia is a useful indicator of inflammatory pathology. Activated microglia have been observed in a number of chronic neurodegenerative diseases including AD (Thangavel R, 2011), ALS and FTD (Brettschneider et al., 2012). The ability to identify activated microglia using IHC techniques is a useful diagnostic tool (Perry et al., 2010). Accordingly, in this study Iba1 antibody has been used as a marker of activated microglia to identify any evidence for neurodegeneration and neuroinflammation.

Histology panels of the frontal cortex (figures 3.7), CA3 region of the hippocampus (figures 3.8) and the cerebellum (figures 3.9) of *Chmp2b* knockout (*Chmp2b*$^{-/-}$) and *Chmp2b* wild type (*Chmp2b*$^{+/+}$) mice at 12, 18 and 24 months stained with hematoxylin and eosin (H&E), GFAP and Iba1 are shown below.

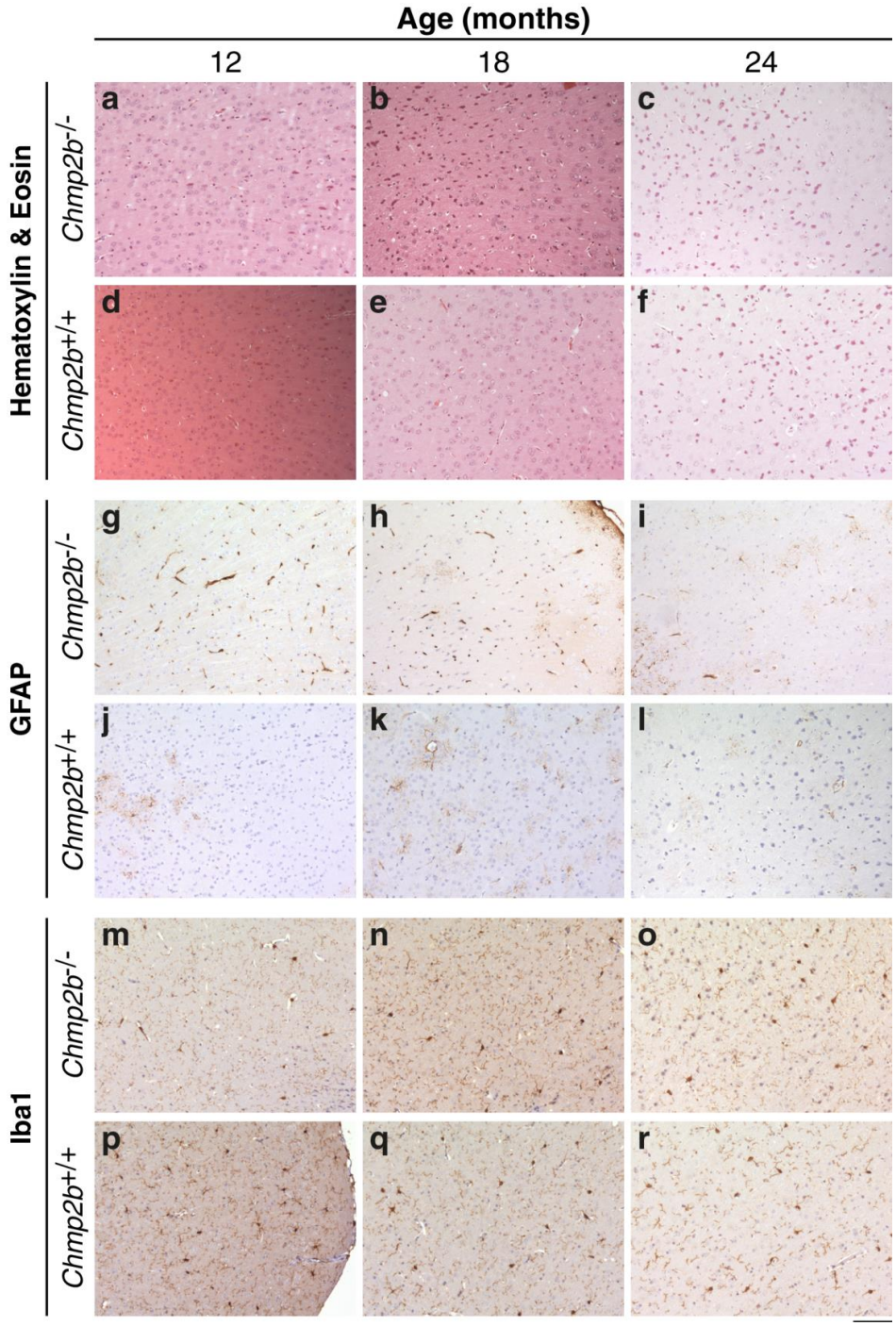

Figure 3.7 Hematoxylin & Eosin (H&E), GFAP and Iba1 staining of the frontal cortex region of *Chmp2b* wild type (*Chmp2b*$^{+/+}$) and *Chmp2b* knockout (*Chmp2b*$^{-/-}$) mice at 12, 18 and 24 months.

No difference is observed in the gross morphology, as assessed by H&E in the frontal cortex of *Chmp2b*$^{-/-}$ mice at any age examined (a-c) compared with the frontal cortex of *Chmp2b*$^{+/+}$ mice at age-matched time points (d-f). Immunostaining with GFAP and Iba1 does not demonstrate increased astrogliosis or activated microglia in *Chmp2b*$^{-/-}$ mice frontal cortex at any time point (g-i; m-o) compared to age-matched *Chmp2b*$^{+/+}$ mice frontal cortex (j-l; p-r). N=3; scale bar=100µm.

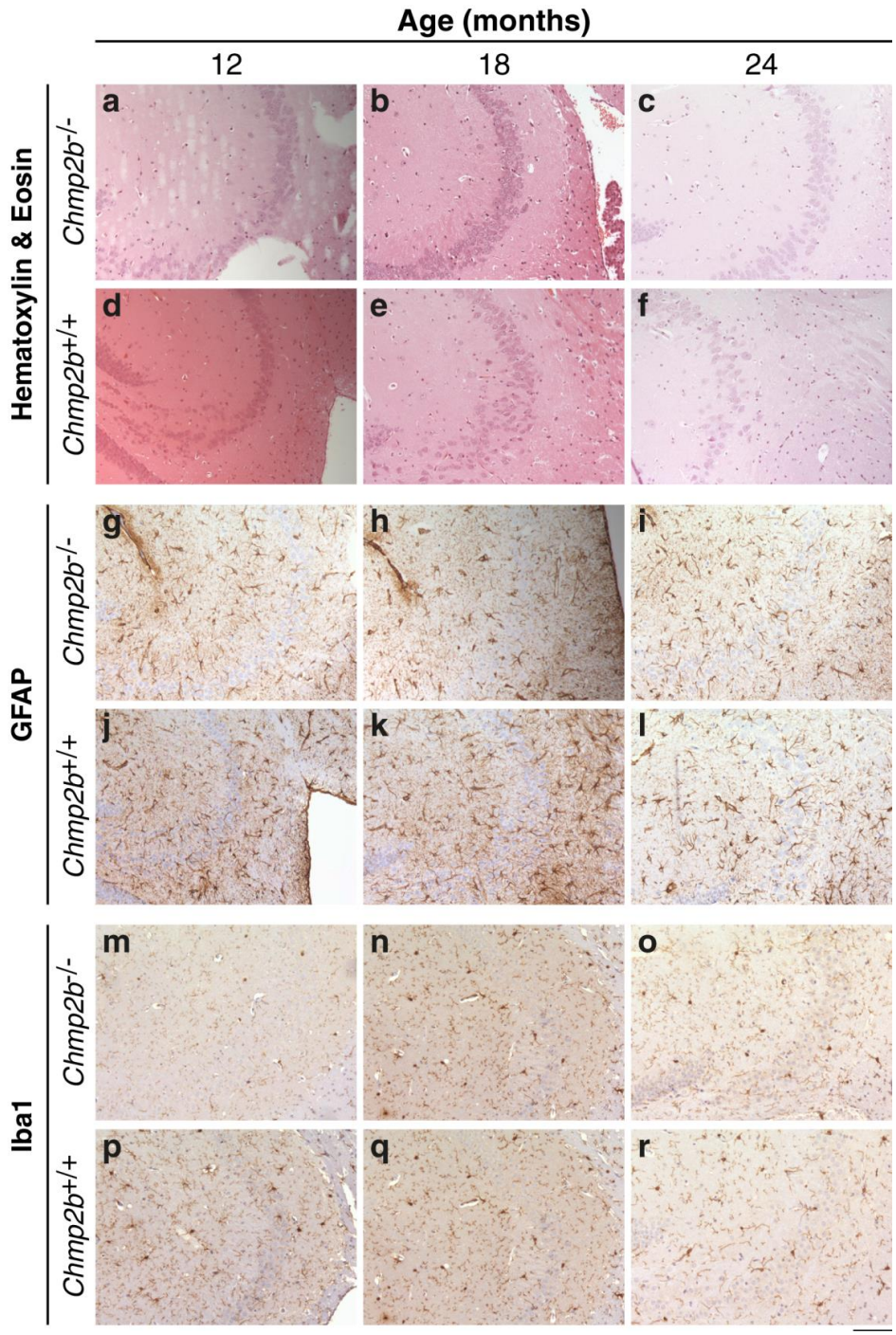

Figure 3.8 Hematoxylin & Eosin (H&E), GFAP and Iba1 staining of the CA3 region of the hippocampus in *Chmp2b* wild type (*Chmp2b*$^{+/+}$) and *Chmp2b* knockout (*Chmp2b*$^{-/-}$) mice at 12, 18 and 24 months.

No difference is observed in the gross morphology, as assessed by H&E in CA3 region of *Chmp2b*$^{-/-}$ mice at any age (a-c) compared with the same region of *Chmp2b*$^{+/+}$ mice at age-matched time points (d-f). Immunostaining with GFAP and Iba1 does not demonstrate increased astrogliosis or activated microglia in *Chmp2b*$^{-/-}$ mice hippocampus at any age (g-i; m-o) compared to age-matched *Chmp2b*$^{+/+}$ mice frontal cortex (j-l; p-r). N=3; scale bar=100µm.

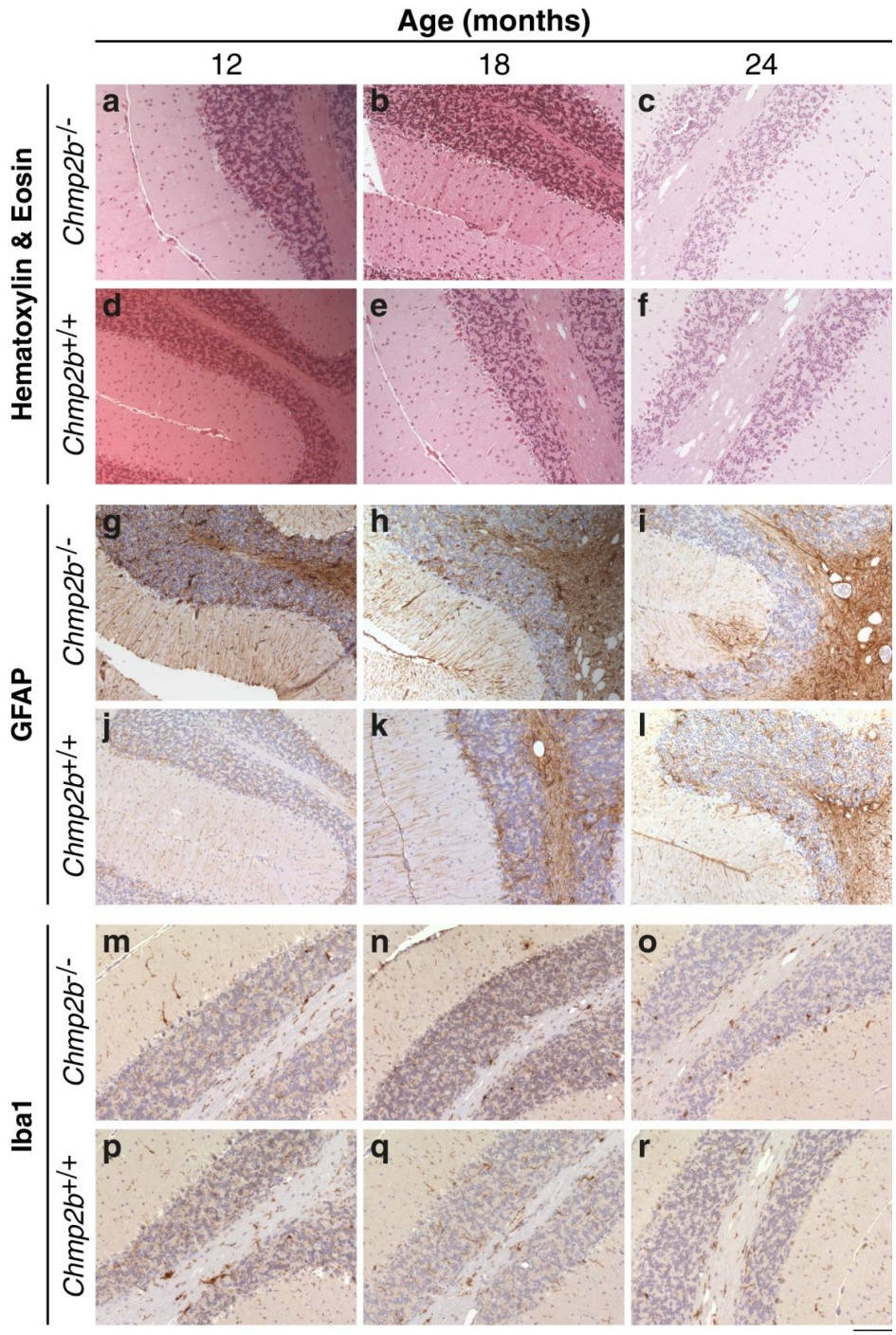

Figure 3.9 Hematoxylin & Eosin (H&E), GFAP and Iba1 staining of the cerebellum in *Chmp2b* wild type (*Chmp2b*$^{+/+}$) and *Chmp2b* knockout (*Chmp2b*$^{-/-}$) mice at 12, 18 and 24 months.

No difference is observed in the gross morphology, as assessed by H&E in the cerebellum of *Chmp2b*$^{-/-}$ mice at any age (a-c) compared with the cerebellum of *Chmp2b*$^{+/+}$ mice at age matched time points (d-f). Immunostaining with GFAP and Iba1 does not demonstrate increased astrogliosis or activated microglia in cerebellum of *Chmp2b*$^{-/-}$ mice (g-i; m-o) compared to age matched *Chmp2b*$^{+/+}$ mice (j-l; p-r). N=3; scale bar=100µm.

Both *Chmp2b* knockout and wild type mouse brains demonstrate a basal increase in GFAP staining with increasing age across all regions analysed (figures 3.7, 3.8 and 3.9). The *Chmp2b* knockout mice show some larger stellate astrocytes and denser GFAP staining in the frontal cortex (figures 3.7g-l) and granule cell layer of the cerebellum (figure 3.9g-l). With increasing age from 12 to 24 months GFAP antibody stains for increasing stellate astrocytes in the frontal cortex of Chmp2b knockout mice (figure 3.10g-l). These observations were not considered significantly different between Chmp2b knockout mice and wild type mice but rather due to aging. All neuropathology was reviewed with a neuropathologist SB to ensure interpretation was correct.

In parallel with GFAP expression, Iba1 expression shows a trend towards increased basal expression with age (12-24 months) in all regions viewed; this is likely due to the normal aging process (figures 3.7m-r, 3.8m-r and 3.9m-r). The microglial cellular morphology is not considered to be consistent with pathological microglial activation which would be expected to show larger microglia with greater branching and an explicit difference when compared with age-matched wild type mice.

In summary, no distinctive pathology is identified in gross or cellular morphology, astrogliosis or microglial activation in *Chmp2b* knockout mouse brains at any of the ages examined.

3.4.1.2 Synaptic density and cell loss

Synaptophysin, also known as major synaptic vesicle protein p38 is a transmembrane glycoprotein highly expressed in neuroendocrine cells and in presynaptic neurotransmitter vesicles of neurons in the brain and spinal cord (Wiedenmann and Franke, 1985; Jahn et al., 1985). Even though the function of synaptophysin has not been fully elucidated, it is known to interact with other synaptic proteins including the v-SNARE vesicle-associated membrane protein 2/synaptobrevin II (VAMP2), suggesting a role in vesicle docking and

neurotransmitter release (Calakos and Scheller, 1994; Washbourne et al., 1995). Synaptophysin has also been implicated in the recycling of synaptic vesicles by associating with dynamin I, a GTPase required for endocytosis (Daly and Ziff, 2002; D'Cruz et al., 2012).

As synaptophysin is extensively expressed in presynaptic nerve terminals it has been adopted as a marker of pre-synaptic density (Calhoun et al., 1996). Studies have reported varying decrease in synaptophysin expression in AD and other neurodegenerative disease brains including HD with dementia and Parkinson's disease (PD) with dementia (Zhan et al., 1993; Masliah et al., 1996).

Calbindin-D28k (molecular mass 28kDa) is an intracellular calcium binding protein that is thought to be involved in trans-cellular calcium transportation and may modulate effects occurring in response to changes in intracellular calcium concentrations as well as having a role in protecting neurons from excitotoxic insult (Mattson et al., 1991; Slomianka et al., 2011). It is expressed both in the peripheral tissues (intestines, kidney), neuroendocrine cells (adrenal glands, the pituitary) as well as in restricted neuronal populations such as Purkinje cells in the cerebellum and mossy fibres of the dentate gyrus (Iacopino et al., 1990; Iacopino and Christakos, 1990; Slomianka et al., 2011).

In aging and neurodegenerative disease, significant decreases have been reported in neuronal calbindin-D mRNA and protein expression (Iacopino et al., 1990; Iacopino and Christakos, 1990). In the aging brain, decrease of calbindin expression is seen in the cerebellum, corpus striatum, and nucleus basalis but not in the neocortex, hippocampus, amygdala, locus ceruleus, or nucleus raphe dorsalis (Iacopino and Christakos, 1990). In neurodegenerative diseases a decrease in calbindin mRNA and protein expression is observed in disease-specific regions; the substantia nigra in Parkinson disease, the corpus striatum in Huntington's disease, the nucleus basalis in Alzheimer's disease and the hippocampus and nucleus raphe dorsalis in Parkinson's disease and Alzheimer's

diseases. However, this decrease in calbindin expression is not seen in the cerebellum, neocortex, amygdala, or locus ceruleus of brains affected by these neurodegenerative disorders (Iacopino et al., 1990; Iacopino and Christakos, 1990).

Since calbindin expression is seen to decrease specifically in brain areas particularly affected during aging and in each of the neurodegenerative diseases, it is thought that decreased calbindin expression may lead to a failure of calcium buffering or intraneuronal calcium homeostasis, which contributes to calcium-mediated excitotoxic neuronal damage during aging and in the pathogenesis of neurodegenerative diseases (Iacopino et al., 1990; Iacopino and Christakos, 1990).

In this study we have examined the expression of synaptophysin in the *Chmp2b* knockout mouse brain (figure 3.10) to investigate whether there is a change in presynaptic density in these mice compared to wild type age-matched mice with increasing age. We have also examined calbindin expression in the brain of *Chmp2b* knockout mice (figure 3.11) as a marker of neuronal integrity and looked for potential cell loss with particular interest in the Purkinje cells of the cerebellum with increasing age.

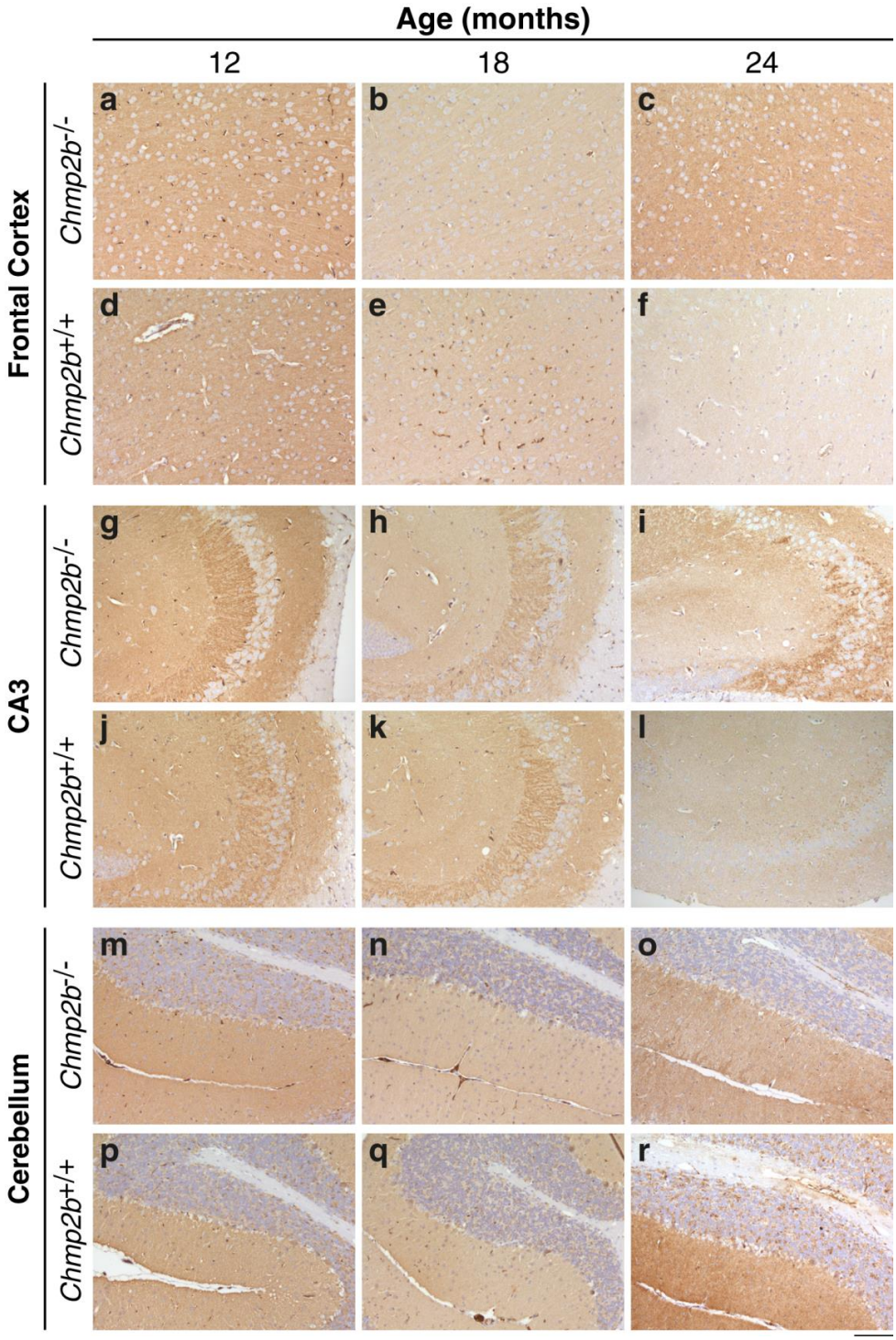

Figure 3.10 Synaptophysin staining in *Chmp2b* knockout (*Chmp2b*$^{-/-}$) and *Chmp2b* wild type (*Chmp2b*$^{+/+}$) mouse brains at 12, 18 and 24 months.

No difference is observed in synaptophysin staining in *Chmp2b*$^{-/-}$ mouse frontal cortex (a-c), CA3 hippocampal region (g-i) or cerebellum (m-o) compared with *Chmp2b*$^{+/+}$ mice at age matched time points. N=3; scale bar=100µm.

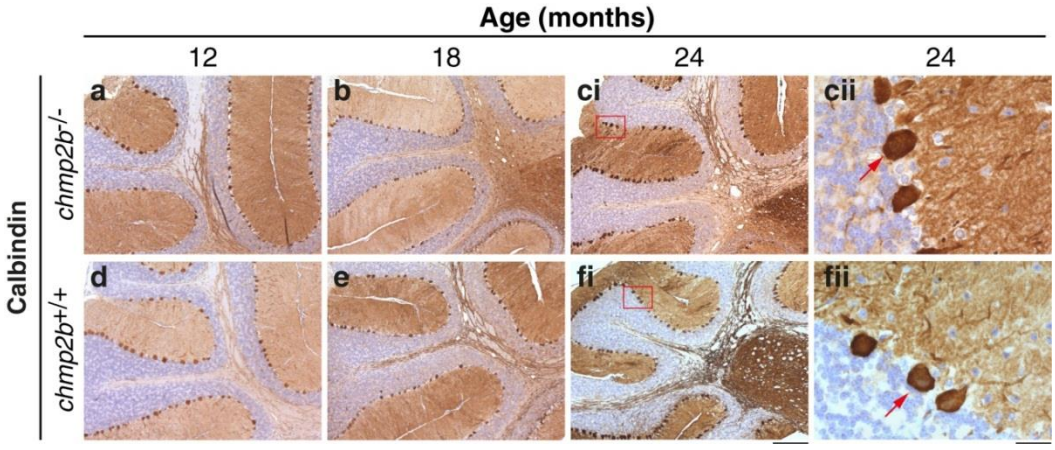

Figure 3.11 Calbindin expression in *Chmp2b* knockout (*Chmp2b*$^{-/-}$) and *Chmp2b* wild type (*Chmp2b*$^{+/+}$) mouse cerebellum at 12, 18 and 24 months.

No difference in calbindin expression is noted in *Chmp2b*$^{-/-}$ mouse cerebellum (a-ci) in comparison with *Chmp2b*$^{+/+}$ mouse (d-fi) at age matched time points. High power images of cerebellar Purkinje cells in *Chmp2b*$^{-/-}$ (cii arrow) and *Chmp2b*$^{+/+}$ (fii arrow) mouse cerebellum at 24 months time point confirms no difference in calbindin expression is noted in *Chmp2b*$^{-/-}$ compared to *Chmp2b*$^{+/+}$ N=3; scale bar=100µm (a-f) and bar= 20µm (cii and fii).

No difference was observed in synaptophysin expression in any of the brain regions examined at any age in *Chmp2b* knockout mice compared to aged matched wild type control mice (figure 3.10). Furthermore, no difference was observed in calbindin expression *Chmp2b* knockout mice compared to wild type age-matched control mice at any time point in any brain region. Representative staining of calbindin staining in the cerebellum is shown in figure 3.11. The Purkinje cell loss phenotype seen in *Atg5* and *Atg7* CNS knockout mice (Hara et al., 2006; Komatsu et al., 2007) is not observed in the *Chmp2b* knockout (figure 3.13).

3.4.1.3 Inclusion pathology: ubiquitin, p62 and TDP-43

Ubiquitin is a small 8.5kDa regulatory protein composed of 76 amino acids found in nearly all eukaryotic cells. It is involved in a vast array of molecular and cellular functions (reviewed in (Rogers et al., 2010)). In yeast and mammals many plasma membrane proteins and receptors destined for degradation are tagged with ubiquitin and directed to either the ubiquitin proteasome system (UPS) or the lysosomal degradation pathway to be broken down and recycled.

One or more ubiquitin molecules bind selectively to proteins, a process termed monoubiquitination and polyubiquitination respectively. The ubiquitin tags act as signals directing proteins and receptors to the proteasome system or lysosomal degradation pathway (reviewed in (Rogers et al., 2010)).

Ubiquitin inclusions localised to the nucleus and cytoplasm are striking pathological features of a significant number of neurodegenerative disorders, including HD, PD, AD, ALS, ataxias, FTLD and FTD-3 (Holm et al., 2007; Nijholt et al., 2011)). Therefore we have used ubiquitin as part of a panel of antibodies that are used in the diagnosis of neuropathological disorders and to investigate whether the depletion of Chmp2b in mice results in ubiquitin inclusions in the mouse brain.

The p62 protein/sequestosome 1 (SQTSM1) (from here on referred to as p62) associates with ubiquitinated proteins and the autophagy marker microtubule associated light chain 3 (LC-3) protein (Pankiv et al., 2007). The C-terminal of the p62 protein contains an ubiquitin association (UBA) amino acid sequence that interacts with ubiquitinated proteins and an LC-3 interacting region (LIR) (also termed the LC3 recognition sequence (LRS) to interact with LC-3 (Tanida et al., 2004a; Tanida et al., 2004b; Ichimura et al., 2008). Ultrastructural data show that p62 is localised to autophagosomes via LC-3 interaction (Komatsu et al., 2007; Nezis et al., 2008; Komatsu and Ichimura, 2010) and that p62 associated with ubiquitinated proteins are transported into autophagosomes suggesting that p62 may act as a receptor for ubiquitinated proteins to be degraded by lysosomes via autophagy (Bjorkoy et al., 2005; Pankiv et al., 2007; Komatsu and Ichimura, 2010).

As p62 is localised to autophagosomes through its interaction with LC-3 and constantly degraded by the autophagosome-lysosome system, disrupting autophagy results in the accumulation of p62 inclusions (Komatsu et al., 2007;

Nezis et al., 2008). Furthermore, mutations in the LRS region of p62 also result in inclusion formation even in the presence of functioning autophagy system. This is thought to be due to p62-LRS mutant escaping efficient autophagy leading to its build up and inclusion formation (Ichimura et al., 2008; Komatsu and Ichimura, 2010).

In FTD-3 human brains, p62 inclusions co-localise with ubiquitin aggregates (Holm et al., 2007), therefore p62 has been used as (1) a marker of pathology and (2) because of its localisation to autophagosomes and interaction with LC-3, it is also used as a surrogate marker of autophagy (Komatsu and Ichimura, 2010). As part of our panel of antibodies, we did attempt to optimise a number of commercially available LC-3 antibodies for immunohistochemistry as a marker of autophagosomes and autophagy but regrettably, none of the antibodies proved successful for IHC in formalin fixed paraffin-embedded tissue in our hands.

The Transactivation response (TAR) *DNA* binding protein with molecular weight 43kDa (TDP-43/TARDTBP) was identified by Neumann and colleagues in 2006 as the component of ubiquitin inclusions (Neumann et al., 2006) in most cases of FTLD with ubiquitin inclusions and in most cases of ALS. TDP-43 is a highly conserved neuronal nuclear protein involved in numerous cellular processes and is ubiquitously expressed in tissues including neurons and glial cells (Buratti et al., 2001; Buratti et al., 2004; Mercado et al., 2005).

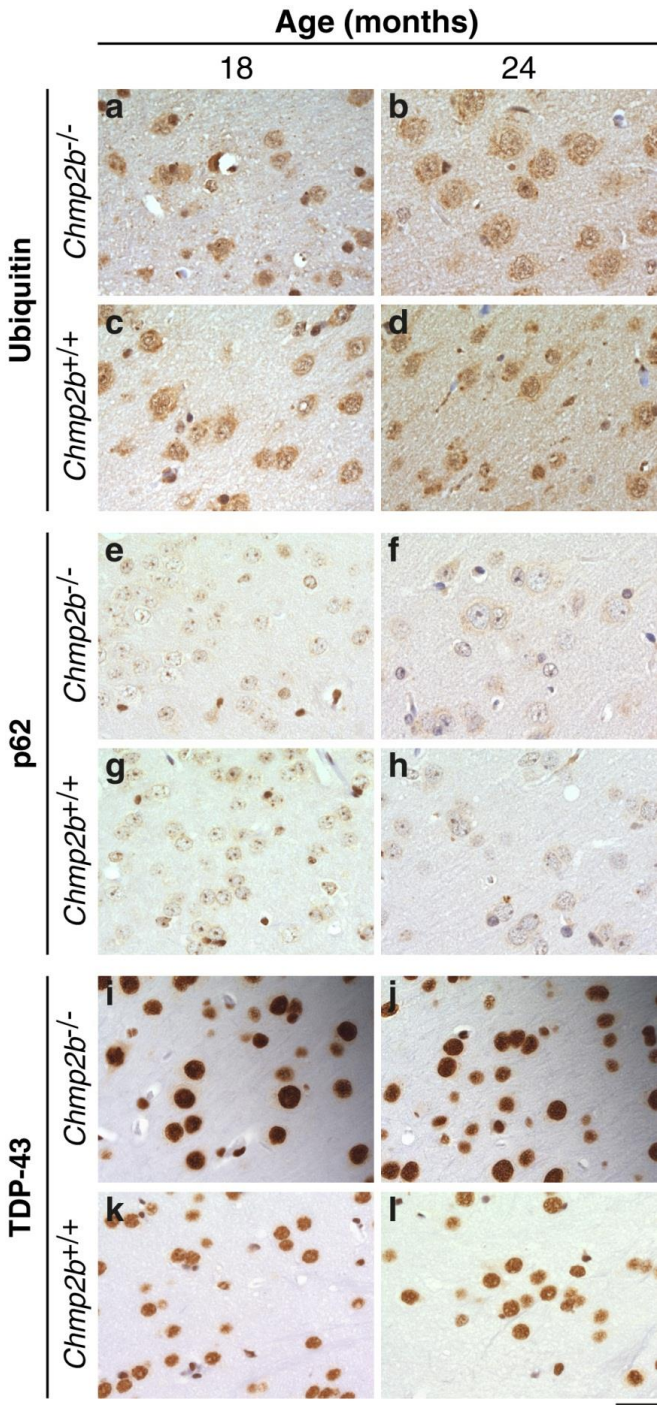

Figure 3.12 Ubiquitin, p62 and TDP-43 staining in the frontal cortex of *Chmp2b* wild type (*Chmp2b*$^{+/+}$) and *Chmp2b* knockout (*Chmp2b*$^{-/-}$) mice at 18 and 24 months of age.

Ubiquitin and p62 inclusions are not observed in the frontal cortex of either *Chmp2b*$^{-/-}$ or *Chmp2b*$^{+/+}$ at any age (a-h). Immunostaining with TDP-43 demonstrates normal nuclear staining but no pathological staining at any age (i-l). Scale bar = 20µm.

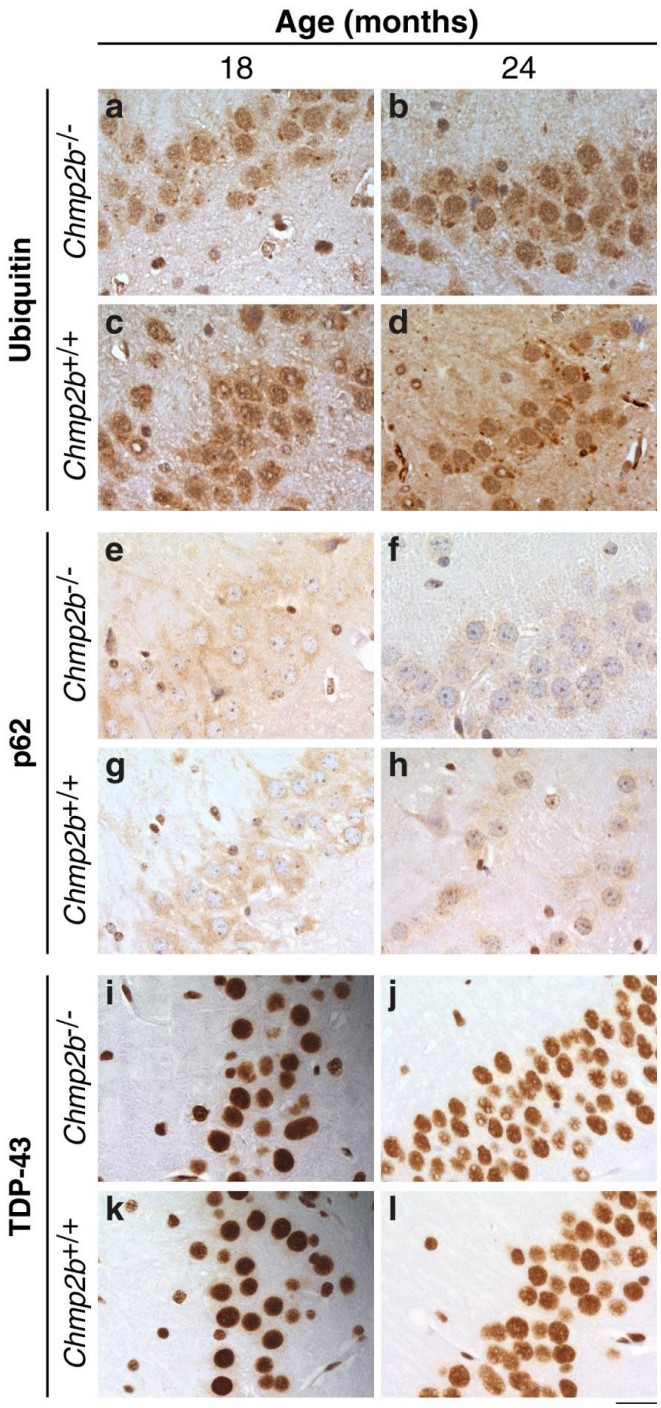

Figure 3.13 Ubiquitin, p62 and TDP-43 staining in the CA3 region of the hippocampus of *Chmp2b* wild type (*Chmp2b*$^{+/+}$) and *Chmp2b* knockout (*Chmp2b*$^{-/-}$) mice at 18 and 24 months.

Ubiquitin and p62 inclusions are not observed in the CA3 region of *Chmp2b*$^{-/-}$ or *Chmp2b*$^{+/+}$ at any age (a-h). Immunostaining with TDP-43 demonstrates normal nuclear staining but no pathological staining at any age (i-l). Scale bar = 20μm.

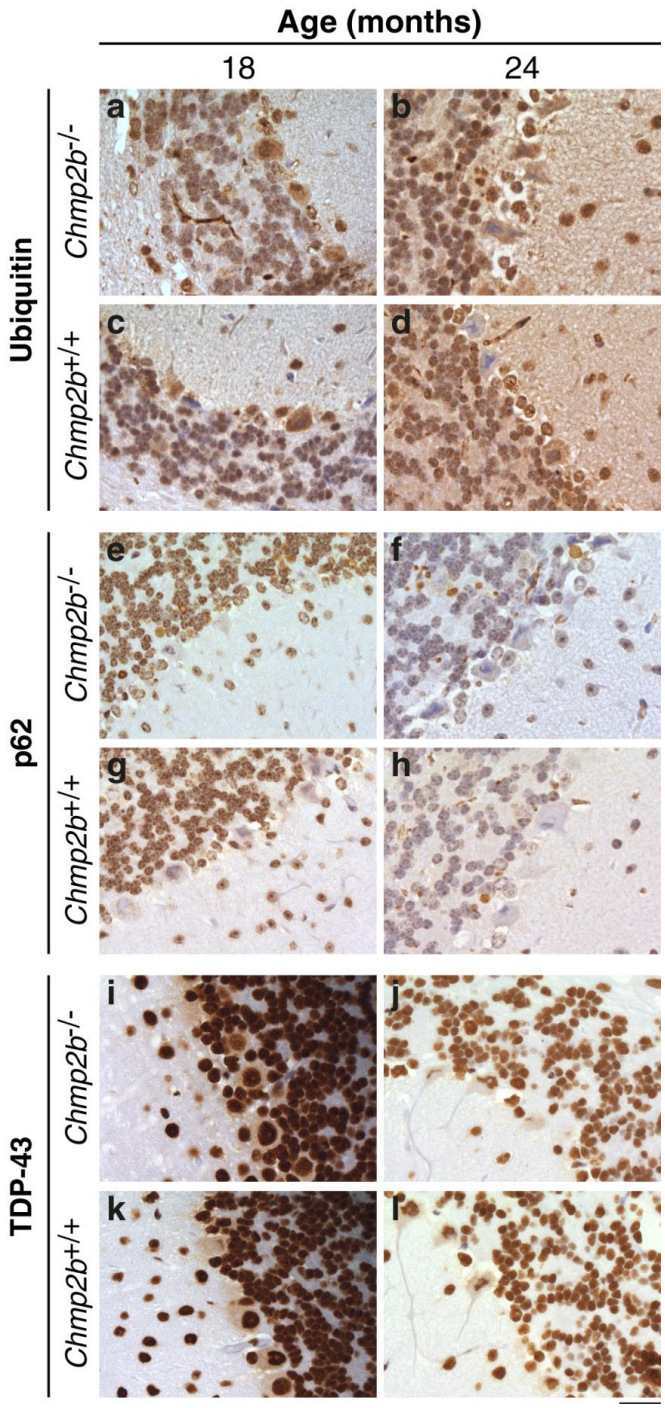

Figure 3.14 Ubiquitin, p62 and TDP-43 staining in the cerebellum of *Chmp2b* wild type (*Chmp2b*$^{+/+}$) and *Chmp2b* knockout (*Chmp2b*$^{-/-}$) mice at 18 and 24 months.

Ubiquitin and p62 inclusions are not observed in the cerebellum of *Chmp2b*$^{-/-}$ or *Chmp2b*$^{+/+}$ at any age (a-h). Immunostaining with TDP-43 demonstrates normal nuclear staining but no pathological staining at any age (i-l). Scale bar = 20µm.

Ubiquitin (figures 3.12a-b, 3.13a-b and 3.14a-b) and p62 (figures 3.12e-f, 3.13e-f and 3.14e-f) neuronal cytoplasmic inclusions (NCI) and nuclear inclusions (NI) are not observed in *Chmp2b* knockout brains in any region examined. Diffuse cytoplasmic staining is retained and the pattern and frequency of ubiquitin and p62 staining likely represent normal physiological staining. This is supported by the observation that the ubiquitin (figures 3.12c-d, 3.13c-d and 3.14c-d) and p62 (figures 3.12g-h, 3.13g-h and 3.14g-h) staining patterns are also present in age-matched wild type *Chmp2b* mouse brains.

FTD-3 cases are found to be negative for pathologic TDP-43 staining, however as TDP-43 positive inclusions are found in tau negative, ubiquitin positive FTLD cases and that TDP-43 is associated with ubiquitin inclusions, we have included TDP-43 in our panel of antibodies. In this study TDP-43 staining shows strong nuclear localisation in both *Chmp2b* knockout and wild type control mice in all regions viewed. No characteristic pathologic TDP-43 staining is identified as reported by Sampathu and colleagues (2006) (Sampathu et al., 2006) and Neumann and colleagues (2006) (Neumann et al., 2006) in the *Chmp2b* knockout or wild type mice at any age examined.

3.4.1.4 Endosome markers

Mannose-6-phosphate (M6P) receptors (M6PR) are integral membrane glycoproteins. Two M6P receptors are recognised; the ~46kDa cation-dependent M6PR (CD-M6PR) and the ~300kDa cation-independent M6PR (CI-M6PR) (Ghosh et al., 2003). M6PR are multifunctional receptors involved in a vast array of cellular processes, one function which CI-M6PR and CD-M6PR share is that they bind to newly synthesized lysosomal hydrolases in the trans-Golgi network (TGN) and deliver them to pre-lysosomal compartments. Subsequently, lysosomal hydrolases are delivered through the endocytic pathway into lysosomes (Ghosh et al., 2003). Hydrolases are recognised by M6PR through binding of their M6P recognition moieties to the receptors. Then the ligand-receptor complex is packaged into molecular carriers that transport their cargo to target endosomes,

followed by recycling of receptors back to the TGN. M6PR sorting is directed by several sorting signals in the cytoplasmic tail of the receptor (Ghosh et al., 2003).

Although M6PR shuttles between early endosomes, TGN, recycling endosomes, late endosomes and the plasma membrane and is notably absent in lysosomes, the steady state distribution of MPRs is predominantly within late endosomes. Therefore it is used as a marker of late endosomes (Ghosh et al., 2003).

Enlarged endosomes positive for M6PR have been identified in human FTD-3 brains and fibroblasts (Holm et al., 2007; Urwin et al., 2010a). In this study M6PR immunostaining has been used as a marker of late endosomes and to investigate whether the enlarged endosome phenotype identified in human tissues is also present in the mouse models. The M6PR antibody (MA1-066 Cambridge Bioscience/Fisher Scientific) used was generated using purified bovine ~300kDa Cl-MPR as the immunogen and recognizes an epitope in the extracellular domain of CI-MPR (M6PR MA1-066 datasheet).

The lysosome associated membrane protein 1 (LAMP-1) is a type I transmembrane protein with a large luminal domain, a transmembrane domain and a C-terminal cytoplasmic tail. LAMP-1 is a 40kDa major lysosomal protein localised to the lysosome limiting membrane. Post glycosylation, the mass of LAMP-1 glycoprotein increases to 120kDa. Late endosome and lysosome limiting membranes are thought to be important in separating the potent acid hydrolases in lysosomes from other cellular constituents (Eskelinen, 2006). Lysosome associated membrane protein 2 (LAMP-2) another lysosomal transmembrane glycoprotein shares significant homology with LAMP-1. These two lysosomal membrane proteins are thought to be involved in the interaction, maturation and fusion of the lysosomes with each other as well as with other cellular compartments including endosomes, phagosomes and the plasma membrane in the endocytosis and phagocytosis pathways (Jager et al., 2004; Eskelinen et al., 2006; Saftig et al., 2008). It is estimated that LAMP-1 and LAMP-

2 contribute up to 50% of total lysosomal proteins (Hunziker et al., 1996) and that the presence of LAMP proteins is a key definition of lysosome compartments (Kornfeld and Mellman, 1989).

Mice deficient in LAMP-1 are found to be viable and fertile and except for mild astrogliosis, tissues do not demonstrate explicit pathology, however an up regulation of LAMP-2 is observed in the kidney, spleen and heart (Andrejewski et al., 1999; Eskelinen, 2006). Strikingly, LAMP-2 deficient mice show a severe phenotype, with 50% mortality at 20-40 days and extensive accumulation of autophagic vacuoles in multiple peripheral organs (Eskelinen, 2006; Saftig et al., 2008). These observations suggest that LAMP-2 is able to compensate for the loss of LAMP-1 but not *vice versa*. Furthermore, double LAMP-1/LAMP-2 deficient mice are embryonic lethal at E14.5-E16.5 and exhibit enlarged autophagic vacuoles (Eskelinen et al., 2004; Eskelinen, 2006).

Early endosomes are a major sorting compartment from which cellular proteins and receptors are transported to lysosomes for degradation or recycled to the plasma membrane. Early Endosome Antigen 1 (EEA1) is an evolutionarily conserved 180kDa protein identified on early endosomes (Raiborg et al., 2001; Stinton et al., 2004).

EEA1 co-localizes with transferrin receptor and Rab5 (early endosome) but not Rab7 (late endosome) (Mu et al., 1995). It is a hydrophilic peripheral membrane protein present in cytosol and membrane fractions. Immunoelectron microscopy reveals EEA1 is associated with tubulovesicular early endosomes (Mu et al., 1995). Autoantibodies to EEA1 have been associated with neurological diseases including Multiple Sclerosis (MS) and Lower Motor Neuron (LMN) disease (Selak et al., 1999).

Other endosomal markers were also tested including late endosome markers Rab-7 and CD63, and lysosome marker LAMP-2. However, the commercially

available antibodies tested did not produce reproducible staining and could not be suitably optimised to be included in our panel of antibodies (data not shown). In this study we have looked at the immunohistological expression of early (EEA1) and late (M6PR and LAMP-1) endosome markers to probe whether the depletion of *Chmp2b* in mice results in endosome pathology.

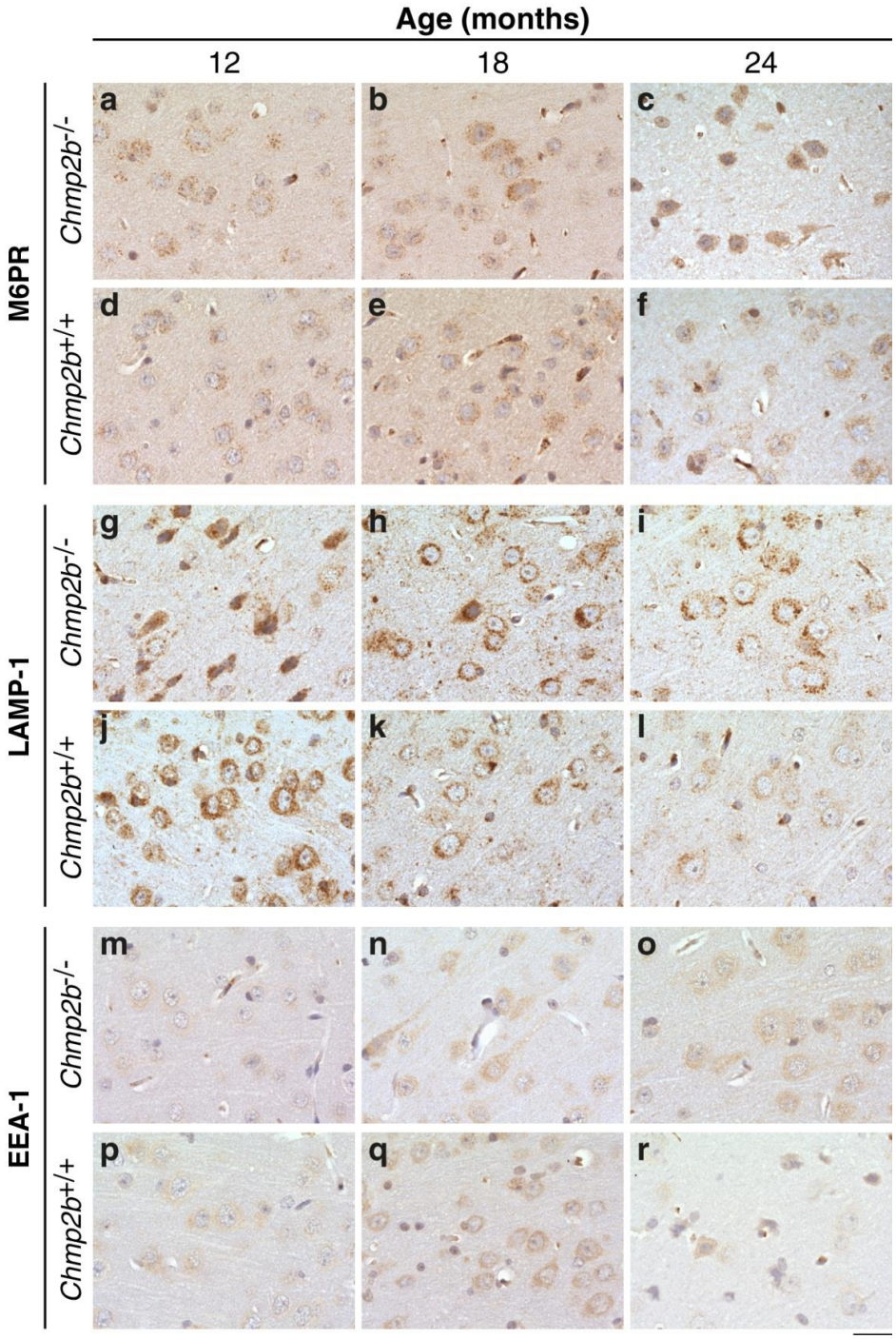

Figure 3.15 M6PR, LAMP-1 and EEA1 endosome markers in the frontal cortex of *Chmp2b* wild type (*Chmp2b*$^{+/+}$) and *Chmp2b* knockout (*Chmp2b*$^{-/-}$) mice at 12, 18 and 24 months.

Endosome markers M6PR (a-f), LAMP-1 (g-l) and EEA1 (l-r) are seen as small punctate granular staining clustering in the perinuclear region and neuronal cell body of cortical neurons and neurites to varying intensity. M6PR is a marker of late endosomes, LAMP-1 is associated with lysosomal membranes and EEA1 an established marker of early endosomes. No difference is observed between *Chmp2b*$^{-/-}$ and *Chmp2b*$^{+/+}$ with any of the markers used. scale bar=20µm.

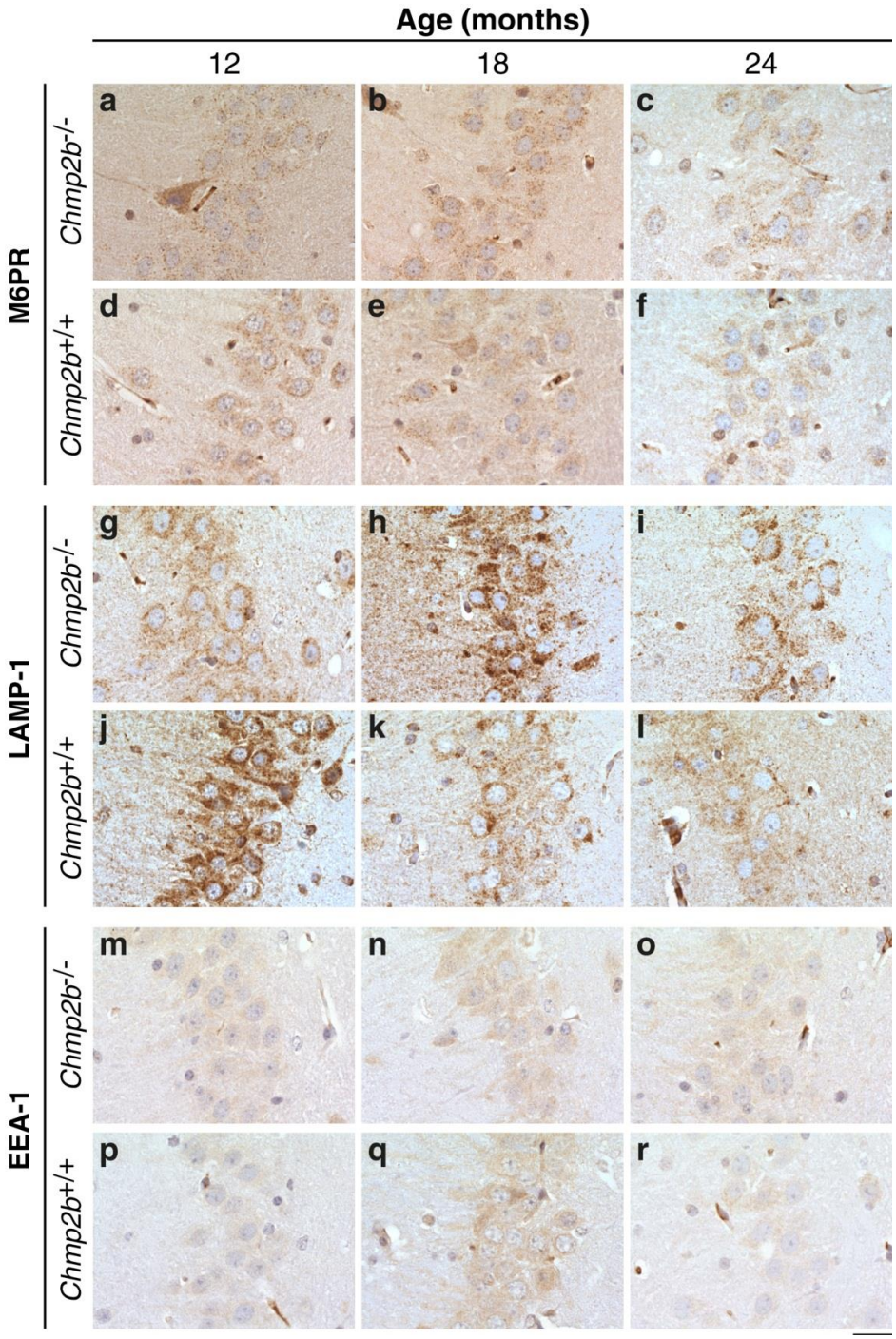

Figure 3.16 M6PR, LAMP-1 and EEA1 endosome markers in CA3 region of the hippocampus of *Chmp2b* wild type (*Chmp2b*$^{+/+}$) and *Chmp2b* knockout (*Chmp2b*$^{-/-}$) mice at 12, 18 and 24 months.

Endosome markers M6PR (a-f), LAMP-1 (g-l) and EEA1 (l-r) are seen as small punctate granular staining clustering in perinuclear and neuronal cell body regions in the molecular layer, granule cell layer and long mossy fibres of the hippocampus to varying intensities. No difference is observed between *Chmp2b*$^{-/-}$ and *Chmp2b*$^{+/+}$ with any of the markers. scale bar=20µm.

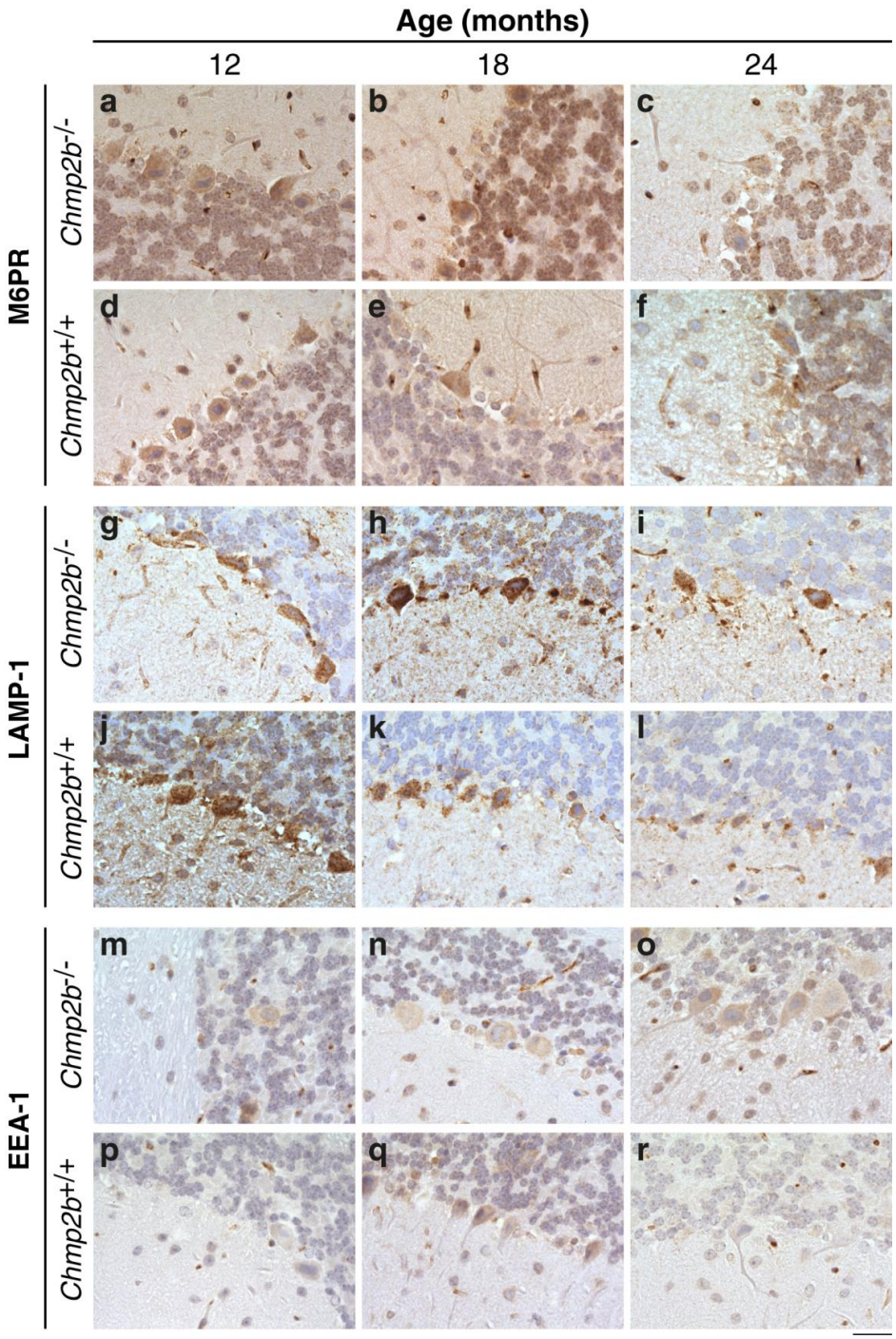

Figure 3.17 M6PR, LAMP-1 and EEA1 endosome markers in the cerebellum of *Chmp2b* wild type (*Chmp2b*$^{+/+}$) and *Chmp2b* knockout (*Chmp2b*$^{-/-}$) mice at 12, 18 and 24 months.

Endosome markers M6PR (a-f), LAMP-1 (g-l) and EEA1 (l-r) are seen as small punctate granular staining clustering in perinuclear and neuronal cell body regions of Purkinje cells, in the cerebellar molecular layer and within the branches of climbing and mossy fibres. No difference is observed between *Chmp2b*$^{-/-}$ and *Chmp2b*$^{+/+}$ with any of the markers. scale bar=20µm.

The endosome and lysosome markers applied, M6PR, LAMP-1 and EEA1 staining are seen as small granular speck-like perinuclear staining with prominent localisation to the neuronal cell body. Some nuclear staining is also evident, however it is also noted that not all nuclei are stained.

In the frontal cortex, large cortical neurons demonstrate positive staining in the neuronal cell body for M6PR, LAMP-1 and EEA1. In the CA3 region of the hippocampus all three endosome markers are present in the molecular layer, granule cell layer and long mossy fibres to varying intensities. This distribution likely reflects the dynamic endosomal activity in transporting and degrading proteins. In a comparable manner M6PR, LAMP-1 and EEA1 are present in the Purkinje cells of the cerebellum, in the cerebellar molecular layer and within the branches of climbing and mossy fibres. No discernible difference is noted in endosome or lysosome staining between *Chmp2b* knockout and wild type brain regions at any age examined. To determine whether morphological changes other than gross enlargement of endosomes/lysosomes occurs, electron microscopic immunogold labelling would need to be applied.

3.4.2 Lumbar spinal cord pathology

The *Chmp2b* knockout mice show a distinctive predominantly lower limb abnormal phenotype most strikingly observed in their gait (chapter 4).

Therefore the ventral horn of lumbar and thoracic spinal cord where motor neurons reside was examined to investigate the possible pathological basis of the gait abnormality identified in the *Chmp2b* knockout mice at 12, 18 and 24 months in comparison to age-matched wild type mice. Data for lumbar spinal cord region only is presented in this chapter.

The spinal cord was dissected and fixed in 10% buffered formalin (as detailed in chapter 2) and subsequently the cervical, thoracic and lumbar regions were

dissected, embedded in paraffin and sectioned. Figure 3.18 shows a representative image of the lumbar spinal cord at low power magnification (x2.5) demonstrating the distinctive butterfly shape of the grey matter and the surrounding white matter, and high power magnification (x40) showing motor neurons with nissl stain.

In a consistent manner to examining the mouse brains, a panel of antibodies as described in section 3.4.1 was used to investigate the histological basis of the spinal cord pathology. H&E staining was used to examine gross morphology and cyto-architecture of the lumbar spinal cord region (figure 3.19). GFAP was used to investigate the presence of astrogliosis (figure 3.20) and Iba1 was used to reveal activated microglia (figure 3.21). Ubiquitin and p62 immunostaining was used to identify neurodegenerative inclusions and M6PR expression used as a marker of late endosomes (figure 3.22).

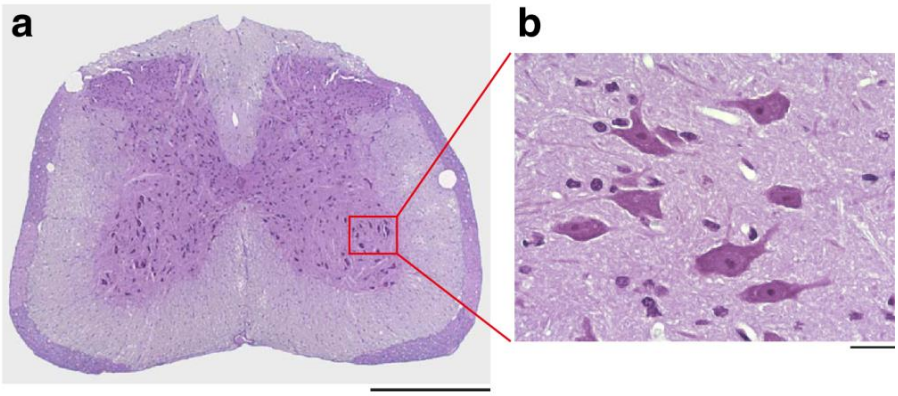

Figure 3.18 Cresyl violet staining of the lumbar spinal cord at low and high magnification.

Cresyl violet staining of the lumber region of the spinal cord shows (a) the classic butterfly shape with grey matter of the spinal and surrounding white matter. The motor neurons reside within the ventral horn of the spinal cord- red boxed region a; and high power magnification showing motor neurons (b) . Scale bars a=500µm and b=20µm.

3.4.2.1 Gross morphology, astrogliosis and activated microglia

Haematoxylin and Eosin staining was used to examine gross cellular morphology and GFAP and Iba1 staining were used to examine the presence of astrogliosis and activated microglia in the lumbar spinal cord of the *Chmp2b* knockout mice at 12, 18 and 24 months to determine whether the gait abnormality is the result of inflammatory or degenerative pathology.

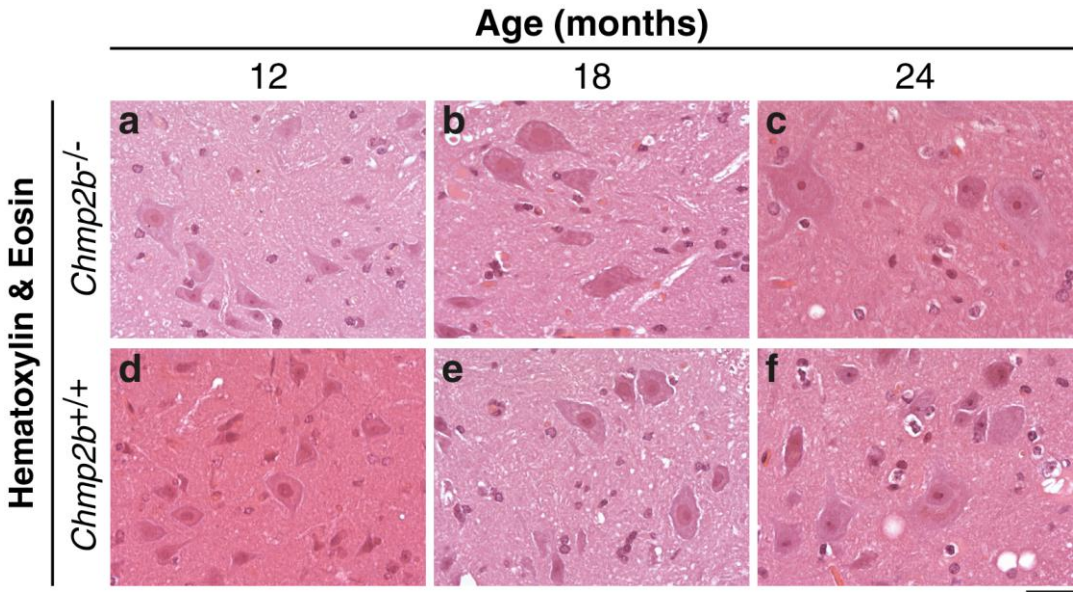

Figure 3.19 Haematoxylin and Eosin staining of lumbar spinal cord.

Ventral horn of the lumbar spinal cord showing intensely stained lower motor neurons (a-f). No difference is observed in $Chmp2b^{-/-}$ (a-c) and $Chmp2b^{+/+}$ (d-f) at any age examined. Scale bar =20µm.

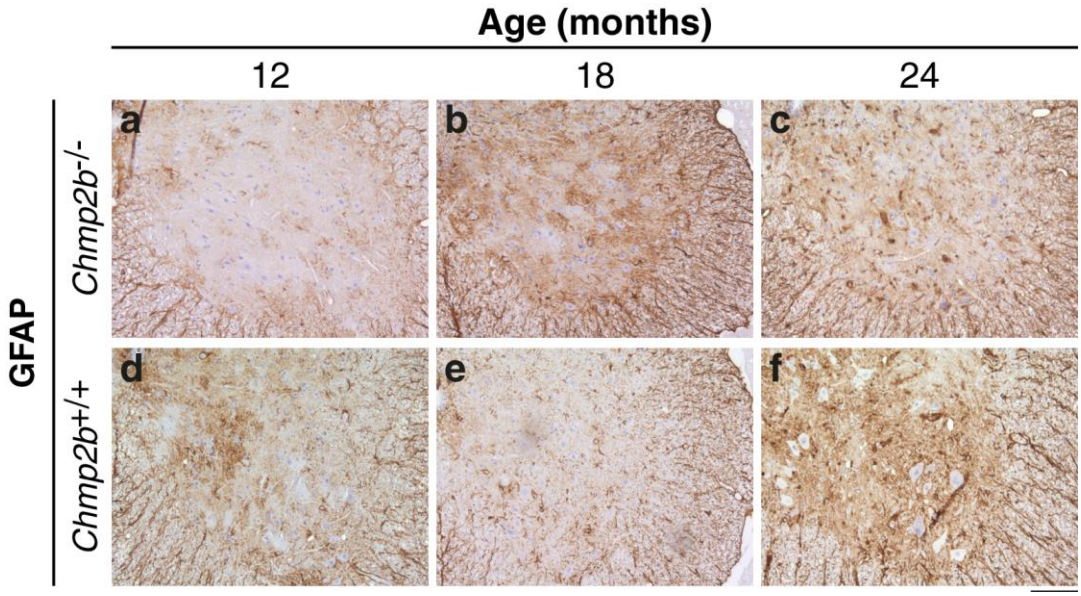

Figure 3.20 GFAP expression in the lumbar spinal cord.

Ventral horn of the lumbar spinal cord reveals an increase of GFAP expression with age in both *Chmp2b*$^{-/-}$ (a-c) and *Chmp2b*$^{+/+}$ (d-f), this increase in GFAP expression is consistent with natural aging and not considered to be pathologic. Scale bar =100µm.

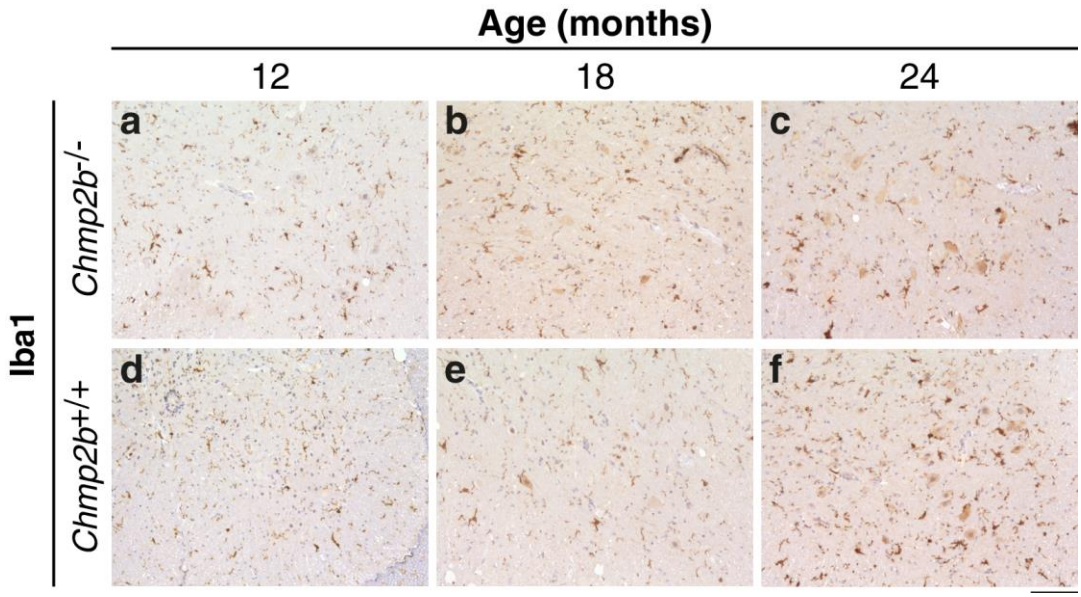

Figure 3.21 Iba1 expression in the lumbar spinal cord.

Ventral horn of the lumbar spinal cord reveals a moderate increase in Iba1 expression with age in both *Chmp2b*$^{-/-}$ (a-c) and *Chmp2b*$^{+/+}$ mice (d-f), this increase in Iba1 expression is consistent with natural aging and is not considered to be pathologic. Scale bar =100µm.

H&E staining does not reveal any distinctive pathology in the ventral horn of the lumbar spinal cord (figure 3.19). Furthermore, the expression of both GFAP and Iba1 is seen to increase with increasing age in both *Chmp2b* knockout and wild type mice (figure 3.20 and 3.21). The increase in expression of GFAP and Iba1 in the spinal cord of *Chmp2b* knockout mice and wild type mice is not considered to be consistent with pathological inflammation, as advised by consultant neuropathologist SB, and is considered consistent with normal aging.

In summary, no pathological difference is identified in gross or cellular morphology, astrogliosis or microglial activation in the *Chmp2b* knockout lumbar spinal cord at any age examined.

3.4.2.2 Ubiquitin, p62 and M6PR

The lumbar spinal cord was examined for the presence of ubiquitin and p62 inclusions to investigate whether the gait phenotype correlates with inclusion formation typical of neurodegenerative disease. Motor neurons in the ventral horn of the lumbar spinal cord in *Chmp2b* knockout mice do not exhibit ubiquitin or p62 inclusions characteristic of neurodegenerative disease at any age examined.

M6PR expression in the lumbar spinal cord of *Chmp2b* knockout mice was examined as a marker of late endosome expression (Ghosh et al., 2003) and showed no difference to wildtype controls.

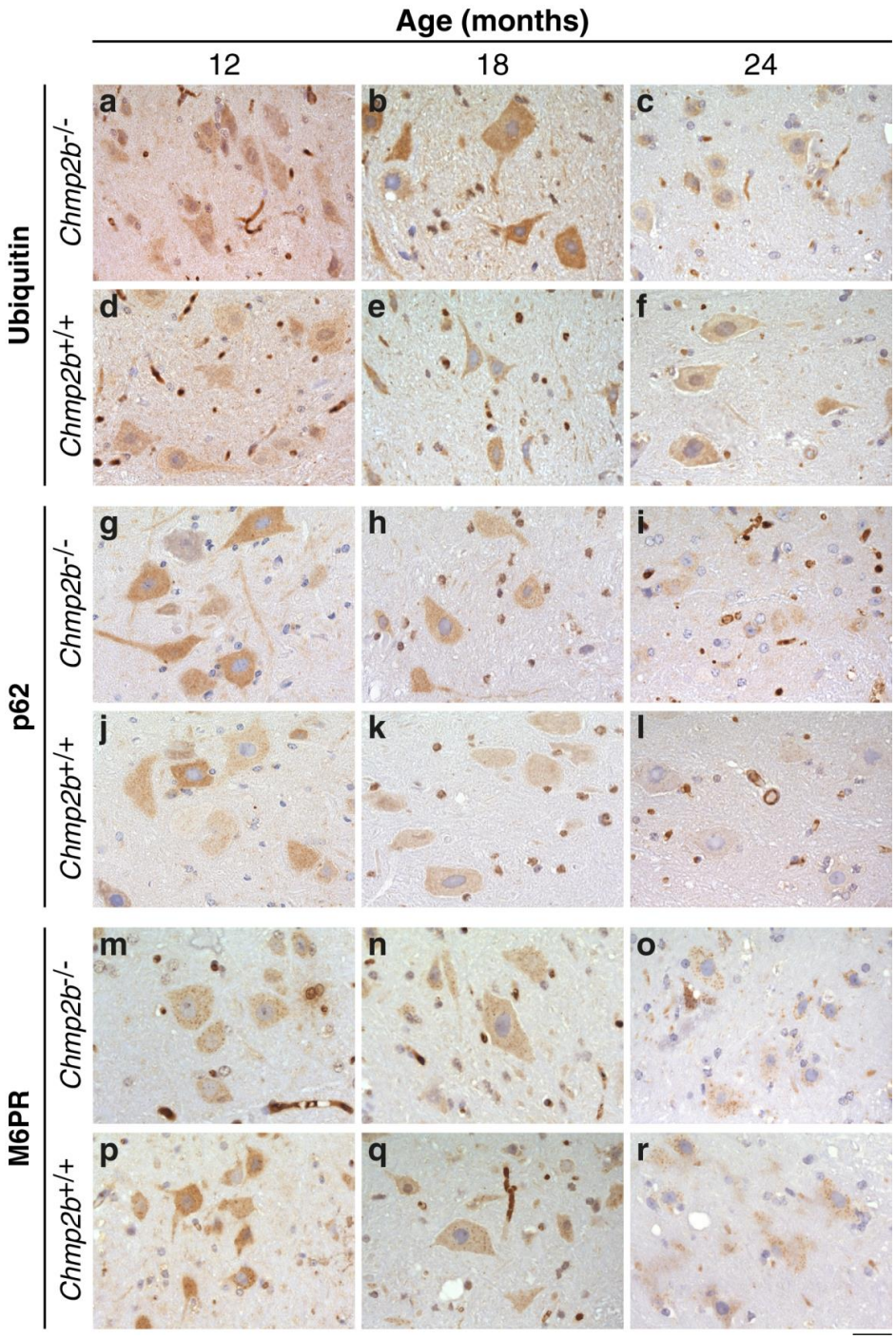

Figure 3.22 Ubiquitin, p62 and M6PR expression in the lumbar spinal cord.

Ventral horn of the lumbar spinal cord reveals a sparse number of ubiquitin (a-f) and p62 (g-l) inclusions in motor neuron cell bodies and grey matter of the ventral horn. These inclusions are present in both *Chmp2b*$^{-/-}$ and *Chmp2b*$^{+/+}$ across all ages examined (a-l). M6PR expression is seen as punctate-granular staining most evident in the large motor neurons, no difference in M6PR expression is evident between *Chmp2b*$^{-/-}$ and *Chmp2b*$^{+/+}$ at any age examined (m-r). Scale bar =20µm.

3.4.3 Sciatic nerve pathology

The sciatic nerve begins in the lower back and runs through the gluteus and down the lower limb. It is the longest and widest single nerve in the body, starting from the top of the leg to the foot on the posterior aspect. The sciatic nerve supplies nearly the whole of the leg, including skin, muscles, and the back of the thigh right down to the foot (Drake et al., 2009).

Sciatic nerve samples were processed in araldite resin and semi-thin (approximately 1 μm) transverse sections stained with toluidine blue and examined under LM.

In peripheral neuropathy, toluidine blue demonstrates axonal loss with typical features including disintegration of the myelin sheath forming oval fragments of myelin and cellular debris. We examined the mouse sciatic nerve to determine whether the abnormal gait in the *Chmp2b* knockout mice may be due to peripheral nerve pathology degeneration.

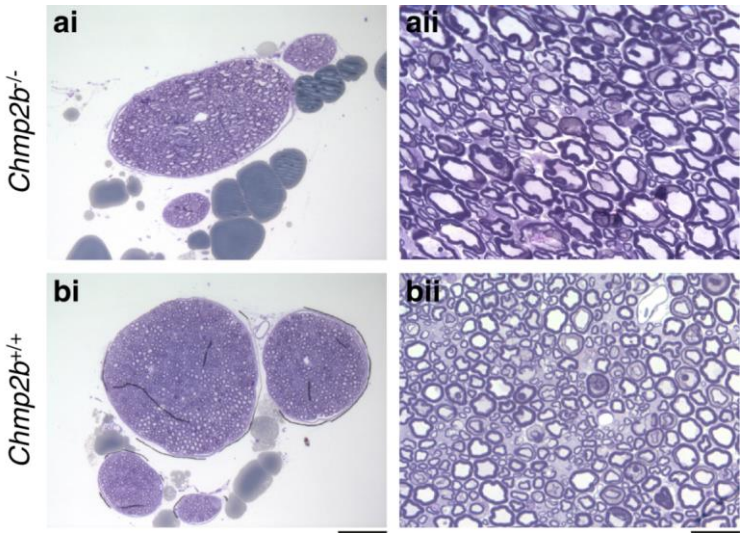

Figure 3.23 Toluidine blue stain of sciatic nerve transverse section at 24-month time point at low and high power magnification.

Low power mouse sciatic nerve demonstrates the gross morphology of the sciatic nerve (ai and bi). High power reveals transverse axons with myelin sheaths (aii and bii). No distinctive difference is noted between *Chmp2b*$^{-/-}$ and *Chmp2b*$^{+/+}$ at 24 months of age. Scale bar; ai and bi =100μm; aii and bii =20μm.

Toluidine blue staining of sciatic nerve does not reveal any distinctive pathology in *Chmp2b* knockout mice at 24 months (figure 3.23).

3.4.4 Muscle pathology

Finally, we examined the quadriceps to determine if the *Chmp2b* knockout mice have muscle pathology. Skeletal muscles such as the quadriceps are neatly aligned long fibres with multiple pericellular nuclei. Critically, skeletal muscles are predominantly post mitotic cells. In the event of muscle damage these long muscle fibres re-enter the cell cycle and undergo mitosis in an effort to repair damage. Damage in skeletal muscle is seen as regions of shorter muscle fibres with centrally located nuclei.

H&E staining is particularly informative in skeletal muscle histology. Hematoxylin and eosin distinguish the muscle fibre nuclei and cytoplasm and connective tissue respectively with good clarity. H&E staining was used on *Chmp2b*$^{-/-}$ and *Chmp2b*$^{+/+}$ mouse quadriceps to reveal any gross pathologic changes (figure 3.25).

H&E staining did not reveal any histological changes consistent with inflammation, damage or degeneration in the *Chmp2b*$^{-/-}$ mouse quadriceps. Specifically, there is no neutrophil infiltration or centrally located nuclei in muscle fibres at any time point examined (figure 3.24).

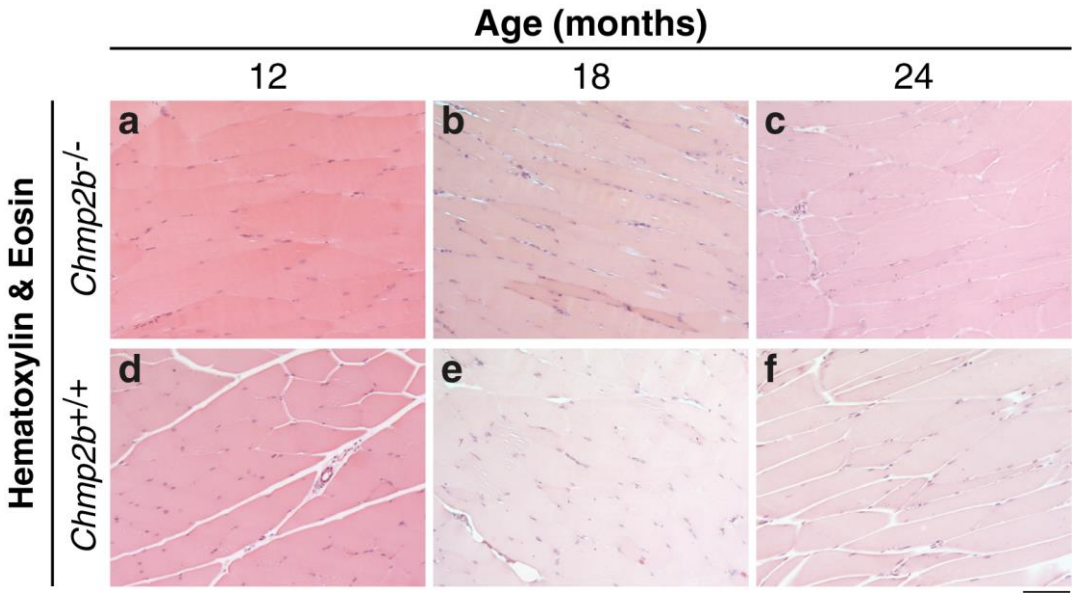

Figure 3.24 H&E staining of quadriceps longitudinal section at 12, 18 and 24 months.

No distinctive gross pathology is observed in the *Chmp2b*$^{-/-}$ and *Chmp2b*$^{+/+}$ quadriceps at any age examined. Scale bar= 20µm.

3.5 Chapter Discussion

C-terminal truncating mutations in *CHMP2B* were first identified in a Danish family presenting with clinical symptoms of FTD and distinctive neuropathology at post-mortem (Gydesen et al., 2002; Skibinski et al., 2005; Holm et al., 2007). To evaluate whether *CHMP2B* mutations result in the loss of function of the native CHMP2B protein and to investigate the function of the native Chmp2b protein, *Chmp2b* knockout mice were generated and examined for pathology in the central nervous system, the sciatic nerve, representative of peripheral nervous tissue as well as muscle sections. This chapter has set out the molecular and histological characterisation of these *Chmp2b* knockout mice.

Chmp2b knockout mice were generated and bred to homozygosity from commercially purchased frozen embryos harbouring the pGT0lxf gene trap within intron 2 of mouse *Chmp2b* gene. Consequently Chmp2b protein was determined to be 85% (p=.0005) depleted (figures 3.5 and 3.6) in knockout mice compared to wild type controls.

Histological examination of mouse brain, spinal cord quadriceps muscle (H&E stain) and sciatic nerve (toluidine blue) did not reveal any evidence of gross pathology. Immunohistochemical analysis did not find evidence for either astrogliosis or microglial activation associated with neuroinflammation and neurodegeneration. In addition, neither p62 nor ubiquitin inclusions were uncovered in the brain or spinal cord associated with neurodegeneration. Light microscopic immunohistochemical analysis of late endosome marker; M6PR, lysosome marker; LAMP-1, and early endosome marker, EEA1 did not identify changes resulting from *Chmp2b* depletion including changes associated with CHMP2B mutations such as enlarged endosomes as seen in cellular models of CHMP2B mutations (Skibinski et al., 2005; Filimonenko et al., 2007; Urwin et al., 2010a).

It has previously been reported that CHMP4B/mSnf7-2 pGT0lxf gene trap knockout mice are embryonic lethal (E7.5-8.5) (Lee et al., 2007) and that selective knockdown of mouse CHMP4B/mSnf7-2 by siRNA in mature cortical neurons results in dendritic retraction of cortical neurons in culture (Lee et al., 2007; Lee et al., 2009). Furthermore, CHMP4B/mSnf7-2 and CHMP2B form a complex in the ESCRT pathway demonstrating they are potentially interdependent in the endosome-lysosome pathway (Lee et al., 2007). Immunohistochemical staining of *Chmp2b* knockout brain sections with synaptophysin or calbindin did not reveal any evidence for neuronal loss even at advanced age of 24 months (figures 3.10 and 3.11).

Histological data presented in this chapter do not identify any pathology or marked difference in *Chmp2b* knockout mice compared to age-matched *Chmp2b* wild type mice in any of the tissues or at any age examined. Even so, *Chmp2b* knockout mice show a definite abnormal gait and rotarod deficit described in chapter 4.

Lack of pathology demonstrated in *Chmp2b* knockout mice may be due to other ESCRT III subunits such as Chmp2a, an orthologue of Chmp2b, compensating for the function Chmp2b protein. It is also important to consider that subtle variations not evident by light microscopic examination may have been detected by quantification of immunohistochemical markers, particularly synaptophysin and endosomal markers described. It is plausible that 85% depletion of Chmp2b is insufficient to cause pathology or that pathology is sufficiently slow and not apparent at the oldest age examined (24 months of age), however this is unlikely as chapter 4 reveals, the *Chmp2b* knockout mice demonstrate a progressive neurological phenotype.

The retention of 15% of Chmp2b protein may possibly be due to splicing out of the pGT0lxf gene trap vector in a subset of cell populations. It is worth considering whether the 15% of Chmp2b protein retention is sufficient to

prevent an embryonic lethal phenotype, and that perhaps the *Chmp2b* knockout neurological phenotype may be developmental due to a reduction of Chmp2b availability during embryonic development.

This chapter does not provide data to support or reject embryonic abnormality in *Chmp2b*$^{-/-}$ mice, however, Lee and colleagues (2007) present data demonstrating that the depletion of Chmp4b/msnf7-2, an ESCRT III subunit that complexes with CHMP2B, results in dendritic retraction in cortical neurons in culture (Lee et al., 2007). Therefore, one rationale may be that the lack of Chmp2b availability to complex with Chmp4b hinders neuronal branching during embryonic development. To address whether the neurological phenotype in the *Chmp2b* knockout mice may be developmental in origin, it would be necessary to perform an embryonic developmental study. Such a study may help provide data as to whether Chmp2b is necessary for nervous system development and maturation and whether significant depletion of Chmp2b results in inefficient neuronal branching and synapse formation during development leading to a consequent neurological phenotype.

The neurological phenotype demonstrated in the *Chmp2b* knockout mice (chapter 4) is principally of the hind limbs. *CHMP2B* point mutations of unconfirmed pathogenicity have been identified in 0.9% of ALS cases (4 out of 433 screened). All four CHMP2B mutation cases had clinical presentations of pure LMN disease termed Progressive Muscular Atrophy (PMA), in the absence of clinical FTD presentation (Cox et al., 2010). Although these mutations are not confirmed to be pathogenic the accepted relationship between FTD and ALS suggests it may be worth considering whether the *Chmp2b* knockout phenotype may be somehow associated with loss or impairment of motor neurons in the spinal cord. To determine this, additional studies would be required for example a study counting motor neurons in the lumbar spinal cord. Ubiquitin inclusions, gliosis and loss of LMN are hallmark features of both human and mouse models of ALS. This study has presented data demonstrating that H&E, GFAP and Iba1

staining do not reveal gross abnormality, gliosis or microglial activation in *Chmp2b* knockout lumbar spinal cord and immunohistochemical examination does not reveal ubiquitin or p62 inclusions. It is plausible that if a more sensitive antibody such as CD68, also a marker of microglia is applied, evidence of microglial activation may be revealed that perhaps Iba1 is not sufficiently sensitive to detect. A similar observation has been reported by Cox and colleagues (2010) where in human PMA cases microglial activation was observed only after applying CD68 antibody (Cox et al., 2010).

In summary, the *Chmp2b* knockout mice generated do not recapitulate key pathology observed in human FTD-3. The data presented in this chapter do not support the hypothesis that C-terminal truncating *CHMP2B* mutations cause FTD-3 by loss of function of the native CHMP2B protein.

4 Phenotyping *Chmp2b* Knockout Mice

An essential component of characterisation of mouse models of disease is a detailed behavioural assessment, which clarifies the functional consequences of pathologies. Since the publication of phenotype evaluation in the first successfully generated transgenic mouse (overexpressing growth hormone, published by Richard Palmiter and colleagues in Nature in 1982) (Palmiter et al., 1982), systematic and quantitative assessment of phenotypes of mutant, transgenic and knockout mice has become standard practice in evaluating how well such mouse models recapitulate the behavioural basis of the associated human disease (Crawley, 2007).

Cohorts from the *Chmp2b* knockout mouse colony have been assessed using the modified-SHIRPA primary screen to assess the presence of any overt phenotype at 12 months of age. Survival analysis and change in weight with age is an established indicator of disease which has also been investigated in *Chmp2b* knockout mice. Further assessment of motor function using rotarod and grip strength analysis and social behaviour using burrowing and nesting was performed at 4, 5 and 6 months of age. It has been reported that the outcome of such rodent activities is related to the integrity of the hippocampus and prefrontal cortex (Deacon and Rawlins, 2005).

4.1 Modified-SHIRPA protocol

The SHIRPA (**S**mithKline Beecham Pharmaceuticals; **H**arwell, MRC Mouse Genome Centre and Mammalian Genetics Unit; **I**mperial College School of Medicine at St Mary's; **R**oyal London Hospital, St Bartholomew's and the Royal London School of Medicine; **P**henotype **A**ssessment) protocol was developed as a tool to standardise phenotyping assessment of mutant, transgenic and knockout mouse models of human disease. The original SHIRPA protocol published by Rogers and colleagues (1997) (Rogers et al., 1997) described a procedure to characterise mouse phenotypes in three stages - termed the

primary, secondary and tertiary screen (Rogers et al., 1997). The primary screen uses observational assessment to compile a behavioural and functional profile, the secondary screen comprises a comprehensive behavioural assessment battery and pathological and biochemical analysis and the tertiary screen is tailored to the analysis of neurological phenotypes and is suitable for the assessment of rodent neurological models of disease (Rogers et al., 1997).

This first SHIRPA protocol has been validated in a number of mouse models of disease including the *Loa* mouse model of ALS (Rogers et al., 2001), the naturally occurring *mdx* mouse model of muscular dystrophy (Rafael et al., 2000), Charcot-Marie Tooth disease type 1 (Norreel et al., 2001) cerebral malaria (Martins et al., 2010) and developing a systematic phenotype database for ENU mice (Isaacs et al., 2002; Masuya et al., 2004).

The modified-SHIRPA protocol used in this study to phenotype *Chmp2b* knockout mice is adopted from the MRC Harwell Mammalian Genome unit (EMPReSS, 2008). The modified-SHIRPA protocol scores defined mouse phenotypes observed in 3 stages; 1) the viewing jar, 2) the observation arena and above the arena and 3) restraint and additional observations. The main difference between the original SHIRPA protocol published by Rogers and colleagues (1997) (Rogers et al., 1997) and the 2008 modified-SHIRPA protocol adopted from MRC Harwell Mammalian Genetics unit (EMPReSS, 2008) is the absence of histological, biochemical, electrophysiology, learning and memory assessments as part of the extended SHIRPA protocol. The modified-SHIRPA protocol is therefore a more rapid and high throughput phenotypic analysis that is designed to allow quantitative comparison of results both over time and between groups. In the event of sufficient N values SHIRPA scores can be analysed using x by *y* Chi squared non-parametric analysis. However, due to insufficient N values for individual phenotypes statistical analysis is not viable in this study and a descriptive commentary is provided using percentage of mice scoring for each phenotype.

The modified-SHIRPA protocol has been used to systematically score defined and additional phenotypes (described in chapter 2) as a primary assessment to identify overt phenotypes at 12 months of age in the *Chmp2b* knockout mice. This late 'middle aged' time point was chosen to allow for any potential progressive or late onset phenotype to become apparent in the initial phenotype screening.

4.1.1 Viewing jar

The first screening stage of the modified-SHIRPA protocol involves placing the mouse in a viewing jar and scoring for phenotypes during undisturbed observation of the mouse. The animal's body position, coat appearance, autonomic functions including defecation and urination as well as signs of over grooming [whiskers] and indicators of anxiety [biting and vocalisation] are scored.

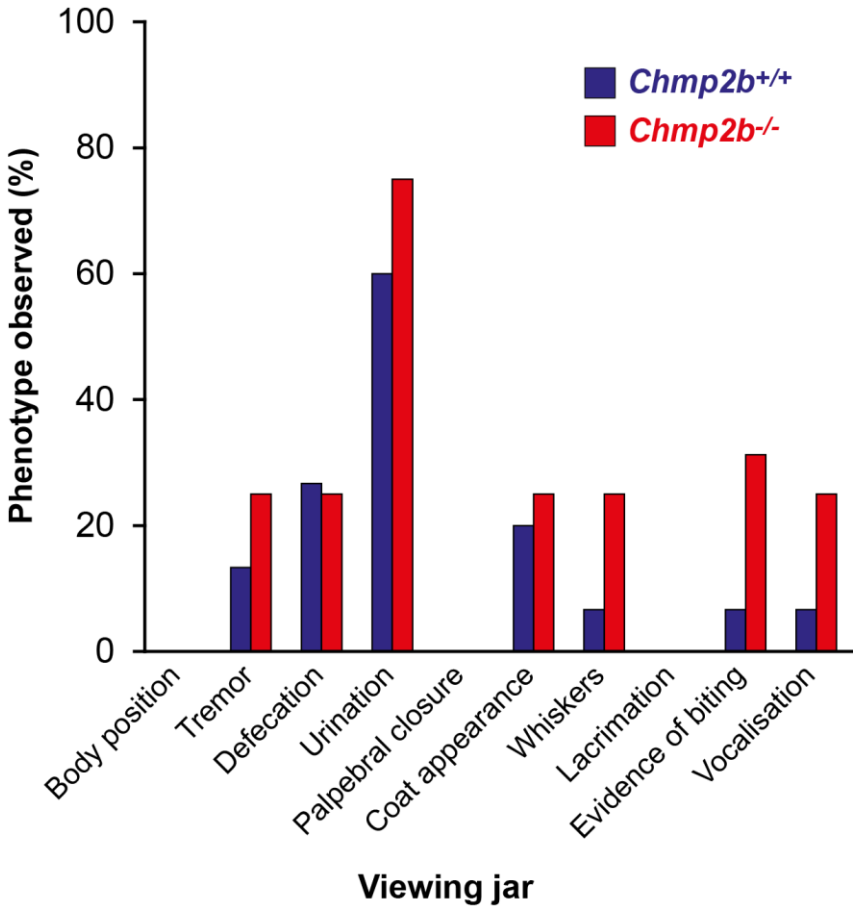

Figure 4.1 Proportion of mice exhibiting phenotypes in viewing jar.

Chmp2b$^{-/-}$ mice demonstrate an increase in over-grooming whiskers [*Chmp2b*$^{-/-}$ mice 25% compared to *Chmp2b*$^{+/+}$ mice 6.7%], evidence of biting [*Chmp2b*$^{-/-}$ mice 31.3% compared to *Chmp2b*$^{+/+}$ mice 6.7%] and vocalisation [*Chmp2b*$^{-/-}$ mice 25% compared to *Chmp2b*$^{+/+}$ mice 6.7%]. *Chmp2b*$^{-/-}$ mouse scores in other phenotypes is comparable to *Chmp2b*$^{+/+}$ mice. *Chmp2b*$^{-/-}$ mice N=16; *Chmp2b*$^{+/+}$ mice N=15.

Results from the first stage of the modified-SHIRPA protocol demonstrate that a greater proportion of *Chmp2b*$^{-/-}$ mice demonstrate an increased grooming phenotype, with 25% of *Chmp2b*$^{-/-}$ mice scoring positive for over-groomed whiskers compared to 6.7% of *Chmp2b*$^{+/+}$ mice (figure 4.1). It is necessary to consider that over-grooming of whiskers may be due to dominant cage mice over-grooming the whiskers of subordinates and not necessarily due to mice over-grooming themselves. Nevertheless, a 3.7 fold difference between *Chmp2b*$^{-/-}$ and *Chmp2b*$^{+/+}$ mice may be of biological importance since over-grooming due to dominant cage effect will be common to both genotypes.

A greater proportion of *Chmp2b*$^{-/-}$ mice (31.3%) demonstrate evidence of biting compared to 6.7% of *Chmp2b*$^{+/+}$ mice. Similarly, Chmp2b$^{-/-}$ mice (25%) demonstrate increased vocalisation phenotype compared to 6.7% of *Chmp2b*$^{+/+}$ mice (figure 4.1). A greater proportion of *Chmp2b*$^{-/-}$ mice exhibiting biting and vocalisation phenotypes may be an indication that *Chmp2b*$^{-/-}$ mice are more anxious. Slightly more *Chmp2b*$^{-/-}$ mice demonstrate tremor and urination phenotypes than *Chmp2b*$^{+/+}$ mice, however the difference is too small to draw a firm conclusion from the data (figure 4.1). Scores for all other phenotypes measured in the viewing jar are comparable between *Chmp2b*$^{-/-}$ mice and *Chmp2b*$^{+/+}$ mice (figure 4.1).

4.1.2 Observation arena

The second screening stage of the modified-SHIRPA protocol involves transferring the mouse from the viewing jar into the observation arena where mice are observed for exploratory behaviour. The observation arena is a transparent rectangular Perspex box measuring L60xW37xH18 cm and containing at its base a white Perspex sheet marked with 15 squares (11x11 cm).

Basic motor function is assessed by scoring locomotor activity, gait and tail elevation. Sensory responses are assessed by scoring mouse startle response and touch escape. Positional passivity scores the extent to which the mouse struggles when held by the tail, when loosely scruffed at the neck and when placed in supine position.

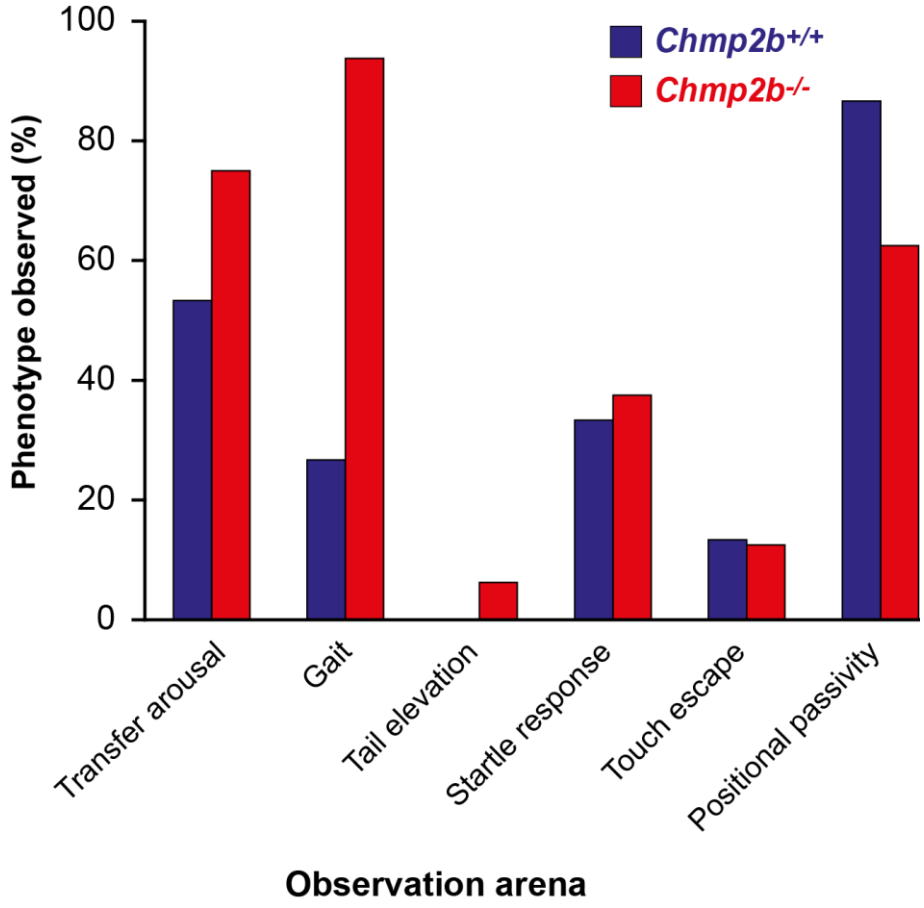

Figure 4.2 Proportion of mice exhibiting phenotypes in observation arena.

93.8% of *Chmp2b*$^{-/-}$ mice demonstrate an irregular gait phenotype compared to 26.7% of *Chmp2b*$^{+/+}$ mice. Other phenotypes in which Chmp2b$^{-/-}$ mice demonstrate a modest score difference include positional passivity; (*Chmp2b*$^{-/-}$ mice 62.5% compared to *Chmp2b*$^{+/+}$ mice 86.7%) and transfer arousal (*Chmp2b*$^{-/-}$ mice 75% compared to *Chmp2b*$^{+/+}$ mice 53.3%). *Chmp2b*$^{-/-}$ mice N=16, *Chmp2b*$^{+/+}$ mice N=15.

The most prominent phenotypic difference identified in the observation arena was an abnormal gait in Chmp2b$^{-/-}$ mice (15 out of 16 mice) (figure 4.2) but no significant difference was found in locomotor activity between Chmp2b$^{-/-}$ and Chmp2b$^{+/+}$ mice (figure 4.3).

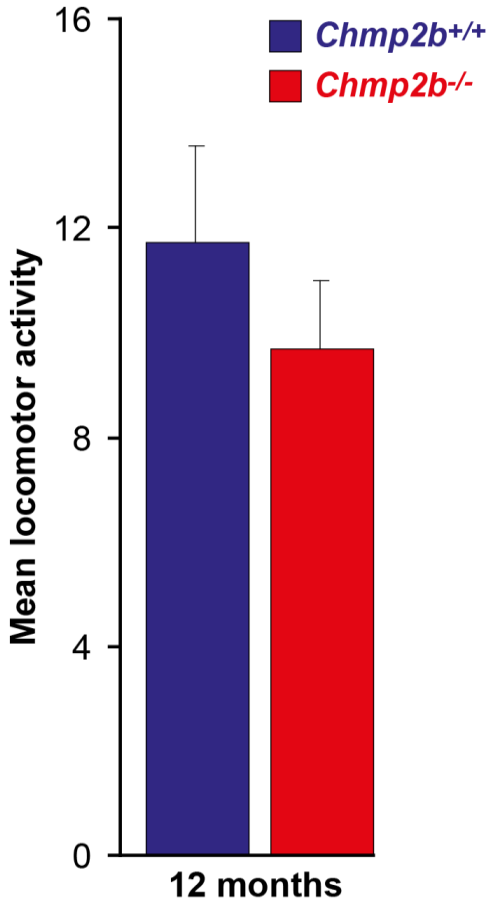

Figure 4.3 Mean locomotor activity (LMA) at 6 and 12 months of age.

Mean locomotor activity is the number of squares crossed on the observational arena in 30 seconds. There is no significant difference in mean LMA between Chmp2b$^{-/-}$ and Chmp2b$^{+/+}$ mice at 12 months of age. Error bars= SEM; p=0.0973; *Chmp2b*$^{-/-}$ mice N=16, *Chmp2b*$^{+/+}$ mice N=15.

75% of *Chmp2b*$^{-/-}$ mice demonstrate enhanced exploratory behaviour on being transferred to the observation arena compared to 63% of *Chmp2b*$^{+/+}$ mice. Only Chmp2b$^{-/-}$ demonstrated an elevated tail phenotype (6.25%). Fewer *Chmp2b*$^{-/-}$ mice (62.5%) demonstrate a positional passivity phenotype compared to *Chmp2b*$^{+/+}$ mice (86.7%) (figure 4.2), demonstrating reduced struggling in *Chmp2b*$^{-/-}$ mice when being handled. In the observation arena the gait phenotype is the most clearly associated with *Chmp2b*$^{-/-}$ mice, although differences in other phenotypes are noted (transfer arousal, tail elevation, positional passivity). It is not possible to conclude based on these data alone that these phenotypes are genotype–specific.

After positional passivity assessment the mouse is held above the arena and assessed for neurological phenotypes including trunk curl and limb grasp. Trunk curl and limb grasp phenotypes are indicative of neurological dysfunction, reviewed by Brooks and Dunnett (2009) while pinna and corneal reflex assess neurosensory function, reviewed by Crawley (2007) (Crawley, 2007; Brooks and Dunnett, 2009). A small proportion of *Chmpb2*$^{-/-}$ mice (6.25%) demonstrate a limb grasp phenotype. Notably *Chmp2b*$^{-/-}$ mice demonstrate prominently reduced pinna and corneal reflex compared to *Chmp2b*$^{+/+}$ mice (figure 4.4).

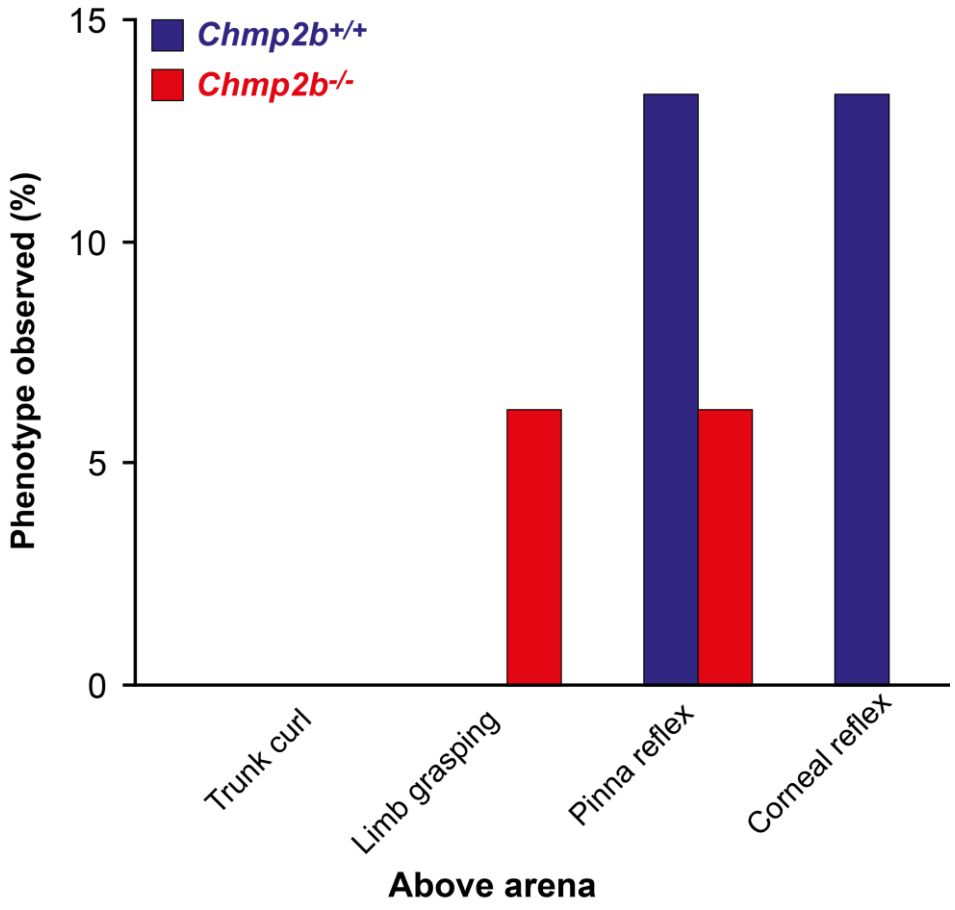

Figure 4.4 Proportion of mice scoring listed phenotypes above arena.

Greater proportion of *Chmp2b*$^{-/-}$ mice demonstrate an increase in limb-grasping (*Chmp2b*$^{-/-}$ mice 6.3% compared to no *Chmp2b*$^{+/+}$ mice) and reduced pinna reflex (*Chmp2b*$^{-/-}$ mice 6.3% compared to *Chmp2b*$^{+/+}$ mice 13.3%) and corneal reflex (*Chmp2b*$^{-/-}$ mice did not score for corneal reflex compared to *Chmp2b*$^{+/+}$ mice 13.3%). Neither *Chmp2b*$^{-/-}$ or *Chmp2b*$^{+/+}$ mouse scored for trunk curl phenotype. *Chmp2b*$^{-/-}$ mice N=16, *Chmp2b*$^{+/+}$ mice N=15.

4.1.3 Restraint and other observations

In the third screening part of the modified-SHIRPA protocol postural reflex is assessed by placing the mouse in a Perspex tube and turning the mouse so that it is rotated on its back. Normal mice will automatically turn themselves over, by righting themselves onto four legs. Neurological and neuromuscular dysfunction will affect the mouse righting reflex so that the mouse is unable to immediately right itself (Crawley, 2007). It was observed that 68.7% of *Chmp2b*$^{-/-}$ mice demonstrated inefficient contact righting reflex, indicating potential underlying neurological or neuromuscular dysfunction (figure 4.5), compared with 6.7% of controls.

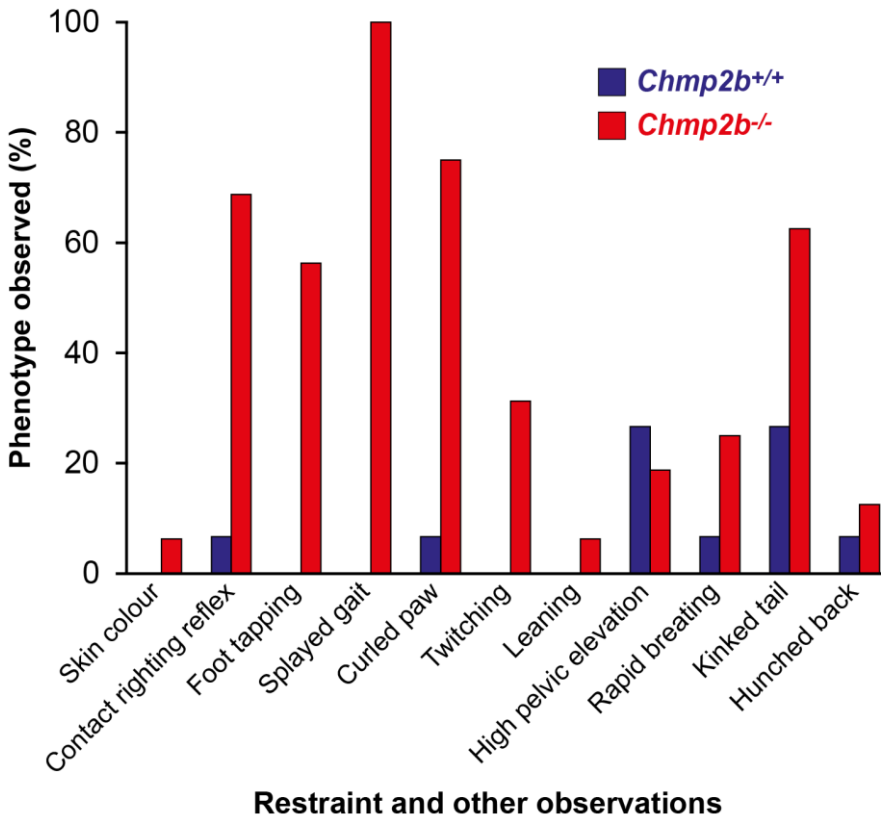

Figure 4.5 Proportion of mice scoring for restraint and other observations.

All *Chmp2b*$^{-/-}$ mice demonstrate an irregular splayed gait (100%) which is not observed in *Chmp2b*$^{+/+}$ mice. Furthermore only *Chmp2b*$^{-/-}$ mice are found to demonstrate foot tapping (56%) and twitching (31%). Other observations of interest include poor contact righting reflex [*Chmp2b*$^{-/-}$ mice 68.8% compared to *Chmp2b*$^{+/+}$ mice 6.7%] an irregular curled paw phenotype [*Chmp2b*$^{-/-}$ mice 75% compared to *Chmp2b*$^{+/+}$ mice 6.7%] and kinked tail [*Chmp2b*$^{-/-}$ mice 62.5% compared to *Chmp2b*$^{+/+}$ mice 26.7%]. *Chmp2b*$^{-/-}$ mice N=16, *Chmp2b*$^{+/+}$ mice N=15

The term 'splayed gait' is used to describe a wide 'waddling' gait detected in the observation arena when scoring gait phenotype. Splayed gait has been recorded under 'other observations' section of the modified-SHIRPA protocol as it is a very distinct observation from generic gait phenotypes, for instance, abnormal gait as a result of fighting scored in section 4.1.2. Splayed gait was the most persistent and systematic phenotype identified in *Chmp2b*$^{-/-}$ mice; 100% of *Chmp2b*$^{-/-}$ mice demonstrated splayed gait; no *Chmp2b*$^{+/+}$ mice were identified to demonstrate splayed gait (figure 4.5). Other additional phenotypes of interest identified in *Chmp2b*$^{-/-}$ mice include 'foot tapping', curled paw (figure 4.6), twitching and kinked tail (figure 4.5 and 4.7). Foot tapping describes repetitive tapping of the hind limb on the floor when initiating movement. The curled paw describes the mouse holding one of its front paws in an abnormal position. Both phenotypes generally occurred unilaterally.

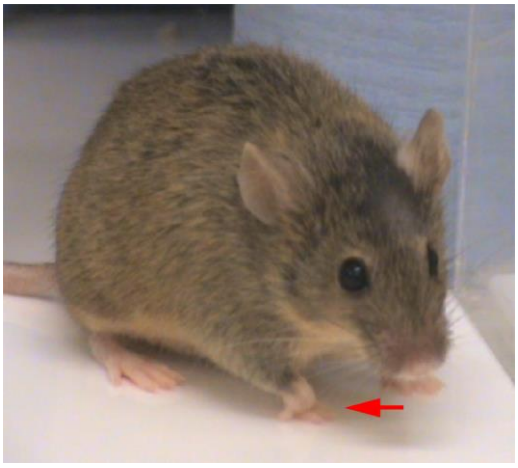

Figure 4.6 Curled paw phenotype.

Image demonstrating curled paw (red arrow) phenotype identified in Chmp2b$^{-/-}$ mice

Figure 4.7 Kinked tail phenotype.

Image demonstrates kinked tail (red arrow) phenotype identified in Chmp2b$^{-/-}$ mice

4.1.3.1 Body weight

Significant change in body weight is a reliable indicator of disease in both humans and mice. If the transgene or gene depletion of interest affects appetite or metabolic function weight will be affected. Genes associated with neurodegeneration may affect locomotor or neuromuscular dysfunction so that the mouse is not able to travel or rear its body to reach food (Crawley, 2007).

At 18 months of age male *Chmp2b*$^{-/-}$ mice show significantly reduced mean body weight (32g) compared to age-matched male *Chmp2b*$^{+/+}$ (49.5g) mice (**p<0.0001) (figure 4.8). Female mice also show a reduction in mean body weight, 30.6g in female *Chmp2b*$^{-/-}$ compared to 41.7g in age-matched female *Chmp2b*$^{+/+}$, however this difference does not reach statistical significance (figure 4.9). Although the weight loss in *Chmp2b*$^{-/-}$ mice occurs at an advanced age it may be suggestive of underlying disease associated with depletion of *chmp2b* protein.

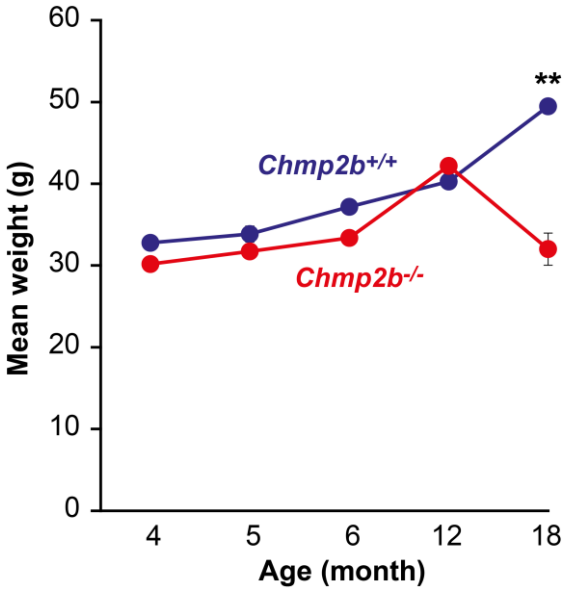

Figure 4.8 Mean weight of male mice in grams of *Chmp2b*$^{-/-}$ and *Chmp2b*$^{+/+}$ from 4 to 18 months of age.

Male *Chmp2b*$^{-/-}$ mice show a significant [ANOVA *p<0.0001] decrease in weight at 18 months compared to age-matched *Chmp2b*$^{+/+}$ mice. Error bars= SEM; Male *Chmp2b*$^{-/-}$ N= 14 at 4 and 5 months, N=15 at 6 months, N=13 at 12 months and N=7 at 18 months. Male *Chmp2b*$^{+/+}$ N= 15 at 4 and 5 months, N=21 at 6 months, N=14 at 12 months and N=8 at 18 months.

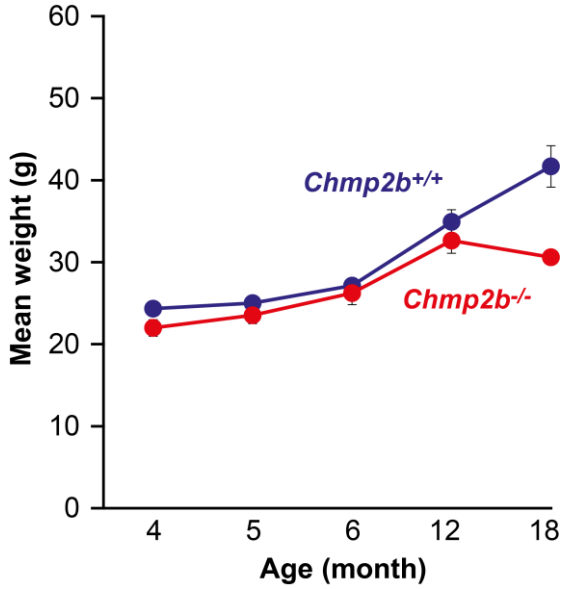

Figure 4.9 Mean weight of female mice in grams of *Chmp2b*$^{-/-}$ and *Chmp2b*$^{+/+}$ from 4 to 18 months of age.

Female *Chmp2b*$^{-/-}$ mice demonstrate weight loss at 18 months, but it does not reach statistical significance compared to age-matched *Chmp2b*$^{+/+}$ mice. Error bars= SEM; Female *Chmp2b*$^{-/-}$ N= 13 at 4 and 5 months, N=23 at 6 months, N=14 at 12 months and N=5 at 18 months. Female *Chmp2b*$^{+/+}$ N= 14 at 4 and 5 months, N=25 at 6 months, N=16 at 12 months and N=12 at 18 months.

4.2 Survival Analysis

Survival analysis of Chmp2b knockout mice reveals that *Chmp2b*$^{-/-}$ mice have significantly reduced survival with median survival of 18 months in *Chmp2b*$^{-/-}$ mice and 22 months in *Chmp2b*$^{+/+}$ mice (***p*=0.0006) (figure 4.10). This data taken together with the weight loss discussed in section 4.1.3.1 above (figure 4.8 and figure 4.9) provide further indication that depletion of *Chmp2b* results in a pathological phenotype.

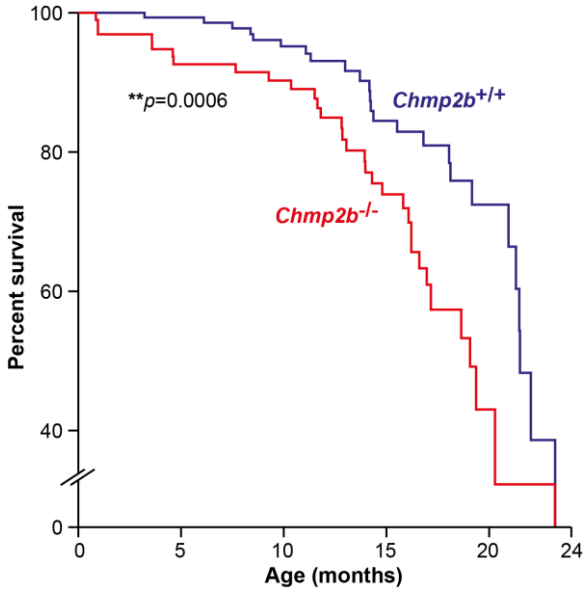

Figure 4.10 Kaplan Meier survival analysis of *Chmp2b*$^{-/-}$ and *Chmp2b*$^{+/+}$ mice.

Survival analysis demonstrates that *Chmp2b*$^{-/-}$ mice have significantly reduced survival compared to *Chmp2b*$^{+/+}$ mice. Log Rank (Mantel-Cox analysis) ** *p*=0.0006. *Chmp2b*$^{-/-}$ N=97; *Chmp2b*$^{+/+}$ N=162.

4.3 Motor Function

Almost all behaviour observed in mice requires movement, including gait and locomotion, change in body position, righting reflex, walking to food, as well as social behaviours such as burrowing, grooming and nesting. Movement is controlled by motor function which when impaired leads to reduced or absence of such behaviour in mice. For this reason standardised assessment of motor function is the most widely explored behavioural phenotype in neurological research (Brooks and Dunnett, 2009). In this study motor function was assessed by using rotarod and grip strength analysis.

4.3.1 Rotarod

In this study the modified-SHIRPA battery screen has revealed that *Chmp2b*$^{-/-}$ mice demonstrate an irregular 'splayed gait' phenotype at 12 months of age. To further investigate this phenotype, a cohort of *Chmp2b* knockout mice was tested using the rotarod protocol (detailed in chapter 2). Rotarod phenotype analysis is a well-established means of testing motor coordination and balance (Crawley, 2007; Brooks and Dunnett, 2009)

In brief, age-matched cohorts of male and female *Chmp2b*$^{-/-}$ and *Chmp2b*$^{+/+}$ mice at 4, 5 and 6 months mice were first given one practice trial on the rotarod. To test motor coordination and balance mice were placed on a rotarod with accelerating speed and timed for how long they could stay on the rotarod before falling off. The latency to falling off the rotarod was recorded and the mean of three rotarod tests per mouse was used for analysis (figure 4.11).

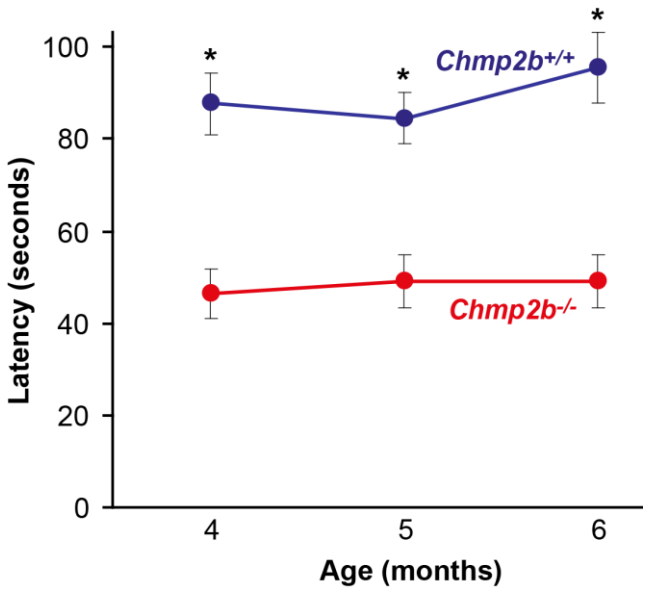

Figure 4.11 Mean rotarod latency in *Chmp2b*$^{-/-}$ and *Chmp2b*$^{+/+}$ mice at 4, 5 and 6 months of age.

Rotarod latency is significantly reduced in *Chmp2b*$^{-/-}$ mice compared to *age-matched Chmp2b*$^{+/+}$ mice at all ages tested (ANOVA and Tukey-Kramer *post hoc* multiple comparison test *p<0.001). Multiple regression analysis reveals highly significant association between rotarod latency and genotype (p<0.0001) but no significant association between rotarod latency and age (p=0.4485) or gender (p=0.4350). Error bars = SEM; *Chmp2b*$^{-/-}$ N= 28 (15 male/13 female) at 4 months, N=27 (15 male/12 female) at 5 months and N=28 (15 male/13 female) at 6 months and *Chmp2b*$^{+/+}$ N= 29 (15 male/14 female) at 4 months, N=29 (15 male/14 female) at 5 months and N=29 (15 male/14 female) at 6 months.

Multiple linear regression analysis reveals there is no significant association between rotarod latency and gender (p=0.4350), therefore male and female mice can be grouped and analysed together. There is also no significant association between rotarod latency and age (p=0.4485). Multiple regression analysis does reveal a highly significant association between rotarod latency and genotype (p<0.0001). Comparing the means of the rotarod latency using ANOVA shows a significant difference between rotarod latency and genotype (*Chmp2b*$^{-/-}$ and *Chmp2b*$^{+/+}$ mice) (p<0.001) and Tukey-Kramer *post hoc* multiple comparisons test reveals that this significance is maintained at all ages tested: 4, 5 and 6 months of age (figure 4.11).

The lack of statistically significant association between rotarod latency and age identified by multiple linear regression analysis and the significant difference between genotype and mean rotarod latency (p=0.001) at each age identified by ANOVA *post hoc* analysis suggests that the rotarod deficit in *Chmp2b*$^{-/-}$ mice is not progressive, meaning that the rotarod deficit does not get worse with age. However, a statistically significant constant poor performance in mean rotarod performance is present in *Chmp2b*$^{-/-}$ mice at all ages tested compared to age-matched wild type mice (figure 4.11).

4.3.2 Grip strength

In order to investigate neuromuscular defects grip strength testing was performed on a cohort of *Chmp2b*$^{-/-}$ mice *Chmp2b*$^{+/+}$ mice at 4, 5 and 6 months of age.

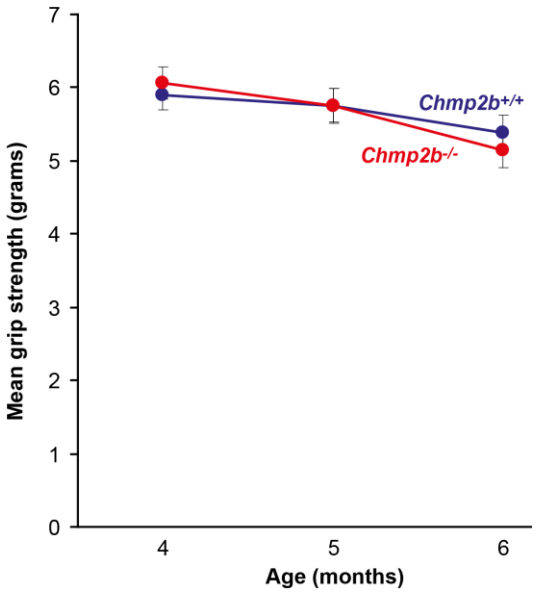

Figure 4.12 Mean grip strength in *Chmp2b*$^{-/-}$ and *Chmp2b*$^{+/+}$ mice at 4, 5 and 6 months of age.

Mean grip strength has been adjusted for weight, therefore male and female data were pooled. There is no significant association between mean grip strength and genotype (multiple linear regression p=0.9023) and no difference in mean grip strength is identified in *Chmp2b*$^{-/-}$ mice compared to *Chmp2b*$^{+/+}$ mice at any age tested (ANOVA; p=0.0513). Multiple linear regression reveals a highly significant association between mean grip strength and age (p<0.00001), likely reflecting weakness associated with aging and not *Chmp2b* depletion. Error bars = SEM; *Chmp2b*$^{-/-}$ N= 28 (15 male/13 female) at 4 months, N=27 (15 male/12 female) at 5 months and N=28 (15 male/13 female) at 6 months and *Chmp2b*$^{+/+}$ N= 29 (15 male/14 female) at 4 months, N=29 (15 male/14 female) at 5 months and N=29 (15 male/14 female) at 6 months.

Multiple linear regression analysis did not identify a significant association between mean grip strength and genotype (p=0.9023) indicating there is no difference in mean grip strength between *Chmp2b*$^{-/-}$ mice and *Chmp2b*$^{+/+}$ mice. This was confirmed by ANOVA analysis (p=0.0513) and can be seen in figure 4.12. Multiple linear regression did identify a highly significant association (*p<0.0001) between mean grip strength and age; this can be seen in figure 4.12 by the decrease in mean grip strength with increasing age for both genotypes (figure 4.12). Therefore this association is an age-dependent phenomenon,

possibly reflecting weakness associated with age and is not as a result of depletion of *Chmp2b*.

4.4 Social Behaviour

Social behaviour, the interaction of an animal with its own and other animal species is fundamental to the survival of all animal kind. Virtually all behaviour such as reproduction, rearing of young, defining territory, nest building, hunting, scavenging, grooming and even death are dictated by social behaviour and convention (Crawley, 2007).

In the wild mice are social species that develop group territories, a colony dependent on food availability. A colony is founded by one dominant male and one or two females. Parents and offspring share burrows and nests built by the adults that provide shelter and safety from predators. Both male and female parents rear pups in the nest and adult offspring move away from the group nest and establish new colonies (Crawley, 2007).

Humans too demonstrate a variety of specific social behaviour and in the event of neuropsychiatric and neurodegenerative disease including FTD, deterioration of social behaviour can be a presenting clinical symptom. Therefore assessing social behaviour in mouse models of neuropsychiatric and neurodegenerative disease is a valuable means of assessing early indictors of disease (Deacon et al., 2001).

Burrowing and nesting are two important social behaviours in mice that can deteriorate with neurodegenerative diseases and were therefore investigated in this study.

4.4.1 Burrowing

Burrowing is considered a primal behaviour necessary for building shelter to provide refuge from weather conditions, to store food, defence against predators and to rear young(Deacon, 2006b; Deacon, 2009).

In this study burrowing behaviour was analysed using a method adopted from a published protocol by Deacon (2006) (Deacon, 2006b). In brief; artificial burrows made of cylindrical plastic tubes were filled with 200g of food pellets and single mice assigned to each food-filled burrow. Male and female *Chmp2b*$^{-/-}$ (N=27) and *Chmp2b*$^{+/+}$ (N=29) mice at 4, 5 and 6 months of age were individually housed with prepared burrows overnight and the weight of the left-over food pellets in the burrow was weighed the following day. The amount (weight in grams) burrowed was determined by subtracting starting food pellet weight (200g) from food pellet weight remaining the following day (detailed in chapter 2) (Deacon, 2006b).

As the data collected does not follow a normal distribution and a ceiling effect has been previously reported in overnight burrowing experiments (Deacon, 2006b), a non-parametric Kruskal-Wallis ANOVA statistical analysis was used, revealing a significant (p<0.0001) difference in amount of food pellet burrowed across ages and between genotypes (figure 4.13). Interestingly, *Chmp2b*$^{+/+}$ mice demonstrate a significant (p<0.001) age-dependent deterioration in burrowing behaviour (figure 4.13) while in *Chmp2b*$^{-/-}$ mice the amount of food pellet burrowed does not decline with age. By 5.5 months of age there is a significant difference (**p=0.0001) between food pellets burrowed by *Chmp2b*$^{+/+}$ mice and that burrowed by *Chmp2b*$^{-/-}$ mice and this significant difference is maintained at 6 and 6.5 months of age (figure 4.13).

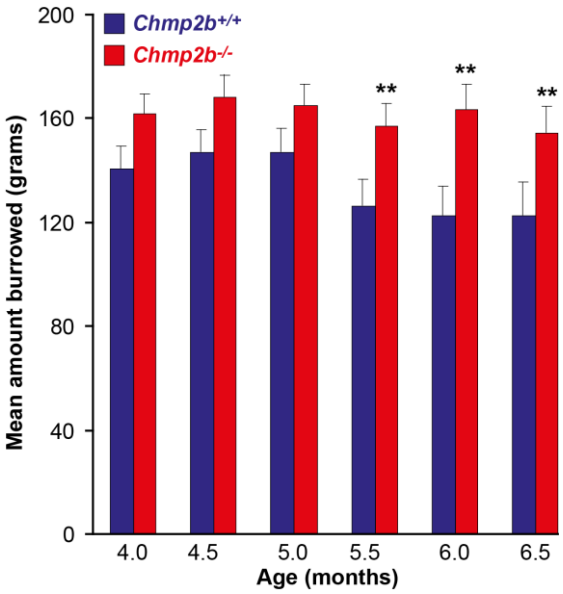

Figure 4.13 Mean weight burrowed by *Chmp2b*$^{-/-}$ and *Chmp2b*$^{+/+}$ mice with increasing age.

Burrowing behaviour declines in *Chmp2b*$^{+/+}$ mice with age as analysed by Kruskal-Wallis ANOVA (<0.001) but there is no significant change in *Chmp2b*$^{-/-}$ mice. By 5.5 months of age a significant difference (Kruskal-Wallis ANOVA (**p<0.0001)) in the amount of food pellet burrowed develops between *Chmp2b*$^{-/-}$ and *Chmp2b*$^{+/+}$ mice which is maintained with increasing age from 5.5 to 6.5 months of age. Error bars = SEM; *Chmp2b*$^{-/-}$ N= 28 (15 male/13 female) at 4 months, N=27 (15 male/12 female) at 5 months and N=28 (15 male/13 female) at 6 months and *Chmp2b*$^{+/+}$ N= 29 (15 male/14 female) at 4 months, N=29 (15 male/14 female) at 5 months and N=29 (15 male/14 female) at 6 months.

In scrapie sick mice burrowing significantly declines compared to non-infected controls with age (Deacon et al., 2001) as would be expected in neurodegeneration. Notably, *Chmp2b*$^{-/-}$ mice do not demonstrate such decline in burrowing with age, in fact, they perform better than age-matched wild type control mice (figure 4.13). The absence of gross neuropathology (chapter 3) is consistent with lack of deterioration in burrowing with age. However, the significantly greater amount of pellets burrowed by *Chmp2b*$^{-/-}$ mice with age remains to be explained.

4.4.2 Nesting behaviour

Nest construction is a common behaviour in animals across the animal kingdom primarily serving as a safe environment to rear offspring. For small mammals such as mice their nests serve as more than just a nursery for the young. Their nests are also used for shelter, hibernation and protection from natural elements. Both male and female mice construct nests, however, female mice may be influenced by reproductive hormonal status, in particular, prolactin (Deacon, 2006a; Keisala et al., 2007).

Nesting behaviour has been shown to be affected in prion infected mice (Cunningham et al., 2003), *Dvl1* (involved in regulation of cell polarity pathway) knockout mice (Lijam et al., 1997) and vitamin D receptor (*VDR)* mutant mice (Keisala et al., 2007). In this study the nesting behaviour protocol was adopted from a published protocol reported in Nature Protocols (Deacon, 2006a). Commercially available cotton Nestlets were placed in cages of individually housed mice at 4, 5 and 6 months of age 1 hour before the dark cycle and scored 1-5 (figure 4.14) the following morning (detailed in chapter 2) (Deacon, 2006a).

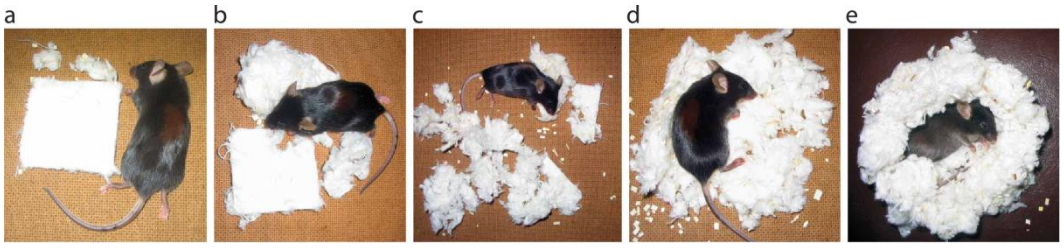

Figure 4.14 Nest building scoring scheme.

Nests are scored 1-5 (a-e respectively) based on degree of Nestlet tearing and nest formation. Adopted from Deacon (2006) protocol (Deacon, 2006a).

As in other published reports of nesting behaviour, male and female nest scores were analysed together as the female mice were housed in single sex cages and none of the female mice being tested were pregnant or lactating, therefore the confounding effect of prolactin status on nest building is considered negligible (Deacon, 2006a; Keisala et al., 2007). Nesting data does not fit the

Normal/Gaussian distribution therefore non-parametric Kruskal-Wallis ANOVA statistical test was used to analyse the nesting behaviour data (Deacon, 2006a).

A box and whisker plot of the nesting scores demonstrates spread of nesting scores using median, minimum (MIN), maximum (MAX) and the first quartile (Q1) and third quartile (Q3) of nesting scores for *Chmp2b*$^{+/+}$ and *Chmp2b*$^{-/-}$ mice across 4, 5 and 6 months of age (figure 4.15). Statistical analysis using Kruskal-Wallis ANOVA identifies a highly significant difference in median scores (p<0.0001) across the nesting data and Dunn's pairwise multiple comparison *post hoc* test identifies a significant difference in median nesting score versus age (p<0.001), nesting score versus genotype (p<0.001) and age versus genotype (p<0.001).

Chmp2b$^{+/+}$ mice demonstrate a constant median nesting score of 4 across ages examined. However, *Chmp2b*$^{-/-}$ mice demonstrate a significantly higher median nesting score of 5 compared to *Chmp2b*$^{+/+}$ mice at 4 and 5 months of age. A ceiling effect is evident as *Chmp2b*$^{+/+}$ and *Chmp2b*$^{-/-}$ mice at all ages demonstrate a maximum score of 5. The median score of 5 overlaps with MAX and Q3 scores for *Chmp2b*$^{-/-}$ mice at 4 and 5 months of age, whereas the median score for Chmp2b$^{+/+}$ mice is 4, demonstrating that more *Chmp2b*$^{-/-}$ mice at these ages build complete nests (scoring 5) compared to age-matched wild type mice (figures 4.15). By 6 months of age both *Chmp2b*$^{+/+}$ and *Chmp2b*$^{-/-}$ mice score equally on median, MIN, Q1 and MAX nest scores, notably Q3 and median scores are equivalent (median and Q3 scores = 4 at 6 months) demonstrating that most mice score 4 at this age, lower than the ceiling score (figure 4.15).

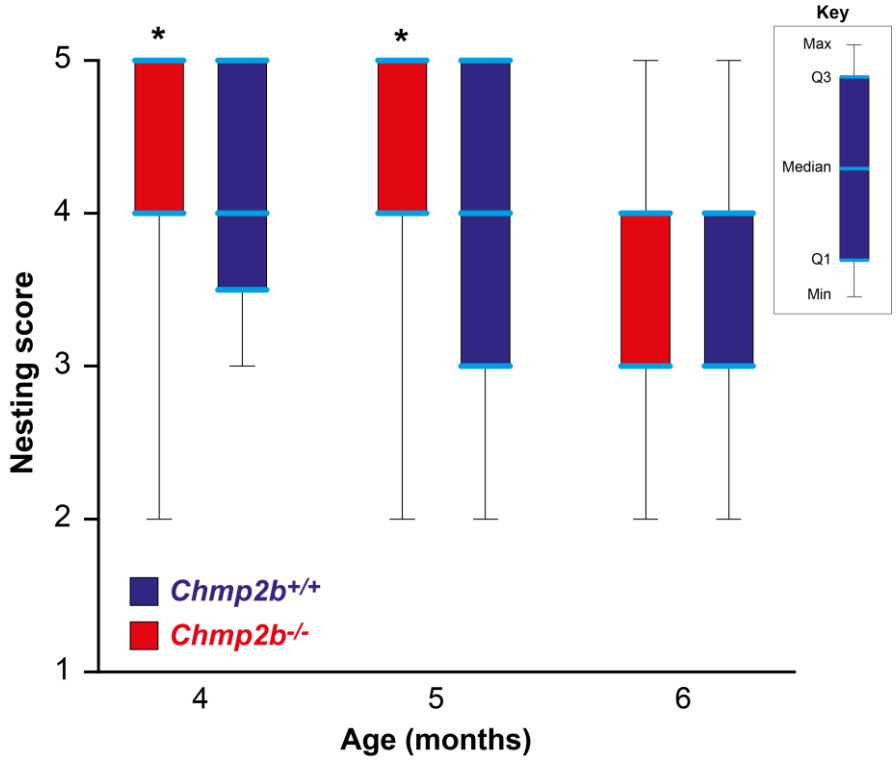

Figure 4.15 Box and whisker plot of nesting score for Chmp2b$^{-/-}$ and Chmp2b$^{+/+}$ mice at 4, 5 and 6 months of age.

Chmp2b$^{+/+}$ and Chmp2b$^{-/-}$ nesting scores are significantly different (variation in median is greater than expected by chance alone) (Kruskal-Wallis ANOVA $p<0.001$). Dunn's pairwise multiple comparison *post hoc* test identifies a significant difference in median scores between nesting score versus age ($p<0.001$), nesting score versus genotype ($^*p<0.001$) and age versus genotype ($p<0.001$). *Chmp2b*$^{-/-}$ N= 13 at 4, 5 and 6 months and *Chmp2b*$^{+/+}$ N= 14 at 4, 5 and 6 months.

4.5 Discussion

The modified-SHIRPA protocol was used as a primary phenotyping screen to identify overt behavioural phenotypes in *Chmp2b* knockout mice. A cohort of 12-month old *Chmp2b*$^{-/-}$ and age-matched *Chmp2b*$^{+/+}$ mice were screened using the modified-SHIRPA battery of tests.

This initial phenotyping screen revealed that *Chmp2b*$^{-/-}$ mice demonstrate an irregular gait termed here as 'splayed gait' as well as foot tapping, curled paw and kinked tail (figure 4.5) phenotypes. Furthermore, *Chmp2b*$^{-/-}$ mice have significantly reduced survival (p=0.0006) (figure 4.10) and male *Chmp2b*$^{-/-}$ mice have significantly reduced weight (p<0.0001) at the later age of 18 months (figure 4.8) compared to age-matched wild type mice.

Examining motor coordination and balance using rotarod test reveals that *Chmp2b*$^{-/-}$ mice also have significantly reduced rotarod performance (p<0.001) compared to age-matched *Chmp2b*$^{+/+}$ (figure 4.11). However, no difference in grip strength between genotypes is identified at any age tested (figure 4.12).

It is interesting to note that impaired rotarod latency in *Chmp2b*$^{-/-}$ mice is not progressive across 4, 5 and 6 months of age but that impaired rotarod performance is consistently maintained with increasing age. This may either be due to a slow rate of decline in the biological basis of rotarod performance, so that if mice are assessed at longer intervals *i.e.* at 4, 8, 12, 16 and 20 months of age, a progressive decline may be detected. Alternatively, the biological basis of rotarod impairment, whether neurological or neuromuscular, may be developmental as opposed to being degenerative. *Chmp5* knockout mice display severe developmental abnormalities; by E8-E9 mutant embryos are severely disorganised with neural tube defect formation, abnormalities in head fold, heart formation and an apparent defect of ventral folding morphogenesis (Shim et al., 2006). Furthermore, a kinked tail phenotype has previously been reported

in Bent tail mice, a model for X-linked neural tube defects (Klootwijk et al., 2000) and the spontaneous Polypodia (*Ppd*) mutant mouse that primarily exhibits ectopic, ventral/caudal limbs and associated pelvic girdle malformation, less penetrant kinked tail and forelimb anomalies (Lehoczky et al., 2006). Although the *Chmp2b*$^{-/-}$ mice do not recapitulate precisely the kinked tail phenotype in the Bent tail and *Ppd* mice, it is worth considering embryonic developmental defects as a potential basis of the phenotype observed in *Chmp2b*$^{-/-}$ mice, especially in the absence of distinctive neuropathology (chapter 3). It is also important to note that some *Chmp2b*$^{+/+}$ mice (although fewer than *Chmp2b*$^{-/-}$ mice) were also observed to have kinked tails and this may simply reflect fighting between mice housed together resulting in damaged tails. In this instance the greater number of *Chmp2b*$^{-/-}$ mice with kinked tails may simply reflect their inability to fight and defend themselves effectively due to lower limb dysfunction.

The observed splayed gait and rotarod deficit suggest neurological or neuromuscular lower limb dysfunction. Abnormal gait phenotypes have been reported in numerous mouse models of neurodegenerative disease including R6/2 mouse models of Huntington's disease (Mangiarini et al., 1996), SCA (Ingram et al., 2012) ALS (Mancuso et al., 2011), Alzheimer's and FTD reviewed by Gotz and Ittner (2008) (Gotz and Ittner, 2008). Histological analysis of *Chmp2b* knockout mouse brains and spinal cord tissue did not reveal any overt neuropathology (chapter 3). Even so, phenotyping data presented in this chapter indicates a motor phenotype in *Chmp2b*$^{-/-}$ mice from 4 months of age which may contribute to the observed reduced survival in these mice, thus for the first time, providing support that depletion of *Chmp2b* may contribute to the observed motor phenotype in FTD-3.

Scrapie infected mice, *Dvl1* and Vitamin D receptor (VDR) mutant mice all demonstrate significantly reduced nest building ability resulting from neuropathology, neurodevelopment, neuroendocrine and vitamin D receptor pathology (Lijam et al., 1997; Deacon, 2006a; Deacon, 2006c; Keisala et al.,

2007). Assessment of burrowing (figure 4.12) and nesting (figure 4.13) behaviour reveals a significant increase in these behaviours in *Chmp2b*$^{-/-}$ mice compared to *Chmp2b*$^{+/+}$ mice. Why *Chmp2b*$^{-/-}$ mice should demonstrate increased burrowing and nesting behaviour is not clear but may be a symptom of increased impulsive behaviour or anxiety symptoms.

The SNAP-25 deficient Colombo mouse displays spontaneous impulsive hyperactivity and impaired inhibition in delayed reinforcement tasks recapitulating some key features of human ADHD behaviour, including obsessive compulsive behaviour (Wilson, 2000; Bruno et al., 2007; Russell, 2011). Transgenic mice expressing tau V337M also display specific effects of transgene expression on the ability to withhold responding in a murine version of the 5-choice serial reaction time task, behaviour consistent with deficits in impulse control which is exacerbated with aging (Lambourne et al., 2007).

SNAP-25 is essential for synaptic vesicle exocytosis and neurotransmitter release regulating membrane trafficking. It is required presynaptically for the release of neurotransmitters and postsynaptically it is also involved in the translocation of proteins and receptor subunits to the cell membrane (Russell, 2011). Interestingly Chmp2b is a subunit of the ESCRT complex and SNAP-25 is a subunit of the SNARE complex which is intrinsically associated via ESCRT-SNARE subunit complex formation. In particular Hrs, an ESCRT I subunit, is a binding partner to SNAP-25 and their association has been hypothesized to regulate synaptic vesicle exocytosis (Kwong et al., 2000) and endosome fusion (Sun et al., 2003). It would be interesting to consider whether the depletion of Chmp2b as in the *Chmp2b*$^{-/-}$ mice might have a cascade effect on ESCRT-SNARE complex formation leading to neurotransmitter irregularity via synaptic vesicle deregulation, thus contributing to impulsive and impaired inhibition behaviour. It is important to clarify that there is no data in this study to support this hypothesis and this is merely speculation, but may be an interesting basis for future investigations.

Neurotransmitters including dopamine (DA) and serotonin (SR) and their associated pathways have been implicated in both human and rodent behaviour (Viggiano et al., 2003; Fernandez and Gaspar, 2012). Dopamine transporter (DAT) knockout and knockdown mice exhibit novelty induced hyperactive behaviour thought to be due to higher levels of brain dopamine, resulting from the lack of clearance of dopamine from the synaptic cleft (Viggiano et al., 2003). Tryptophan is a precursor to serotonin and dietary tryptophan depletion or supplementation results in pronounced behavioural effects, particularly in nesting behaviour where a reduction in nesting is reported following depletion of dietary tryptophan. Interestingly, an increase in nesting behaviour was observed with enhanced dietary tryptophan in BALB/c and C57BL/6J mouse strains (Browne et al., 2012). *Chmp2b* knockout mice are on a 129P2/OlaHsd x C57BL/6J mixed genetic background; it would therefore be interesting to investigate 5HT and other neurotransmitter levels in *Chmp2b*$^{-/-}$ mice on a single strain backcross.

Considering that Chmp proteins, as part of the ESCRT complex, are important in endocytic neurotransmitter recycling (Shim et al., 2006; Lee et al., 2007; Urwin et al., 2010a) and the evidence for altered neurotransmitter regulation in a number of neuropsychiatric disorders (ADHD, clinical anxiety, depression) (Viggiano et al., 2003; Russell, 2011; Fernandez and Gaspar, 2012), it is interesting to consider whether depletion of Chmp2b results in altered neurotransmitter physiology and therefore, behaviour.

In summary, no other mouse model has been identified in the literature that displays the combined phenotypes identified in *Chmp2b*$^{-/-}$ mice but other models demonstrating single common phenotypes may be suitable starting points in identifying the pathological basis of Chmp2b depletion.

To further tease out the age of phenotype onset, future studies would need to assess *Chmp2b* mice from a much younger age, perhaps starting as young as 4

weeks of age for phenotyping studies. Rotarod is a good protocol to maintain; perhaps open field and aggression assessment may also shed further light on the gait defect and changes in aggression and impulsive behaviour in *Chmp2b*$^{-/-}$ mice. No memory or novel task tests such as water maze and object recognition have been used in this study but these may help reveal potential cognitive deficits in *Chmp2b*$^{-/-}$ mice in future studies.

As discussed in chapter 3 developmental, neuronal migration patterns, spinal cord motor neuron counts, study of neurotransmitter levels and distribution, as well as electrophysiological studies may help identify the pathological basis of the observed *Chmp2b*$^{-/-}$ phenotype. *Chmp5* knockout mice result in embryonic lethality and defective late endosome function and dysregulation of signal transduction (Shim et al., 2006). Therefore, parallel studies with *Chmp2b*$^{-/-}$ may reveal that depletion of Chmp2b results in altered embryonic development, trafficking impairment or endosome-lysosome dysfunction important in synaptic integrity (Sweeney et al., 2006; Lee et al., 2007; Belly et al., 2010). Further work is therefore required to determine the molecular basis of the behavioural deficits demonstrated in this chapter.

5 Characterising *CHMP2B* Transgenic Mice

The Danish FTD-3 family CHMP2B mutation is a G>C transition in the splice acceptor site of exon 6 resulting in two novel splice variants *CHMP2B*^{Int5} and *CHMP2B*$^{\Delta 10}$. *CHMP2B*^{Int5} contains the 201bp intronic sequence between exon 5 and 6 resulting in a premature stop codon and a 36 amino acid C-terminal truncation. *CHMP2B*$^{\Delta 10}$ contains a 10bp deletion at the beginning of exon 6 resulting in a frame shift mutation leading to the final 36 amino acids of CHMP2B being replaced with 29 nonsense coding amino acids at the C-terminus (Skibinski et al., 2005). Affected FTD-3 family members present with clinical FTD (Gydesen et al., 1987) and distinctive neuropathology including astrogliosis, microglial infiltration and ubiquitin and p62 inclusions; FTD-3 brains are negative for TDP-43 and FUS pathological staining (Holm et al., 2007; Holm et al., 2009). Furthermore, an additional C-terminal truncating CHMP2B mutation was identified in a Belgian familial FTD case suggesting that the loss of CHMP2B C-terminus may result in a common disease mechanism (van der Zee J. et al., 2008).

Generating transgenic mouse models based on mutations identified from human disease has become an established technique to confirm genetic mutations associated with disease and to explore and examine associated pathology and biochemistry and where appropriate preclinical drug trials of potential therapeutic agents.

This chapter describes the generation, molecular characterisation and neuropathology associated with the CHMP2B transgenic mouse lines generated and sets out initial data exploring the potential basis of autophagic dysfunction in mutant transgenic lines.

Throughout this chapter CHMP2B capitalisation is used to refer to the human transgene and lower case Chmp2b to mouse endogenous gene. *Italicised* script

is used to denote human transgene DNA expressed in transgenic mice *i.e.* genotype *CHMP2B*^{Int5} and non-italicised script to denote transgene protein expression *i.e.* CHMP2B^{Int5}.

5.1 Generating CHMP2B Transgenic Mice

5.1.1 *CHMP2B* transgene constructs

To generate CHMP2B transgenic mouse lines expressing mutant proteins CHMP2B^{Int5} and CHMP2B$^{\Delta 10}$ and overexpressing the native human CHMP2B protein CHMP2B^{WT}, cDNA coding sequences for each respective construct were subcloned into the unique SalI site of the cosmid vector designated SHaCosTet (CosTet vector), which comprises the hamster prion promoter with intron 1 (HaPrP prom) and 3'UTR (figure 5.1) (Scott et al., 1989)

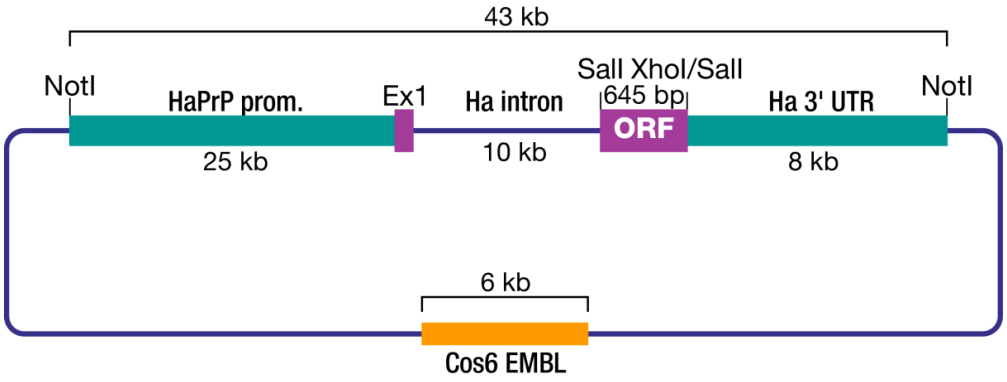

Figure 5.1 Diagrammatic representation of SHaCosTet vector (49kb) showing the 43kb NotI fragment used to generate *CHMP2B* transgenic mice.

The 43kb NotI insert was used to generate the *CHMP2B* transgenic mice. HaPrP prom, Hamster prion promoter; ORF, (open reading frame) cDNA coding sequences of $CHMP2B^{Int5}$, $CHMP2B^{\Delta 10}$ or $CHMP2B^{WT}$; NotI, SalI and XhoI digestion sites; Ha intron, Hamster PrP intron.

The hamster prion promoter was specifically used as it directs expression of transgenes to the brain and spinal cord. This is an important consideration as the aim of this study is to recapitulate the key hallmark neurodegenerative pathology identified in affected FTD-3 family members.

In the SHaCosTet vector, intron sequences are spliced out during transcription. The 3' untranslated region (3'UTR) is not translated but is important in the construct sequence as it contains a polyA sequence (AATAAA) that ensures stability of mRNA. Once the CHMP2B cDNA constructs were successfully subcloned in the SHaCosTet vector, positive clones in the correct orientation were identified through restriction mapping and cloning fidelity was checked by sequencing. High quality DNA was prepared by digesting with restriction enzyme NotI. The digested DNA was subjected to agarose gel electrophoresis to separate the 6kb CosTet vector from the 43kb transgene insert (figure 5.2). The transgene construct was purified using Gene Clean kit and spin columns (Stratech Scientific) ready for microinjection into fertilised single cell eggs.

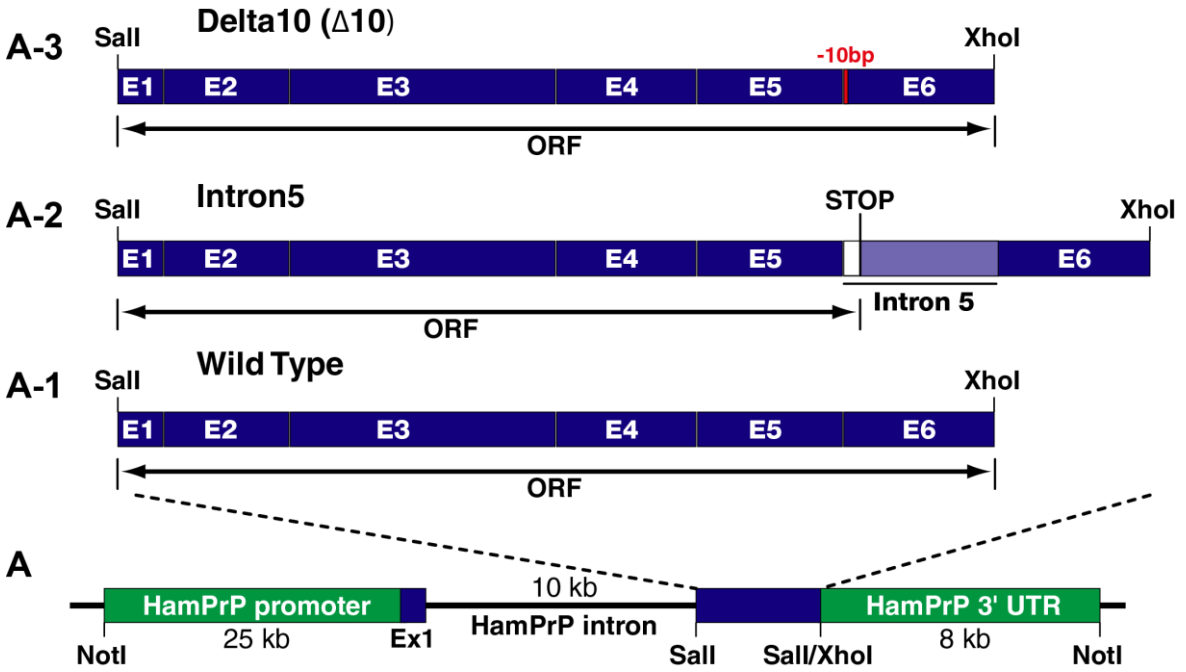

Figure 5.2 A schematic representation of CHMP2B transgene constructs.

(A) CosTet vector incorporating one of the three CHMP2B coding sequences :(A-1) *CHMP2B*^{WT}, (A-2) *CHMP2B*^{Int5} and (A-3) *CHMP2B*$^{\Delta 10}$ that were subcloned into the CosTet vector.

Microinjected eggs were cultured overnight and the resulting two-cell eggs were surgically implanted into the oviducts of pseudopregnant mice. Tail or ear biopsies were taken from the putative transgenics born from these transfers for DNA extraction and genotyping by polymerase chain reaction (PCR) as described in chapter 2**.** Pups positive for *CHMP2B*^{Int5}, *CHMP2B*$^{\Delta 10}$ or *CHMP2B*^{WT} transgenes were designated founders and were mated at 6 weeks of age to wild type C57BL/6J mice. Positive offspring were sampled for RNA expression by Reverse Transcription-PCR (RT-PCR) and protein expression by western blotting using CHMP2B antibodies. Figure 5.3 is a flow diagram illustrating the sequence of steps applied to generate the CHMP2B transgenic mice.

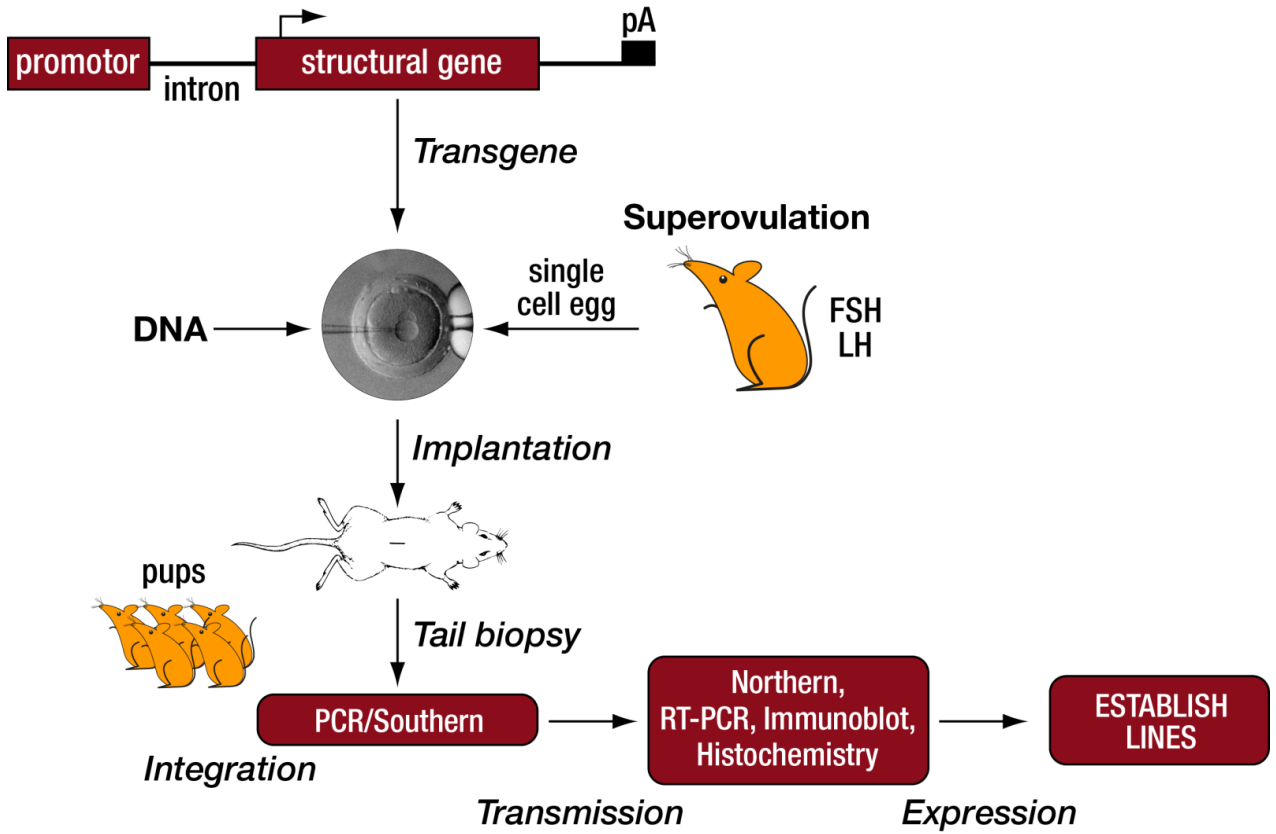

Figure 5.3 Flow diagram of steps to generate CHMP2B transgenic mouse lines.

Each of CHMP2B^{Int5}, CHMP2B$^{\Delta 10}$, and CHMP2B^{WT} construct DNA was microinjected into single cell eggs obtained from superovulated female mice. Two cell eggs harbouring transgene constructs were implanted into pseudopregnant mice. The resulting pups were genotyped for transgene integration to identify founder mice. Founder mice were mated to C57BL/6J mice; the pups from this mating were analysed to assess transmission and expression of the transgenes.

5.1.2 Summary of *CHMP2B* transgenic lines generated

Of the mice identified to be positive for *CHMP2B*^{Int5}, *CHMP2B*$^{\Delta 10}$ and *CHMP2B*^{WT} transgenes, two founder mice from each line were selected and used to establish respective transgenic lines on which molecular characterisation studies were carried out.

The *CHMP2B*^{WT} lines, Tg167 and Tg168; *CHMP2B*^{Int5} lines, Tg153 and Tg156 and *CHMP2B*$^{\Delta 10}$ lines, Tg158 and Tg164 all demonstrate transgene transmission to offspring (section 5.2.1) and RNA expression (section 5.2.2). The RNA expression data is complemented by protein expression (section 5.2.4) in both the *CHMP2B*^{WT} and *CHMP2B*^{Int5} lines but as specific antibodies to CHMP2B$^{\Delta 10}$ protein are currently not available, protein expression in the two *CHMP2B*$^{\Delta 10}$ lines, Tg158 and Tg164 could not be confirmed. The CHMP2B antibodies currently available cannot distinguish between endogenous Chmp2b and CHMP2B$^{\Delta 10}$ proteins as there is only 10 amino acid difference between the two proteins. However, high levels of overexpression would still be detected by western blot as the total CHMP2B protein level would be expected to be higher in the CHMP2B$^{\Delta 10}$ mice when compared to non-transgenic mice. As no clear increase in CHMP2B protein level was detected in the CHMP2B$^{\Delta 10}$ lines compared to endogenous Chmp2b protein even in the homozygous state, both Tg158 and Tg164 lines were culled.

Transgenic lines Tg167 and Tg168 both overexpressed CHMP2B^{WT} protein over 6.6 fold compared to endogenous Chmp2b protein. Such high levels of protein overexpression led to adverse effects in the mice (overgrown teeth) and therefore the decision was taken to utilise these lines in their heterozygous state only. *CHMP2B*^{Int5} lines, Tg153 and Tg156 were both bred to homozygosity and in the homozygous state Tg153 was found to express CHMP2B^{Int5} protein at 0.9 times endogenous Chmp2b protein expression level (section 5.2.4).

The transgenic lines that have been successfully established for each of the CHMP2B transgenes and their expression profiles are summarised in table 5-1. All CHMP2B transgenic mouse lines were established on a CBA x C57BL/6J background.

Transgene	Positive Lines	RNA Expression	Protein Expression	Homozygous Mating
CHMP2B^{WT}	Tg167	✓	✓	×
	Tg168	✓	✓	×
CHMP2B^{Int5}	Tg153	✓	✓	✓
	Tg156	✓	✓	✓
CHMP2B$^{\Delta 10}$	Tg158	✓	?	×
	Tg164	✓	?	×

Table 5.1 Summary table showing characterisation profiles of CHMP2B transgenic lines.

This table lists the transgenic lines generated overexpressing wild type CHMP2B (CHMP2B^{WT}); expressing CHMP2B Intron 5 mutant transgene (CHMP2B^{Int5}) and CHMP2B Delta 10 mutant transgene (CHMP2B$^{\Delta 10}$). The table summarises RNA and protein expression determined for each line and homozygous lines established from homozygous mating.

Because of the vast amount of time and costs involved in the molecular and pathological characterisation of transgenic mouse lines, even though two lines were generated for each of *CHMP2B*^{Int5} *and CHMP2B*^{WT} transgenes, data for only *CHMP2B*^{Int5} Tg153 *and CHMP2B*^{WT} Tg168 are presented in this study as these are the two highest expressing lines for each respective transgene.

Table 5-2 lists the other CHMP2B transgenic lines that were generated but terminated because respective founder mice were either unsuccessful in breeding, did not transmit the relevant transgene to their progeny or did not express the transgene in sufficient amounts at the RNA level. As previously described *CHMP2B*$^{\Delta 10}$ transgenic lines Tg158 and Tg164 were also terminated as protein expression could not be conclusively established.

Transgene	Positive Lines	Fate of Mouse Line
CHMP2B^{WT}	Tg150	Founder died without breeding
	Tg151	No expression line terminated
	Tg166	Insufficient expression line terminated
	Tg169	Founder died without breeding
	Tg178	Founder died without breeding
	Tg179	Line culled- not breeding
CHMP2B^{Int5}	Tg154	Low expression -line culled
	Tg155	Not transmitting transgene –line culled
CHMP2B$^{\Delta 10}$	Tg158	Line culled- Protein expression could not be established
	Tg164	Line culled
	Tg165	Protein expression could not be established Line culled Low RNA expression line culled

Table 5.2 Summary of CHMP2B transgenic lines terminated.

This table lists the transgenic lines that were terminated for reasons listed against each line. *CHMP2B^{WT}* -Wild type CHMP2B overexpressors; *CHMP2B^{Int5}* -CHMP2B Intron 5 mutant lines and *CHMP2B$^{\Delta 10}$* -CHMP2B Delta 10 mutant lines. Mouse lines were terminated if transgene DNA, RNA or protein expression could not be determined in first generation offspring.

5.2 Molecular Characterisation

5.2.1 Genotyping *CHMP2B* Transgenic Mice

DNA amplification of *CHMP2B* by polymerase chain reaction (PCR) was used to screen mice for transgenes of interest *CHMP2B*^{Int5}, *CHMP2B*$^{\Delta 10}$ *and CHMP2B*^{WT}. The same forward and reverse primers, SalF and F19105 were used to amplify all three transgenes. The forward primer SalF (figure 5.4 orange arrow) targets the 5' region of the CHMP2B cDNA sequence and the reverse primer F19105 sits on the hamster prion 3'UTR region of the construct (figure 5.4).

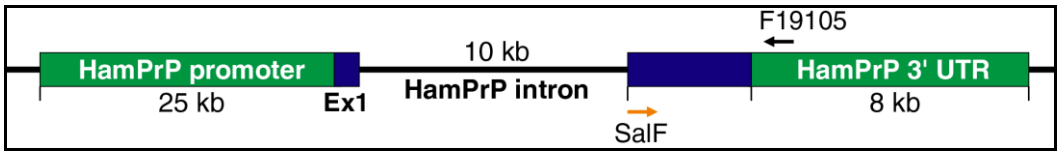

Figure 5.4 Schematic representation of primer positions on transgene construct used for gentoyping.

Region of transgene construct amplified by PCR primers to genotype transgenic mice. SalF-forward primer and F19105 reverse primer.

These primers were predicted to produce PCR products of 939bp when amplifying the *CHMP2B*^{Int5} transgene, 728bp bands when amplifying the *CHMP2B*$^{\Delta 10}$ transgene and 738bp when amplifying the *CHMP2B*^{WT} transgene (figure 5.5).

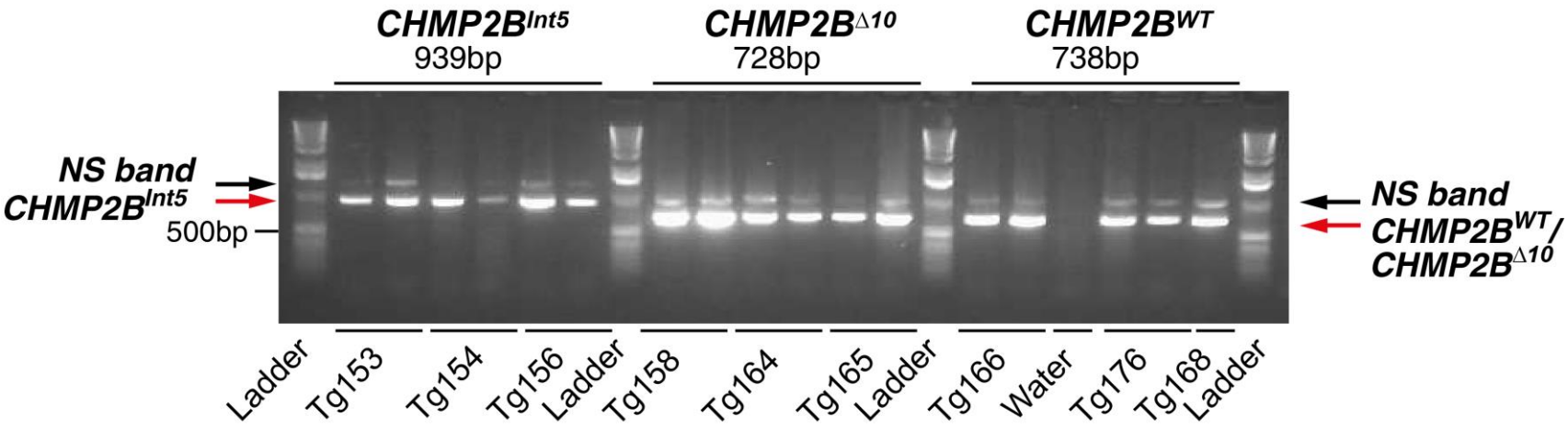

Figure 5.5 Representative PCR DNA bands for each of the *CHMP2B* transgenic lines.

CHMP2B Intron 5 mutant lines (*CHMP2B*^{Int5}) producing 939bp DNA bands, *CHMP2B Delta 10* mutant lines (*CHMP2B*$^{\Delta 10}$) producing 738bp DNA bands and *CHMP2B wild type* overexpressors (*CHMP2B*^{WT}) producing 728pb DNA bands on 1.5% agarose gel stained with ethidium bromide. N>5 for each transgenic line, 1kb DNA ladders used; left to right in lanes 1, 8, 15 and 22 and water control with no DNA template lane 18 from left. NS= non-specific DNA band likely due to non-specific priming of mouse genomic DNA. .

5.2.2 RNA Expression in Transgenic Mice

To determine transgene RNA expression in *CHMP2B* transgenic mice RNA was extracted from *CHMP2B*^{Int5}, *CHMP2B*$^{\Delta 10}$ and *CHMP2B*^{WT} transgenic mouse brains and first strand cDNA template synthesised (described in detail in chapter 2). Primers designed to target *CHMP2B* cDNA were used in a PCR: forward primer SalF targets the 5' end of the *CHMP2B* cDNA sequence and the reverse primer XhoRI targets the 3' end of the *CHMP2B* cDNA sequence (figure .5.6).

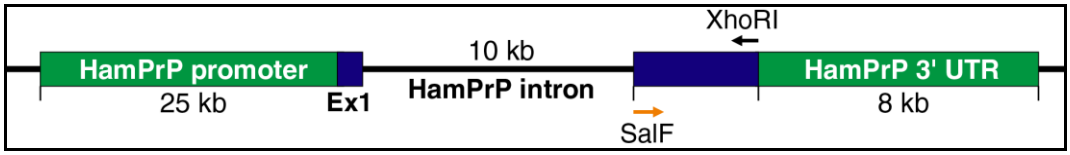

Figure 5.6 Schematic representation of primer positions on transgene construct used in RT-PCR.
cDNA was synthesised by RT-PCR using whole brain RNA. The orange and black arrow indicate region amplified by forward primer SalF and reverse primer XhoRI respectively.

The predicted DNA band sizes are 862pb for *CHMP2B*^{Int5}, 652bp for *CHMP2B*$^{\Delta 10}$ and 662bp for *CHMP2B*^{WT}. RT-PCR products from representative samples from each mouse line are exhibited in figure 5.7. The RNA expression data demonstrates that *CHMP2B*^{Int5} transgenic lines Tg153, Tg154 and Tg156 clearly express *CHMP2B*^{Int5} RNA as the 862bp band is absent in the non-transgenic control lane. In addition, the *CHMP2B*^{Int5} band is 200bp bigger than the endogenous mouse Chmp2b band resulting in two distinct bands in the RT-PCR blot (figure 5.7). This difference in band size is due to the 200bp intronic inclusion in the *CHMP2B*^{Int5} mutant allele. In addition, data from semi-quantitative real-time TaqMan® PCR show that RNA expression in *CHMP2B*^{Int5} Tg153 line is increased ~3.26 (SEM +/-0.37) fold compared to Non-Tg control (AI personal communication).

CHMP2B$^{\Delta 10}$ transgenic lines Tg158 and Tg164 also express *CHMP2B*$^{\Delta 10}$ RNA. As there is only a 10bp difference between the cDNA of *CHMP2B*$^{\Delta 10}$ and endogenous mouse *Chmp2b*, the very small difference in the RT-PCR band sizes cannot be adequately resolved. However, the RT-PCR blot demonstrates a doublet running marginally lower in Tg158 and Tg164, which are therefore adjudged to express the *CHMP2B*$^{\Delta 10}$ RNA (figure 5.7). However, these lines were terminated because the expression levels could not be confirmed at the protein level due to the lack of suitable antibodies. In contrast, Tg165 lacking the doublet and also showing similar signal intensity as the non-transgenic control is considered to be a non-expressing line and was therefore terminated.

Finally, Tg167 and Tg168 but not Tg166 are adjudged to express *CHMP2B*^{WT} RNA (figure 5.7). The human *CHMP2B*^{WT} band is the same size as the endogenous mouse *Chmp2b* and so it is not possible to resolve these as two separate bands. However, as human *CHMP2B*^{WT} is overexpressed, the bands in Tg167 and Tg168 lines are seen to be brighter than non-transgenic control lines. In contrast, Tg166 with signal intensity similar to non-transgenic control is considered to be a non-expressing line. Notably, RNA expression in the Tg168 line is increased ~3.20 (SEM +/-0.04) fold compared to Non-Tg; this semi-quantitative real-time TaqMan® PCR data is kindly provided by AI (Ghazi-Noori et al., 2012)

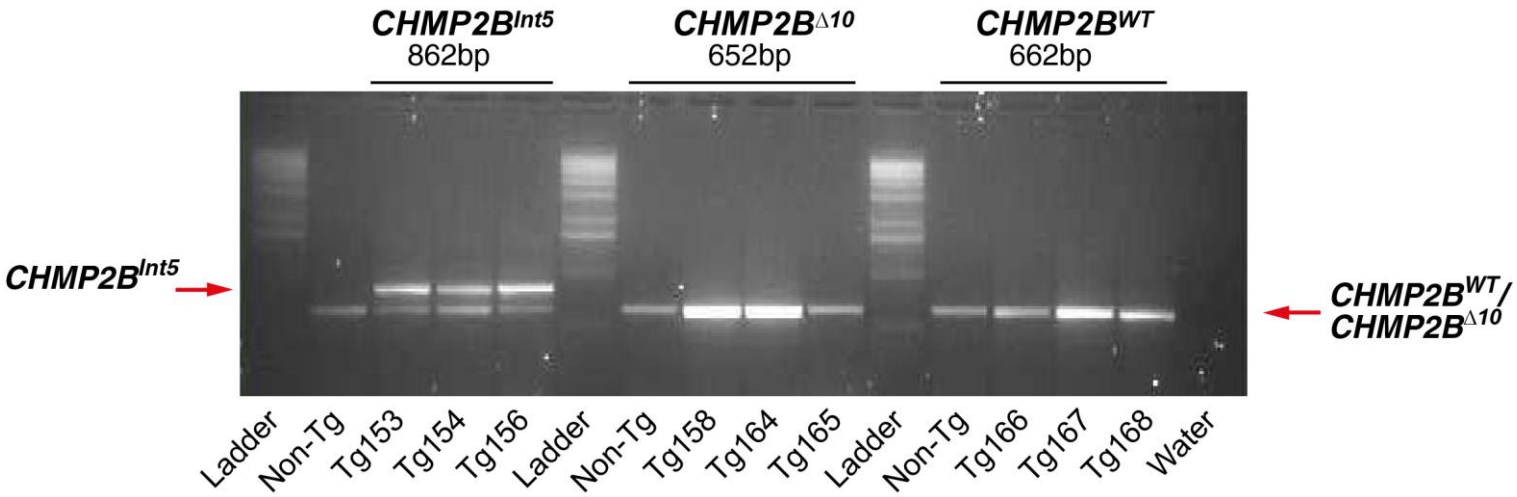

Figure 5.7 Representative RNA bands for each of *CHMP2B* transgenic lines and non-transgenic control.

Tg153, Tg154, Tg156 are *CHMP2B Intron 5* mutant lines (*CHMP2B*^{Int5}) producing 862bp DNA bands; Tg158, Tg164, Tg165 are *CHMP2B Delta 10* mutant lines (*CHMP2B*$^{\Delta 10}$) producing 652bp DNA bands; Tg166, Tg167 and Tg168 are *CHMP2B wild type* overexpressors (*CHMP2B*^{WT}) producing 552bp DNA bands on a 1.5% agarose gel following PCR amplification. 1kb DNA ladders were used to size the bands seen left to right in lanes 1, 6, and 11; No RNA template water control showing no amplification product is seen in lane 16 from left. (Representative image of N=3 for each transgenic line).

5.2.3 Screening for Homozygous Mice

A real-time TaqMan PCR assay was used to determine the zygosity of mice (chapter 2). Mice that were assayed to be homozygous by Taqman were confirmed in progeny test matings to non-transgenic mice. If the mice are true homozygotes, the offspring from the non-transgenic x homozygous matings would all be expected to be positive (hemizygotes) when genotyped using PCR amplification for *CHMP2B* transgenes.

Figure 5.8 shows a Real-Time PCR amplification plot from Tg158 transgenic line as a representative example. Zygosity for all other transgenic lines was determined using the same protocol and homozygotes were identified using the delta Ct method detailed in chapter 2 section 2.4.5.1.

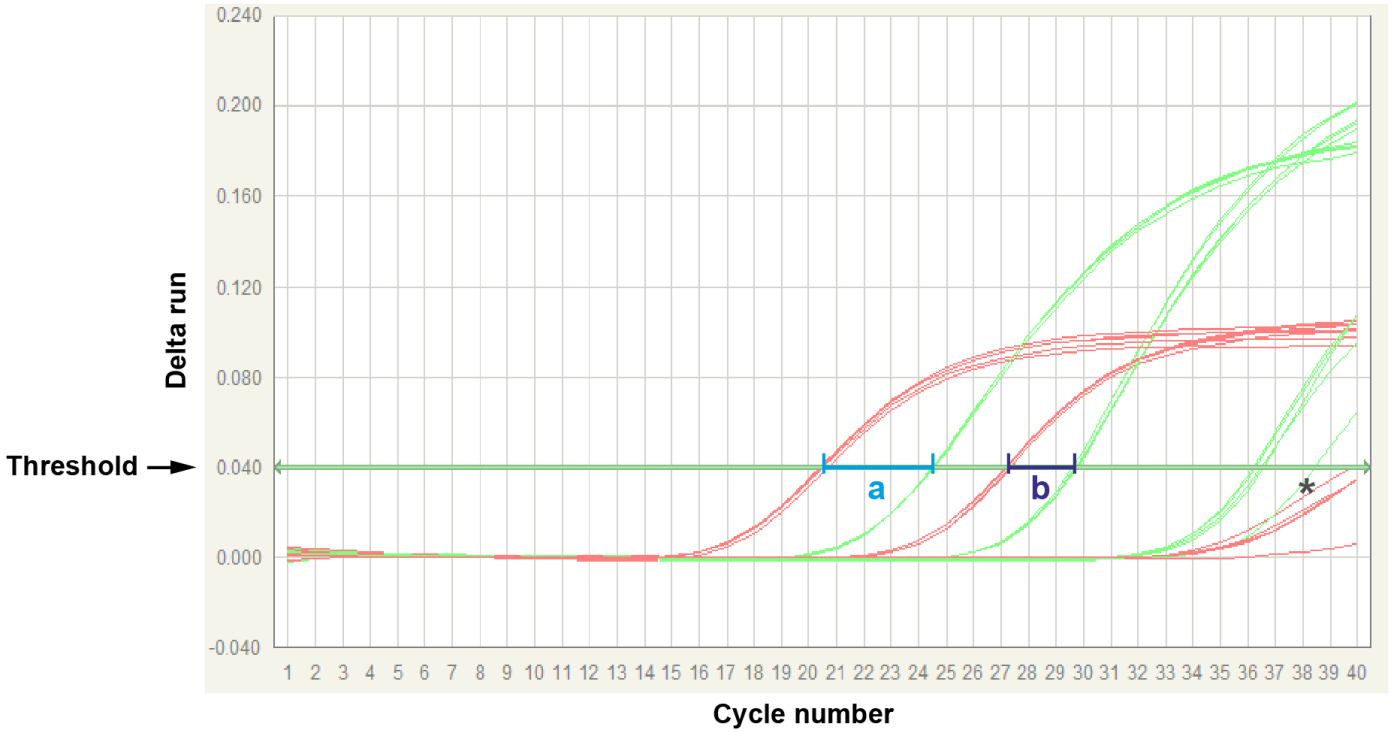

Figure 5.8 Screen print of Real-Time TaqMan® PCR amplification plot used to identify *CHMP2B* transgenic homozygous mice.

Green lines are amplification profiles for *CHMP2B* and red lines are plots for GAPDH amplification. Example of representative amplification plot showing homozygous and heterozygous sample (a; light blue) and homozygous (b; dark blue) and no template water (star). (Representative of N=5 for each sample).

5.2.4 CHMP2B Protein Expression

To determine transgene protein expression in the *CHMP2B* transgenic lines, custom made rabbit polyclonal antibodies were generated by 21 Century Biochemicals using *CHMP2B* N-terminal peptides. Testing several bleeds from three different rabbits on transgenic and non-transgenic 10% mouse brain homogenates, western blot analysis demonstrated that two antibodies detected specific CHMP2B bands. One antibody corresponding to bleed 7 produced the most suitable detection to $CHMP2B^{WT}$ protein and was designated as antibody 0762-B7. A second antibody, CHMP2B-3335 demonstrated specific detection of both $CHMP2B^{WT}$ and $CHMP2B^{int5}$ proteins in optimisation studies and was used to quantify $CHMP2B^{WT}$ and $CHMP2B^{Int5}$ transgene protein expression.

5.2.4.1 Initial detection of $CHMP2B^{WT}$ transgene protein

As human and mouse wild type CHMP2B proteins have the same molecular weight, overexpression of human $CHMP2B^{WT}$ protein was determined by producing greater band intensity, that is increased CHMP2B protein in comparison to non-transgenic mice. The predicted band size for wild type CHMP2B protein is 24kDa, however the band observed on Western blots is just below 36kDa. This may be due to the protein's highly charged nature or due to glycosylation or phosphorylation of the intracellular protein.

CHMP2B protein expression is demonstrated in each of the *CHMP2B* transgenic lines by western blotting 10% brain homogenates from hemizygous transgenic mice (figure 5.9). The blot has been probed with 0762-B7 antibody which detects N-terminal amino acids 10-28 (VDDVIKEQNRELRGTQRAI) of wild type CHMP2B.

Bands are present just below 36kDa corresponding to wild type Chmp2b protein for each sample except *Chmp2b*$^{-/-}$ which does not express Chmp2b protein, confirming specificity of the antibody. Lanes corresponding to Tg167 and Tg168

(*CHMP2B*^{WT} lines) show bands of much greater intensity compared to other transgenic lines and non-transgenic samples, confirming overexpression of *CHMP2B*^{WT} transgene protein (figure 5.9). The same increased band intensity is not observed in Tg166, also a *CHMP2B*^{WT} line suggesting this line does not overexpress the transgene protein (figure 5.9).

The actin blot (figure 5.9) shows the same blot re-probed with anti-actin antibody demonstrating that all the samples were loaded equally.

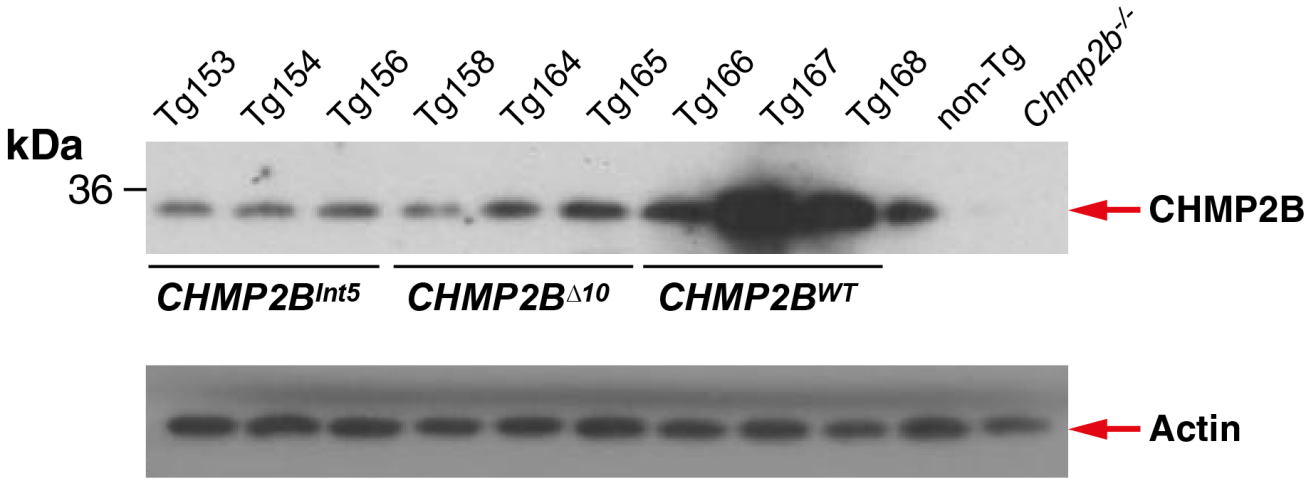

Figure 5.9 Western blot of CHMP2B lines using N-Terminal antibody 0762-B7.

CHMP2B^{WT} lines Tg167 and Tg168 demonstrate a much stronger CHMP2B band intensity compared to Non-Tg sample confirming overexpression of transgenic CHMP2B relative to endogenous Chmp2b. CHMP2B^{Int5} or CHMP2B$^{\Delta 10}$ protein bands are not detected in the respective lines. As expected the Chmp2b knockout (*Chmp2b*$^{-/-}$) sample does not produce a Chmp2b band, further supporting the specificity of the antibody used (representative of N=3 for each transgenic line; 1 minute exposure).

5.2.4.2 Detection of CHMP2B^{Int5} transgene protein

CHMP2B antibody 0762-B7 was designed to target a common N-terminal amino acid sequence of the CHMP2B protein so that in principle it may detect CHMP2B^{Int5}, CHMP2B$^{\Delta 10}$ and CHMP2B^{WT} proteins. However, CHMP2B^{Int5} and CHMP2B$^{\Delta 10}$ protein bands were not initially detected (figure 5.9). Optimisation of the blotting protocol was therefore performed and CHMP2B^{Int5} protein was detected for the first time by using 0762-B7 antibody at a 3 fold higher concentration and exposing blots to film for a longer (30 minutes) duration as detailed in chapter 2 (figure 5.10).

Western blot of homozygous and hemizygous Tg153 (*CHMP2B*^{Int5}) mouse brain homogenates shows the endogenous mouse chmp2b protein band present in Tg153 and Non-Tg samples (figure 5.10). This blot also shows an additional band below the endogenous mouse Chmp2b band. This additional band is most intense in the homozygous (Tg153+/+) samples, less intense in hemizygous (Tg153+/-) samples and absent in Non-Tg samples. This band runs lower than mouse wild type endogenous Chmp2b band, below 36kDa and above 22kDa and is consistent with the expected size of CHMP2B^{Int5} protein (figure 5.10). The actin blot shows samples are loaded equally (figure 5.10).

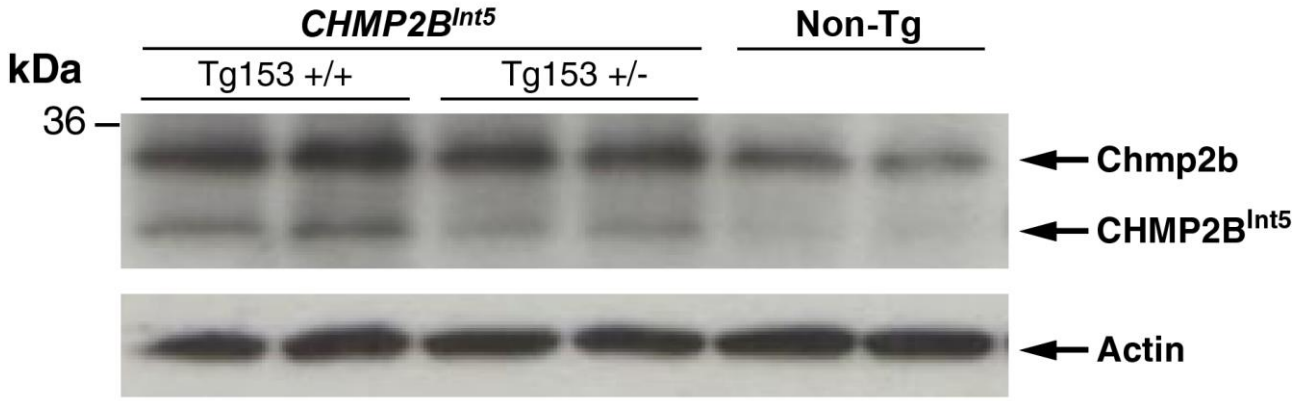

Figure 5.10 Initial detection of CHMP2B-Intron 5 band in Tg153 line.

The strongest CHMP2B^{Int5} protein band is observed in Tg153+/+ homozygous samples, less intense CHMP2B^{Int5} protein band is observed in Tg153+/- hemizygous samples and a distinct CHMP2B^{Int5} protein band is not present in Non-Tg samples (N=2 for each genotype; 30-minute exposure).

To confirm CHMP2B^{Int5} protein expression in the Tg153 line and achieve a cleaner and more distinct CHMP2B^{Int5} protein band, the western blot protocol was further optimised and a fresh aliquot of 0762-B7 used and additional control samples were included in the western blot. *CHMP2B^{Int5}* or *CHMP2B^{WT}* transfected HEK cell lysates were used as positive and negative CHMP2B^{Int5} transgene protein controls respectively. Human FTD-3 and control brain lysates were also included. Furthermore, short (10 minutes) and long (25 minutes) film exposure times were tested to reveal CHMP2B^{Int5} bands (figure 5.11).

As with the first western blot (figure 5.10), figure 5.11 also shows an endogenous CHMP2B band in mouse and human brain samples. This blot too shows a second band (below 36kDa and above 22kDa) running below the endogenous Chmp2b band. This protein band which is consistent with the CHMP2B^{Int5} band in figure 5.10 is identified in *CHMP2B^{Int5}* Tg153 mouse brain samples in both short (10 minutes) and long (25 minutes) film exposure blots. Critically, this smaller band in the *CHMP2B^{Int5}* mouse brain samples runs at the same size as the CHMP2B^{Int5} protein band from *CHMP2B^{Int5}* transfected HEK positive control cell lysates. Of note, in the FTD-3 sample, this CHMP2B^{Int5} band is also seen in the long (25-minute) exposure blot (figure 5.11).

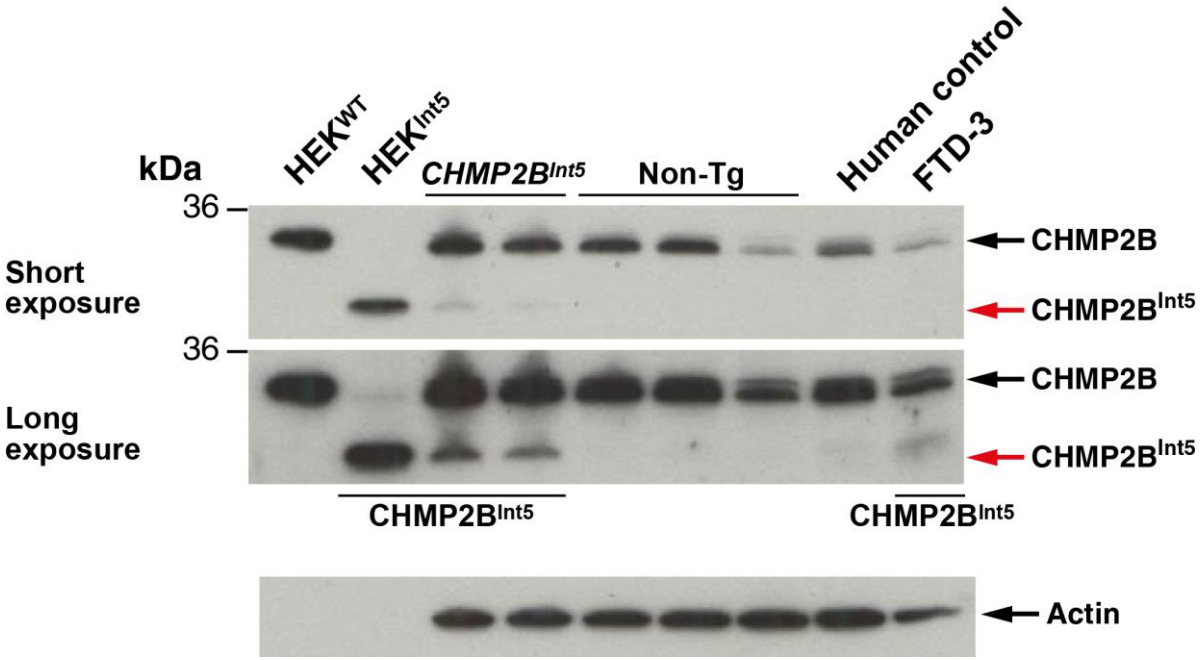

Figure 5.11 Western blot demonstrating identification of CHMP2B^{Int5} protein in Tg153 mouse brain.

CHMP2B^{Int5} protein band is identified in *CHMP2B^{Int5}* mouse brain running at the same size as HEK^{Int5} samples at both short (10 minutes) and long (30 minutes) exposure; CHMP2B^{Int5} protein band also observed in human FTD-3 brain homogenate, but is absent in Non-Tg, human control and HEK^{WT} sample (N=3 for each genotype).

In summary, figure 5.11 confirms that Tg153 *CHMP2B*^{Int5} transgenic mouse brains express CHMP2B^{Int5} protein and that this protein is not present in non-transgenic (Non-Tg) brain samples, control human brain or *CHMP2B*^{WT} transfected cells. The actin blot shows even sample loading in mouse and human brain lanes (figure 5.11). Actin bands are not present in either of the cell lysate lanes. This is because transfected cells express a disproportionately greater amount of transfected constructs and therefore a lot less of cell lysate volume is loaded onto the gel, accounting for the absence of actin bands in the actin blot of figure 5.11.

CHMP2B$^{\Delta 10}$ protein expression could not be detected in Tg158, Tg164 or Tg165 *CHMP2B*$^{\Delta 10}$ lines due to lack of antibodies specific to CHMP2B$^{\Delta 10}$ protein. However, overexpression of CHMP2B$^{\Delta 10}$ protein, above endogenous mouse Chmp2b levels, would be expected to be detected by western blot. It has previously been demonstrated that *CHMP2B*$^{\Delta 10}$ protein is degraded more quickly than CHMP2B^{Int5} or *CHMP2B*^{WT} protein (Lee et al., 2007), which could explain the lack of overexpressed protein, particularly as CHMP2B$^{\Delta 10}$ RNA was detected.

Having demonstrated *CHMP2B*^{WT} transgene expression in Tg167 and Tg168 lines and *CHMP2B*^{Int5} transgene protein expression in Tg153 line, a consensus was reached to move forward using only *one* of each transgenic line. Therefore, for transgene protein quantification and histological analysis Tg168 was used as *CHMP2B*^{WT} representative line and Tg153 as the *CHMP2B*^{Int5} representative line.

5.2.4.3 Quantification of transgene proteins

A significant limitation to using 0762-B7 antibody was the different antibody concentration and film exposure times needed to reveal CHMP2B^{Int5} and CHMP2B^{WT} bands, making it impractical to analyse Non-Tg samples, Tg153 *CHMP2B*^{Int5} samples and Tg168 *CHMP2B*^{WT} on the same western blot for quantification.

To overcome this limitation and to quantify Tg153 CHMP2B^{Int5} and Tg168 CHMP2B^{WT} transgene protein expression, a different CHMP2B antibody designated CHMP2B-3335 and generated from a recombinant full-length CHMP2B protein immunogen was used (figure 5.12).

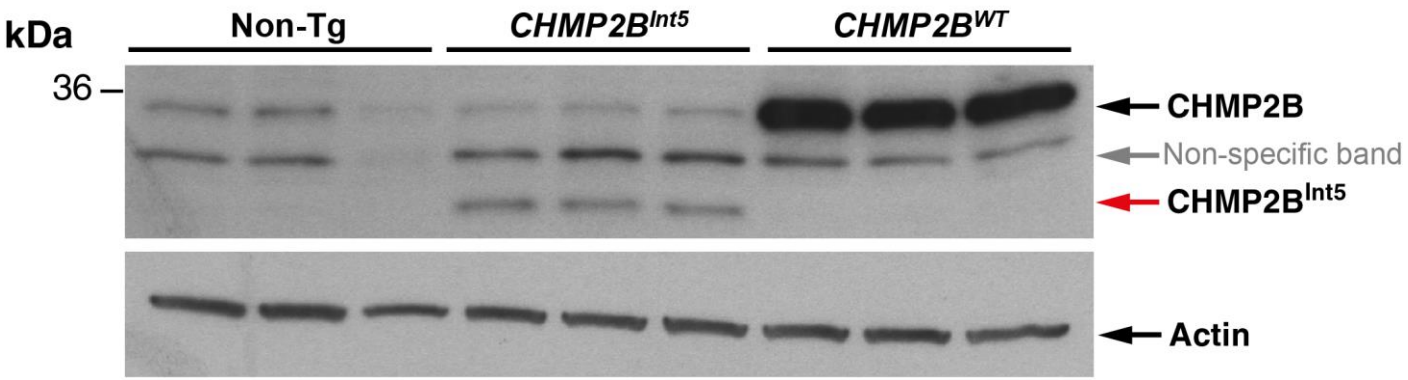

Figure 5.12 Western blot of CHMP2B lines using full-length anti-CHMP2B antibody.

CHMP2B^{WT} samples show a strong CHMP2B protein band (CHMP2B black arrow) compared to Non-Tg samples which demonstrate only the endogenous mouse Chmp2b protein band. *CHMP2B*^{Int5} samples demonstrate an additional protein band consistent with CHMP2B^{Int5} (red arrow) that is absent in all other samples. Antibody used is full-length anti-CHMP2B antibody CHMP2B-3335 (N=3 for each genotype).

To quantify CHMP2B^{Int5} and CHMP2B^{WT} transgene protein expression, exposed films were scanned and analysed using the Volocity program. Transgenic samples were all normalised to Non-Tg samples (described in chapter 2). CHMP2B^{WT} protein is expressed 6.6 fold higher than endogenous Chmp2b (p= 0.00005*) and CHMP2B^{Int5} protein is expressed 0.9 fold in comparison to endogenous Chmp2b protein and is not considered an overexpression as CHMP2B^{Int5} mutant protein expression is almost equal to endogenous Chmp2b protein expression (figure 5.13).

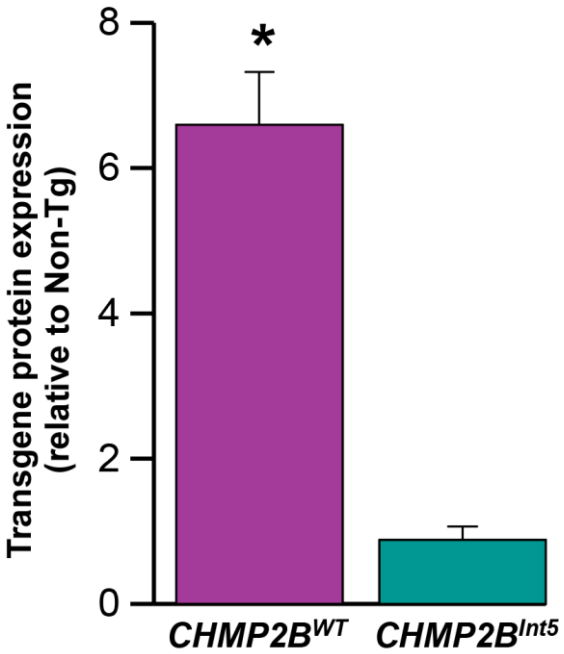

Figure 5.13 Quantification of transgenic proteins.

Graph shows a significant (6.6 times) increase in Tg168 (*CHMP2B^{WT}*) protein expression (*p*= 0.00005). CHMP2B Intron 5 protein expression in Tg153 (*CHMP2B^{Int5}*) is ~0.9, almost equivalent to endogenous Chmp2b protein expression (N=3 for each genotype; error bars=SEM).

5.3 Pathology

Having determined relative transgene expression levels for *CHMP2B^{Int5}* Tg153 (0.9 times) and *CHMP2B^{WT}* Tg168 (6.6 times) mouse lines relative to endogenous Chmp2b protein expression in non-transgenic lines (Non-Tg), a systematic histological study was carried out to examine the brain and spinal cord (lumbar region) of Tg153 *CHMP2B^{Int5}* (from here on referred to as *CHMP2B^{Int5}*), Tg168 *CHMP2B^{WT}* (from here on referred to as *CHMP2B^{WT}*) and Non-Tg mice at 6, 12 and 18 months of age.

Immunohistochemical staining for markers of neuroinflammation, inclusion pathology and neuronal loss have been studied to investigate whether the mutant *CHMP2B^{Int5}* expressed in the brain and spinal cord recapitulates the distinctive neuropathology reported in affected members of the FTD-3 family (Holm et al., 2007; Holm et al., 2009).

The gross morphology of sciatic nerve samples were examined from *CHMP2B^{Int5}*, *CHMP2B^{WT}* and Non-Tg mice at the latest time point, 18 months of age, to investigate whether peripheral nerve pathology was present. Finally an EM study was carried out on *CHMP2B^{Int5}* mouse brains compared to Non-Tg mouse brains to explore the ultra-structural neuropathology.

5.3.1 Brain Pathology

5.3.1.1 Astrogliosis and microglial activation

Transgenic mouse brains were examined for evidence of astrogliosis and microglial activation, using two established immunohistochemical markers, Glial Fibrillary Acidic Protein (GFAP) and Ionized calcium binding adaptor molecule 1 (Iba1) (Middeldorp and Hol, 2011) (described in detail in chapter 3).

Proliferation of GFAP-positive astrocytes is observed in an age-dependent progressive manner in *CHMP2B*^{Int5} brains (figure 5.14a-c). Few proliferating astrocytes are observed in 6-month *CHMP2B*^{Int5} brain (figure 5.14a). Abundant astrogliosis is initially identified at 12 months in *CHMP2B*^{Int5} brain (figure 5.14b). By 18 months astrogliosis increases in *CHMP2B*^{Int5} brains compared to both 12 months *CHMP2B*^{Int5} brain (figure 5.14b), 18 months Non-Tg (figure 5.14f) and *CHMP2B*^{WT} brain (figure 5.14i). Non-Tg (figure 5.14d-f) and *CHMP2B*^{WT} (figure 5.14g-i) do not demonstrate comparable progressive astrogliosis at age-matched time points.

Quantitative analysis of percent GFAP coverage verifies a progressive increase in *CHMP2B*^{Int5} (not statistically significant at 6 months in any brain region examined), progressing to be statistically significant in the cortex at 12 months (*p<0.05 figure 5.15A) and 18 months (**p<0.01 figure 5.15A) as well as in the thalamus at 12 months (***p<0.001 figure 5.15B) and 18 months (****p<0.0001 figure 5.15B) compared to age- and brain region- matched Non-Tg sections (figure 5.15A and B respectively). No significant changes are demonstrated in *CHMP2B*^{WT} at any age in any brain region examined (figure 5.15A and 5.15B).

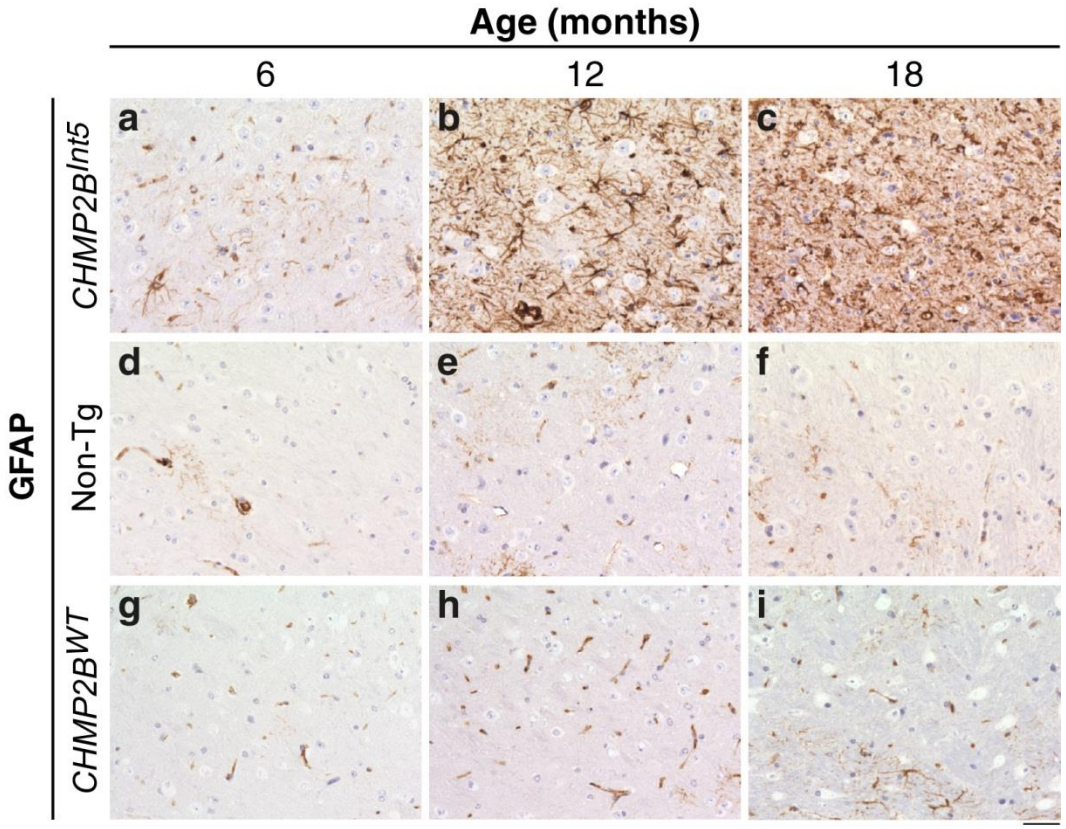

Figure 5.14 Progressive astrogliosis in *CHMP2B^{Int5}* thalamus

Representative images from Tg153 *CHMP2B^{Int5}*, Non-Tg and Tg168 *CHMP2B^{WT}* mouse thalamus at 6, 12 and 18 months. *CHMP2B^{Int5}* thalamus shows specific proliferation of GFAP positive astrocytes at all ages examined with a slight but non-significant increase at 6 months. Significant astrogliosis is observed initially at 12 months (b) and increases at 18 months (c) demonstrating progressive astrogliosis. There is no significant evidence of GFAP positive astrocytes at any age in Non-Tg (d-f) and *CHMP2B^{WT}* (g-i) mouse thalamus. (N=3 for each genotype at each age; scale bar= 160µm).

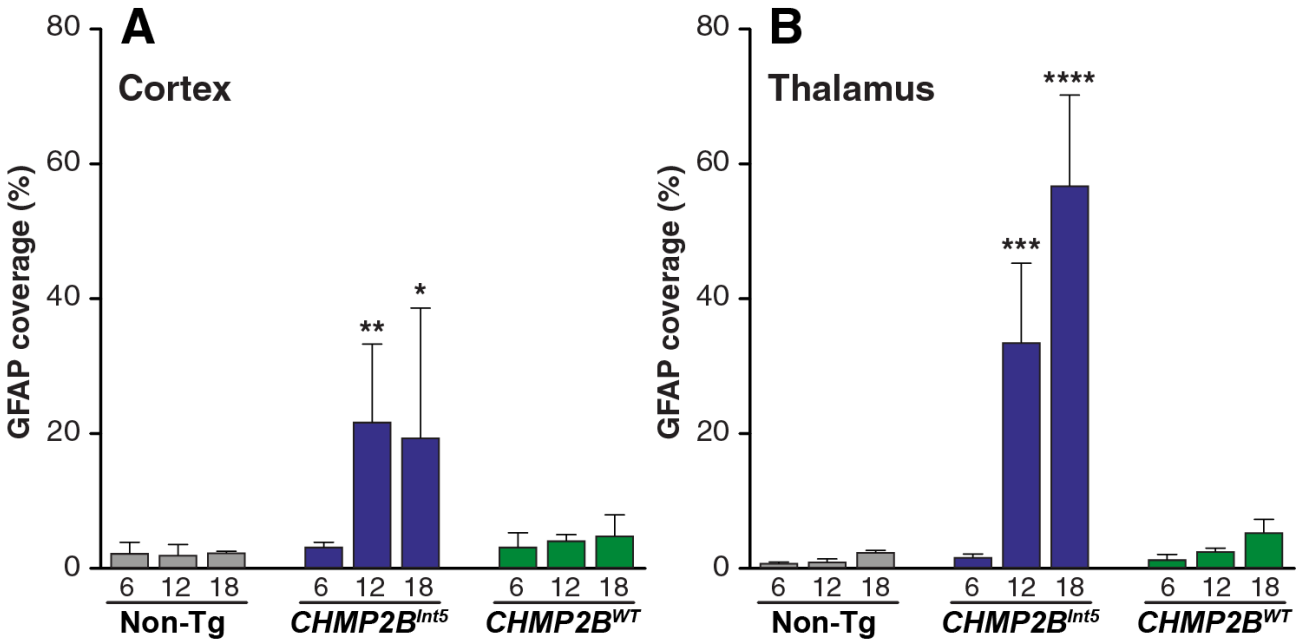

Figure 5.15 Quantification of astrogliosis using GFAP coverage in the cortex and thalamus of CHMP2B^{Int5} mice.

Astrogliosis is significantly increased in the cortex (A) and thalamus (B) of Tg153 *CHMP2B^{Int5}* mice at 12 and 18 months of age compared to age matched Non-Tg mice. No significant changes are identified in Tg168 *CHMP2B^{WT}*at any age. (N=5 for each genotype at each age; error bars % SEM; *p<0.05, **p<0.01,***p<0.001, ****p<0.0001 obtained by two-way ANOVA and Bonferroni post-hoc test).

Activated Iba1-positive microglia with intensely staining cell bodies and thickened processes are also detected in an age-dependent progressive manner in *CHMP2B*^{Int5} brains (figure 5.16a-c). Few activated microglia with extended processes are seen in 6 month-old *CHMP2B*^{Int5} brain (figure 5.16a). Microglial activation increases at 12 (figure 5.16b) and 18 months (figure 5.16c) observed as increasing number of activated microglia, greater staining intensity of the cell bodies and activated morphology (figure 5.16a-c). Non-Tg (figure 5.16d-f) and *CHMP2B*^{WT} brains (figure 5.16g-i) do not exhibit comparable activated microglia at age-matched time points.

Microglial activation can be classified according to cellular morphology. In order of increasing activation, microglia are classified as ramified (normal), reactive, amoeboid or phagocytic (most activated state) (Ghazi-Noori et al., 2012).

Non-parametric Kruskal-Wallis ANOVA statistical analysis of Iba1 scores was performed using this classification scheme with a score of 1 for ramified morphology up to 4 for phagocytic morphology. This analysis reveals a significant increase in microglial activation at 6 months (*p<0.05 figure 5.17B) 12 months (**p<0.001 figure 5.15B) and 18 months (****p<0.0001) compared to age matched Non-Tg brain (figure 5.15B). No significant changes are demonstrated in *CHMP2B*^{WT} at any age in any brain region examined (figure 5.17A and 5.15B).

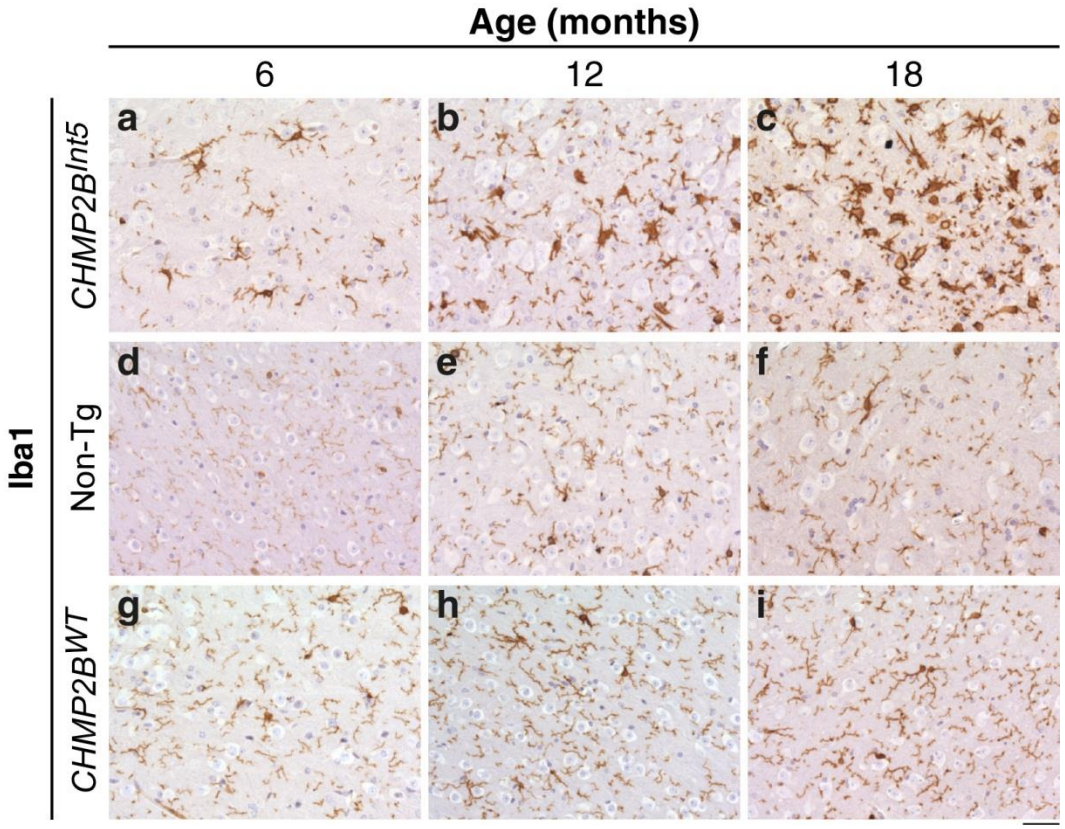

Figure 5.16 Progressive microglial activation in *CHMP2B^{Int5}* thalamus.

Representative images from Tg153 *CHMP2B^{Int5}*, Non-Tg and Tg168 *CHMP2B^{WT}* mouse thalamus at 6, 12 and 18 months. *CHMP2B^{Int5}* thalamus shows specific activation of Iba1 positive microglia at all ages examined with a few at 6 months (a) and progressively increasing at 12 months (b) and 18 months (c) demonstrating progressive microglial activation. There are very few microglia demonstrating activated morphology at any age in Non-Tg (d-f) and *CHMP2B^{WT}* (g-i) mouse thalamus. (N=3 for each genotype at each age; scale bar= 160µm).

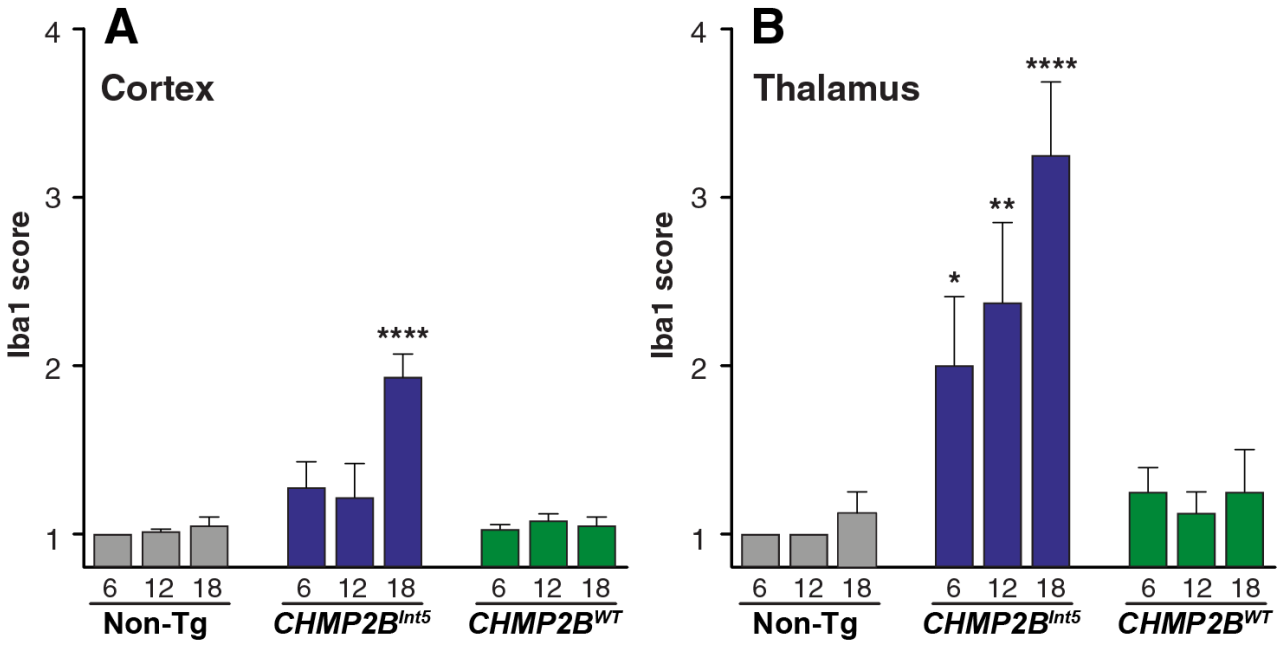

Figure 5.17 Scores of progressive microglial activation in the cortex and thalamus of CHMP2B^{Int5} mice.

Microglial activation is significantly increased in the cortex (A) of *CHMP2B*^{Int5} at 18 months compared to age matched Non-Tg mice and in a progressive age-dependent manner in *CHMP2B*^{Int5} thalamus (B) at 6, 12 and 18 months compared to age matched Non-Tg mice. No significant changes are identified in *CHMP2B*^{WT} mice at any age. (N=5 for each genotype at each age; *p<0.05, **p<0.01, ****p<0.0001 obtained using non-parametric Kruskal-Wallis ANOVA statistical analysis)

Quantitative immunohistochemical analysis of GFAP and Iba1 has revealed significant and age-dependent progressive astrogliosis and microglial activation specific to *CHMP2B*^{Int5} mouse cortex and thalamus. Data not shown but recently reported by AI also demonstrates progressive astrogliosis and microglial activation in Tg153 *CHMP2B*^{Int5} corpus callosum representative of brain white matter (Ghazi-Noori et al., 2012). Astrogliosis demonstrated in *CHMP2B*^{Int5} mouse brain is consistent with reported FTD-3 pathology (Holm et al., 2007).

5.3.1.2 Inclusion pathology

Ubiquitin and p62 inclusions co-localise in FTD-3 human brains (Holm et al., 2007), therefore in this study p62 has been used as (1) a marker of inclusion pathology and (2) because of its localisation to autophagosomes and interaction with LC-3 as a surrogate marker of autophagy (Komatsu and Ichimura, 2010).

Ubiquitin and p62 immunostaining was performed on brain sections of 6, 12 and 18 months old *CHMP2B*^{Int5}, *CHMP2B*^{WT} and Non-Tg mice. The most distinctive pathology identified is the progressive age-dependent accumulation of p62 inclusions specific to *CHMP2B*^{Int5} mouse brain in many brain regions (figure 5.18 and 5.19).

Progressive age-dependent accumulation of p62 inclusions is seen in the cortex, corpus callosum, thalamus (figure 5.18) and brain stem of *CHMP2B*^{Int5} mice. At 6 months only a few small p62 inclusions are seen (figure 5.18 g arrow), the number and size of p62 inclusions increases at 12 months (figure 5.18 b,e,h) and by 18 months p62 inclusions are abundant and include both large neuronal inclusions (figure 5.18 c, blue arrows) and smaller dot and thread-like inclusions (figure 5.18 f and i red arrows).

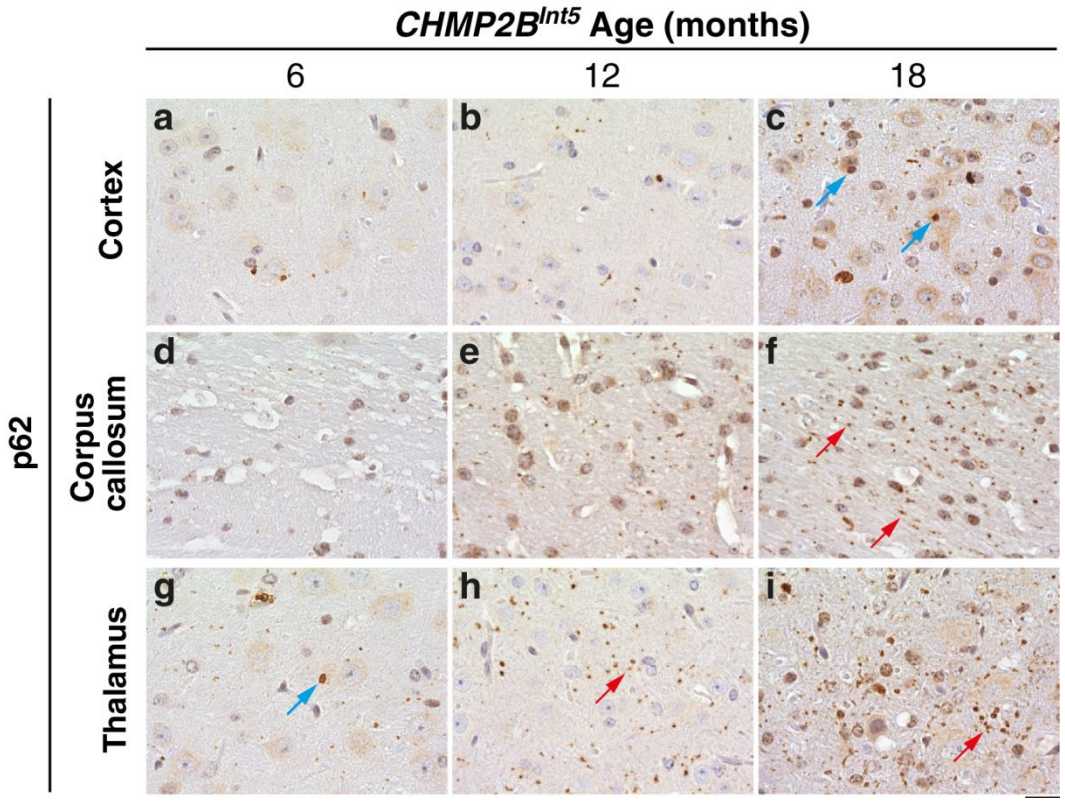

Figure 5.18 Progressive age-dependent accumulation of p62 inclusions in CHMP2B^{Int5} brain. Representative images from Tg153 CHMP2B^{Int5} mouse cortex, corpus callosum and thalamus at 6, 12 and 18 months of age. p62 neuronal inclusions (arrows) show progressive age-dependent accumulation, the size and density of p62 inclusions also increases in an age-dependent manner**.** (a-i) two types of inclusions are seen- neuronal inclusions (blue arrows) and dot and thread like inclusions (red arrows). (N=3 for each genotype at each age; scale bar= 160µm).

The thalamus exhibits the greatest amount of p62 inclusions of all regions examined (figure 5.19 and 5.20C). Non-Tg and *CHMP2B*^{WT} brain sections do not exhibit p62 inclusions at any age in the thalamus (figure 5.19) or any other region examined including the cortex, corpus callosum or brain stem (figure 5.30).

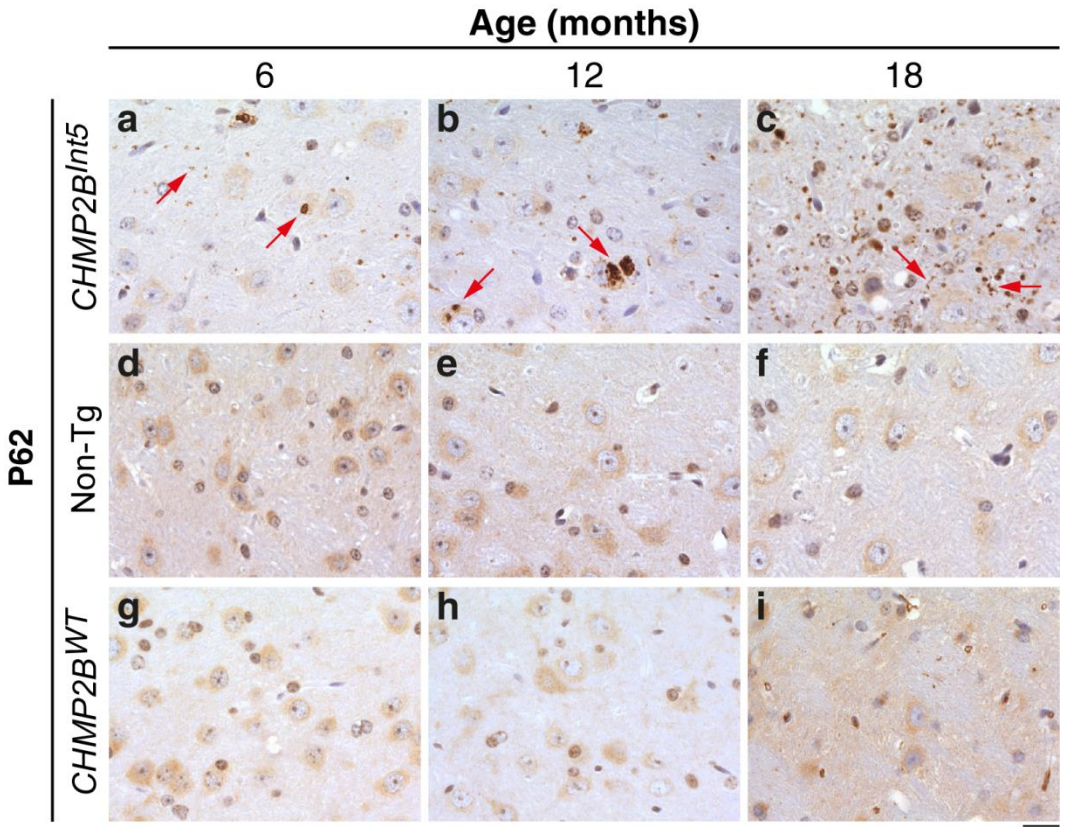

Figure 5.19 Progressive age-dependent p62 inclusions are unique to CHMP2BI^{nt5} brain. Representative images from CHMP2B^{Int5}, Non-Tg and CHMP2B^{WT} transgenic mice showing p62 inclusion formation at 6, 12 and 18 months of age only in CHMP2B^{Int5} thalamus. Very few p62 inclusions are observed at (a) 6 months increasing in size and density at (b) 12 and (c) 18 months (a, b and c arrows). p62 inclusions comparable to those seen in CHMP2BInt5 are not observed in age-matched Non-Tg (d-f) or CHMP2B^{WT} (g-i) brain. (N=3 for each genotype at each age; scale bar= 160µm).

Quantitative analysis of the cortex, corpus callosum and thalamus confirms a statistically significant age-dependent progressive accumulation of p62 inclusions in *CHMP2B*^{Int5} compared to Non-Tg brain (figure 5.20). In the cortex (figure 5.20A) a marginal statistical significance is identified at 12 months (p<0.05) and 18 months (p<0.01). In the corpus callosum (figure 5.20B) and thalamus (figure 5.20C) a greater statistical significance is observed at 12 and 18 months (p<0.0001) and of all the regions analysed quantitatively, the thalamus demonstrates the greatest amount of p62 accumulation in *CHMP2B*^{Int5} relative to other brain regions at 18 months (figure 5.20).

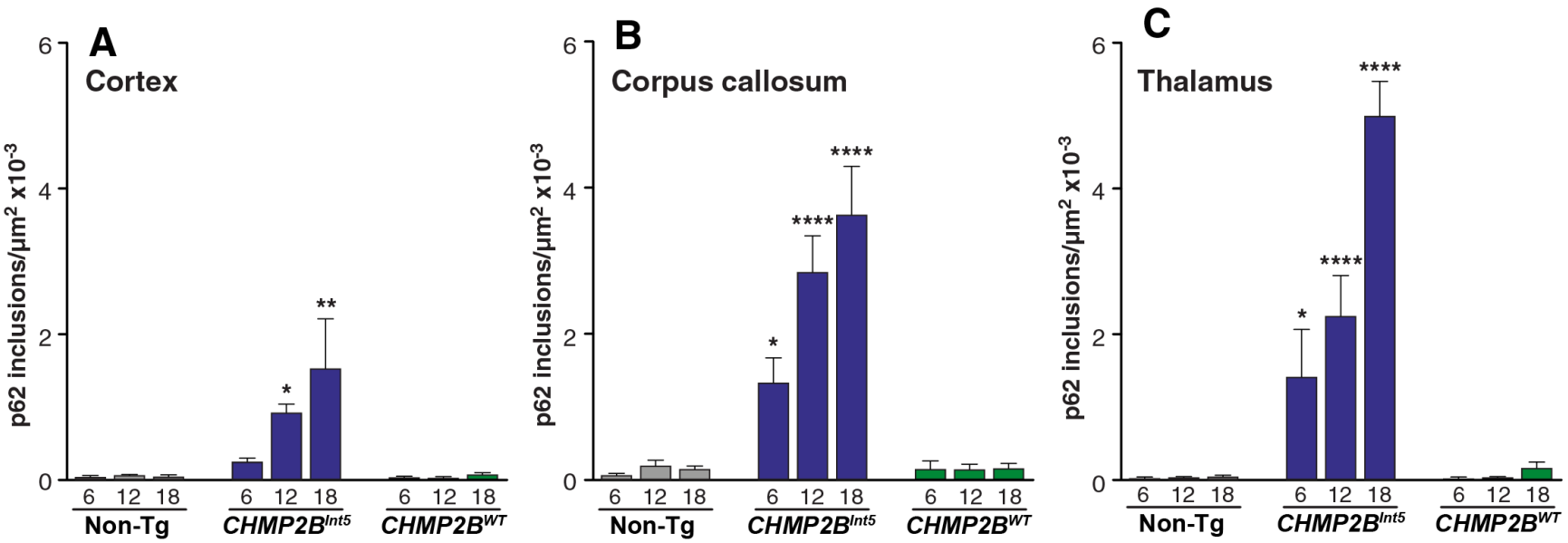

Figure 5.20 Quantification of p62 inclusions in the cortex, corpus callosum and thalamus of CHMP2B mouse lines.

Progressive age-dependent p62 inclusion accumulation is found to be statistically significant in all regions analysed, including the cortex (A), corpus callosum (B) and thalamus (C) of *CHMP2B*^{Int5} mouse brain compared to age-matched Non-Tg and *CHMP2B*^{WT} mice. p62 inclusion accumulation is only marginally significant in the cortex and highly significant in the corpus callosum and thalamus. Furthermore, the thalamus demonstrates the greatest density of p62 inclusion accumulation at 18 months. (N=5 for each genotype at each age; *p<0.05, **p<0.01, ****p<0.0001 obtained by two-way ANOVA and Bonferroni post-hoc test).

Immunostaining with anti-CHMP2B antibody demonstrates CHMP2B inclusions in *CHMP2B^{Int5}* thalamus at 18 months (figure 5.21a arrows) and increased staining in *CHMP2B^{WT}* thalamus (figure 5.21c) compared to Non-Tg thalamus (figure 5.21b). Ubiquitin inclusions are also detected in *CHMP2B^{Int5}* thalamus at 18 months (figure 5.21d arrow). Ubiquitin inclusions demonstrate a comparable staining pattern to p62 inclusions in *CHMP2B^{Int5}* brain, including neuronal and dot and thread like ubiquitin inclusions (figure 5.21d arrows). CHMP2B inclusions are not observed in 18 months Non-Tg or *CHMP2B^{WT}* thalamus (figure 5.21b and c respectively). Ubiquitin inclusions are not observed either in 18 months Non-Tg thalamus (figure 5.21e), however intranuclear neuronal ubiquitin inclusions are seen in 18 months *CHMP2B^{WT}* thalamus (figure 5.21f), but the size and staining pattern is distinct from that seen in *CHMP2B^{Int5}* thalamus, there are also far fewer ubiquitin inclusions in *CHMP2B^{WT}* thalamus at 18 months.

Accumulation of presynaptic marker synaptophysin is observed in 18-month *CHMP2B^{Int5}* thalamus (figure 5.21g arrow) but not age-matched *CHMP2B^{WT}* or Non-Tg thalamus (figure 5.21h and i respectively). Translocation of TDP-43 from the nucleus to the cytoplasm has been reported in FTLD-TDP cases (Sampathu et al., 2006). TDP-43 staining is specifically nuclear in *CHMP2B^{Int5}*, *CHMP2B^{WT}* and Non-Tg brains and translocation from the nucleus to the cytoplasm or skein-like staining is not observed (figure 5.21j-l)

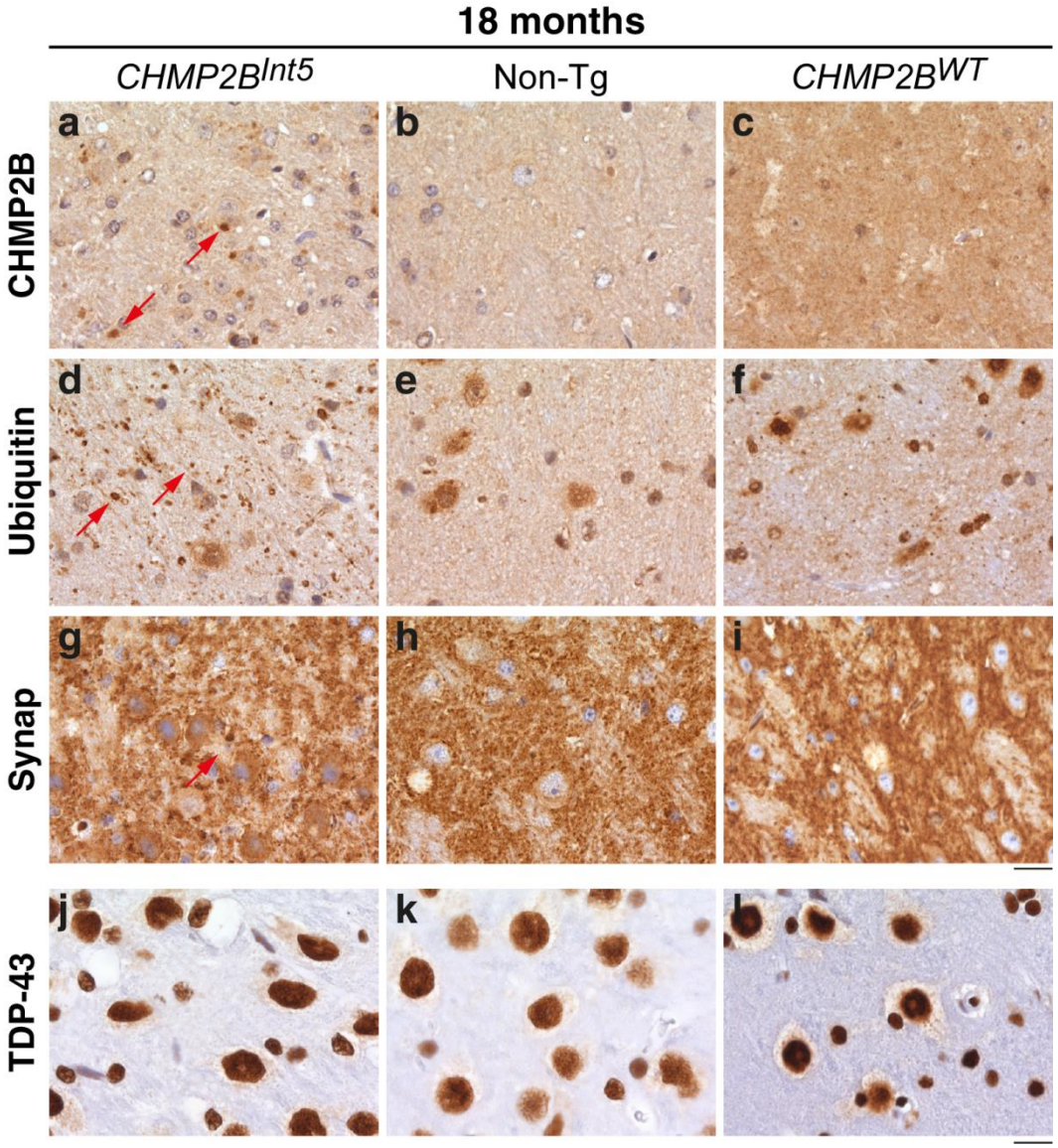

Figure 5.21 Representative CHMP2B, ubiquitin, synaptophysin and TDP-43 staining in *CHMP2B*^{Int5}, Non-Tg and *CHMP2B*^{WT} thalamus at 18 months.

CHMP2B-positive inclusions are detected at 18 months in *CHMP2B*^{Int5} thalamus (a arrows); *CHMP2B*^{WT} transgenic mice which overexpress human wild type CHMP2B show greater CHMP2B immunostaining (c) compared to Non-Tg brain (b). Ubiquitin inclusions are also observed in *CHMP2B*^{Int5} thalamus (d) but not Non-Tg thalamus (e). Neuronal nuclear ubiquitin inclusions are seen in *CHMP2B*^{WT} brain (f) but these inclusions are distinct from inclusions observed in *CHMP2B*^{Int5} brain and only appear at 18 months. Accumulation of synaptophysin, a marker of presynaptic terminals is observed in *CHMP2B*^{Int5} thalamus at 18 months (g) but not age-matched Non-Tg (h) or *CHMP2B*^{WT} (i) thalamus. Translocation of TDP-43 or skein-like staining typical of FTLD-TDP pathology is not observed in *CHMP2B*^{Int5}, Non-Tg or *CHMP2B*^{WT}. (N=3 for each genotype at each age; scale bar= 160µm).

5.3.2 Brain Ultrastructure

Ultrastructural electron microscopic (EM) analysis demonstrated enlarged endosome structures consistent with dysmorphic multivesicular bodies in three FTD-3 patient fibroblast lines, which were absent in age-matched controls. The dysmorphic structures were reported as being enlarged vacuoles positive for the late endosome marker CD63, with aberrant membranes or sparse interluminal vesicles (Urwin et al., 2010a). To investigate whether the *CHMP2B* transgenic mice recapitulate this ultrastructural pathology and to further elucidate the neuropathology observed in the *CHMP2B*^{Int5} mouse brains under light microscopy (LM), including inclusion morphology, mouse brains were processed appropriately and viewed under EM. As the thalamus was shown to be the region of greatest pathology in LM analysis, the focus of the EM examination was primarily the thalamus.

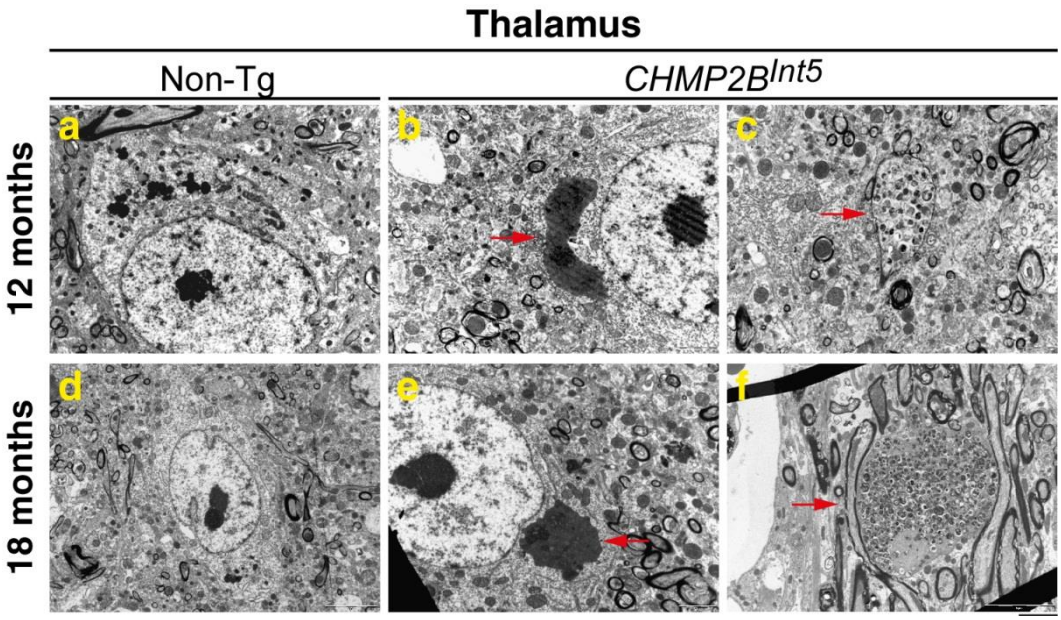

Figure 5.22 Electron microscopic images of *CHMP2B^{Int5}* and Non-Tg thalamus.

Neuronal inclusions are observed at both 12 months (b) and 18 months (e) (arrows) in *CHMP2B^{Int5}* thalamus. Additional pathology identified includes enlarged axons at 12 months (c) and 18 months (f) (arrows) . Neuronal inclusions and enlarged axons are absent in Non-Tg mouse brains at both 12 months (a) and 18 months (d) (N=3 for each genotype at each age; scale bar a-c and e = 2µm, d and f = 5µm).

Examination of *CHMP2B^{Int5}* transgenic thalamus reveals the presence of electron dense structures with a rough perimeter identified close to neuronal nuclei at 12 and 18 months (figures 5.22 b and e arrows); these structures are considered to be consistent with the p62-positive neuronal inclusions, observed under LM.

Data not shown but reported by AI demonstrates axonal pathology using amyloid precursor protein staining in *CHMP2B^{Int5}* transgenic mouse brain first evident at 6 months and progressive with age; axonal swellings are absent in age-matched Non-Tg brains (Ghazi-Noori et al., 2012). Consistent with this data, axonal swellings are also identified under EM in CHMP2B^{Int5} thalamus at both 12 and 18 month (figures 5.22 c and f arrows). The axonal swellings contain an accumulation of mitochondria, and vesicles likely from the endosome-lysosome and autophagy pathways. Neuronal inclusions and axonal swellings are not observed in age matched Non-Tg brains (figures 5.22 a and d).

5.3.3 Spinal Cord Pathology

5.3.3.1 Astrogliosis

The hamster prion promoter directs *CHMP2B* transgene expression to the spinal cord as well as the brain. To further characterise the *CHMP2B* transgenic mice and investigate the effect of the *CHMP2B* transgenes in the spinal cord, a systematic study was undertaken to examine the lumbar spinal cord for astrogliosis and inclusion pathology.

Astrogliosis is observed in a progressive age-dependent manner in the lumbar spinal cord of *CHMP2B*^{Int5} mice first apparent at 12 months (figure 5.23b) and increasing at 18 months (figure 5.23c) indicating a chronic and progressive inflammatory pathology. Some variation is noted in GFAP staining in Non-Tg and *CHMP2B*^{WT} lumbar spinal cord, reflecting inflammation that is not progressive with age and distinct from the progressive age-dependent inflammatory pathology identified in *CHMP2B*^{Int5} lumbar spinal cord (figure 5.23). Critically there is greater GFAP staining at 12 months and 18 months in *CHMP2B*^{Int5} lumbar spinal cord (figure 5.23 b and c respectively) compared to age matched *CHMP2B*^{WT} (figure 5.23e and f) and Non-Tg (figure 5.23h and i) lumbar spinal cord.

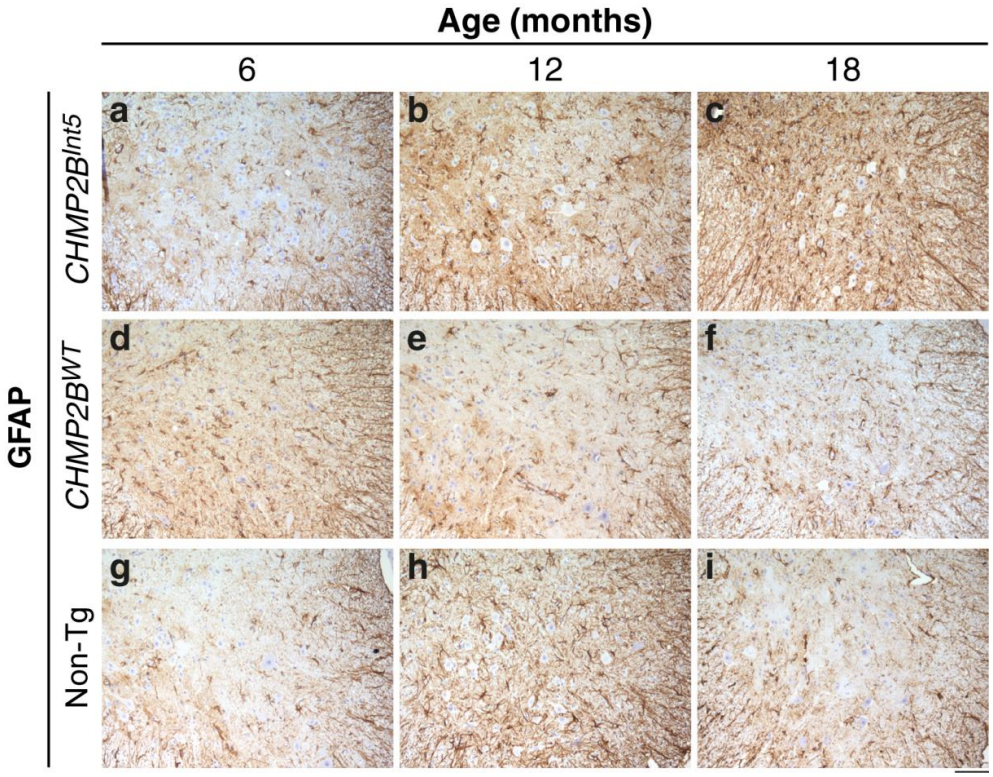

Figure 5.23 GFAP expression in lumbar spinal cord at 6, 12 and 18 months.

Astrogliosis is observed in an age-dependent progressive manner at 12 and18 months in *CHMP2B*^{Int5} lumbar spinal cord demonstrated by increased GFAP expression (b and c). The same degree of astrogliosis depicted by the increase in GFAP is not present in age-matched *CHMP2B*^{WT} or Non-Tg lumbar spinal cord. (N=3 for each genotype at each age; scale bar=100µm).

5.3.3.2 Inclusion pathology

CHMP2B transgenic mouse lumbar spinal cord sections were subjected to immunostaining with anti-CHMP2B, ubiquitin and p62 antibodies to investigate whether these mice present with inclusion accumulation typical of neurodegenerative pathology.

Neuronal CHMP2B-positive inclusions are observed in motor neurons of the lumbar spinal cord initially at 12 months (figure 5.24b, arrow); the size and number of these CHMP2B-positive inclusions increases with age so that at 18 months larger and a greater number of CHMP2B-positive inclusions are evident (figure 5.24c, arrows). Notably the CHMP2B-positive inclusions are unique to *CHMP2B*^{Int5} mice and not observed in age-matched *CHMP2B*^{WT} (figure 5.24d-f) or Non-Tg (figure 5.24g-1) lumbar spinal cord.

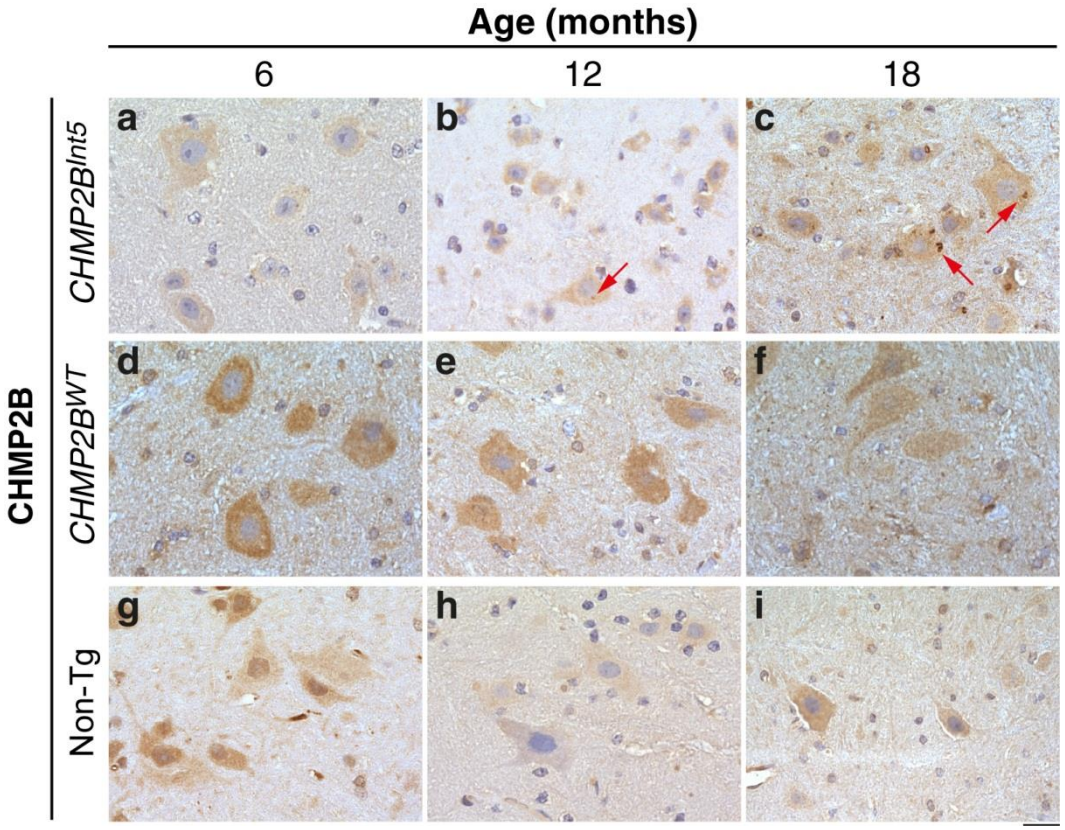

Figure 5.24 CHMP2B expression in lumbar spinal cord motor neurons at 6, 12 and 18 months.

CHMP2B immunostaining reveals inclusions in 12 and 18 months *CHMP2B*^{Int5} motor neurons (b and c arrows) in a progressive age-dependent manner but are absent in age-matched *CHMP2B*^{WT} (e and f) and Non-Tg (h and i) lumbar spinal cord. *CHMP2B*^{WT} motor neurons (d, e and f) show more intense CHMP2B staining compared to Non-Tg spinal cord (g, h and i). (N=3 for each genotype at each age; scale bar=20µm)

Parallel to the CHMP2B-positive inclusions observed in the lumbar spinal cord motor neurons of *CHMP2B*^{Int5} mice, immunostaining with ubiquitin and p62 reveals a corresponding age-dependent progressive accumulation of ubiquitin (figure 5.25) and p62 (figure 5.26) inclusions also unique to *CHMP2B*^{Int5} motor neurons.

Small neuronal ubiquitin inclusions are first identified at 12 months (figure 5.25b, arrow) in lumbar spinal cord motor neurons of *CHMP2B*^{Int5} mice. The size and number of ubiquitin inclusions is seen to increase at 18 months (figure 5.25c, arrows). p62 inclusions are initially identified at 6 months (figure 5.26a, arrow); and are relatively larger in size at 12 months compared to ubiquitin inclusions at the same age (compare figure 5.25b against figure 5.26b). The number of p62 inclusions increases further by 18 months (figure 5.26c, arrows). Ubiquitin and p62 inclusions are not identified in age-matched *CHMP2B*^{WT} or Non-Tg spinal cord motor neurons (figure 5.25d-i and 5.26d-i respectively).

Quantification of p62 inclusions (% of motor neurons containing inclusions) confirms a progressive age-dependent increase in p62 inclusions in *CHMP2B*^{Int5} spinal cord motor neurons compared to Non-Tg spinal cord motor neurons; at 12 months (p<0.001) and 18 months (p<0.0001) (figure 5.27). This effect is not replicated in age-matched *CHMP2B*^{WT} spinal cord motor neurons (figure 5.27)

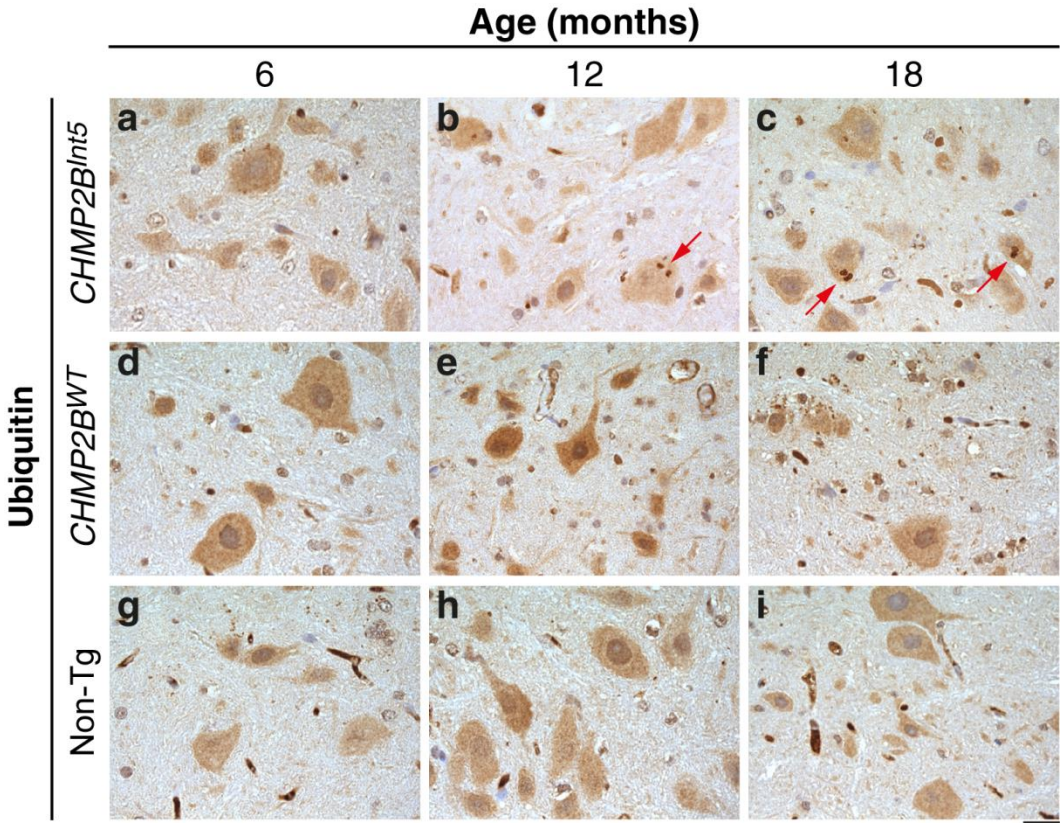

Figure 5.25 Ubiquitin expression in lumbar spinal cord motor neurons at 6, 12 and 18 months.

Ubiquitin inclusions are observed in 6, 12 and 18 months *CHMP2B*^{Int5} motor neurons (b and c arrows) in a progressive age-dependent manner but are absent in age-matched *CHMP2B*^{WT} (d,e,f) and Non-Tg (g, h, i) lumbar spinal cord. (N=3 for each genotype at each age; scale bar=20µm).

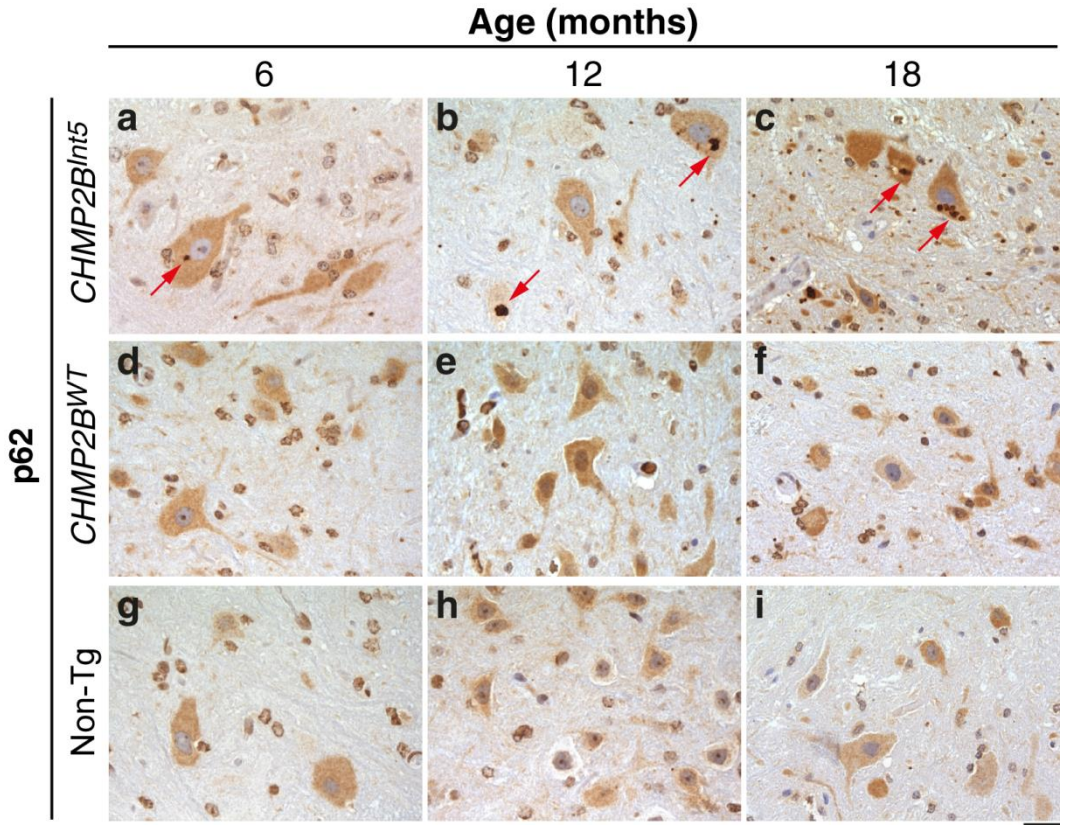

Figure 5.26 p62 Immunostaining of the lumbar spinal cord at 6, 12 and 18 months.

p62 inclusions are observed in 12 and 18 months *CHMP2B*^{Int5} motor neurons (a, b and c arrows) in a progressive age-dependent manner but are absent in age-matched *CHMP2B*^{WT} (d,e,f) and Non-Tg (g, h, i) lumbar spinal cord. (N=3 for each genotype at each age; scale bar=20µm).

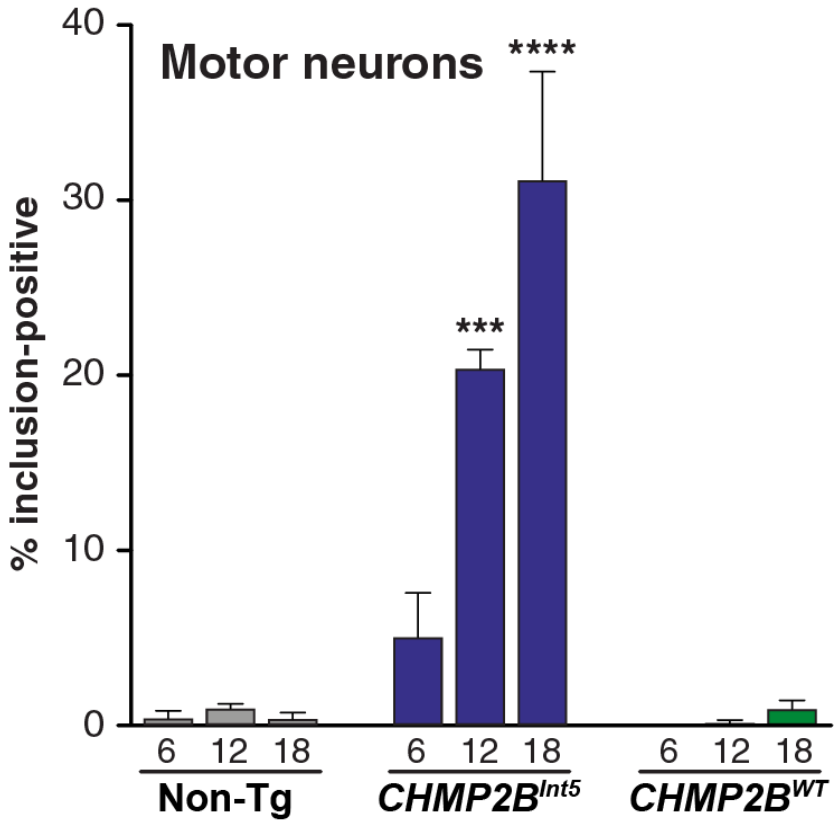

Figure 5.27 Quantification of p62 inclusions in lumbar spinal cord.

Progressive age-dependent p62 inclusion accumulation is found to be statistically significant in *CHMP2B*^{Int5} lumbar spinal cord motor neurons compared to age-matched Non-Tg lumbar spinal cord motor neurons. This effect is not replicated in *CHMP2B*^{WT} lumbar spinal cord motor neurons (N=5 for each genotype at each age; error bars % SEM ***p<0.001, ****p<0.0001 obtained by two-way ANOVA and Bonferroni post-hoc test).

5.3.4 Sciatic Nerve

The sciatic nerve from CHMP2B transgenic mice was used to investigate any potential peripheral nerve pathology. The gross morphology of sciatic nerve from 18 months *CHMP2B*^{Int5}, *CHMP2B*^{WT} and Non-Tg mice was examined under low and high magnification (figure 5.28). No distinctive difference or features of sciatic nerve pathology were idenitifed in *CHMP2B*^{Int5} or *CHMP2B*^{WT} compared to Non-Tg sciatic nerves (figure 5.28).

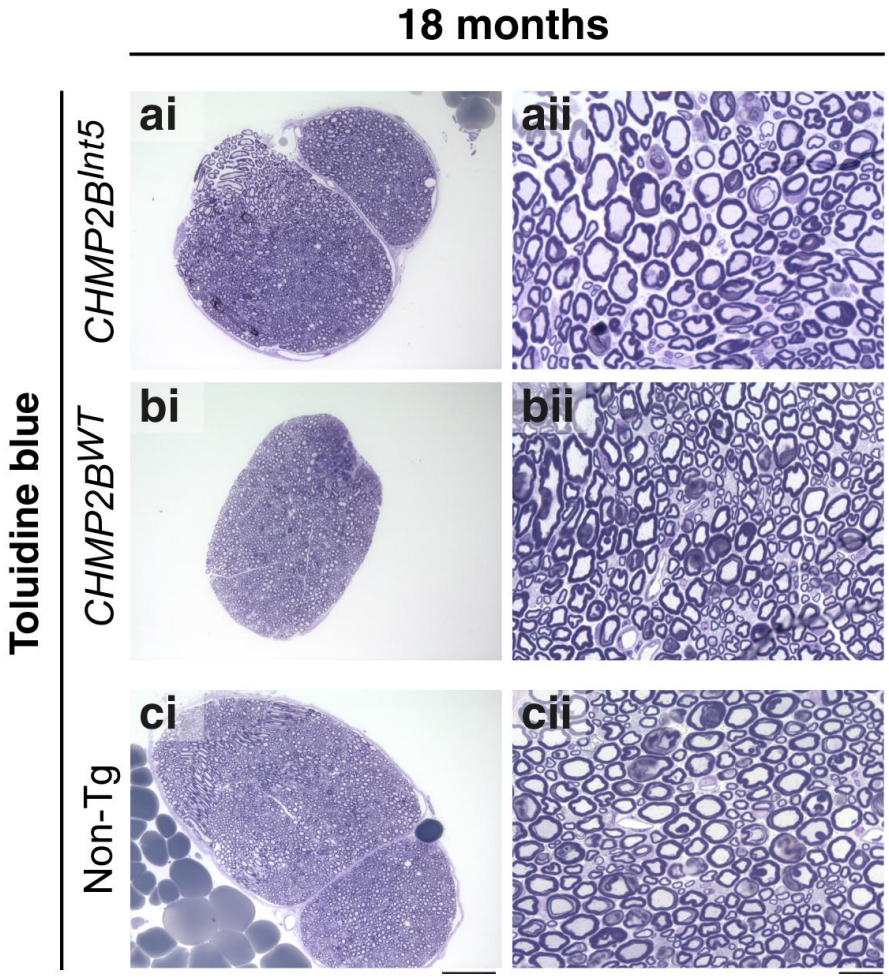

Figure 5.28 *CHMP2B*^{Int5}, *CHMP2B*^{WT} and Non-Tg sciatic nerve transverse sections at 18 months stained with toluidine blue.

Low magnification mouse sciatic nerve demonstrates gross morphology of the sciatic nerve with numerous nerve fibres (ai, bi and ci); high magnification of the nerve fibres showing transverse myelinated axonal profiles (aii, bii and cii). No distinctive difference is noted in any genotype at 18 months. (N=3 for each genotype; scale bar= ai-ci =100µm; aii-cii =20µm).

5.4 Exploring the Molecular Basis of CHMP2B^{Int5} Pathology

Autophagy is an intracellular bulk degradation process employed by cells to degrade and recycle organelles and ubiquitinated proteins from the cytoplasm. The molecular basis of autophagy has received much interest in the field of neurodegenerative research in recent years as a potential mechanistic basis for a number of neurodegenerative disorders (reviewed by Harris and Rubinsztein) (Harris and Rubinsztein, 2012). Autophagy is initiated by the formation of double-membrane structures termed phagophores, which engulf portions of cytoplasm and cargo destined for degradation (Harris and Rubinsztein, 2012).

During the second maturation stage of autophagy, LC3 is cleaved at its C-terminus by ATG4 to form cytosolic LC3-I which is conjugated with lipid phosphatidylethanolamine to form LC3-II which in turn aids the closure of the membrane to form autophagosomes (Mizushima et al., 2003; Ravikumar et al., 2010). The resulting autophagosomes ultimately fuse with lysosomes, where their contents are degraded by lysosomal acid hydrolases (Ravikumar et al., 2010; Harris and Rubinsztein, 2012).

In section 5.3 of this chapter 'inclusion pathology' data demonstrating progressive age-dependent accumulation of ubiquitin and p62 inclusions unique to *CHMP2B^{Int5}* transgenic mice is presented. These *CHMP2B^{Int5}* specific p62 inclusions are identified in many brain regions (figure 5.30) and in motor neurons of the lumbar spinal cord (figure 5.26). Furthermore quantification of inclusions reveals a statistically significant progressive increase of p62 with increasing age (figure 5.20). Western blot data of soluble and insoluble fractions from *CHMP2B^{Int5}* brains reveals an increase in p62 expression only in the insoluble fraction and not the soluble fraction, compared to Non-Tg brain samples (figure 5.29), very likely reflecting the accumulation of insoluble p62 inclusions (data kindly provided by AI) (Ghazi-Noori et al., 2012).

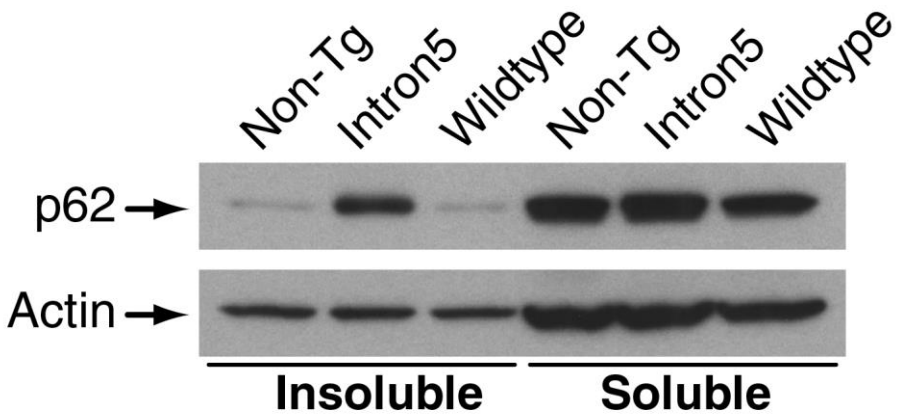

Figure 5.29 Insoluble p62 is increased in CHMP2B^{Int5} mouse brain.

Western blot demonstrates accumulation of p62 in the insoluble *CHMP2B^{Int5}* brain fraction only, reflecting accumulation of non-soluble p62 inclusions. Adapted from Ghazi-Noori *et al* 2012 (Ghazi-Noori et al., 2012).

The progressive age-dependent accumulation of p62 inclusions is of particular interest as p62 acts as a linker protein and presents substrates to be degraded to the autophagic machinery by simultaneously binding to both ubiquitinated proteins (via its UBA domain) and LC3-II (via its LRS/LIR region) and consequently p62 is degraded by autophagy itself (Tanida et al., 2004b; Pankiv et al., 2007; Ichimura et al., 2008).

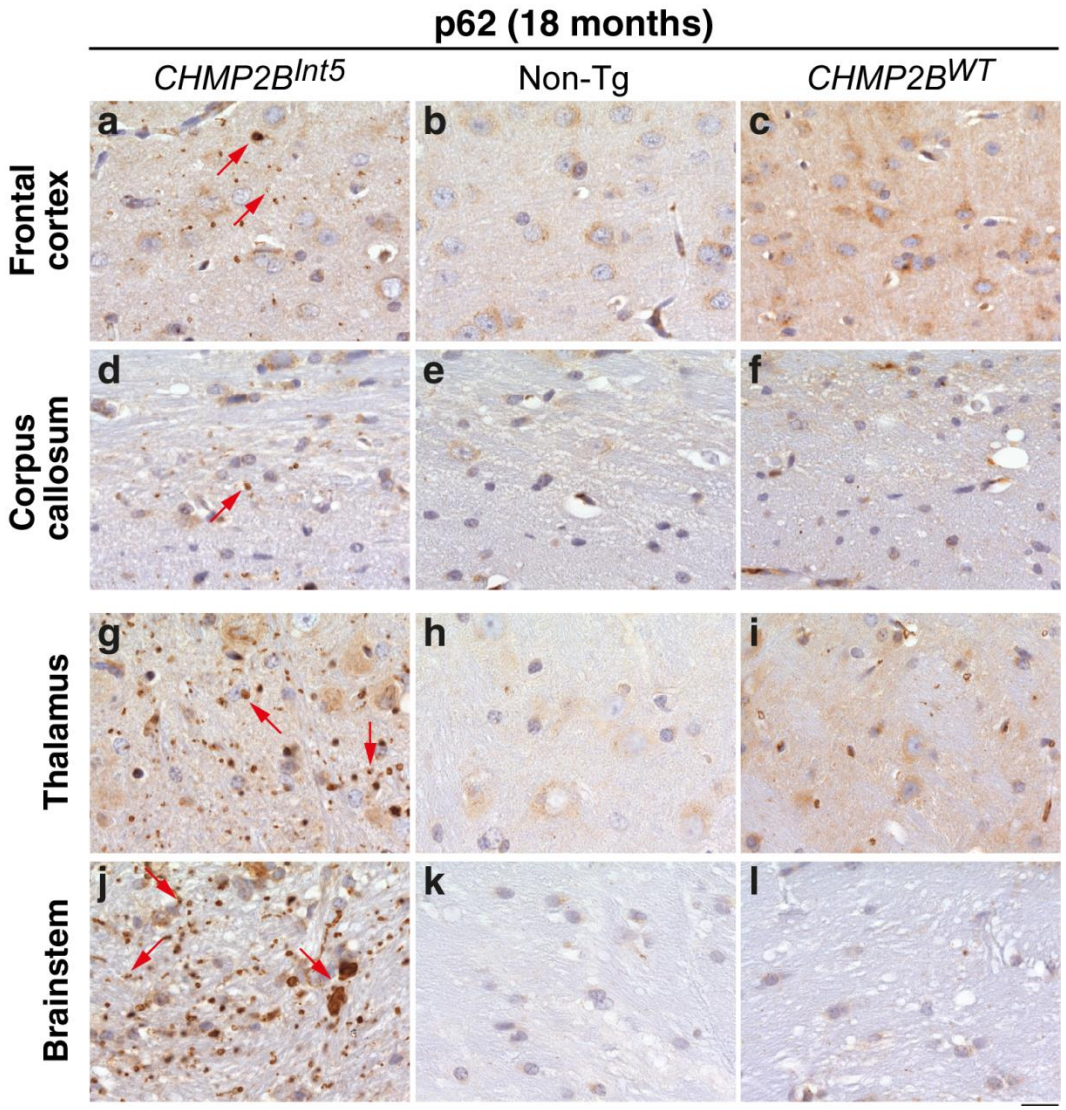

Figure 5.30 p62 inclusions identified in a range of *CHMP2B^{Int5}* brain regions.

p62 inclusions are present in many *CHMP2B^{Int5}* brain regions at 18 months of age (a, d, g and j). p62 inclusions are not identified in age-matched *CHMP2B^{WT}* (c, f, I and l) or Non-Tg brains (b, e, h and k). Representative images of N=3; scale bar = 160µm.

In an attempt to explore whether the basis of the neuropathology phenotype identified in the *CHMP2B*^{Int5} mouse brain is associated with autophagy dysregulation, LC3-II expression was quantified in 6 months (low levels of p62 inclusions) and 18 months (high levels of p62 inclusion formation) in mouse brains.

Observing LC3 western blots by eye alone does not reveal a distinct difference in LC3-II protein expression in *CHMP2B*^{Int5} or *CHMP2B*^{WT} compared to Non-Tg samples at either 6 months (figures 5.31) or 18 months (figure 5.32). Quantification of LC3-II normalised to Non-Tg in *CHMP2B*^{Int5} shows a non-significant increase in LC3-II expression at 18 months (146.5%) compared to 6 months (115.4%) (figure 5.33). Even this conservative increase in LC3-II expression from 6 months to 18 months may potentially be suggestive of autophagosome accumulation. Conversely, quantification of LC3-II in *CHMP2B*^{WT} demonstrates a reduction in LC3-II expression at 18 months (102.9%) compared to 6 months (144.8%); again this is not a statistically significant change (figure 5.33).

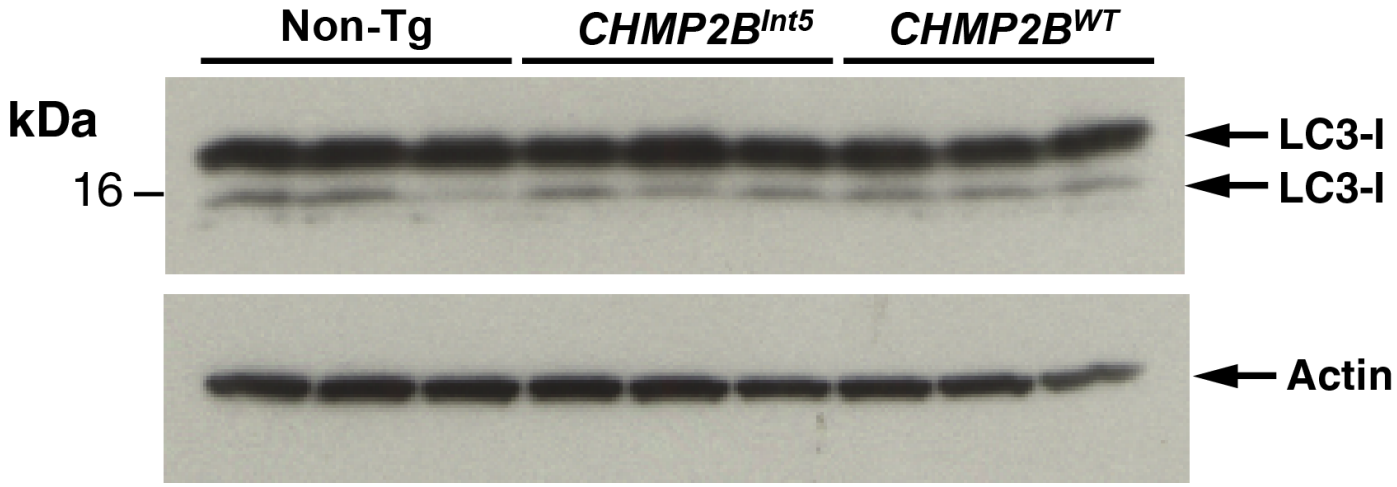

Figure 5.31 LC3 expression at 6 months in *CHMP2B^{Int5}*, *CHMP2B^{WT}* and Non-Tg whole brain homogenates.

No distinct difference is identified in LC3-II expression in CHMP2B^{Int5}or CHMP2B^{WT} compared to Non-Tg samples. Actin blot demonstrates equal loading across all samples (N=3 for each genotype).

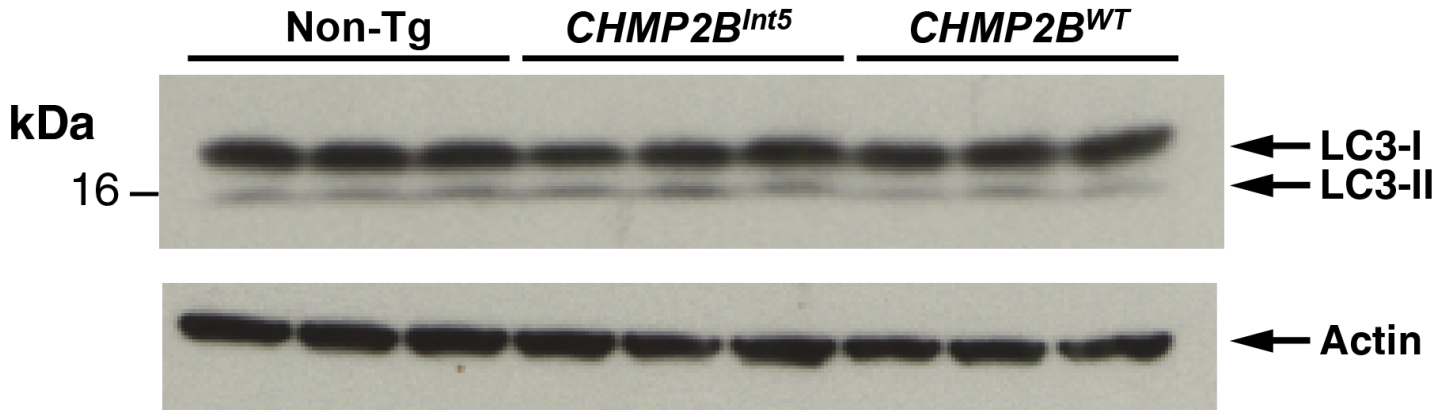

Figure 5.32 LC3 expression at 18 months in *CHMP2B^{Int5}*, *CHMP2B^{WT}* and Non-Tg whole brain homogenate.

No distinct difference is identified in LC3-II expression in CHMP2B^{Int5}or CHMP2B^{WT} compared to Non-Tg samples. Actin blot demonstrates equal loading across all samples (N=3 for each genotype).

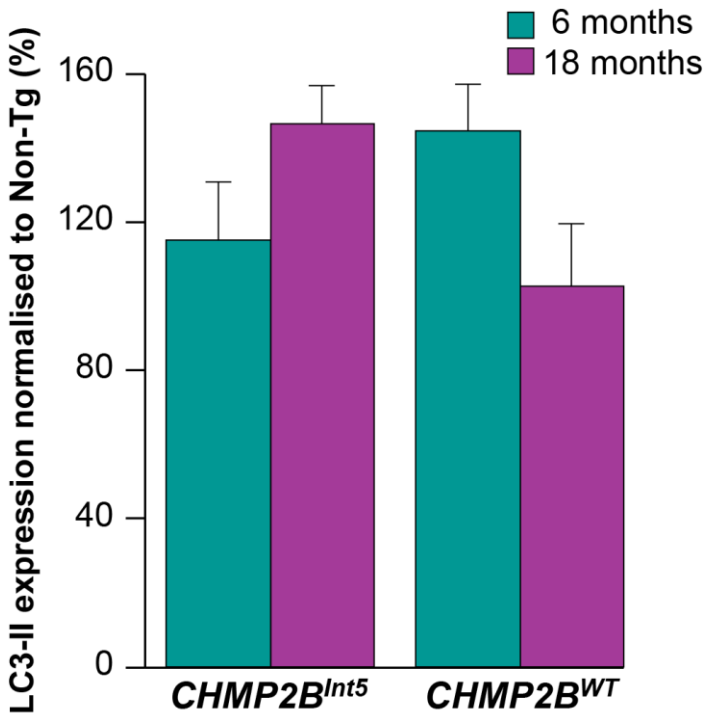

Figure 5.33 Quantification of LC3-II expression.

LC3-II expression was normalised to Non-Tg LC3-II expression for *CHMP2B*^{Int5} and *CHMP2B*^{WT} at 6 months and 18 months. A non-significant increase in LC3-II expression is observed in 18 months *CHMP2B*^{Int5} (146.5% SEM +/- 16.9) samples compared to 6 months samples (115.4% SEM+/-12.4). Conversely, a reduction in LC3-II expression is observed in 18 months (102.9 SEM+/-16.1) *CHMP2B*^{WT} samples compared to 6 months (144.8 SEM±13.4) samples; this too is not statistically significant. (N=3 for each genotype at each age; error bars= SEM (%); two-sample t-test).

5.5 Discussion

To investigate the pathogenic basis of CHMP2B mutations *in vivo*, transgenic mice harbouring human *CHMP2B^{Int5}* and *CHMP2B$^{\Delta 10}$* mutations and overexpressing human wild type CHMP2B (*CHMP2B^{WT}*) were generated and analysed in comparison to non-transgenic mice (Non-Tg).

In summary, the *CHMP2B^{Int5}* mice demonstrate brain and spinal cord pathology characterised by progressive age-dependent astrogliosis, microglial activation and inclusion formation first apparent at 6-12 months. The progressive increase in astrogliosis in the cortex, thalamus and motor neurons of the lumbar spinal cord in *CHMP2B^{Int5}* mice at 12 and 18 months is statistically significant compared to age matched Non-Tg mice. No significant astrogliosis was identified in *CHMP2B^{WT}* at any age.

Ubiquitin and p62 inclusions are identified in many brain regions and in the lumbar spinal cord motor neurons. CHMP2B-positive inclusions are also identified in the brain and lumbar spinal cord motor neurons, however CHMP2B-positive inclusions first appear at 12 months at low frequency and then appear more robustly at 18 months. The late appearance of CHMP2B inclusions may reflect mutant CHMP2B^{Int5} protein being recruited into aggregated inclusions at a late stage of pathology or that the antibody used in this study to detect CHMP2B^{Int5} inclusions is not sufficiently sensitive to detect smaller inclusions or the protein conformation of inclusions when they first start to form.

Quantification of p62 inclusions in the brain and spinal cord confirms a statistically significant progressive age-dependent p62 inclusion accumulation in the cortex, corpus callosum, thalamus and motor neurons of the lumbar spinal cord compared to age-matched Non-Tg mice. This p62 inclusion accumulation is only marginally significant in the cortex and highly significant in the corpus callosum

and thalamus. The pattern of inclusion pathology likely reflects the distribution of transgene expression driven by the hamster prion protein gene promoter (figure 5.34).

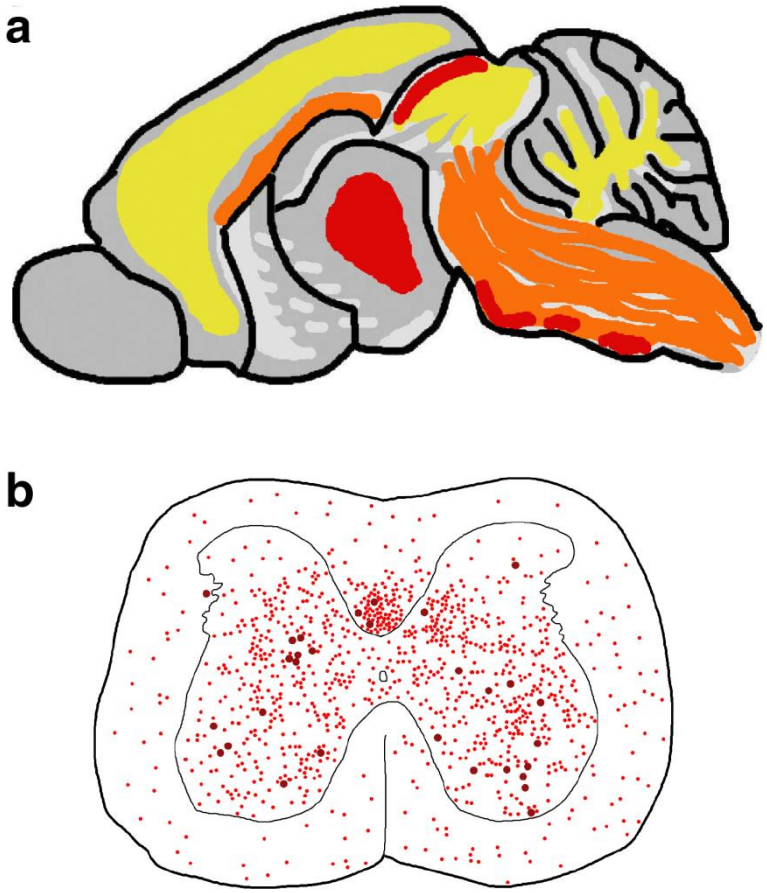

Figure 5.34 Diagrammatic representation of regions of p62 inclusion pathology in 18-month-old *CHMP2B^{Int5}* mice.

(A) areas shaded yellow demonstrate low levels of brain pathology (cortex, cerebellar white matter); orange greater pathology (brain stem and corpus callosum) and red areas of greatest pathology (thalamus and occasional brain stem axonal tracts); grey shading indicates no overt pathology. (B) red dots depict inclusion pathology size and density in the lumbar spinal cord. Greatest inclusion pathology is identified in the grey matter and dorsal corticospinal tract and less so in the white matter (Ghazi-Noori et al., 2012).

Additional data provided by AI demonstrates that p62 levels are increased in the insoluble fraction of *CHMP2B^{Int5}* brain lysates only, likely reflecting the accumulation of insoluble p62 aggregates in *CHMP2B^{Int5}* brain (Ghazi-Noori et al., 2012). The progressive inclusion pathology is unique to *CHMP2B^{Int5}* mice and not replicated in *CHMP2B^{WT}* mice and no pathology is identified in age-matched Non-

Tg mice. Data kindly provided by AI shows that a second *CHMP2B*^{Int5} line, Tg156 demonstrates comparable pathology (figure 5.35) to the *CHMP2B*^{Int5} Tg153 line described in this chapter (Ghazi-Noori et al., 2012). This confirms that the pathology is caused by the *CHMP2B*^{Int5} transgene and is not due to insertional mutagenesis.

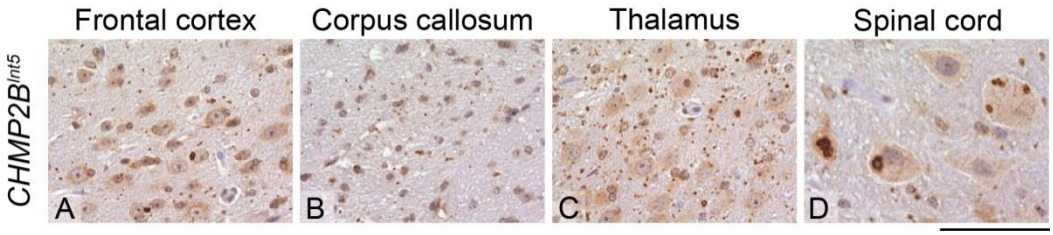

Figure 5.35 p62 inclusion pathology in *CHMP2B*^{Int5} line Tg156 at 18 months.

p62 pathology in *CHMP2B*^{Int5} Tg156 line is consistent with *CHMP2B*^{Int5} line Tg153 line described in section 5.3 of this chapter, confirming that pathology is the result of *CHMP2B*^{Int5} isoform and not due to insertional mutagenesis. Data provided by AI, figure adopted from Ghazi-Noori *et al* 2012 (Ghazi-Noori et al., 2012)

Examination of 12 and 18 months *CHMP2B*^{Int5} brain ultrastructure confirms the presence of neuronal inclusions and the presence of axonal swellings containing an accumulation of mitochondria and vesicles, likely from the endosome-lysosome and autophagy pathways. Neuronal inclusions and axonal swellings are not observed in age-matched Non-Tg brains (section 5.3.2, figure 5.22)

Examination of the sciatic nerve does not reveal any pathology; this may reflect the hamster prion protein promoter driving transgene expression to the brain and spinal cord.

Expression of *CHMP2B*^{Int5} in cells results in the accumulation of ubiquitin, p62 and GFP-LC3 (Filimonenko et al., 2007) and expression of *CHMP2B*^{Int5} in the fly eye results, increased expression of LC3-II and autophagosome structures identified under EM (Lee et al., 2007). The accumulation of autophagosomes may potentially be due to inhibition of autophagic or autophagosome degradation or

impaired fusion of autophagosomes with lysosomes (Harris and Rubinsztein, 2012). LC3-II expression *in vivo* in *CHMP2B*^{Int5} mouse brains shows a modest increase in LC3-II from 6 months (115.4% compared to Non-Tg) to 18 months (146.5%); this increase is not statistically significant. Furthermore, autophagosome accumulation is not identified under EM examination.

This disparity between *CHMP2B*^{Int5} transfected *in vitro* cell models and *CHMP2B*^{Int5} expressed *in vivo* in *CHMP2B*^{Int5} mouse models may reflect the relative expression levels in *in vitro* and *in vivo* models. Cellular systems transfected with mutant protein produce very high protein expression levels compared to *in vivo* models. In mouse brain *CHMP2B*^{Int5} RNA expression is 3 fold higher than endogenous mouse Chmp2b expression and CHMP2B^{Int5} protein expression is almost equivalent to endogenous mouse Chmp2b protein expression at 0.9 times; the likely lower expression *in vivo* does not appear to result in autophagosome accumulation.

It is also conceivable that significant autophagosome accumulation may only be present in a subset of brain cells such as the thalamic or cortical neurons. As whole brain lysates have been used in this study it is potentially possible that an effect associated with a subset of neuronal population could be masked, particularly as EM is only able to view a small number of neurons. It is possible that *CHMP2B*^{Int5} mutant proteins may be processed more effectively *in vivo* for example aggregated proteins could be diverted to the UPS system for degradation to maintain physiological homeostasis or that autophagosomes only significantly accumulate at a much later age and 18 months may be too early to detect such changes.

Even in the absence of data for autophagosome accumulation, ultimately the cumulative effect of glial and inclusion pathology as well as axonal swelling identified in *CHMP2B*^{Int5} mouse brain and spinal cord is lethal and *CHMP2B*^{Int5} mice

have significantly (p=0.001) reduced survival compared to Non-Tg mice (figure 5.36) (data kindly provided by AI) (Ghazi-Noori et al., 2012).

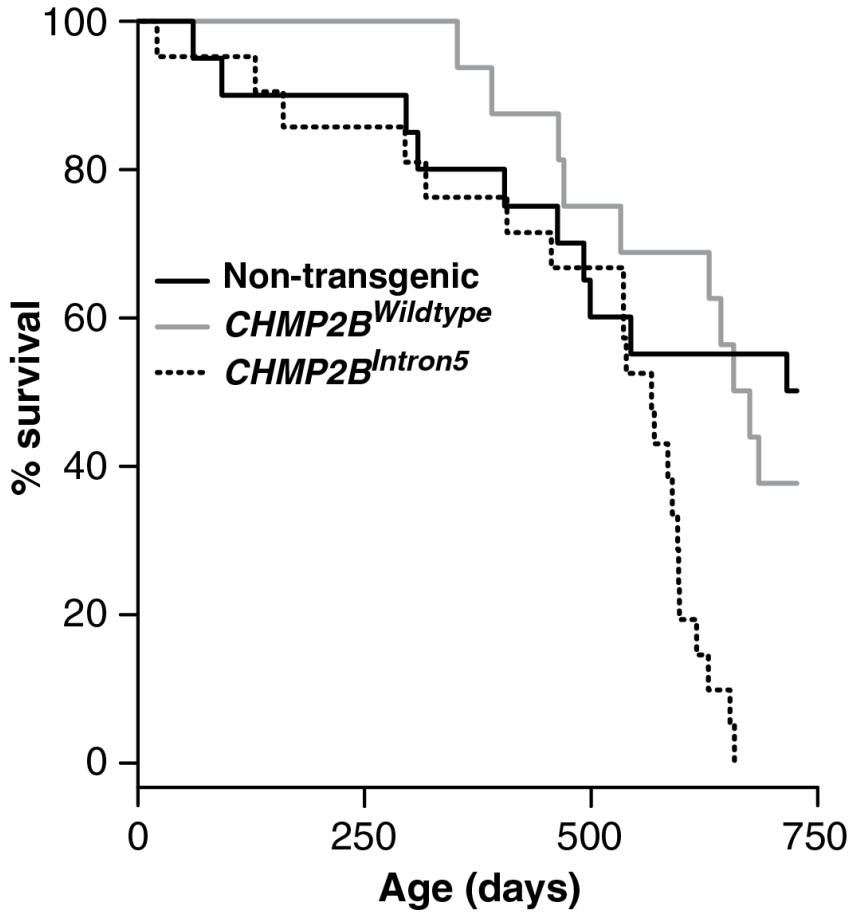

Figure 5.36 CHMP2B transgenic mice survival analysis.

Decreased survival in CHMP2B^{Int5} mice (p=0.001), Kaplan-Meier analysis and Log Rank test. Data kindly provided by AI (Ghazi-Noori et al., 2012).

In summary, this chapter has set out data presenting the first mouse model of FTD-3 associated with *CHMP2B^{Int5}* mutation. These mice recapitulate some of the key neuropathological features of the human disease and will be useful models for further investigations into the disease and potentially testing therapeutic strategies and compounds.

6 General Discussion

6.1 *In Vivo* Mouse Models of FTD-3

This thesis has presented data for the first time demonstrating the effect of depleting endogenous mouse *Chmp2b* in an *in vivo* murine model and the significance of expression of mutant *CHMP2B*^{Int5} in transgenic mice.

Frontotemporal dementia with *CHMP2B* mutations are a rare cause of FTD accounting for less than 1% of all FTD cases (Mackenzie et al., 2011), however it is likely that there are common mechanisms of disease associated with FTD pathology for example *CHMP2B* and progranulin have both been implicated in the lysosomal degradation pathway (Filimonenko et al., 2007; Hu et al., 2010; Urwin et al., 2010a). Therefore studying *CHMP2B* depletion and *CHMP2B* mutant expression in *in vivo* mammalian systems is an important way of deducing both the normal function of *Chmp2b* and the effect of mutant *CHMP2B* species *in vivo,* as well as providing insight into a potential common FTD mechanism of disease.

6.2 *Chmp2b* Knockout Mice

6.2.1 *Chmp2b* Knockout Mice Do Not Recapitulate FTD-3 Neuropathology

Chmp2b$^{-/-}$ mice do not recapitulate FTD-3 neuropathology (Holm et al., 2007; Urwin et al., 2010a; Ghazi-Noori et al., 2012)as described in Chapter 3 and furthermore, there is no evidence of an aberrant endosomal phenotype in *Chmp2b*$^{-/-}$ mice as reported in other *Chmp* knockout mice (Shim et al., 2006; Lee et al., 2007) or RNAi depletion of CHMP2B in hippocampal neurons (Belly et al., 2010). The absence of pathology may be due to the incomplete knockout of endogenous *Chmp2b* in *Chmp2b*$^{-/-}$ mice. *Chmp2b*, as part of the ESCRT III complex, is one subunit in an intricate multi-molecular pathway. It is therefore possible that other ESCRT subunits may compensate for the depleted levels of *Chmp2b,* with its

closest homologue, *Chmp2a,* being the prime candidate. Indeed, it has been shown that CHMP2A and CHMP2B can compensate for each other in the context of viral budding, another ESCRT-dependent pathway. In this context single CHMP2A or CHMP2B knockdowns have small effects on viral budding, but double knockdowns have a pronounced effect (Morita et al., 2011). It is also possible that the 15% Chmp2b protein expression generated in this study may be sufficient for essential biological functions.

Even though Chapter 3 sets out data demonstrating that *Chmp2b*$^{-/-}$ mice do not recapitulate FTD-3 specific pathology, it is still possible that *Chmp2b*$^{-/-}$ mice may have other more discrete pathology not identified in this study. There is a precedence for abnormal embryonic development in *Chmp* knockout mice including neural tube defects (Shim et al., 2006; Lee et al., 2007) and Chmp2b has been associated with the Toll pathway in *drosophila* (Ahmad et al., 2009) involved in dorsoventralization of the *drosophila* embryo as a regulator of early morphogenetic patterning (Rock et al., 1998). Studying *Chmp2b*$^{-/-}$ embryos and young pups would address whether *Chmp2b* depletion results in an embryonic neurodevelopmental phenotype.

CHMP2B missense mutations have been identified in cases of progressive muscular atrophy (PMA); a type of lower motor neurone disease (Cox et al., 2010) and *Chmp2b*$^{-/-}$ mice demonstrate a distinct gait phenotype. Although histological assessment of *Chmp2b*$^{-/-}$ mice has not shown pathology, performing motor neuron counts would be a more sensitive method of determining motor neuron loss. Chronic neurogenic change is a characteristic ALS symptom and electrophysiological tests such as EMG and nerve conduction tests are used as part of a battery of criteria to diagnose ALS (de Carvalho et al., 2008). It is possible that *Chmp2b*$^{-/-}$ mice may harbour electrophysiological abnormalities such as nerve conduction abnormalities which should be investigated in the future.

6.2.2 Depletion of *Chmp2b* Results in a Motor and Behavioural Phenotype

6.2.2.1 *Chmp2b*$^{-/-}$ mice have reduced survival and weight loss

The most critical indicator that depletion of Chmp2b results in a deleterious phenotype are demonstrated by the significantly reduced survival (p=0.0006) of *Chmp2b*$^{-/-}$ mice. In addition, male *Chmp2b*$^{-/-}$ mice demonstrate significant weight loss at 18 months of age (p=0.001) and female mice show a trend for weight loss at 18 months, but this does not reach statistical significance likely due to low number of female *Chmp2b*$^{-/-}$ mice surviving at 18 months of age.

6.2.2.2 *Chmp2b*$^{-/-}$ mice demonstrate a movement phenotype

The initial SHIRPA phenotype assessment has shown that a greater proportion of *Chmp2b*$^{-/-}$ mice at 12 months of age *do* demonstrate gross phenotypes that are either absent in age-matched *Chmp2b*$^{+/+}$ mice or are only observed in smaller proportions of *Chmp2b*$^{+/+}$ mice.

To further define the gross phenotypes identified from the modified-SHIRPA protocol, more sensitive motor and behavioural phenotyping assessments were performed on a cohort of *Chmp2b* knockout mice at 4, 5 and 6 months of age.

6.2.2.3 *Chmp2b*$^{-/-}$ mice have rotarod deficits

Chmp2b$^{-/-}$ mice demonstrate a statistically significant rotarod deficiency (p<0.001) at 4, 5 and 6 months of age compared to age matched *Chmp2b*$^{+/+}$ mice. The poor rotarod performance in *Chmp2b*$^{-/-}$ mice is not observed to be progressive between 4 to 6 months of age, which may reflect a slowly progressive phenotype *i.e*. a two-month difference is not sufficient to identify a progressive trait which would otherwise be detected if mice where tested at longer intervals; for example at 4, 8, 12, 16 and 24 months of age.

Numerous transgenic and mutant mouse models of neurodegenerative disease demonstrate rotarod deficit due to impaired gait and/or poor coordination. These include mouse models of polyglutamine disease including the R6/2 mice (Mangiarini et al., 1996), mouse models of spinocerebellar ataxia (SCA) subtypes (reviewed by Ingram 2012 and Orr 2012 (Ingram et al., 2012; Orr, 2012)), mouse models associated with mutation in the dynein complex associated with MND (reviewed by Kuta 2011 (Kuta, 2011)), as well as spontaneously occurring mutants identified in the ENU project at MRC Harwell such as the moonwalker (Mwk) mice that harbor a gain-of-function mutation in the Trpc3 gene encoding the non-selective transient receptor potential cation channel, type C3 (TRPC3), resulting in altered TRPC3 channel gating (Becker et al., 2009).

Many factors can influence mouse rotarod performance and interpreting rotarod deficits is not straightforward and may reflect impairment within different sites of the neuromuscular system. For example, abnormalities of neuromuscular junctions are observed in mice expressing mutant DCTN1/P150Glued (Chevalier-Larsen et al., 2008) and impaired growth and differentiation of Purkinje cell dendritic arbors as in *Mwk* mice (Becker et al., 2009). It is also possible that deficits may be the result of neurodevelopmental abnormalities (Shim et al., 2006; Lee et al., 2007) such as impaired synaptic branching during development (Belly et al., 2010).

6.2.2.4 *Chmp2b*$^{-/-}$ mice do not have grip strength deficits

No statistically significant difference in grip strength was identified between *Chmp2b*$^{-/-}$ and *Chmp2b*$^{+/+}$ mice at the ages tested. The grip strength test is used to measure the neuromuscular function as maximal muscle strength of combined forelimbs and hind limbs.

The grip strength test has been especially useful in revealing neuromuscular deficits in mouse models of MND. For example the *Legs at odd angles' (Loa)*

mutant mice which carry a missense point mutation in the *Dync1h1* gene demonstrate neurological deficits in heterozygous mice including abnormal body posture, limb grasping and reduced grip strength (Hafezparast *et al.*, 2003).

The *'Sprawling' (Swl)* mutant generated via radiation induced mutagenesis carries a 9 bp deletion within the dimerisation domain of the dynein heavy chain (Chen et al., 2007) resulting in neurological deficits in heterozygous mice identified by an unsteady gait and decrease in the grip strength of hind limbs. Neurological deficits results from a neuropathy of sensory neurons and degeneration of muscle spindles in hind limbs. Histological analysis shows decreased number of proprioceptors and sensory neurons located in the dorsal root ganglion. At the same time peripheral and spinal motor neurons were not affected (Kuta, 2011). The *Wobbler* mice, a mouse model of ALS carry a missense mutation in the *Vps54* gene (Schmitt-John et al., 2005). At 4 weeks of age *wobbler* mice show rapid neuromuscular deficit progression, as demonstrated by gait abnormality and reduced foreleg grip-strength (Schmitt-John et al., 2005; De Paola et al., 2012).

Taken together, these examples show that a primary muscle defect is not required for rotarod deficits. This concept is supported by the absence of gross pathology in the quadriceps muscle of *Chmp2b* knockout mice even in the presence of the abnormal gait phenotype.

6.2.2.5 *Chmp2b*$^{-/-}$ mice show altered behaviour

Assessment of burrowing behaviour showed a statistically significant age-dependent decline (p<0.001) in *Chmp2b*$^{+/+}$ mice. Interestingly in *Chmp2b*$^{-/-}$ mice the amount of food pellets burrowed does not decline with age. By 5.5 months of age there is a significant reduction (p=0.001) in food pellets burrowed by *Chmp2b*$^{+/+}$ mice compared to *Chmp2b*$^{-/-}$ mice and this significant difference is sustained until 6.5 months of age. It is important to note that the significant difference in burrowing between *Chmp2b*$^{-/-}$ and *Chmp2b*$^{+/+}$ mice arises from *Chmp2b*$^{-/-}$ mice not replicating the decline in burrowing behaviour with age demonstrated by *Chmp2b*$^{+/+}$ mice rather than *Chmp2b*$^{-/-}$ mice increasing the amount of food pellets they burrow.

Mice burrow spontaneously regardless of the material available, and burrowing has been suggested to be a rewarding activity (Deacon, 2009). Therefore the difference in burrowing behaviour in *Chmp2b*$^{-/-}$ mice is interesting and may potentially reflect changes in CNS neurotransmitter homeostasis, trafficking or recycling associated with Chmp2b depletion. Although this study does not have data to support this concept specifically in *Chmp2b* knockout mice, there are reports of dopamine transporter mutant mice and SNAP-25 deficient mice displaying impulsive hyperactivity and impaired inhibition in delayed reinforcement tasks, recapitulating some key features of human ADHD behaviour including obsessive compulsive behaviour (Wilson, 2000; Bruno et al., 2007; Russell, 2011).

The challenge in generating successful models of disease is to an extent recapitulating clinical symptoms observed in human disease. The defining clinical symptoms of FTD include personality change and language deficits, which at initial consideration may seem specific only to humans and therefore not possible to model in mice. However, it has been suggested that several aspects of FTD are potentially amenable to mouse modelling (Roberson, 2012).

Progressive loss of interest in others, disinhibition and aggressive behaviour are examples of social dysfunction and cardinal signs of FTD. Social interaction can be tested in mice using sociability tests, by quantifying interaction with cage mates over time and assessing social dominance which is diminished or lost in FTD (Roberson, 2012). Interesting parallels of neuroanatomy and behaviour have also been reported with social abnormalities being mapped to the prefrontal cortex (Rankin et al., 2006). Repetitive behaviour is also a core feature of FTD and patients develop some form of repetitive behaviour during their post morbid life (Miller et al., 1995). Repetitive behaviour where the striatum is reported to be highly involved, is commonly observed as repetitive grooming in mice (Greer and Capecchi, 2002; Werner et al., 2007; Roberson, 2012; Halabi et al., 2013). Incidentally in this study more *Chmp2b*$^{-/-}$ mice were observed to demonstrate more whisker grooming than *Chmp2*$^{+/+}$ mice in the SHIRPA experiments. Emotional behaviour such as fear, anger and disgust are also impaired in FTD correlating with atrophy of the amygdala (Ledoux, 2003; Werner et al., 2007). Fear response can be relatively easily tested in mice by assessing aversion to stimuli such as mild foot shock or hot plate avoidance (Roberson, 2012).

The FTD genes and their respective proteins are highly conserved between humans and mice with the added finding that mouse brain architecture and network connections are similar to humans, mouse models provide very important tools for studying FTD. FTD caused by progranulin mutations results in haploinsufficiency and a number of progranulin knockout mice have been generated to model loss of progranulin function (Gotz and Ittner, 2008; Roberson, 2012). Progranulin knockout lines exhibit early abnormality in social behaviour such as anxiety (Suzuki et al., 2009) but without noted effect on motor function or general health (Kayasuga et al., 2007; Yin et al., 2010b; Ghoshal et al., 2012). Specifically, Yin and colleagues (2010) demonstrated deficits in hippocampal dependent spatial learning and memory in aged (18 months) progranulin deficient mice using the Morris Water Maze paradigm (Yin et al., 2010b). This study

showed that these progranulin deficient mice also demonstrate depression-like behaviour such as being immobile for longer in forced swimming test from 4 months of age and reduced social recognition. In the social recognition paradigm, test mice have reduced preference for a container containing a second 'intruder mouse' compared to an empty container. As this recognition assessment depends on olfaction, the mouse's sense of smell was tested by their preference for sesame oil over water; the authors reported no difference in preference between progranulin deficient mice and wild type mice. Therefore it was concluded that the reduced preference for the container with the mouse against an empty container reflects social interaction abnormality (Yin et al., 2010b).

Reduced levels of social engagement and cognitive deficits were also reported in another progranulin knockout mouse model at late middle age (Ghoshal et al., 2012). In this study robust differences were reported in more socially orientated indices of the resident-intruder test such as pawing, following and time spent alone. Progranulin knockout mice interacted less frequently with young male intruders compared to wild type control mice. Although no differences were observed in locomotor or exploratory behaviour the Morris Water Maze revealed mild impaired learning and memory performance likely due to cognitive deficits (Ghoshal et al., 2012). A homozygous progranulin knockout line generated using a targeted genomic recombination approach and *Cre-LoxP* technology showed no difference to heterozygous progranulin mice until 10 months of age (Wils et al., 2012). From this age onwards homozygous progranulin deficient mice showed reduced survival, that the other two studies had not reported (Ghoshal et al., 2012). The differences in the phenotypes reported by the different groups likely reflect differences in mouse genetic background and level of progranulin deficiency resulting from different molecular approaches used to establish each respective progranulin knockout mice.

Interestingly, two patients with homozygous progranulin mutation causing complete progranulin deficiency have recently been shown to develop a clinically distinct neurodegenerative disease; neuronal ceroid lipofuscinosis (NCL) (Smith et al., 2012) suggesting that the degree of progranulin deficiency is clinically relevant and therefore differences between homozygous and heterozygous progranulin mice are likely. Indeed a cardinal pathological feature of human NCL is accumulation of lipofuscin which has also been reported in an age-dependent manner in homozygous progranulin knockout mice by a number of groups (Ahmed et al., 2010; Ghoshal et al., 2012; Petkau et al., 2012; Wils et al., 2012).

As discussed in section 1.6.2 progranulin mutations are characterised by the presence of TDP-43 protein inclusions. In addition mutation in FTD-MND spectrum disorders resulting from *TARDBP* (gene coding TDP-43 protein) are missense changes in the genes glycine-rich domain(Benajiba et al., 2009; Kovacs et al., 2009; Barmada and Finkbeiner, 2010; Ticozzi et al., 2011). Complete TDP-43 knockout mouse models are embryonic lethal, while heterozygous knockouts display no obvious pathology and normal TDP-43 protein levels (Wu et al., 2010; Sephton et al., 2010; Kraemer et al., 2010). Only Kreamer and colleagues (2010) reported subtle motor weakness with age (Kraemer et al., 2010) while conditional knockout of *TARDBP* at 4-6 weeks results in rapid weight loss and death within 9 days (Chiang et al., 2010; Wu et al., 2012). Numerous TDP-43 mouse models have been generated to date and reviewed elsewhere (Roberson, 2012; Tsao et al., 2012; Rademakers and van Blitterswijk, 2013). The first TDP-43 mouse models were generated using heterologous promoters to drive human TDP-43 expression throughout the nervous system. These mice developed significant motor impairment leading to death (Wegorzewska et al., 2009; Wils et al., 2012). While restricted expression of TDP-43 to the forebrain using CaMKII promoter resulted in neurodegeneration and behavioural deficits (Tsai et al., 2010; Igaz et al., 2011). Recently the entire human TDP-43 gene, driven by its own promoter has been expressed in mice. Researchers report 3x TDP-43 endogenous brain levels in these

mouse models which develop learning, memory and motor deficits from 7 months of age in addition to earlier onset astrogliosis. Interestingly, these phenotypes are present whether wild type or mutant TDP-43 is expressed (Swarup et al., 2011).

TDP-43 protein inclusions are also a hallmark of C9orf72 FTD cases. However, at time of writing there are no reports of published C9orf72 mouse models. However, it has been reported that C9orf72 is highly transcribed in neuronal populations sensitive to degeneration in FTD and ALS using transgenic mice harbouring a LacZ insertion (Suzuki et al., 2013).

Mutations in tau were the first mutations found in FTD patients and many mouse models of tau have been described and recent reviews include Roberson 2012 and Gots 2007 (Gotz and Ittner, 2008; Roberson, 2012). Interesting findings from decades of tau mouse models include the observation that tau pathology and neuronal death have been dissociated from function deficit phenotypes (Roberson, 2012). For example, Yoshiyama and colleagues (2007) report that in the PS19 tauopathy mouse model, behavioural deficits and synaptic deficits are observed several months before tangle formation (Yoshiyama et al., 2007). Also a number of groups have reported that in regulatable tau lines, even though turning off mutant tau expression reverses synaptic and behavioural deficits, tau pathology and neuronal loss continues (SantaCruz et al., 2005; Mocanu et al., 2008; Sydow et al., 2011; Roberson, 2012). Interesting in relation to the *Chmp2b* data, it has been reported that transgenic mice expressing tau V337M also display deficits in impulse control which is exacerbated with aging (Lambourne et al., 2007).

As burrowing is considered a spontaneous and rewarding activity, one might consider whether *Chmp2b* knockout mice are unable to regulate their impulse control and therefore continue to burrow when wild type *Chmp2b* counterparts demonstrate reduced burrowing activity.

Nesting behaviour too is a spontaneous and rewarding behaviour and is demonstrated in both male and female mice. *Chmp2b*$^{+/+}$ mice demonstrate a constant median nesting score of 4 (score range 2 to 5) from 4 to 6 months of age. However, *Chmp2b*$^{-/-}$ mice demonstrate a significantly higher median nesting score of 5 (score range 2 to 5) at 4 and 5 months of age. By 6 months of age both *Chmp2b*$^{+/+}$ and *Chmp2b*$^{-/-}$ mice have a median score of 4.

In a comparable manner to the burrowing results, *Chmp2b*$^{-/-}$ mice demonstrate an increase in nesting behaviour compared to *Chmp2b*$^{+/+}$ mice. Most reports of nesting phenotype identified in the literature report a significant decline in nesting behaviour associated with neurodegeneration mouse models, including scrapie sick mice (Cunningham et al., 2003). The only report identified at this time in a literature search showing an *increase* in nesting behaviour is in BALB/c and C57BL/6J mouse on enhanced dietary tryptophan (Browne et al., 2012). Tryptophan is a serotonin precursor and dietary tryptophan depletion or supplementation results in pronounced behavioural effects, particularly in nesting behaviour (Browne et al., 2012). As previously suggested for the burrowing data the increase in nesting behaviour observed in *Chmp2b*$^{-/-}$ mice may be associated with the potential effect of Chmp2b depletion on receptor regulation, although this study does not provide evidence of this phenomenon and additional work is needed to test this hypothesis.

It is interesting that an 85*%* depletion of Chmp2b is sufficient to produce a distinct motor and behavioural phenotype in *Chmp2b*$^{-/-}$mice, without resulting in embryonic lethality. Notably, other ESCRT III protein knockout mouse models reported to date, *Chmp5 and Chmp4b* knockouts are embryonic lethal (Shim et al., 2006; Lee et al., 2007).

In conclusion this body of work has demonstrated evidence that depletion of *Chmp2b* in mice results in motor and behaviour deficits as well as significantly reduced survival, which is consistent with other mouse models of FTD discussed above and likely reflects broader neurodegenerative pathology. In order to assess memory and learning abilities of these mice additional tests such as the Morris Water Maze will need to be carried out in future studies.

6.3 *CHMP2B* Transgenic Mice

Affected FTD-3 family members present with characteristic neuropathology including global cortical atrophy involving the frontal and temporal cortices, astrogliosis, microglial infiltration together with ubiquitin and p62 inclusions, however FTD-3 brains are negative for TDP-43 and FUS pathological staining (Holm et al., 2007; Holm et al., 2009).

One of the aims of this thesis was to investigate whether expression of mutant $CHMP2B^{Int5}$ and $CHMP2B^{\Delta 10}$ transcripts in mice recapitulates key neuropathological hallmarks found in post-mortem FTD-3 brains and therefore whether mutant CHMP2B causes disease by a gain of function mechanism.

As protein overexpression was not demonstrated in $CHMP2B^{\Delta 10}$ mice, $CHMP2B^{\Delta 10}$ lines Tg158 and Tg164, were terminated after initial molecular characterisation and further pathological studies were not performed on these lines.

6.3.1 $CHMP2B^{Int5}$ transgenic mice demonstrate progressive gliosis and microglial activation pathology

$CHMP2B^{Int5}$ mouse brain sections show progressive gliosis and microglial activation in an age-dependent progressive manner not observed in age-matched Non-Tg and $CHMP2B^{WT}$ brain sections. A consistent pattern of age-dependent progressive

gliosis is also identified in the *CHMP2B*^{Int5} lumber spinal cord region. Although some variation is noted in GFAP staining of the spinal cord, comparable progressive age-dependent gliosis is not identified in the lumber spinal cord region of age-matched Non-Tg and *CHMP2B*^{WT} mice.

Progressive gliosis including astrocyte activation is a cardinal feature of FTLD and is evident in both grey and white matter regions often accompanying neuronal loss (Brun and et al, 1994; Josephs et al., 2004; Cairns et al., 2007a). Therefore not surprisingly mouse models of FTD harbouring mutant proteins or knockout models reproducing loss of function paradigms also demonstrate progressive gliosis and microglial activation (reviewed by Roberson 2012 (Roberson, 2012)). For example a number of published progranulin deficient mouse (*GRN*$^{-/-}$) lines demonstrate high degrees of progressive gliosis and microgliosis (reviewed by Roberson 2012 (Roberson, 2012)). Specifically in FTD-3, gliosis and astrocyte infiltration is present in layer II of the frontal cortex with involvement of the entire thickness of the cortex to some degree, so that progressive gliosis and microglial activation in *CHMP2B*^{Int5} mouse brain is consistent with FTD-3 pathology and other reported FTD mouse models.

6.3.2 *CHMP2B*^{Int5} transgenic mice demonstrate progressive inclusion pathology

The most striking pathology identified in *CHMP2B*^{Int5} mouse brain and lumbar spinal cord is the age-dependent progressive accumulation of ubiquitin, p62 and CHMP2B inclusions. The presence of these inclusions unique to *CHMP2B*^{Int5} mice suggests that these inclusions are intrinsically linked to the presence of *CHMP2B*^{Int5} mutant isoform.

Ubiquitin and p62-positive neuronal cytoplasmic inclusions are observed in FTD-3 brains in the dentate granule cell layer of the hippocampus and to a lesser extent in the frontal cortex (Holm et al., 2007). In *CHMP2B*^{Int5} mice p62 inclusions are identified in the cortex, corpus callosum, thalamus and brain stem which very

likely reflects the expression pattern of the hamster prion promoter used for driving *CHMP2B*^{Int5} expression as previously described (Scott et al., 1989; Asante et al., 2002)

A fundamental characteristic of FTLD pathology is the presence of abnormal intracellular accumulation of disease-specific proteins on which recent FTLD classification is based (Mackenzie et al., 2009; Neumann et al., 2009b; Mackenzie et al., 2010; Rademakers et al., 2012). Furthermore, such proteins including TDP-43 and FUS colocalise with ubiquitin and p62 inclusions suggesting their targeting to UPS or autophagy pathway for degradation (Neumann et al., 2007; Mackenzie and Rademakers, 2007; Mackenzie et al., 2009; Neumann et al., 2009a; Neumann et al., 2009b; Mackenzie et al., 2010; Rademakers et al., 2012). Consequently some FTD mouse models including a number of progranulin null and *Vcp* mutant mice demonstrate ubiquitinated TDP-43 protein (Roberson, 2012).

Ubiquitin inclusions in FTD-3 do not colocalise to TDP-43 or FUS protein (Holm et al., 2009), which may indicate the presence of an as yet unidentified protein inclusion possibly a CHMP protein or members of the DNA/RNA binding proteins other than TDP-43 or FUS. Remarkably *CHMP2B*^{Int5} mouse brains demonstrate CHMP2B-positive inclusions not yet reported in human FTD-3 brains. The CHMP2B inclusions in *CHMP2B*^{Int5} mouse brains demonstrate a similar staining pattern and distribution as ubiquitin inclusions, a strong indicator that they co-localise. The inability to detect CHMP2B inclusions in FTD-3 brains may be due to poor CHMP2B antibodies that cannot detect CHMP2B inclusions in human brains which have often been preserved in formalin for long durations.

The transgenic mice described here are not on a *Chmp2b* null background and therefore mice retain the wild type endogenous mouse Chmp2b protein. Both the endogenous mouse Chmp2b and the human mutant *CHMP2B*^{Int5} protein are shown to be expressed (chapter 5, figure 5.10). It can therefore be hypothesised

that mutant *CHMP2B^{Int5}* protein and endogenous wild type mouse Chmp2b protein would potentially interact, resulting in the inclusion formation seen. This may also address the absence of CHMP2B inclusions in human brains as FTD-3 patients carry only one wild type CHMP2B allele and therefore only have half of the wild type protein available.

6.3.3 *CHMP2B^{Int5}* mouse brain cortex ultrastructure shows inclusions and axonal swelling

Ultrastructural EM examination of 12 and 18 months *CHMP2B^{Int5}* brain cortex confirms the presence of neuronal inclusions and further reveals the presence of axonal swellings containing an accumulation of mitochondria and vesicles, likely from the endosome-lysosome and autophagy pathways. Neuronal inclusions and axonal swellings are not observed in age-matched Non-Tg brains confirming that the inclusions are not an age-related artefact but are transgene specific. This observation may also suggest that *CHMP2B^{Int5}* transgenic mice may have impaired vesicular transport. Consistent with this is the observation that Chmp4b knockout mice and expression of *CHMP2B^{Int5}* in cortical neurons results in autophagosome accumulation (Lee et al., 2009). Furthermore, expression of the human P^{150Glued} subunit of dynactin associated with MND results in distal degeneration associated with axonal swelling and changes in the NMJs and although axonal transport is not impaired, enlarged tertiary lysosomes and cytoplasmic granules are observed in neuronal cells, suggesting impairment in vesicular transport and degradation (Kuta, 2011).

6.3.4 Autophagy is not up regulated in *CHMP2B^{Int5}* Transgenic Mice

The autophagy degradation process has received much attention in the field of neurodegeneration. Loss of autophagy in neurons results in inclusion accumulation and neurodegeneration (Hara et al., 2006; Komatsu et al., 2006) and upregulation of autophagy by pharmacological administration of mTOR inhibiting

drugs such as FK506 reduces levels of soluble huntingtin and formation of intracellular aggregates *in vitro* (Ravikumar et al., 2004) and ameliorates pathogenesis in TDP-43 proteinopathy mouse models (Fang Wang et al., 2013).

Mutant *CHMP2B*^{Int5} leads to formation of aberrant enlarged endosomes and delayed EGFR degradation in cell culture and in patient fibroblasts due to impaired endosome-lysosome fusion (Urwin et al., 2010a). CHMP2B mutants have also been shown to inhibit autophagic degradation, leading to accumulation of ubiquitin, p62, and GFP-LC3 (Filimonenko et al., 2007). In *CHMP2B*^{Int5} transgenic mouse brain homogenates, accumulation of p62 is predominantly in the insoluble *CHMP2B*^{Int5} brain fraction, reflecting accumulation of insoluble p62 inclusions (Ghazi-Noori et al., 2012). No difference is identified in LC3-II expression in *CHMP2B*^{Int5} mouse whole brain homogenates compared to Non-Tg mice at 6 or 18 months. This suggests that autophagy is not altered in *CHMP2B*^{Int5} mouse brain, however it is possible that autophagy may be altered in only parts of the brain for example the thalamus where most pathology is identified and using whole brain homogenate may mask any autophagy deregulation unique to only particular brain regions.

Post-mortem FTD-3 brain tissues demonstrate enlarged vacuoles positive for the late endosome marker M6PR (Urwin et al., 2010a). Furthermore, CHMP2B has been implicated in granulovacuolar degeneration (GVD) in PD and AD (Yamazaki et al., 2010; Kurashige et al., 2012). GVD involves the accumulation of large, double membrane-bound bodies. Because of the two-layer membrane morphology it has been proposed that the bodies are related to autophagic organelles. Funk and colleagues (2011) have shown that granulovacuolar degeneration bodies (GVBs) in AD contain late-stage autophagic markers which colocalized strongly with CHMP2B and accumulate proteins at the nexus of autophagic and endocytic pathways, suggesting that failure to complete autolysosome formation may be an important correlate of GVB accumulation (Funk et al., 2011).

CHMP2B^{Int5} mice do not replicate the enlarged M6PR positive vacuoles seen in human FTD-3 brains or presence of GVD. This may simply be that such process is a late phenotype and the pathology assessed in the mice is not sufficiently progressed to permit identification of these, or that light microscopy does not have sufficient resolution to reveal endosomal phenotype and immuno-gold EM of endosomal markers would reveal an endosome-autophagosome phenotype. Alternatively interaction between *CHMP2B*^{Int5} and *CHMP2B*$^{\Delta 10}$ proteins may be a factor in the formation of the vacuolar phenotype in FTD-3 brain. This is not modelled in *CHMP2B*^{Int5} mice as *CHMP2B*$^{\Delta 10}$ is not co-expressed. Another possibility is that a loss of function/dominant negative effect is masked by the presence of endogenous mouse Chmp2b protein in the transgenic lines, as loss of Chmp5 and Chmp4b have been reported to result in autophagosome accumulation (Shim et al., 2006; Lee et al., 2009).

6.4 Summary

CHMP2B^{Int5} mice demonstrate key neuropathological features consistent with human FTD-3 disease. They demonstrate neuroinflammation characterised by progressive gliosis and microglial activation and p62 and ubiquitin inclusions that are negative for TDP-43 and FUS proteins, all cardinal features of FTD-3 neuropathology. In addition the mice also develop CHMP2B protein inclusions, axonal swelling and have reduced survival. This neuropathology is not observed in Non-Tg, *CHMP2B*^{WT} mice *Chmp2b*$^{-/-}$ mice, taken together these observations are consistent with a gain-of-function effect unique to the *CHMP2B*^{Int5} isoform.

No mouse model is perfect and *CHMP2B*^{Int5} mice also have some limitations. Critically, the transgenic mice are not on a *Chmp2b* null background meaning that all the transgenic mice express the endogenous mouse Chmp2b in addition to the human wild type or mutant CHMP2B transgenic proteins. This is likely to be

important as in human FTD-3 there is a loss of one wild type *CHMP2B* allele, in principle suggesting that up to 50% of CHMP2B expression may be lost. This loss of expression may contribute to disease pathology and clinical presentation so that in *CHMP2B*^{Int5} mice, endogenous Chmp2b is compensating for some expected pathology. For example it is likely that *CHMP2B*^{Int5} mice on a *Chmp2b* null background may develop earlier disease onset, more aggressive pathology as well as motor and behavioural phenotype. Preliminary observation suggests *CHMP2B*^{Int5} mice do not have an obvious motor phenotype (personal communication with AI). In addition *CHMP2B*^{Int5} mice demonstrate CHMP2B inclusions not seen in human FTD-3 which may reflect interaction of mutant CHMP2B^{Int5} protein with endogenous wild type mouse Chmp2b. Moreover, although axonal swelling is seen under EM in *CHMP2B*^{Int5} mice, enlarged late endosome marker positive vacuoles are not seen again raising the possibility that endogenous mouse Chmp2b may play a molecular compensatory role.

Chmp2b$^{-/-}$ mice do not reveal any overt pathology with the techniques applied; they do however show distinct motor coordination deficits and behavioural abnormalities. This contrasting observation to the *CHMP2B*^{Int5} mice suggests loss of function of CHMP2B may contribute to other aspects of the disease phenotype. This phenomenon has been described for SCA1 knockout mice in which loss of *Atxn1* does not lead to neuropathological changes (Matilla et al., 1998) while expression of the expanded CAG repeat does (Watase et al., 2002). However, comparable to the observation in *Chmp2b*$^{-/-}$ mice it has been demonstrated that partial loss of function of *Atxn1* contributes to disease phenotype, including behavioural changes (Lim *et al*., 2008; Crespo-Barreto *et al*., 2010). Consistent with this Belly and colleagues (2010) have demonstrated that in cultured hippocampal neurons depletion of endogenous CHMP2B by RNAi resulted in morphological changes similar to those induced by mutant CHMP2B (Belly et al., 2010) further supporting that loss of function could contribute to the disease phenotype.

Mouse models are important tools for studying neurodegenerative disorders because they meet the need for an experimentally manipulable system that shares sufficient genetic and neural similarity with humans. Mice and humans also share a number of conserved genes and a high degree of chromosomal synteny as well as conserved patterns of gene expression across brain regions. The FTD proteins in particular are highly conserved between humans and mice and as neurodegenerative diseases target networks of connected brain regions the finding that mice have brain architecture and network connections that are similar to humans is an important advantage over non mammalian models (Roberson, 2012).

6.5 Future directions

As both the *Chmp2b*$^{-/-}$ and transgenic mice are on mixed genetic background they need to be backcrossed onto a homogenous genetic background. Genetic background can influence the performance and phenotype of animals therefore it would be beneficial to characterise *Chmp2b* knockout and CHMP2B transgenic mice bred on at least 2 distinct genetic backgrounds. For example different genetic backgrounds may affect the behavioural phenotype observed in *Chmp2b*$^{-/-}$ mice. The modifying effects of genetic background on disease associated phenotypes have been described using a transgenic model of amyotropic lateral sclerosis (ALS) (Acevedo-Arozena et al., 2011).

Future work will also need to further characterise *CHMP2B*^{Int5} and *Chmp2b*$^{-/-}$ mice as several aspects of FTD are potentially amenable to mouse modelling.

CHMP2B^{Int5} and *Chmp2b*$^{-/-}$ mice will also be good sources to harvest neuronal cells for functional studies, for example functional receptor degradation,

autophagosome formation, transcriptional regulation in cortical neurons and *in vivo* electrophysiological studies. The use of primary neuronal cells has advantages over other *in vitro* paradigms as they are more physiologically relevant because they are neuronal cells and have stably expressed mutant *CHMP2B* gene expression at endogenous levels or *Chmp2b* depletion. They will also be a good source to test potential therapeutic compounds.

To date research into neurodegenerative disease including FTD has systematically classified clinical and neuropathological characteristics. Neuropathologists have painstakingly identified regions and patterns of pathology distinct to FTLD, inclusion pathology and recently the subclassification of FTLD into respective proteinopathies and genetics has identified sporadic and familial genetic causes while *in vivo* studies have recapitulated respective genetic mutation pathologies in mouse and fly models and *in vitro* studies have attempted to shed light on the functional aspects of genetic dysfunction.

Moving forward it is critical to direct research into examining interaction of neuronal cells and the neuronal systems they form and how disease associated mutations affect such interactions perhaps through signalling and transcription pathways, receptor homeostasis and reactive neuroinflammation.

The overall aim is ultimately to identify effective treatment strategies for FTD patients. To achieve this, experience and knowledge will need to be drawn from other clinical specialities, for example effective cancer treatment and management has evolved from extensive genetic, molecular and pathological research critically combined with pre-symptomatic screening. The greatest challenge in FTD treatment is that by the time an individual is diagnosed, they would have advanced disease symptoms. Even today conclusive diagnosis *i.*e. type of FTD proteinopathy is only possible at post-mortem, raising the need for therapeutic intervention that can reverse at the very least clinical symptoms and ideally pathology. Treatment and management of FTD as well as other

neurodegenerative disorders will ultimately involve extensive research and development of disease biomarkers. For genetically inherited cases screening of *asymptomatic* carriers is important as they will be the most suitable group to test potential therapeutic interventions that aim to halt rather than reverse disease progression. The development of the first mouse model of FTD-3 described in this thesis is the first step on this pathway to therapy.

Publications arising from this thesis

1. **Ghazi-Noori, S., Froud, K., Mizielinska, S., Powell, C., Smidak, M., Fernandez de Marco, M., O'Malley, C., Farmer, M., Parkinson, N., Fisher, E.M.C., Asante, E.A., Brandner, S., Collinge, J., and Isaacs, A.M.** (2012). Progressive neuronal inclusion formation and axonal degeneration in CHMP2B mutant transgenic mice. **Brain *135*; 819–832**

2. **Urwin,H., Ghazi-Noori, S., Collinge, J., and Isaacs, A.** (2009). The role of CHMP2B in frontotemporal dementia. **Biochem Soc Trans *37*,** 208-212.

Reference List

Acevedo-Arozena,A., Kalmar,B., Essa,S., Ricketts,T., Joyce,P., Kent,R., Rowe,C., Parker,A., Gray,A., Hafezparast,M., Thorpe,J.R., Greensmith,L., and Fisher,E.M.C. (2011). A comprehensive assessment of the SOD1(G93A) low-copy transgenic mouse, which models human amyotrophic lateral sclerosis. Disease Models & Mechanisms *4*, 686-700.

Ahmad,S.T., Sweeney,S.T., Lee,J.A., Sweeney,N.T., and Gao,F.B. (2009). Genetic screen identifies serpin5 as a regulator of the toll pathway and CHMP2B toxicity associated with frontotemporal dementia. Proc Natl Acad Sci U S A *106*, 12168-12173.

Ahmed,Z., Sheng,H., Xu,Y.F., Lin,W.L., Innes,A.E., Gass,J., Yu,X., Hou,H., Chiba,S., Yamanouchi,K., Leissring,M., Petrucelli,L., Nishihara,M., Hutton,M.L., McGowan,E., Dickson,D.W., and Lewis,J. (2010). Accelerated Lipofuscinosis and Ubiquitination in Granulin Knockout Mice Suggest a Role for Progranulin in Successful Aging. American Journal of Pathology *177*, 311-324.

Alzheimer A (1911). Uber eigenartige Krankheitsfalle des spateren alters. Z Ges Neurol Psychiatr *4*, 356-385.

Alzheimer,A., Stelzmann,R.A., Schnitzlein,H.N., and Murtagh,F.R. (1995). An English translation of Alzheimer's 1907 paper, "Uber eine eigenartige Erkankung der Hirnrinde". Clin. Anat. *8*, 429-431.

Andrejewski,N., Punnonen,E.L., Guhde,G., Tanaka,Y., Lullmann-Rauch,R., Hartmann,D., von Figura,K., and Saftig,P. (1999). Normal lysosomal morphology and function in LAMP-1-deficient mice. Journal of Biological Chemistry *274*, 12692-12701.

Asante,E.A., Linehan,J.M., Desbruslais,M., Joiner,S., Gowland,I., Wood,A.L., Welch,J., Hill,A.F., Lloyd,S.E., Wadsworth,J.D., and Collinge,J. (2002). BSE prions propagate as either variant CJD-like or sporadic CJD-like prion strains in transgenic mice expressing human prion protein. EMBO J *21*, 6358-6366.

Baba,Y., Baker,M.C., Le Ber,I., Brice,A., Maeck,L., Kohlhase,J., Yasuda,M., Stoppe,G., Bugiani,O., Sperfeld,A.D., Tsuboi,Y., Uitti,R.J., Farrer,M.J., Ghetti,B., Hutton,M.L., and Wszolek,Z.K. (2007). Clinical and genetic features of families with frontotemporal dementia and parkinsonism linked to chromosome 17 with a P301S tau mutation. Journal of Neural Transmission *114*, 947-950.

Babst,M., Katzmann,D.J., Estepa-Sabal,E.J., Meerloo,T., and Emr,S.D. (2002). Escrt-III: an endosome-associated heterooligomeric protein complex required for mvb sorting. Dev. Cell *3*, 271-282.

Bancroft,J. and Gamble,M. (2002). Theory and Practice of Histological Techniques Fifth edition.

Barmada,S.J. and Finkbeiner,S. (2010). Pathogenic TARDBP Mutations in Amyotrophic Lateral Sclerosis and Frontotemporal Dementia: Disease-Associated Pathways. Reviews in the Neurosciences *21*, 251-272.

Bathgate,D., Snowden,J.S., Varma,A., Blackshaw,A., and Neary,D. (2001). Behaviour in frontotemporal dementia, Alzheimer's disease and vascular dementia. Acta Neurologica Scandinavica *103*, 367-378.

BayGenomics. http://www.mmrrc.org/catalog/overview_BG.php. http://www.mmrrc.org/catalog/overview_BG.php . 2012.
Ref Type: Electronic Citation

Becker,E.B.E., Olivera,P.L., Glitsch,M.D., Banks,G.T., Achilli,F., Hardy,A., Nolan,P.M., Fisher,E.M.C., and Davies,K.E. (2009). A point mutation in TRPC3 causes abnormal Purkinje cell development and cerebellar ataxia in moonwalker mice. Proceedings of the National Academy of Sciences of the United States of America *106*, 6706-6711.

Belly,A., Bodon,G., Blot,B., Bouron,A., Sadoul,R., and Goldberg,Y. (2010). CHMP2B mutants linked to frontotemporal dementia impair maturation of dendritic spines. J Cell Sci *123*, 2943-2954.

Benajiba,L., Le,B., I, Camuzat,A., Lacoste,M., Thomas-Anterion,C., Couratier,P., Legallic,S., Salachas,F., Hannequin,D., Decousus,M., Lacomblez,L., Guedj,E., Golfier,V., Camu,W., Dubois,B., Campion,D., Meininger,V., and Brice,A. (2009). TARDBP mutations in motoneuron disease with frontotemporal lobar degeneration. Ann Neurol *65*, 470-473.

Bjorkoy,G., Lamark,T., Brech,A., Outzen,H., Perander,M., Overvatn,A., Stenmark,H., and Johansen,T. (2005). p62/SQSTM1 forms protein aggregates degraded by autophagy and has a protective effect on huntingtin-induced cell death. J Cell Biol. *171*, 603-614.

Boeve,B.F. (2011). The Multiple Phenotypes of Corticobasal Syndrome and Corticobasal Degeneration: Implications for Further Study. Journal of Molecular Neuroscience *45*, 350-353.

Brettschneider,J., Libon,D.J., Toledo,J.B., Xie,S.X., McCluskey,L., Elman,L., Geser,F., Lee,V.M.Y., Grossman,M., and Trojanowski,J.Q. (2012). Microglial activation and

TDP-43 pathology correlate with executive dysfunction in amyotrophic lateral sclerosis. Acta Neuropathologica *123*, 395-407.

Broe,M., Hodges,J.R., Schofield,E., Shepherd,C.E., Kril,J.J., and Halliday,G.M. (2003). Staging disease severity in pathologically confirmed cases of frontotemporal dementia. Neurology *60*, 1005-1011.

Brooks,S.P. and Dunnett,S.B. (2009). Tests to assess motor phenotype in mice: a user's guide. Nature Reviews Neuroscience *10*, 519-529.

Brown,J. (1998). Chromosome 3-linked frontotemporal dementia. Cellular and Molecular Life Sciences *54*, 925-927.

Brown,J., Ashworth,A., Gydesen,S., Sorensen,A., Rossor,M., Hardy,J., and Collinge,J. (1995). Familial non-specific dementia maps to chromosome 3. Hum Mol Genet *4*, 1625-1628.

Brown,J., Gydesen,S., Johannsen,P., Gade,A., Skibinski,G., Chakrabarti,L., Brun,A., Spillantini,M., Yancopoulou,D., Thusgaard,T., Sorensen,A., Fisher,E., and Collinge,J. (2004). Frontotemporal dementia linked to chromosome 3. Dementia and Geriatric Cognitive Disorders *17*, 274-276.

Brown,J., Gydesen,S., Sorensen,S.A., Brun,A., Smith,S., Houlden,H., Twells,R., Mullan,M., Rossor,M., Collinge,J., Palmer,M., Goate,A., and Hardy,J. (1993). Genetic-Characterization of A Familial Nonspecific Dementia Originating in Jutland, Denmark. Journal of the Neurological Sciences *114*, 138-143.

Brown,J., Smith,S., Brun,A., Collinge,J., Gydesen,S., Hardy,J., Mullan,M., and Goate,A. (1991). Genetic-Characterization of A Novel Familial Dementia. Annals of the New York Academy of Sciences *640*, 181-183.

Browne,C.A., Clarke,G., Dinan,T.G., and Cryan,J.F. (2012). An effective dietary method for chronic tryptophan depletion in two mouse strains illuminates a role for 5-HT in nesting behaviour. Neuropharmacology *62*, 1903-1915.

Brun,A. and et al (1994). Clinical and neuropathological criteria for frontotemporal dementia. The Lund and Manchester Groups. J Neurol. Neurosurg. Psychiatry *57*, 416-418.

Bruno,K.J., Freet,C.S., Twining,R.C., Egami,K., Grigson,P.S., and Hess,E.J. (2007). Abnormal latent inhibition and impulsivity in coloboma mice, a model of ADHD. Neurobiology of Disease *25*, 206-216.

Buratti,E., Brindisi,A., Pagani,F., and Baralle,F.E. (2004). Nuclear factor TDP-43 binds to the polymorphic TG repeats in CFTR intron 8 and causes skipping of exon 9: a functional link with disease penetrance. Am J Hum Genet *74*, 1322-1325.

Buratti,E., Dork,T., Zuccato,E., Pagani,F., Romano,M., and Baralle,F.E. (2001). Nuclear factor TDP-43 and SR proteins promote in vitro and in vivo CFTR exon 9 skipping. EMBO J *20*, 1774-1784.

Burrell,J.R. and Hodges,J.R. (2010). From FUS to Fibs: What's New in Frontotemporal Dementia? Journal of Alzheimers Disease *21*, 349-360.

Burrell,J.R., Kiernan,M.C., Vucic,S., and Hodges,J.R. (2011). Motor Neuron dysfunction in frontotemporal dementia. Brain *134*, 2582-2594.

Cairns,N.J., Bigio,E.H., Mackenzie,I.R., Neumann,M., Lee,V.M., Hatanpaa,K.J., White,C.L., III, Schneider,J.A., Grinberg,L.T., Halliday,G., Duyckaerts,C., Lowe,J.S., Holm,I.E., Tolnay,M., Okamoto,K., Yokoo,H., Murayama,S., Woulfe,J., Munoz,D.G., Dickson,D.W., Ince,P.G., Trojanowski,J.Q., and Mann,D.M. (2007a). Neuropathologic diagnostic and nosologic criteria for frontotemporal lobar degeneration: consensus of the Consortium for Frontotemporal Lobar Degeneration. Acta Neuropathol. (Berl) *114*, 5-22.

Cairns,N.J., Neumann,M., Bigio,E.H., Holm,I.E., Troost,D., Hatanpaa,K.J., Foong,C., White,C.L., III, Schneider,J.A., Kretzschmar,H.A., Carter,D., Taylor-Reinwald,L., Paulsmeyer,K., Strider,J., Gitcho,M., Goate,A.M., Morris,J.C., Mishra,M., Kwong,L.K., Stieber,A., Xu,Y., Forman,M.S., Trojanowski,J.Q., Lee,V.M., and Mackenzie,I.R. (2007b). TDP-43 in familial and sporadic frontotemporal lobar degeneration with ubiquitin inclusions. Am J Pathol *171*, 227-240.

Calakos,N. and Scheller,R.H. (1994). Vesicle-Associated Membrane-Protein and Synaptophysin Are Associated on the Synaptic Vesicle. Journal of Biological Chemistry *269*, 24534-24537.

Calhoun,M.E., Jucker,M., Martin,L.J., Thinakaran,G., Price,D.L., and Mouton,P.R. (1996). Comparative evaluation of synaptophysin-based methods for quantification of synapses. Journal of Neurocytology *25*, 821-828.

Cannon,A., Baker,M., Boeve,B., Josephs,K., Knopman,D., Petersen,R., Parisi,J., Dickison,D., Adamson,J., Snowden,J., Neary,D., Mann,D., Hutton,M., and Pickering-Brown,S.M. (2006). CHMP2B mutations are not a common cause of frontotemporal lobar degeneration. Neurosci. Lett *398*, 83-84.

Chen,X.J., Levedakou,E.N., Millen,K.J., Wollmann,R.L., Soliven,B., and Popko,B. (2007). Proprioceptive sensory neuropathy in mice with a mutation in the cytoplasmic dynein heavy chain 1 gene. Journal of Neuroscience *27*, 14515-14524.

Chevalier-Larsen,E.S., Wallace,K.E., Pennise,C.R., and Holzbaur,E.L.F. (2008). Lysosomal proliferation and distal degeneration in motor neurons expressing the G59S mutation in the p150(Glued) subunit of dynactin. Human Molecular Genetics *17*, 1946-1955.

Chiang,P.M., Ling,J., Jeong,Y.H., Price,D.L., Aja,S.M., and Wong,P.C. (2010). Deletion of TDP-43 down-regulates Tbc1d1, a gene linked to obesity, and alters body fat metabolism. Proceedings of the National Academy of Sciences of the United States of America *107*, 16320-16324.

Chow,T.W., Miller,B.L., Hayashi,V.N., and Geschwind,D.H. (1999). Inheritance of frontotemporal dementia. Arch Neurol *56*, 817-822.

Cox,L.E., Ferraiuolo,L., Goodall,E.F., Heath,P.R., Higginbottom,A., Mortiboys,H., Hollinger,H.C., Hartley,J.A., Brockington,A., Burness,C.E., Morrison,K.E., Wharton,S.B., Grierson,A.J., Ince,P.G., Kirby,J., and Shaw,P.J. (2010). Mutations in CHMP2B in lower motor neuron predominant amyotrophic lateral sclerosis (ALS). PLoS One *5*, e9872.

Crawley,J.N. (2007). What's wrong with my mouse? Behavioural phenotyping of transgenic and knockout mice second edition. Wiley).

Cruts,M., Rademakers,R., Gijselinck,I., van der,Z.J., Dermaut,B., De Pooter,T., de Rijk,P., Del Favero,J., and Van Broeckhoven,C. (2005). Genomic architecture of human 17q21 linked to frontotemporal dementia uncovers a highly homologous family of low-copy repeats in the tau region. Hum. Mol. Genet. *14*, 1753-1762.

Cunningham,C., Deacon,R., Wells,H., Boche,D., Waters,S., Diniz,C.P., Scott,H., Rawlins,J.N.P., and Perry,V.H. (2003). Synaptic changes characterize early behavioural signs in the ME7 model of murine prion disease. European Journal of Neuroscience *17*, 2147-2155.

D'Cruz,T., Weibley,B., Kimball,S., and Barber,A. (2012). Post-Translational Processing of Synaptophysin in the Rat Retina Is Disrupted by Diabetes. PLoS One *7*, e44711.

Daly,C. and Ziff,E.B. (2002). Ca2+-dependent formation of a dynamin-synaptophysin complex - Potential role in synaptic vesicle endocytosis. Journal of Biological Chemistry *277*, 9010-9015.

de Carvalho,M., Dengler,R., Eisen,A., England,J.D., Kaji,R., Kimura,J., Mills,K., Mitsumoto,H., Nodera,H., Shefner,J., and Swash,M. (2008). Electrodiagnostic criteria for diagnosis of ALS. Clinical Neurophysiology *119*, 497-503.

De Paola,M., Mariani,A., Bigini,P., Peviani,M., Ferrara,G., Molteni,M., Gemma,S., Veglianese,P., Castellaneta,V., Boldrin,V., Rossetti,C., Chiabrando,C., Forloni,G., Mennini,T., and Fanelli,R. (2012). Neuroprotective Effects of Toll-Like Receptor 4 Antagonism in Spinal Cord Cultures and in a Mouse Model of Motor Neuron Degeneration. Molecular Medicine *18*, 971-981.

Deacon,R.M.J. (2006a). Assessing nest building in mice. Nature Protocols *1*, 1117-1119.

Deacon,R.M.J. (2006b). Burrowing in rodents: a sensitive method for detecting behavioral dysfunction. Nature Protocols *1*, 118-121.

Deacon,R.M.J. (2006c). Housing, husbandry and handling of rodents for behavioral experiments. Nature Protocols *1*, 936-946.

Deacon,R.M.J. (2009). Burrowing: A sensitive behavioural assay, tested in five species of laboratory rodents. Behavioural Brain Research *200*, 128-133.

Deacon,R.M.J., Raley,J.M., Perry,V.H., and Rawlins,J.N.P. (2001). Burrowing into prion disease. Neuroreport *12*, 2053-2057.

Deacon,R.M.J. and Rawlins,J.N.P. (2005). Hippocampal lesions, species-typical behaviours and anxiety in mice. Behavioural Brain Research *156*, 241-249.

Dejesus-Hernandez,M., Mackenzie,I.R., Boeve,B.F., Boxer,A.L., Baker,M., Rutherford,N.J., Nicholson,A.M., Finch,N.A., Flynn,H., Adamson,J., Kouri,N., Wojtas,A., Sengdy,P., Hsiung,G.Y., Karydas,A., Seeley,W.W., Josephs,K.A., Coppola,G., Geschwind,D.H., Wszolek,Z.K., Feldman,H., Knopman,D.S., Petersen,R.C., Miller,B.L., Dickson,D.W., Boylan,K.B., Graff-Radford,N.R., and Rademakers,R. (2011). Expanded GGGGCC Hexanucleotide Repeat in Noncoding Region of C9ORF72 Causes Chromosome 9p-Linked FTD and ALS. Neuron *72*, 245-256.

Deters,N., Ittner,L.M., and Gotz,J. (2008). Divergent phosphorylation pattern of tau in P301L tau transgenic mice. European Journal of Neuroscience *28*, 137-147.

Drake,R., Vogl,A., and Mitchell,AW. (2009). Gray's Anatomy for students. Churchill Livingston).

EMPReSS. http://empress.har.mrc.ac.uk/. http://empress.har.mrc.ac.uk/ . 26-6-2008.
Ref Type: Electronic Citation

Eng,L.F. and Ghirnikar,R.S. (1994). Gfap and Astrogliosis. Brain Pathology *4*, 229-237.

Eng,L.F., Ghirnikar,R.S., and Lee,Y.L. (2000). Glial fibrillary acidic protein: GFAP-thirty-one years (1969-2000). Neurochemical Research *25*, 1439-1451.

Eskelinen,E.L. (2006). Roles of LAMP-1 and LAMP-2 in lysosome biogenesis and autophagy. Molecular Aspects of Medicine *27*, 495-502.

Eskelinen,E.L., Huynh,K., Schmidt,C.K., Grinstein,S., and Saftig,P. (2006). The role of lysosomal membrane proteins in (auto)phagocytosis and intracellular cholesterol traffic. Autophagy *2*, 336.

Eskelinen,E.L., Schmidt,C.K., Neu,S., Willenborg,M., Fuertes,G., Salvador,N., Tanaka,Y., Lullmann-Rauch,R., Hartmann,D., Heeren,J., von Figura,K., Knecht,E., and Saftig,P. (2004). Disturbed cholesterol traffic but normal proteolytic function in LAMP-1/LAMP-2 double-deficient fibroblasts. Molecular Biology of the Cell *15*, 3132-3145.

Eskildsen,S.F., Ostergaard,L.R., Rodell,A.B., Ostergaard,L., Nielsen,J.E., Isaacs,A.M., and Johannsen,P. (2009). Cortical volumes and atrophy rates in FTD-3 CHMP2B mutation carriers and related non-carriers. Neuroimage *45*, 713-721.

Espay,A.J. and Litvan,I. (2011). Parkinsonism and Frontotemporal Dementia: The Clinical Overlap. Journal of Molecular Neuroscience *45*, 343-349.

Fang Wang,I., Tsai,K., and Shen,C.K.J. (2013). Autophagy activation ameliorates neuronal pathogenesis
of FTLD-U mice. Autophagy *9*, 239-240.

Fernandez,S.P. and Gaspar,P. (2012). Investigating anxiety and depressive-like phenotypes in genetic mouse models of serotonin depletion. Neuropharmacology *62*, 144-154.

Ferrari,R., Hardy,J., and Momeni,P. (2011). Frontotemporal Dementia: From Mendelian Genetics Towards Genome Wide Association Studies. Journal of Molecular Neuroscience *45*, 500-515.

Filimonenko,M., Stuffers,S., Raiborg,C., Yamamoto,A., Malerod,L., Fisher,E.M., Isaacs,A., Brech,A., Stenmark,H., and Simonsen,A. (2007). Functional multivesicular bodies are required for autophagic clearance of protein aggregates associated with neurodegenerative disease. J Cell Biol *179*, 485-500.

Forman,M.S., Mackenzie,I.R., Cairns,N.J., Swanson,E., Boyer,P.J., Drachman,D.A., Jhaveri,B.S., Karlawish,J.H., Pestronk,A., Smith,T.W., Tu,P.H., Watts,G.D.J., Markesbery,W.R., Smith,C.D., and Kimonis,V.E. (2006). Novel ubiquitin neuropathology in frontotemporal dementia with valosin-containing protein gene mutations. Journal of Neuropathology and Experimental Neurology *65*, 571-581.

Foster,N.L., Wilhelmsen,K., Sima,A.A.F., Jones,M.Z., Damato,C.J., Gilman,S., Spillantini,M.G., Lynch,T., Mayeux,R.P., Gaskell,P.C., Hulette,C.M., PericakVance,M.A., WelshBohmer,K.A., Dickson,D.W., Heutink,P., Kros,J., vanSwieten,J.C., Arwert,F., Ghetti,M.B., Murrell,J., Lannfelt,L., Hutton,M., Jones,M., Phelps,C.H., Snyder,D.S., Oliver,E., Ball,M.J., Cummings,J.L., Miller,B.L., Katzman,R., Reed,L., Schelper,R.L., Landska,D.J., Brun,A., Fink,J.K., Kuhl,D.E., Knopman,D.S., Wszolek,Z., Miller,C.A., Bird,T.D., Lendon,C., and Elechi,C. (1997). Frontotemporal dementia and parkinsonism linked to chromosome 17: A consensus conference. Annals of Neurology *41*, 706-715.

Fujioka,S. and Wszolek,Z.K. (2011). Clinical Aspects of Familial Forms of Frontotemporal Dementia Associated with Parkinsonism. Journal of Molecular Neuroscience *45*, 359-365.

Funk,K.E., Mrak,R.E., and Kuret,J. (2011). Granulovacuolar degeneration (GVD) bodies of Alzheimer's disease (AD) resemble late-stage autophagic organelles. Neuropathology and Applied Neurobiology *37*, 295-306.

Ghanim,M., Guillot-Noel,L., Pasquier,F., Jornea,L., Deramecourt,V., Dubois,B., Le Ber,I., and Brice,A. (2010). CHMP2B mutations are rare in French families with frontotemporal lobar degeneration. Journal of Neurology *257*, 2032-2036.

Ghazi-Noori,S., Froud,K.E., Mizielinska,S., Powell,C., Smidak,M., de Marco,M.F., O'Malley,C., Farmer,M., Parkinson,N., Fisher,E.M.C., Asante,E.A., Brandner,S., Collinge,J., and Isaacs,A.M. (2012). Progressive neuronal inclusion formation and axonal degeneration in CHMP2B mutant transgenic mice. Brain *135*, 819-832.

Ghosh,P., Dahms,N.M., and Kornfeld,S. (2003). Mannose 6-phosphate receptors: New twists in the tale. Nature Reviews Molecular Cell Biology *4*, 202-212.

Ghoshal,N., Dearborn,J.T., Wozniak,D.F., and Cairns,N.J. (2012). Core features of frontotemporal dementia recapitulated in progranulin knockout mice. Neurobiol Dis *45*, 395-408.

Gijselinck,I., Engelborghs,S., Maes,G., Cuijt,I., Peeters,K., Mattheijssens,M., Joris,G., Cras,P., Martin,J.J., De Deyn,P.P., Kumar-Singh,S., Van Broeckhoven,C., and Cruts,M. (2010). Identification of 2 Loci at Chromosomes 9 and 14 in a Multiplex Family With Frontotemporal Lobar Degeneration and Amyotrophic Lateral Sclerosis. Archives of Neurology *67*, 606-616.

Gijselinck,I., Van Broeckhoven,C., and Cruts,M. (2008). Granulin Mutations Associated With Frontotemporal Lobar Degeneration and Related Disorders: An Update. Human Mutation *29*, 1373-1386.

Gislason,T.B., Sjogren,M., Larsson,L., and Skoog,I. (2003). The prevalence of frontal variant frontotemporal dementia and the frontal lobe syndrome in a population based sample of 85 year olds. Journal of Neurology Neurosurgery and Psychiatry *74*, 867-871.

Goedert,M., Crowther,R.A., and Spillantini,M.G. (1998). Tau mutations cause frontotemporal dementias. Neuron *21*, 955-958.

Goedert,M., Spillantini,M.G., Jakes,R., Rutherford,D., and Crowther,R.A. (1989). Multiple isoforms of human microtubule-associated protein tau: sequences and localization in neurofibrillary tangles of Alzheimer's disease. Neuron *3*, 519-526.

Goldman,J.S., Farmer,J.M., Wood,E.M., Johnson,J.K., Boxer,A., Neuhaus,J., Lomen-Hoerth,C., Wilhelmsen,K.C., Lee,V.M.Y., Grossman,M., and Miller,B.L. (2005). Comparison of family histories in FTLD subtypes and related tauopathies. Neurology *65*, 1817-1819.

Gorno-Tempini,M.L., Dronkers,N.F., Rankin,K.P., Ogar,J.M., Phengrasamy,L., Rosen,H.J., Johnson,J.K., Weiner,M.W., and Miller,B.L. (2004). Cognition and anatomy in three variants of primary progressive aphasia. Annals of Neurology *55*, 335-346.

Goss,J.R., Finch,C.E., and Morgan,D.G. (1991). Age-Related-Changes in Glial Fibrillary Acidic Protein Messenger-Rna in the Mouse-Brain. Neurobiology of Aging *12*, 165-170.

Gotz,J. and Ittner,L.M. (2008). Animal models of Alzheimer's disease and frontotemporal dementia. Nature Reviews Neuroscience *9*, 532-544.

Graff-Radford,N.R. and Woodruff,B.K. (2007). Frontotemporal dementia. Semin Neurol *27*, 48-57.

Greer,J.M. and Capecchi,M.R. (2002). Hoxb8 is required for normal grooming behavior in mice. Neuron *33*, 23-34.

Gruenberg,J. and Stenmark,H. (2004). The biogenesis of multivesicular endosomes. Nat Rev. Mol. Cell Biol *5*, 317-323.

Gydesen,S., Brown,J.M., Brun,A., Chakrabarti,L., Gade,A., Johannsen,P., Rossor,M., Thusgaard,T., Grove,A., Yancopoulou,D., Spillantini,M.G., Fisher,E.M., Collinge,J., and Sorensen,S.A. (2002). Chromosome 3 linked frontotemporal dementia (FTD-3). Neurology *59*, 1585-1594.

Gydesen,S., Hagen,S., Klinken,L., Abelskov,J., and Sorensen,S.A. (1987). Neuropsychiatric Studies in A Family with Presenile-Dementia Different from Alzheimer and Pick Disease. Acta Psychiatrica Scandinavica *76*, 276-284.

Halabi,C., Halabi,A., Dean,D.L., Wang,P.N., Boxer,A.L., Trojanowski,J.Q., DeArmond,S.J., Miller,B.L., Kramer,J.H., and Seeley,W.W. (2013). Patterns of Striatal Degeneration in Frontotemporal Dementia. Alzheimer Disease & Associated Disorders *27*, 74-83.

Hanisch,U.K. and Kettenmann,H. (2007). Microglia: active sensor and versatile effector cells in the normal and pathologic brain. Nature Neuroscience *10*, 1387-1394.

Hara,T., Nakamura,K., Matsui,M., Yamamoto,A., Nakahara,Y., Suzuki-Migishima,R., Yokoyama,M., Mishima,K., Saito,I., Okano,H., and Mizushima,N. (2006).

Suppression of basal autophagy in neural cells causes neurodegenerative disease in mice. Nature *441*, 885-889.

Harris,H. and Rubinsztein,D.C. (2012). Control of autophagy as a therapy for neurodegenerative disease. Nature Reviews Neurology *8*, 108-117.

Harvey,R.J., Skelton-Robinson,M., and Rossor,M.N. (2003). The prevalence and causes of dementia in people under the age of 65 years. J Neurol. Neurosurg. Psychiatry *74*, 1206-1209.

Hassel,B., Tessler,S., Faull,R.L.M., and Emson,P.C. (2008). Glutamate uptake is reduced in prefrontal cortex in Huntington's disease. Neurochemical Research *33*, 232-237.

Hatanpaa,K.J., Bigio,E.H., Cairns,N.J., Womack,K.B., Weintraub,S., Morris,J.C., Foong,C., Xiao,G., Hladik,C., Mantanona,T.Y., and White,C.L., III (2008). TAR DNA-binding protein 43 immunohistochemistry reveals extensive neuritic pathology in FTLD-U: a midwest-southwest consortium for FTLD study. J Neuropathol Exp Neurol *67*, 271-279.

Hodges,J.R., Davies,R., Xuereb,J., Kril,J., and Halliday,G. (2003). Survival in frontotemporal dementia. Neurology *61*, 349-354.

Hodges,J.R., Patterson,K., Oxbury,S., and Funnell,E. (1992). Semantic dementia. Progressive fluent aphasia with temporal lobe atrophy. Brain *115 (Pt 6)*, 1783-1806.

Holm,I.E., Englund,E., Mackenzie,I.R., Johannsen,P., and Isaacs,A.M. (2007). A Reassessment of the Neuropathology of Frontotemporal Dementia Linked to Chromosome 3. J Neuropathol Exp. Neurol *66*, 884-891.

Holm,I.E., Isaacs,A.M., and Mackenzie,I.R. (2009). Absence of FUS-immunoreactive pathology in frontotemporal dementia linked to chromosome 3 (FTD-3) caused by mutation in the CHMP2B gene. Acta Neuropathol *118*, 719-720.

Horii,M., Shibata,H., Kobayashi,R., Katoh,K., Yorikawa,C., Yasuda,J., and Maki,M. (2006). CHMP7, a novel ESCRT-III-related protein, associates with CHMP4b and functions in the endosomal sorting pathway. Biochem. J. *400*, 23-32.

Hosler,B.A., Siddique,T., Sapp,P.C., Sailor,W., Huang,M.C., Hossain,A., Daube,J.R., Nance,M., Fan,C., Kaplan,J., Hung,W.Y., McKenna-Yasek,D., Haines,J.L., Pericak-Vance,M.A., Horvitz,H.R., and Brown,R.H., Jr. (2000). Linkage of Familial Amyotrophic Lateral Sclerosis With Frontotemporal Dementia to Chromosome 9q21-q22. JAMA *284*, 1664-1669.

Hsiung,G.Y., Dejesus-Hernandez,M., Feldman,H., Sengdy,P., Bouchard-Kerr,P., Dwosh,E., Leung,B., Fok,A., Rutherford,N., Baker,M., Rademakers,R., and

Mackenzie,I.R.A. (2012a). Clinical Heterogeneity in Familial Frontotemporal Dementia and Amyotrophic Lateral Sclerosis Caused by C9ORF72 Mutation. Neurology *78*.

Hsiung,G.Y.R., Dejesus-Hernandez,M., Feldman,H.H., Sengdy,P., Bouchard-Kerr,P., Dwosh,E., Butler,R., Leung,B., Fok,A., Rutherford,N.J., Baker,M., Rademakers,R., and Mackenzie,I.R.A. (2012b). Clinical and pathological features of familial frontotemporal dementia caused by C9ORF72 mutation on chromosome 9p. Brain *135*, 709-722.

Hu,F., Padukkavidana,T., Vaegter,C.B., Brady,O.A., Zheng,Y., Mackenzie,I.R., Feldman,H.H., Nykjaer,A., and Strittmatter,S.M. (2010). Sortilin-mediated endocytosis determines levels of the frontotemporal dementia protein, progranulin. Neuron *68*, 654-667.

Hunziker,W., Simmen,T., and Honing,S. (1996). Trafficking of lysosomal membrane proteins in polarized kidney cells. Nephrologie *17*, 347-350.

Hurley,J.H. (2008). ESCRT complexes and the biogenesis of multivesicular bodies. Curr. Opin. Cell Biol. *20*, 4-11.

Hurley,J.H. (2010). The ESCRT complexes. Critical Reviews in Biochemistry and Molecular Biology *45*, 463-487.

Hurley,J.H. and Emr,S.D. (2006). THE ESCRT COMPLEXES: Structure and Mechanism of a Membrane-Trafficking Network *. Annu. Rev. Biophys Biomol. Struct. *35*, 277-298.

Hutton,M., Lendon,C.L., Rizzu,P., Baker,M., Froelich,S., Houlden,H., Pickering-Brown,S., Chakraverty,S., Isaacs,A., Grover,A., Hackett,J., Adamson,J., Lincoln,S., Dickson,D., Davies,P., Petersen,R.C., Stevens,M., de Graaff,E., Wauters,E., van Baren,J., Hillebrand,M., Joosse,M., Kwon,J.M., Nowotny,P., Che,L.K., Norton,J., Morris,J.C., Reed,L.A., Trojanowski,J., Basun,H., Lannfelt,L., Neystat,M., Fahn,S., Dark,F., Tannenberg,T., Dodd,P.R., Hayward,N., Kwok,J.B., Schofield,P.R., Andreadis,A., Snowden,J., Craufurd,D., Neary,D., Owen,F., Oostra,B.A., Hardy,J., Goate,A., van Swieten,J., Mann,D., Lynch,T., and Heutink,P. (1998). Association of missense and 5'-splice-site mutations in tau with the inherited dementia FTDP-17. Nature *393*, 702-705.

Iacopino,A.M. and Christakos,S. (1990). Specific Reduction of Calcium-Binding Protein (28-Kilodalton Calbindin-D) Gene-Expression in Aging and Neurodegenerative Diseases. Proceedings of the National Academy of Sciences of the United States of America *87*, 4078-4082.

Iacopino,A.M., Rhoten,W.B., and Christakos,S. (1990). Calcium-Binding Protein (Calbindin-D28K) Gene-Expression in the Developing and Aging Mouse Cerebellum. Molecular Brain Research *8*, 283-290.

Ichimura,Y., Kumanomidou,T., Sou,Y.S., Mizushima,T., Ezaki,J., Ueno,T., Kominami,E., Yamane,T., Tanaka,K., and Komatsu,M. (2008). Structural basis for sorting mechanism of p62 in selective autophagy. Journal of Biological Chemistry *283*, 22847-22857.

Igaz,L.M., Kwong,L.K., Lee,E.B., Chen-Plotkin,A., Swanson,E., Unger,T., Malunda,J., Xu,Y., Winton,M.J., Trojanowski,J.Q., and Lee,V.M.Y. (2011). Dysregulation of the ALS-associated gene TDP-43 leads to neuronal death and degeneration in mice. Journal of Clinical Investigation *121*, 726-738.

Ince,P.G., Lowe,J., and Shaw,P.J. (1998). Amyotrophic lateral sclerosis: current issues in classification, pathogenesis and molecular pathology. Neuropathology and Applied Neurobiology *24*, 104-117.

Ingram,M.A.C., Orr,H.T., and Clark,H.B. (2012). Genetically engineered mouse models of the trinucleotide-repeat spinocerebellar ataxias. Brain Research Bulletin *88*, 33-42.

Isaacs,A.M., Jeans,A., Oliver,P.L., Vizor,L., Brown,S.D., Hunter,A.J., and Davies,K.E. (2002). Identification of a new Pmp22 mouse mutant and trafficking analysis of a Pmp22 allelic series suggesting that protein aggregates may be protective in Pmp22-associated peripheral neuropathy. Mol. Cell Neurosci. *21*, 114-125.

Isaacs,A.M., Johannsen,P., Holm,I., and Nielsen,J.E. (2011). Frontotemporal Dementia Caused by CHMP2B Mutations. Curr Alzheimer Res.

Ito,D., Imai,Y., Ohsawa,K., Nakajima,K., Fukuuchi,Y., and Kohsaka,S. (1998). Microglia-specific localisation of a novel calcium binding protein, Iba1. Molecular Brain Research *57*, 1-9.

Jager,S., Bucci,C., Tanida,I., Ueno,T., Kominami,E., Saftig,P., and Eskelinen,E.L. (2004). Role for Rab7 in maturation of late autophagic vacuoles. J Cell Sci *117*, 4837-4848.

Jahn,R., Schiebler,W., Ouimet,C., and Greengard,P. (1985). A 38,000-Dalton Membrane-Protein (P38) Present in Synaptic Vesicles. Proceedings of the National Academy of Sciences of the United States of America *82*, 4137-4141.

Johnson,J.K., Diehl,J., Mendez,M.F., Neuhaus,J., Shapira,J.S., Forman,M., Chute,D.J., Roberson,E.D., Pace-Savitsky,C., Neumann,M., Chow,T.W., Rosen,H.J., Forstl,H., Kurz,A., and Miller,B.L. (2005). Frontotemporal lobar degeneration: demographic characteristics of 353 patients. Arch Neurol *62*, 925-930.

Josephs,K.A., Hodges,J.R., Snowden,J.S., Mackenzie,I.R., Neumann,M., Mann,D.M., and Dickson,D.W. (2011). Neuropathological background of phenotypical variability in frontotemporal dementia. Acta Neuropathologica *122*, 137-153.

Josephs,K.A., Holton,J.L., Rossor,M.N., Godbolt,A.K., Ozawa,T., Strand,K., Khan,N., Al Sarraj,S., and Revesz,T. (2004). Frontotemporal lobar degeneration and ubiquitin immunohistochemistry. Neuropathol. Appl. Neurobiol. *30*, 369-373.

Katzmann,D.J., Odorizzi,G., and Emr,S.D. (2002). Receptor downregulation and multivesicular-body sorting. Nat Rev. Mol. Cell Biol *3*, 893-905.

Kayasuga,Y., Chiba,S., Suzuki,M., Kikusui,T., Matsuwaki,T., Yamanouchi,K., Kotaki,H., Horai,R., Iwakura,Y., and Nishihara,M. (2007). Alteration of behavioural phenotype in mice by targeted disruption of the progranulin gene. Behavioural Brain Research *185*, 110-118.

Keisala,T., Minasyan,A., Jarvelin,U., Wang,J.H., Hamalainen,T., Kalueff,A.V., and Tuohimaa,P. (2007). Aberrant nest building and prolactin secretion in vitamin D receptor mutant mice. Journal of Steroid Biochemistry and Molecular Biology *104*, 269-273.

Kertesz,A. (2004). Frontotemporal Dementia/Pick's disease. Archives of Neurology *61*, 969-971.

Kertesz,A., Kawarai,T., Rogaeva,E., George-Hyslop,P., Poorkaj,P., Bird,T.D., and Munoz,D.G. (2000). Familial frontotemporal dementia with ubiquitin-positive, tau-negative inclusions. Neurology *54*, 818-827.

Kipps,C., Nestor,P.J., Dawson,K., Mitchell,J., and Hodges,J.R. (2008). Measuring progression of disease in frontotemporal dementia: Therapeutic trial implications. Neurology *70*, A98.

Klootwijk,R., Franke,B., van der Zee,C.E.E.M., de Boer,R.T., Wilms,W., Hol,F.A., and Mariman,E.C.M. (2000). A deletion encompassing Zic3 in Bent tail, a mouse model for X-linked neural tube defects. Human Molecular Genetics *9*, 1615-1622.

Knopman,D.S., Petersen,R.C., Edland,S.D., Cha,R.H., and Rocca,W.A. (2004). The incidence of frontotemporal lobar degeneration in Rochester, Minnesota, 1990 through 1994. Neurology *62*, 506-508.

Kobayashi,T., Beuchat,M.H., Chevallier,J., Makino,A., Mayran,N., Escola,J.M., Lebrand,C., Cosson,P., Kobayashi,T., and Gruenberg,J. (2002). Separation and characterization of late endosomal membrane domains. J Biol Chem. *277*, 32157-32164.

Komatsu,M. and Ichimura,Y. (2010). Physiological significance of selective degradation of p62 by autophagy. Febs Letters *584*, 1374-1378.

Komatsu,M., Waguri,S., Chiba,T., Murata,S., Iwata,J., Tanida,I., Ueno,T., Koike,M., Uchiyama,Y., Kominami,E., and Tanaka,K. (2006). Loss of autophagy in the central nervous system causes neurodegeneration in mice. Nature *441*, 880-884.

Komatsu,M., Waguri,S., Koike,M., Sou,Y.S., Ueno,T., Hara,T., Mizushima,N., Iwata,J., Ezaki,J., Murata,S., Hamazaki,J., Nishito,Y., Iemura,S., Natsume,T., Yanagawa,T., Uwayama,J., Warabi,E., Yoshida,H., Ishii,T., Kobayashi,A., Yamamoto,M., Yue,Z., Uchiyama,Y., Kominami,E., and Tanaka,K. (2007). Homeostatic levels of p62 control cytoplasmic inclusion body formation in autophagy-deficient mice. Cell *131*, 1149-1163.

Kornfeld,S. and Mellman,I. (1989). The Biogenesis of Lysosomes. Annual Review of Cell Biology *5*, 483-525.

Kovacs,G.G., Murrell,J.R., Horvath,S., Haraszti,L., Majtenyi,K., Molnar,M.J., Budka,H., Ghetti,B., and Spina,S. (2009). TARDBP variation associated with frontotemporal dementia, supranuclear gaze palsy, and chorea. Mov. Disord *24*, 1843-1847.

Kraemer,B.C., Schuck,T., Wheeler,J.M., Robinson,L.C., Trojanowski,J.Q., Lee,V.M.Y., and Schellenberg,G.D. (2010). Loss of murine TDP-43 disrupts motor function and plays an essential role in embryogenesis. Acta Neuropathologica *119*, 409-419.

Kurashige,T., Takahashi,T., Yamazaki,Y., Hiji,M., Izumi,Y., Yamawaki,T., and Matsumoto,M. (2012). Localization of CHMP2B-immunoreactivity in the brain stem of Lewy body disease. Neuropathology *September*, 1-9.

Kuta, A. Investigation of subunits of the cytoplasmic dynein complex using novel mouse models. 2011.
Ref Type: Thesis/Dissertation

Kwiatkowski,T.J., Bosco,D.A., LeClerc,A.L., Tamrazian,E., Vanderburg,C.R., Russ,C., Davis,A., Gilchrist,J., Kasarskis,E.J., Munsat,T., Valdmanis,P., Rouleau,G.A., Hosler,B.A., Cortelli,P., de Jong,P.J., Yoshinaga,Y., Haines,J.L., Pericak-Vance,M.A., Yan,J., Ticozzi,N., Siddique,T., McKenna-Yasek,D., Sapp,P.C., Horvitz,H.R., Landers,J.E., and Brown,R.H. (2009). Mutations in the FUS/TLS Gene on Chromosome 16 Cause Familial Amyotrophic Lateral Sclerosis. Science *323*, 1205-1208.

Kwong,J., Roudabush,F.L., Moore,P.H., Montague,M., Oldham,W., Li,Y., Chin,L., and Li,L. (2000). Hrs interacts with SNAP-25 and regulates Ca2+-dependent exocytosis. Journal of Cell Science *113*, 2273-2284.

Laaksovirta,H., Peuralinna,T., Schymick,J.C., Scholz,S.W., Lai,S.L., Myllykangas,L., Sulkava,R., Jansson,L., Hernandez,D.G., Gibbs,J.R., Nalls,M.A., Heckerman,D., Tienari,P.J., and Traynor,B.J. (2010). Chromosome 9p21 in amyotrophic lateral sclerosis in Finland: a genome-wide association study. Lancet Neurology *9*, 978-985.

Lambourne,S.L., Humby,T., Isles,A.R., Emson,P.C., Spillantini,M.G., and Wilkinson,L.S. (2007). Impairments in impulse control in mice transgenic for the human FTDP-17 tau(V337M) mutation are exacerbated by age. Human Molecular Genetics *16*, 1708-1719.

Lashley,T., Rohrer,J.D., Bandopadhyay,R., Fry,C., Ahmed,Z., Isaacs,A.M., Brelstaff,J.H., Borroni,B., Warren,J.D., Troakes,C., King,A., Al Saraj,S., Newcombe,J., Quinn,N., Ostergaard,K., Schroder,H.D., Bojsen-Moller,M., Braendgaard,H., Fox,N.C., Rossor,M.N., Lees,A.J., Holton,J.L., and Revesz,T. (2011). A comparative clinical, pathological, biochemical and genetic study of fused in sarcoma proteinopathies. Brain *134*, 2548-2564.

Lata,S., Roessle,M., Solomons,J., Jamin,M., Gottlinger,H.G., Svergun,D.I., and Weissenhorn,W. (2008). Structural basis for autoinhibition of ESCRT-III CHMP3. J. Mol. Biol. *378*, 818-827.

Ledoux,J. (2003). The emotional brain, fear, and the amygdala. Cellular and Molecular Neurobiology *23*, 727-738.

Lee,J.A., Beigneux,A., Ahmad,S.T., Young,S.G., and Gao,F.B. (2007). ESCRT-III dysfunction causes autophagosome accumulation and neurodegeneration. Curr Biol *17*, 1561-1567.

Lee,J.A., Liu,L., and Gao,F.B. (2009). Autophagy defects contribute to neurodegeneration induced by dysfunctional ESCRT-III. Autophagy *5*, 1070-1072.

Lee, J. A., Liu, L., R, Kreitzer A.C, Delaloy C, and Gao, F. B. ESCRT III subunits Snf7-1 and Snf7-2 differentially regulate transmembrane cargos in hESC-derived human neurons. Molecular Brain 4:37, 1-8. 2011. BioMed Central Open Access.
Ref Type: Generic

Lehoczky,J.A., Cai,W.W., Douglas,J.A., Moran,J.L., Beier,D.R., and Innis,J.W. (2006). Description and genetic mapping of Polypodia: an X-linked dominant mouse mutant with ectopic caudal limbs and other malformations. Mammalian Genome *17*, 903-913.

Lewis,J., McGowan,E., Rockwood,J., Melrose,H., Nacharaju,P., Van Slegtenhorst,M., Gwinn-Hardy,K., Murphy,M.P., Baker,M., Yu,X., Duff,K., Hardy,J., Corral,A., Lin,W.L., Yen,S.H., Dickson,D.W., Davies,P., and Hutton,M. (2000). Neurofibrillary tangles, amyotrophy and progressive motor disturbance in mice expressing mutant (P301L) tau protein. Nature Genetics *25*, 402-405.

Leyton,C.E., Villemagne,V.L., Savage,S., Pike,K.E., Ballard,K.J., Piguet,O., Burrell,J.R., Rowe,C.C., and Hodges,J.R. (2011). Subtypes of progressive aphasia: application of the international consensus criteria and validation using beta-amyloid imaging. Brain *134*, 3030-3043.

Lijam,N., Paylor,R., McDonald,M.P., Crawley,J.N., Deng,C.X., Herrup,K., Stevens,K.E., Maccaferri,G., Mcbain,C.J., Sussman,D.J., and WynshawBoris,A. (1997). Social interaction and sensorimotor gating abnormalities in mice lacking Dvl1. Cell *90*, 895-905.

Lillo,P., Garcin,B., Hornberger,M., Bak,T.H., and Hodges,J.R. (2010). Neurobehavioral Features in Frontotemporal Dementia With Amyotrophic Lateral Sclerosis. Archives of Neurology *67*, 826-830.

Lillo,P. and Hodges,J.R. (2009). Frontotemporal dementia and motor neurone disease: Overlapping clinic-pathological disorders. Journal of Clinical Neuroscience *16*, 1131-1135.

Lindquist,S.G., Braedgaard,H., Svenstrup,K., Isaacs,A.M., and Nielsen,J.E. (2008). Frontotemporal dementia linked to chromosome 3 (FTD-3)--current concepts and the detection of a previously unknown branch of the Danish FTD-3 family. Eur J Neurol *15*, 667-670.

Lomen-Hoerth,C., Anderson,T., and Miller,B. (2002). The overlap of amyotrophic lateral sclerosis and frontotemporal dementia. Neurology *59*, 1077-1079.

Lynch,T., Sano,M., Marder,K.S., Bell,K.L., Foster,N.L., Defendini,R.F., Sima,A.A.F., Keohane,C., Nygaard,T.G., Fahn,S., Mayeux,R., Rowland,L.P., and Wilhelmsen,K.C. (1994). Clinical Characteristics of A Family with Chromosome 17-Linked Disinhibition-Dementia-Parkinsonism-Amyotrophy Complex. Neurology *44*, 1878-1884.

Mackenzie,I.R., Baborie,A., Pickering-Brown,S., Plessis,D.D., Jaros,E., Perry,R.H., Neary,D., Snowden,J.S., and Mann,D.M. (2006a). Heterogeneity of ubiquitin pathology in frontotemporal lobar degeneration: classification and relation to clinical phenotype. Acta Neuropathol. (Berl) *112*, 539-549.

Mackenzie,I.R., Neumann,M., Bigio,E.H., Cairns,N.J., Alafuzoff,I., Kril,J., Kovacs,G.G., Ghetti,B., Halliday,G., Holm,I.E., Ince,P.G., Kamphorst,W., Revesz,T., Rozemuller,A.J., Kumar-Singh,S., Akiyama,H., Baborie,A., Spina,S., Dickson,D.W., Trojanowski,J.Q., and Mann,D.M. (2009). Nomenclature for neuropathologic subtypes of frontotemporal lobar degeneration: consensus recommendations. Acta Neuropathol *117*, 15-18.

Mackenzie,I.R., Neumann,M., Bigio,E.H., Cairns,N.J., Alafuzoff,I., Kril,J., Kovacs,G.G., Ghetti,B., Halliday,G., Holm,I.E., Ince,P.G., Kamphorst,W., Revesz,T., Rozemuller,A.J., Kumar-Singh,S., Akiyama,H., Baborie,A., Spina,S., Dickson,D.W., Trojanowski,J.Q., and Mann,D.M. (2010). Nomenclature and nosology for neuropathologic subtypes of frontotemporal lobar degeneration: an update. Acta Neuropathol *119*, 1-4.

Mackenzie,I.R. and Rademakers,R. (2007). The molecular genetics and neuropathology of frontotemporal lobar degeneration: recent developments. Neurogenetics *8*, 237-248.

Mackenzie,I.R., Shi,J., Shaw,C.L., Duplessis,D., Neary,D., Snowden,J.S., and Mann,D.M. (2006b). Dementia lacking distinctive histology (DLDH) revisited. Acta Neuropathol. (Berl) *112*, 551-559.

Mackenzie,I.R.A., Neumann,M., Baborie,A., Sampathu,D.M., Du Plessis,D., Jaros,E., Perry,R.H., Trojanowski,J.Q., Mann,D.M.A., and Lee,V.M.Y. (2011). A harmonized classification system for FTLD-TDP pathology. Acta Neuropathologica *122*, 111-113.

Majounie,E., Renton,A.E., Mok,K., Dopper,E.G.P., Waite,A., Rollinson,S., Chio,A., Restagno,G., Nicolaou,N., Simon-Sanchez,J., van Swieten,J.C., Abramzon,Y., Johnson,J.O., Sendtner,M., Pamphlett,R., Orrell,R.W., Mead,S., Sidle,K.C., Houlden,H., Rohrer,J.D., Morrison,K.E., Pall,H., Talbot,K., Ansorge,O., Hernandez,D.G., Arepalli,S., Sabatelli,M., Mora,G., Corbo,M., Giannini,F., Calvo,A., Englund,E., Borghero,G., Foris,G.L., Remes,A.M., Laaksovirta,H., McCluskey,L., Trojanowski,J.Q., Van Deerlin,V.M., Schellenberg,G.D., Nalls,M.A., Drory,V.E., Lu,C.S., Yeh,T.H., Ishiura,H., Takahashi,Y., Tsuji,S., Le Ber,I., Brice,A., Drepper,C., Williams,N., Kirby,J., Shaw,P., Hardy,J., Tienari,P.J., Heutink,P., Morris,H.R., Pickering-Brown,S., and Traynor,B.J. (2012). Frequency of the C9orf72 hexanucleotide repeat expansion in patients with amyotrophic lateral sclerosis and frontotemporal dementia: a cross-sectional study. Lancet Neurology *11*, 323-330.

Mancuso,R., Olivan,S., Osta,R., and Navarro,X. (2011). Evolution of gait abnormalities in SOD1(G93A) transgenic mice. Brain Research *1406*, 65-73.

Mangiarini,L., Sathasivam,K., Seller,M., Cozens,B., Harper,A., Hetherington,C., Lawton,M., Trottier,Y., Lehrach,H., Davies,S.W., and Bates,G.P. (1996). Exon 1 of the HD gene with an expanded CAG repeat is sufficient to cause a progressive neurological phenotype in transgenic mice. Cell *87*, 493-506.

Martins,Y.C., Werneck,G.L., Carvalho,L.J., Silva,B.P.T., Andrade,B.G., Souza,T.M., Souza,D.O., and Daniel-Ribeiro,C.T. (2010). Algorithms to predict cerebral malaria in murine models using the SHIRPA protocol. Malaria Journal *9*.

Masliah,E., Alford,M., DeTeresa,R., Mallory,M., and Hansen,L. (1996). Deficient glutamate transport is associated with neurodegeneration in Alzheimer's disease. Annals of Neurology *40*, 759-766.

Massman,P.J., Sims,J., Cooke,N., Haverkamp,L.J., Appel,V., and Appel,S.H. (1996). Prevalence and correlates of neuropsychological deficits in amyotrophic lateral sclerosis. Journal of Neurology Neurosurgery and Psychiatry *61*, 450-455.

Masuya,H., Nakai,Y., Motegi,H., Niinaya,N., Kida,Y., Kaneko,Y., Aritake,H., Suzuki,N., Ishii,J., Koorikawa,K., Suzuki,T., Inoue,M., Kobayashi,K., Toki,H., Wada,Y., Kaneda,H., Ishijima,J., Takahashi,K.R., Minowa,O., Noda,T., Wakana,S., Gondo,Y., and Shiroishi,T. (2004). Development and implementation of a database system to manage a large-scale mouse ENU-mutagenesis program. Mammalian Genome *15*, 404-411.

Matilla,A., Roberson,E.D., Banfi,S., Morales,J., Armstrong,D.L., Burright,E.N., Orr,H.T., Sweatt,J.D., Zoghbi,H.Y., and Matzuk,M.M. (1998). Mice lacking ataxin-1 display learning deficits and decreased hippocampal paired-pulse facilitation. J Neurosci *18*, 5508-5516.

Mattson,M.P., Rychlik,B., Chu,C., and Christakos,S. (1991). Evidence for Calcium-Reducing and Excito-Protective Roles for the Calcium-Binding Protein Calbindin-D(28K) in Cultured Hippocampal-Neurons. Neuron *6*, 41-51.

McKhann,G.M., Albert,M.S., Grossman,M., Miller,B., Dickson,D., and Trojanowski,J.Q. (2001). Clinical and pathological diagnosis of frontotemporal dementia: report of the Work Group on Frontotemporal Dementia and Pick's Disease. Arch. Neurol. *58*, 1803-1809.

Mercado,P.A., Ayala,Y.M., Romano,M., Buratti,E., and Baralle,F.E. (2005). Depletion of TDP 43 overrides the need for exonic and intronic splicing enhancers in the human apoA-II gene. Nucleic Acids Res *33*, 6000-6010.

Merck. H&E staining. Merk , 1-6. 2012.
Ref Type: Electronic Citation

Mercy,L., Hodges,J.R., Dawson,K., Barker,R.A., and Brayne,C. (2008). Incidence of early-onset dementias in Cambridgeshire, United Kingdom. Neurology *71*, 1496-1499.

Metcalf,D. and Isaacs,A.M. (2010). The role of ESCRT proteins in fusion events involving lysosomes, endosomes and autophagosomes. Biochem. Soc Trans *38*, 1469-1473.

Middeldorp,J. and Hol,E.M. (2011). GFAP in health and disease. Progress in Neurobiology *93*, 421-443.

Miller,B.L., Darby,A.L., Swartz,J.R., Yener,G.G., and Mena,I. (1995). Dietary-Changes, Compulsions and Sexual-Behavior in Frontotemporal Degeneration. Dementia *6*, 195-199.

Mizushima,N., Kuma,A., Kobayashi,Y., Yamamoto,A., Matsubae,M., Takao,T., Natsume,T., Ohsumi,Y., and Yoshimori,T. (2003). Mouse Apg16L, a novel WD-repeat protein, targets to the autdphagic isolation membrane with the Apg12-Apg5 conjugate. Journal of Cell Science *116*, 1679-1688.

Mizushima,N., Levine,B., Cuervo,A.M., and Klionsky,D.J. (2008). Autophagy fights disease through cellular self-digestion. Nature *451*, 1069-1075.

Mocanu,M.M., Nissen,A., Eckermann,K., Khlistunova,I., Biernat,J., Drexler,D., Petrova,O., Schonig,K., Bujard,H., Mandelkow,E., Zhou,L., Rune,G., and Mandelkow,E.M. (2008). The potential for beta-structure in the repeat domain of Tau protein determines aggregation, synaptic decay, neuronal loss, and coassembly with endogenous Tau in inducible mouse models of tauopathy. Journal of Neuroscience *28*, 737-748.

Mok,K., Traynor,B.J., Schymick,J., Tienari,P.J., Laaksovirta,H., Peuralinna,T., Myllykangas,L., Chio,A., Shatunov,A., Boeve,B.F., Boxer,A.L., Dejesus-Hernandez,M., Mackenzie,I.R., Waite,A., Williams,N., Morris,H.R., Simon-Sanchez,J., van Swieten,J.C., Heutink,P., Restagno,G., Mora,G., Morrison,K.E., Shaw,P.J., Rollinson,P.S., Al Chalabi,A., Rademakers,R., Pickering-Brown,S., Orrell,R.W., Nalls,M.A., and Hardy,J. (2012). The chromosome 9 ALS and FTD locus is probably derived from a single founder. Neurobiology of Aging *33*.

Momeni,P., Bell,J., Duckworth,J., Hutton,M., Mann,D., Brown,S.P., and Hardy,J. (2006a). Sequence analysis of all identified open reading frames on the frontal temporal dementia haplotype on chromosome 3 fails to identify unique coding variants except in CHMP2B. Neurosci Lett *410*, 77-79.

Momeni,P., Rogaeva,E., Van,D., V, Yuan,W., Grafman,J., Tierney,M., Huey,E., Bell,J., Morris,C.M., Kalaria,R.N., van Rensburg,S.J., Niehaus,D., Potocnik,F., Kawarai,T., Salehi-Rad,S., Sato,C., George-Hyslop,P., and Hardy,J. (2006b). Genetic variability in CHMP2B and frontotemporal dementia. Neurodegener. Dis *3*, 129-133.

Morgan,T.E., Rozovsky,I., Goldsmith,S.K., Stone,D.J., Yoshida,T., and Finch,C.E. (1997). Increased transcription of the astrocyte gene GFAP during middle-age is attenuated by food restriction: Implications for the role of oxidative stress. Free Radical Biology and Medicine *23*, 524-528.

Morgan,T.E., Xie,Z., Goldsmith,S., Yoshida,T., Lanzrein,A.S., Stone,D., Rozovsky,I., Perry,G., Smith,M.A., and Finch,C.E. (1999). The mosaic of brain glial hyperactivity during normal ageing and its attenuation by food restriction. Neuroscience *89*, 687-699.

Morita,E., Sandrin,V., McCullough,J., Katsuyama,A., Baci,H., I, and Sundquist,W.I. (2011). ESCRT-III protein requirements for HIV-1 budding. Cell Host Microbe *9*, 235-242.

Morita,M., Al Chalabi,A., Andersen,P.M., Hosler,B., Sapp,P., Englund,E., Mitchell,J.E., Habgood,J.J., de Belleroche,J., Xi,J., Jongjaroenprasert,W., Horvitz,H.R., Gunnarsson,L.G., and Brown,R.H., Jr. (2006). A locus on chromosome 9p confers susceptibility to ALS and frontotemporal dementia. Neurology *66*, 839-844.

Mu,F.T., Callaghan,J.M., Steelemortimer,O., Stenmark,H., Parton,R.G., Campbell,P.L., Mccluskey,J., Yeo,J.P., Tock,E.P.C., and Toh,B.H. (1995). Eea1, An Early Endosome-Associated Protein - Eea1 Is A Conserved Alpha-Helical Peripheral Membrane-Protein Flanked by Cysteine Fingers and Contains A Calmodulin-Binding Iq Motif. Journal of Biological Chemistry *270*, 13503-13511.

Muramori,F., Kobayashi,K., and Nakamura,I. (1998). A quantitative study of neurofibrillary tangles, senile plaques and astrocytes in the hippocampal subdivisions and entorhinal cortex in Alzheimer's disease, normal controls and non-Alzheimer neuropsychiatric diseases. Psychiatry and Clinical Neurosciences *52*, 593-599.

Muziol,T., Pineda-Molina,E., Ravelli,R.B., Zamborlini,A., Usami,Y., Gottlinger,H., and Weissenhorn,W. (2006). Structural Basis for Budding by the ESCRT-III Factor CHMP3. Dev. Cell *10*, 821-830.

Neary,D. (1990). Dementia of Frontal-Lobe Type. Journal of the American Geriatrics Society *38*, 71-72.

Neary,D., Snowden,J.S., Gustafson,L., Passant,U., Stuss,D., Black,S., Freedman,M., Kertesz,A., Robert,P.H., Albert,M., Boone,K., Miller,B.L., Cummings,J., and Benson,D.F. (1998). Frontotemporal lobar degeneration: a consensus on clinical diagnostic criteria. Neurology *51*, 1546-1554.

Neary,D., Snowden,J.S., and Mann,D.M.A. (1993). Familial Progressive Aphasia - Its Relationship to Other Forms of Lobar Atrophy. Journal of Neurology Neurosurgery and Psychiatry *56*, 1122-1125.

Neary,D., Snowden,J.S., and Mann,D.M.A. (2000a). Classification and description of frontotemporal dementias. Molecular Basis of Dementia *920*, 46-51.

Neary,D., Snowden,J.S., and Mann,D.M.A. (2000b). Cognitive change in motor neurone disease/amyotrophic lateral sclerosis (MND/ALS). Journal of the Neurological Sciences *180*, 15-20.

Neary,D., Snowden,J.S., Mann,D.M.A., Northen,B., Goulding,P.J., and Macdermott,N. (1990). Frontal-Lobe Dementia and Motor Neuron Disease. Journal of Neurology Neurosurgery and Psychiatry *53*, 23-32.

Neary,D., Snowden,J., and Mann,D. (2005). Frontotemporal dementia. The Lancet Neurology *4*, 771-780.

Neumann,M., Kwong,L.K., Truax,A.C., Vanmassenhove,B., Kretzschmar,H.A., Van Deerlin,V.M., Clark,C.M., Grossman,M., Miller,B.L., Trojanowski,J.Q., and Lee,V.M. (2007). TDP-43-positive white matter pathology in frontotemporal lobar degeneration with ubiquitin-positive inclusions. J Neuropathol. Exp. Neurol *66*, 177-183.

Neumann,M., Rademakers,R., Roeber,S., Baker,M., Kretzschmar,H.A., and Mackenzie,I.R. (2009a). A new subtype of frontotemporal lobar degeneration with FUS pathology. Brain *132*, 2922-2931.

Neumann,M., Sampathu,D.M., Kwong,L.K., Truax,A.C., Micsenyi,M.C., Chou,T.T., Bruce,J., Schuck,T., Grossman,M., Clark,C.M., McCluskey,L.F., Miller,B.L., Masliah,E., Mackenzie,I.R., Feldman,H., Feiden,W., Kretzschmar,H.A., Trojanowski,J.Q., and Lee,V.M. (2006). Ubiquitinated TDP-43 in frontotemporal lobar degeneration and amyotrophic lateral sclerosis. Science *314*, 130-133.

Neumann,M., Tolnay,M., and Mackenzie,I.R.A. (2009b). The molecular basis of frontotemporal dementia. Expert Reviews in Molecular Medicine *11*.

Nezis,I.P., Simonsen,A., Sagona,A.P., Finley,K., Gaumer,S., Contamine,D., Rusten,T.E., Stenmark,H., and Brech,A. (2008). Ref(2)P, the Drosophila melanogaster homologue of mammalian p62, is required for the formation of protein aggregates in adult brain. J Cell Biol *180*, 1065-1071.

Nichols,N.R., Day,J.R., Laping,N.J., Johnson,S.A., and Finch,C.E. (1993). Gfap Messenger-Rna Increases with Age in Rat and Human Brain. Neurobiology of Aging *14*, 421-429.

Nickerson,D.P., Russell,M.R.G., and Odorizzi,G. (2007). A concentric circle model of multivesicular body cargo sorting. Embo Reports *8*, 644-650.

Nijholt,D.A.T., De Kimpe,L., Elfrink,H.L., Hoozemans,J.J.M., and Scheper,W. (2011). Removing Protein Aggregates: The Role of Proteolysis in Neurodegeneration. Current Medicinal Chemistry *18*, 2459-2476.

Norreel,J.C., Jamon,M., Riviere,G., Passage,E., Fontes,M., and Clarac,F. (2001). Behavioural profiling of a murine Charcot-Marie-Tooth disease type 1A model. European Journal of Neuroscience *13*, 1625-1634.

Obita,T., Saksena,S., Ghazi-Tabatabai,S., Gill,D.J., Perisic,O., Emr,S.D., and Williams,R.L. (2007). Structural basis for selective recognition of ESCRT-III by the AAA ATPase Vps4. Nature *449*, 735-739.

Orr,H.T. (2012). Cell biology of spinocerebellar ataxia. Journal of Cell Biology *197*, 167-177.

Palmiter,R.D., Brinster,R.L., Hammer,R.E., Trumbauer,M.E., Rosenfeld,M.G., Birnberg,N.C., and Evans,R.M. (1982). Dramatic Growth of Mice That Develop from Eggs Micro-Injected with Metallothioneine-Growth Hormone Fusion Genes. Nature *300*, 611-615.

Pankiv,S., Clausen,T.H., Lamark,T., Brech,A., Bruun,J.A., Outzen,H., Overvatn,A., Bjorkoy,G., and Johansen,T. (2007). p62/SQSTM1 binds directly to Atg8/LC3 to facilitate degradation of ubiquitinated protein aggregates by autophagy. J Biol Chem *282*, 24131-24145.

Parkinson,N., Ince,P.G., Smith,M.O., Highley,R., Skibinski,G., Andersen,P.M., Morrison,K.E., Pall,H.S., Hardiman,O., Collinge,J., Shaw,P.J., and Fisher,E.M. (2006). ALS phenotypes with mutations in CHMP2B (charged multivesicular body protein 2B). Neurology *67*, 1074-1077.

Pearson,J.P., Williams,N.M., Majounie,E., Waite,A., Stott,J., Newsway,V., Murray,A., Hernandez,D., Guerreiro,R., Singleton,A.B., Neal,J., and Morris,H.R. (2011). Familial frontotemporal dementia with amyotrophic lateral sclerosis and a shared haplotype on chromosome 9p. Journal of Neurology *258*, 647-655.

Peavy,G.M., Herzog,A.G., Rubin,N.P., and Mesulam,M.M. (1992). Neuropsychological Aspects of Dementia of Motor-Neuron Disease - A Report of 2 Cases. Neurology *42*, 1004-1008.

Perry,V.H., Nicoll,J.A.R., and Holmes,C. (2010). Microglia in neurodegenerative disease. Nature Reviews Neurology *6*, 193-201.

Petkau,T.L., Neal,S.J., Milnerwood,A., Mew,A., Hill,A.M., Orban,P., Gregg,J., Lu,G., Feldman,H.H., Mackenzie,I.R.A., Raymond,L.A., and Leavitt,B.R. (2012). Synaptic dysfunction in progranulin-deficient mice. Neurobiology of Disease *45*, 711-722.

Pick A (1892). Ueber die Beziegungen der senilen Hirnatrophie sur aphasia. Prag med Wochenscher *17*, 165-167.

Pickering-Brown,S.M., Baker,M., Nonaka,T., Ikeda,K., Sharma,S., Mackenzie,J., Simpson,S.A., Moore,J.W., Snowden,J.S., de Silva,R., Revesz,T., Hasegawa,M., Hutton,M., and Mann,D.M. (2004). Frontotemporal dementia with Pick-type histology associated with Q336R mutation in the tau gene. Brain *127*, 1415-1426.

Portet,F., Touchon,J., and Camu,W. (2001). Amyotrophic lateral sclerosis and cognitive disorders: review and analysis of the literature. Revue Neurologique *157*, 139-150.

Rabinovici,G.D. and Miller,B.L. (2010). Frontotemporal Lobar Degeneration Epidemiology, Pathophysiology, Diagnosis and Management. Cns Drugs *24*, 375-398.

Rademakers,R., Neumann,M., and Mackenzie,I.R. (2012). Advances in understanding the molecular basis of frontotemporal dementia. Nature Reviews Neurology *8*, 423-434.

Rademakers,R. and van Blitterswijk,M. (2013). Novel causal genes and disease modifiers. Nature Reviews Neurology *9*, 63-64.

Rafael,J.A., Nitta,Y., Peters,J., and Davies,K.E. (2000). Testing of SHIRPA, a mouse phenotypic assessment protocol, on Dmd(mdx) and Dmd(mdx3cv) dystrophin-deficient mice. Mammalian Genome *11*, 725-728.

Raiborg,C., Bremnes,B., Mehlum,A., Gillooly,D.J., D'Arrigo,A., Stang,E., and Stenmark,H. (2001). FYVE and coiled-coil domains determine the specific localisation of Hrs to early endosomes. Journal of Cell Science *114*, 2255-2263.

Ramsden,M., Kotilinek,L., Forster,C., Paulson,J., McGowan,E., SantaCruz,K., Guimaraes,A., Yue,M., Lewis,J., Carlson,G., Hutton,M., and Ashe,K.H. (2005). Age-dependent neurofibrillary tangle formation, neuron loss, and memory impairment in a mouse model of human tauopathy (P301L). Journal of Neuroscience *25*, 10637-10647.

Rankin,K.P., Gorno-Tempini,M.L., Allison,S.C., Stanley,C.M., Glenn,S., Weiner,M.W., and Miller,B.L. (2006). Structural anatomy of empathy in neurodegenerative disease. Brain *129*, 2945-2956.

Rascovsky,K., Salmon,D.P., Hansen,L.A., Thal,L.J., and Galasko,D. (2007). Disparate letter and semantic category fluency deficits in autopsy-confirmed frontotemporal dementia and Alzheimer's disease. Neuropsychology *21*, 20-30.

Rascovsky,K., Salmon,D.P., Lipton,A.M., Leverenz,J.B., DeCarli,C., Jagust,W.J., Clark,C.M., Mendez,M.F., Tang-Wai,D.F., Graff-Radford,N.R., and Galasko,D. (2005). Rate of progression differs in frontotemporal dementia and Alzheimer disease. Neurology *65*, 397-403.

Ratnavalli,E., Brayne,C., Dawson,K., and Hodges,J.R. (2002). The prevalence of frontotemporal dementia. Neurology *58*, 1615-1621.

Ravikumar,B., Sarkar,S., Davies,J.E., Futter,M., Garcia-Arencibia,M., Green-Thompson,Z.W., Jimenez-Sanchez,M., Korolchuk,V.I., Lichtenberg,M., Luo,S.Q.,

Massey,D.C.O., Menzies,F.M., Moreau,K., Narayanan,U., Renna,M., Siddiqi,F.H., Underwood,B.R., Winslow,A.R., and Rubinsztein,D.C. (2010). Regulation of Mammalian Autophagy in Physiology and Pathophysiology. Physiological Reviews *90*, 1383-1435.

Ravikumar,B., Vacher,C., Berger,Z., Davies,J.E., Luo,S., Oroz,L.G., Scaravilli,F., Easton,D.F., Duden,R., O'Kane,C.J., and Rubinsztein,D.C. (2004). Inhibition of mTOR induces autophagy and reduces toxicity of polyglutamine expansions in fly and mouse models of Huntington disease. Nat Genet *36*, 585-595.

Renton,A.E., Majounie,E., Waite,A., Simon-Sanchez,J., Rollinson,S., Gibbs,J.R., Schymick,J.C., Laaksovirta,H., van Swieten,J.C., Myllykangas,L., Kalimo,H., Paetau,A., Abramzon,Y., Remes,A.M., Kaganovich,A., Scholz,S.W., Duckworth,J., Ding,J., Harmer,D.W., Hernandez,D.G., Johnson,J.O., Mok,K., Ryten,M., Trabzuni,D., Guerreiro,R.J., Orrell,R.W., Neal,J., Murray,A., Pearson,J., Jansen,I.E., Sondervan,D., Seelaar,H., Blake,D., Young,K., Halliwell,N., Callister,J.B., Toulson,G., Richardson,A., Gerhard,A., Snowden,J., Mann,D., Neary,D., Nalls,M.A., Peuralinna,T., Jansson,L., Isoviita,V.M., Kaivorinne,A.L., Holtta-Vuori,M., Ikonen,E., Sulkava,R., Benatar,M., Wuu,J., Chio,A., Restagno,G., Borghero,G., Sabatelli,M., Heckerman,D., Rogaeva,E., Zinman,L., Rothstein,J.D., Sendtner,M., Drepper,C., Eichler,E.E., Alkan,C., Abdullaev,Z., Pack,S.D., Dutra,A., Pak,E., Hardy,J., Singleton,A., Williams,N.M., Heutink,P., Pickering-Brown,S., Morris,H.R., Tienari,P.J., and Traynor,B.J. (2011). A Hexanucleotide Repeat Expansion in C9ORF72 Is the Cause of Chromosome 9p21-Linked ALS-FTD. Neuron.

Rizzu,P., van Mil,S.E., Anar,B., Rosso,S.M., Kaat,L.D., Heutink,P., and van Swieten,J.C. (2006). CHMP2B mutations are not a cause of dementia in Dutch patients with familial and sporadic frontotemporal dementia. Am J Med Genet B Neuropsychiatr. Genet *141B*, 944-946.

Roberson,E.D. (2012). Mouse Models of Frontotemporal Dementia. Annals of Neurology *72*, 837-849.

Roberson,E.D., Hesse,J.H., Rose,K.D., Slama,H., Johnson,J.K., Yaffe,K., Forman,M.S., Miller,C.A., Trojanowski,J.Q., Kramer,J.H., and Miller,B.L. (2005). Frontotemporal dementia progresses to death faster than Alzheimer disease. Neurology *65*, 719-725.

Rock,F.L., Hardiman,G., Timans,J.C., Kastelein,R.A., and Bazan,J.F. (1998). A family of human receptors structurally related to Drosophila Toll. Proceedings of the National Academy of Sciences of the United States of America *95*, 588-593.

Roeber,S., Mackenzie,I.R., Kretzschmar,H.A., and Neumann,M. (2008). TDP-43-negative FTLD-U is a significant new clinico-pathological subtype of FTLD. Acta Neuropathol *116*, 147-157.

Rogers,D.C., Fisher,E.M.C., Brown,S.D.M., Peters,J., Hunter,A.J., and Martin,J.E. (1997). Behavioral and functional analysis of mouse phenotype: SHIRPA, a proposed protocol for comprehensive phenotype assessment. Mammalian Genome *8*, 711-713.

Rogers,D.C., Peters,J., Martin,J.E., Ball,S., Nicholson,S.J., Witherden,A.S., Hafezparast,M., Latcham,J., Robinson,T.L., Quilter,C.A., and Fisher,E.M.C. (2001). SHIRPA, a protocol for behavioral assessment: validation for longitudinal study of neurological dysfunction in mice. Neuroscience Letters *306*, 89-92.

Rogers,N., Paine,S., Bedford,L., and Layfield,R. (2010). Review: The ubiquitin-proteasome system: contributions to cell death or survival in neurodegeneration. Neuropathology and Applied Neurobiology *36*, 113-124.

Rohrer,J.D., Ahsan,R.L., Isaacs,A.M., Nielsen,J.E., Ostergaard,L., Scahill,R., Warren,J.D., Rossor,M.N., Fox,N.C., and Johannsen,P. (2009a). Presymptomatic generalized brain atrophy in frontotemporal dementia caused by CHMP2B mutation. Dement Geriatr Cogn Disord *27*, 182-186.

Rohrer,J.D., Guerreiro,R., Vandrovcova,J., Uphill,J., Reiman,D., Beck,J., Isaacs,A.M., Authier,A., Ferrari,R., Fox,N.C., Mackenzie,I.R., Warren,J.D., de Silva,R., Holton,J., Revesz,T., Hardy,J., Mead,S., and Rossor,M.N. (2009b). The heritability and genetics of frontotemporal lobar degeneration. Neurology *73*, 1451-1456.

Rohrer,J.D., Lashley,T., Holton,J., Revesz,T., Urwin,H., Isaacs,A.M., Fox,N.C., Rossor,M.N., and Warren,J. (2011a). The clinical and neuroanatomical phenotype of FUS associated frontotemporal lobar degeneration. Journal of Neurology Neurosurgery and Psychiatry *82*, 1405-1407.

Rohrer,J.D., Lashley,T., Schott,J.M., Warren,J.E., Mead,S., Isaacs,A.M., Beck,J., Hardy,J., de Silva,R., Warrington,E., Troakes,C., Al Sarraj,S., King,A., Borroni,B., Clarkson,M.J., Ourselin,S., Holton,J.L., Fox,N.C., Revesz,T., Rossor,M.N., and Warren,J.D. (2011b). Clinical and neuroanatomical signatures of tissue pathology in frontotemporal lobar degeneration. Brain *134*, 2565-2581.

Rohrer,J.D. and Warren,J.D. (2011). Phenotypic signatures of genetic frontotemporal dementia. Current Opinion in Neurology *24*, 542-549.

Rosso,S.M., Donker,K.L., Baks,T., Joosse,M., de,K., I, Pijnenburg,Y., de Jong,D., Dooijes,D., Kamphorst,W., Ravid,R., Niermeijer,M.F., Verheij,F., Kremer,H.P., Scheltens,P., van Duijn,C.M., Heutink,P., and van Swieten,J.C. (2003). Frontotemporal dementia in The Netherlands: patient characteristics and prevalence estimates from a population-based study. Brain *126*, 2016-2022.

Russell,V. (2011). Overview of Animal Models of Attention Deficit Hyperactivity Disorder (ADHD). John Wiley and sons Inc).

Saftig,P., Beertsen,W., and Eskelinen,E.L. (2008). LAMP-2: a control step for phagosome and autophagosome maturation. Autophagy *4*, 510-512.

Saksena,S., Wahlman,J., Teis,D., Johnson,A.E., and Emr,S.D. (2009). Functional reconstitution of ESCRT-III assembly and disassembly. Cell *136*, 97-109.

Sampathu,D.M., Neumann,M., Kwong,L.K., Chou,T.T., Micsenyi,M., Truax,A., Bruce,J., Grossman,M., Trojanowski,J.Q., and Lee,V.M. (2006). Pathological heterogeneity of frontotemporal lobar degeneration with ubiquitin-positive inclusions delineated by ubiquitin immunohistochemistry and novel monoclonal antibodies. Am J Pathol *169*, 1343-1352.

SantaCruz,K., Lewis,J., Spires,T., Paulson,J., Kotilinek,L., Ingelsson,M., Guimaraes,A., DeTure,M., Ramsden,M., McGowan,E., Forster,C., Yue,M., Orne,J., Janus,C., Mariash,A., Kuskowski,M., Hyman,B., Hutton,M., and Ashe,K.H. (2005). Tau suppression in a neurodegenerative mouse model improves memory function. Science *309*, 476-481.

Schmitt-John,T., Drepper,C., Mussmann,A., Hahn,P., Kuhlmann,M., Thiel,C., Hafner,M., Lengeling,A., Heimann,P., Jones,J.M., Meisler,M.H., and Jockusch,H. (2005). Mutation of Vps54 causes motor neuron disease and defective spermiogenesis in the wobbler mouse. Nature Genetics *37*, 1213-1215.

Scott,M., Foster,D., Mirenda,C., Serban,D., Coufal,F., Walchli,M., Torchia,M., Groth,D., Carlson,G., DeArmond,S.J., Westaway,D., and Prusiner,S.B. (1989). Transgenic mice expressing hamster prion protein produce species-specific scrapie infectivity and amyloid plaques. Cell *59*, 847-857.

Seelaar,H., Kamphorst,W., Koning,I., Rizzu,P., and van Swieten,J.C. (2008a). Genetic forms of frontotemporal dementia. Neurology *70*, A315-A316.

Seelaar,H., Kamphorst,W., Rosso,S.M., Azmani,A., Masdjedi,R., de Koning,I., Maat-Kievit,J.A., Anar,B., Kaat,L.D., Breedveld,G.J., Dooijes,D., Rozemuller,J.M., Bronner,I.F., Rizzu,P., and van Swieten,J.C. (2008b). Distinct genetic forms of frontotemporal dementia. Neurology *71*, 1220-1226.

Seelaar,H., Klijnsma,K.Y., de Koning,I., van der Lugt,A., Chiu,W.Z., Azmani,A., Rozemuller,A.J.M., and Swieten,J.C. (2010). Frequency of ubiquitin and FUS-positive, TDP-43-negative frontotemporal lobar degeneration. Journal of Neurology *257*, 747-753.

Seelaar,H., Rohrer,J.D., Pijnenburg,Y.A., Fox,N.C., and van Swieten,J.C. (2011). Clinical, genetic and pathological heterogeneity of frontotemporal dementia: a review. J Neurol Neurosurg Psychiatry *82*, 476-486.

Seelaar,H., Schelhaas,H.J., Azmani,A., Kusters,B., Rosso,S., Majoor-Krakauer,D., de Rijk,M.C., Rizzu,P., ten Brummelhuis,M., van Doorn,P.A., Kamphorst,W.,

Willemsen,R., and van Swieten,J.C. (2007). TDP-43 pathology in familial frontotemporal dementia and motor neuron disease without Progranulin mutations. Brain *130*, 1375-1385.

Seilhean,D., Le Ber,I., Sarazin,M., Lacomblez,L., Millecamps,S., Salachas,F., Pradat,P.F., Le Forestier,N., LeGuern,E., Dubois,B., Meininger,V., Brice,A., Hauw,J.J., and Duyckaerts,C. (2011). Fronto-temporal lobar degeneration: neuropathology in 60 cases. Journal of Neural Transmission *118*, 753-764.

Selak,S., Chan,E.K.L., Schoenroth,L., Senecal,J.L., and Fritzler,M.J. (1999). Early endosome antigen 1: An autoantigen associated with neurological diseases. Journal of Investigative Medicine *47*, 311-318.

Sephton,C.F., Good,S.K., Atkin,S., Dewey,C.M., Mayer,P., Herz,J., and Yu,G. (2010). TDP-43 Is a Developmentally Regulated Protein Essential for Early Embryonic Development. Journal of Biological Chemistry *285*, 6826-6834.

Shatunov,A., Mok,K., Newhouse,S., Weale,M.E., Smith,B., Vance,C., Johnson,L., Veldink,J.H., van Es,M.A., van den Berg,L.H., Robberecht,W., Van Damme,P., Hardiman,O., Farmer,A.E., Lewis,C.M., Butler,A.W., Abel,O., Andersen,P.M., Fogh,I., Silani,V., Chio,A., Traynor,B.J., Melki,J., Meininger,V., Landers,J.E., McGuffin,P., Glass,J.D., Pall,H., Leigh,P.N., Hardy,J., Brown,R.H., Powell,J.F., Orrell,R.W., Morrison,K.E., Shaw,P.J., Shaw,C.E., and Al Chalabi,A. (2010). Chromosome 9p21 in sporadic amyotrophic lateral sclerosis in the UK and seven other countries: a genome-wide association study. Lancet Neurology *9*, 986-994.

Shim,J.H., Xiao,C., Hayden,M.S., Lee,K.Y., Trombetta,E.S., Pypaert,M., Nara,A., Yoshimori,T., Wilm,B., Erdjument-Bromage,H., Tempst,P., Hogan,B.L., Mellman,I., and Ghosh,S. (2006). CHMP5 is essential for late endosome function and down-regulation of receptor signaling during mouse embryogenesis. J Cell Biol *172*, 1045-1056.

Shim,S., Kimpler,L.A., and Hanson,P.I. (2007). Structure/function analysis of four core ESCRT-III proteins reveals common regulatory role for extreme C-terminal domain. Traffic *8*, 1068-1079.

Simon-Sanchez,J., Dopper,E.G.P., Cohn-Hokke,P.E., Hukema,R.K., Nicolaou,N., Seelaar,H., de Graaf,J.R.A., de Koning,I., van Schoor,N.M., Deeg,D.J.H., Smits,M., Raaphorst,J., van den Berg,L.H., Schelhaas,H.J., Die-Smulders,C.E.M., Majoor-Krakauer,D., Rozemuller,A.J.M., Willemsen,R., Pijnenburg,Y.A.L., Heutink,P., and van Swieten,J.C. (2012). The clinical and pathological phenotype of C9ORF72 hexanucleotide repeat expansions. Brain *135*, 723-735.

Sjogren,M. and Andersen,C. (2006). Frontotemporal dementia--a brief review. Mech. Ageing Dev *127*, 180-187.

Skibinski,G., Parkinson,N.J., Brown,J.M., Chakrabarti,L., Lloyd,S.L., Hummerich,H., Nielsen,J.E., Hodges,J.R., Spillantini,M.G., Thusgaard,T., Brandner,S., Brun,A., Rossor,M.N., Gade,A., Johannsen,P., Sorensen,S.A., Gydesen,S., Fisher,E.M., and Collinge,J. (2005). Mutations in the endosomal ESCRTIII-complex subunit CHMP2B in frontotemporal dementia. Nat Genet. *37*, 806-808.

Slomianka,L., Amrein,I., Knuesel,I., Sorensen,J.C., and Wolfer,D.P. (2011). Hippocampal pyramidal cells: the reemergence of cortical lamination. Brain Structure & Function *216*, 301-317.

Smith,K.R., Damiano,J., Franceschetti,S., Carpenter,S., Canafoglia,L., Morbin,M., Rossi,G., Pareyson,D., Mole,S.E., Staropoli,J.F., Sims,K.B., Lewis,J., Lin,W.L., Dickson,D.W., Dahl,H.H., Bahlo,M., and Berkovic,S.F. (2012). Strikingly Different Clinicopathological Phenotypes Determined by Progranulin-Mutation Dosage. American Journal of Human Genetics *90*, 1102-1107.

Snowden,J.S., Bathgate,D., Varma,A., Blackshaw,A., Gibbons,Z.C., and Neary,D. (2001). Distinct behavioural profiles in frontotemporal dementia and semantic dementia. Journal of Neurology Neurosurgery and Psychiatry *70*, 323-332.

Snowden,J.S. and Neary,D. (1993). Progressive Language Dysfunction and Lobar Atrophy. Dementia *4*, 226-231.

Snowden,J.S., Neary,D., and Mann,D.M. (2002). Frontotemporal dementia. Br. J Psychiatry *180*, 140-143.

Spillantini,M.G., Murrell,J.R., Goedert,M., Farlow,M.R., Klug,A., and Ghetti,B. (1998). Mutation in the tau gene in familial multiple system tauopathy with presenile dementia. Proc. Natl. Acad. Sci U. S A *95*, 7737-7741.

Spitalnik, Patrice and Witkin, Joan. Histology Laboratory Manual. Colombia CNMTL . 10-9-2012. 1-9-0012.
Ref Type: Electronic Citation

Stevens,M., van Duijn,C.M., Kamphorst,W., de Knijff,P., Heutink,P., van Gool,W.A., Scheltens,P., Ravid,R., Oostra,B.A., Niermeijer,M.F., and van Swieten,J.C. (1998). Familial aggregation in frontotemporal dementia. Neurology *50*, 1541-1545.

Stinton,L.M., Eystathioy,T., Selak,S., Chan,E.K.L., and Fritzler,M.J. (2004). Autoantibodies to protein transport and messenger RNA processing pathways: endosomes, lysosomes, Golgi complex, proteasomes, assemblyosomes, exosomes, and GW bodies. Clinical Immunology *110*, 30-44.

Stryke,D., Kawamoto,M., Huang,C.C., Johns,S.J., King,L.A., Harper,C.A., Meng,E.C., Lee,R.E., Yee,A., L'Italien,L., Chuang,P.T., Young,S.G., Skarnes,W.C., Babbitt,P.C., and Ferrin,T.E. (2003). BayGenomics: a resource of insertional mutations in mouse embryonic stem cells. Nucleic Acids Research *31*, 278-281.

Stuchell-Brereton,M.D., Skalicky,J.J., Kieffer,C., Karren,M.A., Ghaffarian,S., and Sundquist,W.I. (2007). ESCRT-III recognition by VPS4 ATPases. Nature *449*, 740-744.

Sun,W., Yan,Q., Vida,T.A., and Bean,A.J. (2003). Hrs regulates early endosome fusion by inhibiting formation of an endosomal SNARE complex. Journal of Cell Biology *162*, 125-137.

Suzuki,M., Lee,H.C., Kayasuga,Y., Chiba,S., Nedachi,T., Matsuwaki,T., Yamanouchi,K., and Nishihara,M. (2009). Roles of Progranulin in Sexual Differentiation of the Developing Brain and Adult Neurogenesis. Journal of Reproduction and Development *55*, 351-355.

Suzuki,N., Maroof,A., Merkle,F., Koszka,K., Intoh,A., Armstrong,I., Moccia,R., Davis-Dusenbury,B., and Eggan,K. (2013). The mouse C9ORF72 ortholog is enriched in neurons known to degenerate in ALS and FTD. Nature Neuroscience *16*, 1725-1728.

Swarup,V., Phaneuf,D., Bareil,C., Robertson,J., Rouleau,G.A., Kriz,J., and Julien,J.P. (2011). Pathological hallmarks of amyotrophic lateral sclerosis/frontotemporal lobar degeneration in transgenic mice produced with TDP-43 genomic fragments. Brain *134*, 2610-2626.

Sweeney,N.T., Brenman,J.E., Jan,Y.N., and Gao,F.B. (2006). The coiled-coil protein shrub controls neuronal morphogenesis in Drosophila. Curr. Biol *16*, 1006-1011.

Sydow,A., Van der Jeugd,A., Zheng,F., Ahmed,T., Balschun,D., Petrova,O., Drexler,D., Zhou,L.P., Rune,G., Mandelkow,E., D'Hooge,R., Alzheimer,C., and Mandelkow,E.M. (2011). Tau-Induced Defects in Synaptic Plasticity, Learning, and Memory Are Reversible in Transgenic Mice after Switching Off the Toxic Tau Mutant. Journal of Neuroscience *31*, 2511-2525.

Tamai,K., Tanaka,N., Nara,A., Yamamoto,A., Nakagawa,I., Yoshimori,T., Ueno,Y., Shimosegawa,T., and Sugamura,K. (2007). Role of Hrs in maturation of autophagosomes in mammalian cells. Biochem Biophys Res Commun *360*, 721-727.

Tamai,K., Toyoshima,M., Tanaka,N., Yamamoto,N., Owada,Y., Kiyonari,H., Murata,K., Ueno,Y., Ono,M., Shimosegawa,T., Yaegashi,N., Watanabe,M., and Sugamura,K. (2008). Loss of Hrs in the Central Nervous System Causes Accumulation of Ubiquitinated Proteins and Neurodegeneration. American Journal of Pathology *173*, 1806-1817.

Tanida,I., Ueno,T., and Kominami,E. (2004a). Human light chain 3/MAP1LC3B is cleaved at its carboxyl-terminal Met(121) to expose Gly(120) for lipidation and targeting to autophagosomal membranes. Journal of Biological Chemistry *279*, 47704-47710.

Tanida,I., Ueno,T., and Kominami,E. (2004b). LC3 conjugation system in mammalian autophagy. International Journal of Biochemistry & Cell Biology *36*, 2503-2518.

Taniguchi,S., McDonagh,A.M., Pickering-Brown,S.M., Umeda,Y., Iwatsubo,T., Hasegawa,M., and Mann,D.M. (2004). The neuropathology of frontotemporal lobar degeneration with respect to the cytological and biochemical characteristics of tau protein. Neuropathol. Appl. Neurobiol. *30*, 1-18.

Thangavel R,S.D.Y.X.A.P.Z.A. (2011). EXPRESSION OF GLIA MATURATION FACTOR IN NEUROPATHOLOGICAL LESIONS OF ALZHEIMER'S DISEASE. Neuropathol Appl Neurobiol.

Ticozzi,N., LeClerc,A.L., van Blitterswijk,M., Keagle,P., McKenna-Yasek,D.M., Sapp,P.C., Silani,V., Wills,A.M., Brown,R.H., and Landers,J.E. (2011). Mutational analysis of TARDBP in neurodegenerative diseases. Neurobiology of Aging *32*, 2096-2099.

Tsai,K.J., Yang,C.H., Fang,Y.H., Cho,K.H., Chien,W.L., Wang,W.T., Wu,T.W., Lin,C.P., Fu,W.M., and Shen,C.K.J. (2010). Elevated expression of TDP-43 in the forebrain of mice is sufficient to cause neurological and pathological phenotypes mimicking FTLD-U. Journal of Experimental Medicine *207*, 1661-1673.

Tsao,W., Jeong,Y.H., Lin,S., Ling,J., Price,D.L., Chiang,P.M., and Wong,P.C. (2012). Rodent models of TDP-43: Recent advances. Brain Research *1462*, 26-39.

Urwin,H., Authier,A., Nielsen,J.E., Metcalf,D., Powell,C., Froud,K., Malcolm,D.S., Holm,I., Johannsen,P., Brown,J., Fisher,E.M., van der,Z.J., Bruyland,M., Van Broeckhoven,C., Collinge,J., Brandner,S., Futter,C., and Isaacs,A.M. (2010a). Disruption of endocytic trafficking in frontotemporal dementia with CHMP2B mutations. Hum Mol Genet *19*, 2228-2238.

Urwin,H., Ghazi-Noori,S., Collinge,J., and Isaacs,A. (2009). The role of CHMP2B in frontotemporal dementia. Biochem Soc Trans *37*, 208-212.

Urwin,H., Josephs,K.A., Rohrer,J.D., Mackenzie,I.R., Neumann,M., Authier,A., Seelaar,H., van Swieten,J.C., Brown,J.M., Johannsen,P., Nielsen,J.E., Holm,I.E., Dickson,D.W., Rademakers,R., Graff-Radford,N.R., Parisi,J.E., Petersen,R.C., Hatanpaa,K.J., White,C.L., Weiner,M.F., Geser,F., Van Deerlin,V.M., Trojanowski,J.Q., Miller,B.L., Seeley,W.W., van der Zee,J., Kumar-Singh,S., Engelborghs,S., De Deyn,P.P., Van Broeckhoven,C., Bigio,E.H., Deng,H.X., Halliday,G.M., Kril,J.J., Munoz,D.G., Mann,D.M., Pickering-Brown,S.M., Doodeman,V., Adamson,G., Ghazi-Noori,S., Fisher,E.M.C., Holton,J.L., Revesz,T., Rossor,M.N., Collinge,J., Mead,S., and Isaacs,A.M. (2010b). FUS pathology defines the majority of tau- and TDP-43-negative frontotemporal lobar degeneration. Acta Neuropathologica *120*, 33-41.

Valdmanis,P.N., Dupre,N., Bouchard,J.P., Camu,W., Meininger,V., Strong,M., and Rouleau,G.A. (2007). Three families with amyotrophic lateral sclerosis and frontotemporal dementia with evidence of linkage to chromosome 9p. Archives of Neurology *64*, 240-245.

van der Zee J., Rademakers,R., Engelborghs,S., Gijselinck,I., Bogaerts,V., Vandenberghe,R., Santens,P., Caekebeke,J., De Pooter,T., Peeters,K., Lubke,U., Van den,B.M., Martin,J.J., Cruts,M., De Deyn,P.P., Van Broeckhoven,C., and Dermaut,B. (2006). A Belgian ancestral haplotype harbours a highly prevalent mutation for 17q21-linked tau-negative FTLD. Brain *129*, 841-852.

van der Zee J., Urwin,H., Engelborghs,S., Bruyland,M., Vandenberghe,R., Dermaut,B., De Pooter,T., Peeters,K., Santens,P., De Deyn,P.P., Fisher,E.M., Collinge,J., Isaacs,A.M., and Van Broeckhoven,C. (2008). CHMP2B C-truncating mutations in frontotemporal lobar degeneration are associated with an aberrant endosomal phenotype in vitro. Hum Mol Genet *17*, 313-322.

van Es,M.A., Veldink,J.H., Saris,C.G.J., Blauw,H.M., van Vught,P.W.J., Birve,A., Lemmens,R., Schelhaas,H.J., Groen,E.J.N., Huisman,M.H.B., van der Kooi,A.J., de Visser,M., Dahlberg,C., Estrada,K., Rivadeneira,F., Hofman,A., Zwarts,M.J., van Doormaal,P.T.C., Rujescu,D., Strengman,E., Giegling,I., Muglia,P., Tomik,B., Slowik,A., Uitterlinden,A.G., Hendrich,C., Waibel,S., Meyer,T., Ludolph,A.C., Glass,J.D., Purcell,S., Cichon,S., Nothen,M.M., Wichmann,H.E., Schreiber,S., Vermeulen,S.H.H.M., Kiemeney,L.A., Wokke,J.H.J., Cronin,S., McLaughlin,R.L., Hardiman,O., Fumoto,K., Pasterkamp,R.J., Meininger,V., Melki,J., Leigh,P.N., Shaw,C.E., Landers,J.E., Al Chalabi,A., Brown,R.H., Robberecht,W., Andersen,P.M., Ophoff,R.A., and van den Berg,L.H. (2009). Genome-wide association study identifies 19p13.3 (UNC13A) and 9p21.2 as susceptibility loci for sporadic amyotrophic lateral sclerosis. Nature Genetics *41*, 1083-1U53.

van Swieten,J.C. (2007). Genetic basis of frontotemporal dementia. Lancet Neurology *6*, 840-841.

van Swieten,J.C. and Heutink,P. (2008). Mutations in progranulin (GRN) within the spectrum of clinical and pathological phenotypes of frontotemporal dementia. Lancet Neurol *7*, 965-974.

Vance,C., Al Chalabi,A., Ruddy,D., Smith,B.N., Hu,X., Sreedharan,J., Siddique,T., Schelhaas,H.J., Kusters,B., Troost,D., Baas,F., de,J., V, and Shaw,C.E. (2006). Familial amyotrophic lateral sclerosis with frontotemporal dementia is linked to a locus on chromosome 9p13.2-21.3. Brain *129*, 868-876.

Vance,C., Rogelj,B., Hortobagyi,T., De Vos,K.J., Nishimura,A.L., Sreedharan,J., Hu,X., Smith,B., Ruddy,D., Wright,P., Ganesalingam,J., Williams,K.L., Tripathi,V., Al Saraj,S., Al Chalabi,A., Leigh,P.N., Blair,I.P., Nicholson,G., de Belleroche,J., Gallo,J.M., Miller,C.C., and Shaw,C.E. (2009). Mutations in FUS, an RNA Processing

Protein, Cause Familial Amyotrophic Lateral Sclerosis Type 6. Science *323*, 1208-1211.

Viggiano,D., Ruocco,L.A., and Sadile,A.G. (2003). Dopamine phenotype and behaviour in animal models: in relation to attention deficit hyperactivity disorder. Neuroscience and Biobehavioral Reviews *27*, 623-637.

Washbourne,P., Schiavo,G., and Montecucco,C. (1995). Vesicle-Associated Membrane Protein-2 (Synaptobrevin-2) Forms A Complex with Synaptophysin. Biochemical Journal *305*, 721-724.

Watase,K., Weeber,E.J., Xu,B., Antalffy,B., Yuva-Paylor,L., Hashimoto,K., Kano,M., Atkinson,R., Sun,Y., Armstrong,D.L., Sweatt,J.D., Orr,H.T., Paylor,R., and Zoghbi,H.Y. (2002). A long CAG repeat in the mouse Sca1 locus replicates SCA1 features and reveals the impact of protein solubility on selective neurodegeneration. Neuron *34*, 905-919.

Weder,N.D., Aziz,R., Wilkins,K., and Tampi,R.R. (2007). Frontotemporal dementias: a review. Ann Gen Psychiatry *6*, 15.

Wegorzewska,I., Bell,S., Cairns,N.J., Miller,T.M., and Baloh,R.H. (2009). TDP-43 mutant transgenic mice develop features of ALS and frontotemporal lobar degeneration. Proceedings of the National Academy of Sciences of the United States of America *106*, 18809-18814.

Werner,K.H., Roberts,N.A., Rosen,H.J., Dean,D.L., Kramer,J.H., Weiner,M.W., Miller,B.L., and Levenson,R.W. (2007). Emotional reactivity and emotion recognition in frontotemporal lobar degeneration. Neurology *69*, 148-155.

Wiedenmann,B. and Franke,W.W. (1985). Identification and Localization of Synaptophysin, An Integral Membrane Glycoprotein of Mr 38,000 Characteristic of Presynaptic Vesicles. Cell *41*, 1017-1028.

Wilhelmsen,K.C., Lynch,T., Pavlou,E., Higgins,M., and Nygaard,T.G. (1994). Localization of Disinhibition-Dementia-Parkinsonism-Amyatrophy Complex to 17Q21-22. American Journal of Human Genetics *55*, 1159-1165.

Williams,R.L. and Urbe,S. (2007). The emerging shape of the ESCRT machinery. Nat Rev Mol Cell Biol *8*, 355-368.

Wils,H., Kleinberger,G., Pereson,S., Janssens,J., Capell,A., Van Dam,D., Cuijt,I., Joris,G., De Deyn,P.P., Haass,C., Van Broeckhoven,C., and Kumar-Singh,S. (2012). Cellular ageing, increased mortality and FTLD-TDP-associated neuropathology in progranulin knockout mice. Journal of Pathology *228*, 67-76.

Wilson,M.C. (2000). Coloboma mouse mutant as an animal model of hyperkinesis and attention deficit hyperactivity disorder. Neuroscience and Biobehavioral Reviews *24*, 51-57.

Wollert,T. and Hurley,J.H. (2010). Molecular mechanism of multivesicular body biogenesis by ESCRT complexes. Nature *464*, 864-869.

Wollert,T., Wunder,C., Lippincott-Schwartz,J., and Hurley,J.H. (2009). Membrane scission by the ESCRT-III complex. Nature *458*, 172-177.

Wu,L.S., Cheng,W.C., Hou,S.C., Yan,Y.T., Jiang,S.T., and Shen,C.K.J. (2010). TDP-43, a Neuro-Pathosignature Factor, is Essential for Early Mouse Embryogenesis. Genesis *48*, 56-62.

Wu,L.S., Cheng,W.C., and Shen,C.K.J. (2012). Targeted Depletion of TDP-43 Expression in the Spinal Cord Motor Neurons Leads to the Development of Amyotrophic Lateral Sclerosis-like Phenotypes in Mice. Journal of Biological Chemistry *287*, 27335-27344.

www.molgen.ua.ac.be/FTDMutations/. Alzheimer's and Frontotemporal Dementia Mutation Database. 2012.

Yamazaki,Y., Takahashi,T., Hiji,M., Kurashige,T., Izumi,Y., Yamawaki,T., and Matsumoto,M. (2010). Immunopositivity for ESCRT-III subunit CHMP2B in granulovacuolar degeneration of neurons in the Alzheimer's disease hippocampus. Neuroscience Letters *477*, 86-90.

Yancopoulou,D., Crowther,R.A., Chakrabarti,L., Gydesen,S., Brown,J.M., and Spillantini,M.G. (2003). Tau protein in frontotemporal dementia linked to chromosome 3 (FTD-3). J Neuropathol. Exp. Neurol. *62*, 878-882.

Yin,F., Banerjee,R., Thomas,B., Zhou,P., Qian,L., Jia,T., Ma,X., Ma,Y., Iadecola,C., Beal,M.F., Nathan,C., and Ding,A. (2010a). Exaggerated inflammation, impaired host defense, and neuropathology in progranulin-deficient mice. J Exp Med *207*, 117-128.

Yin,F., Dumont,M., Banerjee,R., Ma,Y., Li,H., Lin,M.T., Beal,M.F., Nathan,C., Thomas,B., and Ding,A. (2010b). Behavioral deficits and progressive neuropathology in progranulin-deficient mice: a mouse model of frontotemporal dementia. FASEB J *24*, 4639-4647.

Yoshiyama,Y., Higuchi,M., Zhang,B., Huang,S.M., Iwata,N., Saido,T.C., Maeda,J., Suhara,T., Trojanowski,J.Q., and Lee,V.M.Y. (2007). Synapse loss and microglial activation precede tangles in a P301S tauopathy mouse model. Neuron *53*, 337-351.

Zamborlini,A., Usami,Y., Radoshitzky,S.R., Popova,E., Palu,G., and Gottlinger,H. (2006). Release of autoinhibition converts ESCRT-III components into potent inhibitors of HIV-1 budding. Proc Natl Acad Sci U S A *103*, 19140-19145.

Zhan,S.S., Beyreuther,K., and Schmitt,H.P. (1993). Quantitative Assessment of the Synaptophysin Immuno-Reactivity of the Cortical Neuropil in Various Neurodegenerative Disorders with Dementia. Dementia *4*, 66-74.

Zhang, Y., Schuff, N., Ching C, Tosun D, Zhan W, Nezamzadeh M, Rosen, H. J., Kramer, B. M., Gorno'-Tempini, M. L., Miller, B., and Weiner, M. W. Joint Assessment of Structural, Perfusion and Diffussion MRI in Alzheimer's Disease and Frontotemporal Dementia. International Journal of Alzheimer's Disease 2011, 1-11. 26-4-2011. SAGE-Hindawi Access to Research.